THE UNIVERSITY
of EDINBURGH

Hydrogel and Other Polymer Arrays for Biomedical Applications

Sara Schmidt

THE UNIVERSITY *of* EDINBURGH

Doctorate of Philosophy

The University of Edinburgh

School of Chemistry

2019

Abstract

The need for efficient and reproducible cell culture is necessary for the development of novel biological applications. Traditional two-dimensional cell culture is traditionally done using monolayer cultures on tissue culture plastic. Such surfaces however, do not mimic the natural three-dimensional (3D) *in vivo* setting in which cells reside, namely the complex 3D extracellular matrix (ECM), which is composed of multiple components, including proteins, polysaccharides and proteoglycans. Clearly monolayer cell culture is unable to recapitulate this environment and consequently results in altered gene expression profiles, changes to cell metabolism, signalling and morphology when compared to cells grown in 3D.

Therefore, there is a need to develop 3D matrices that can support *in vitro* cell culture. Commonly used 3D matrices tend to be based on animal-derived products that are subject to batch-to-batch variations with variable compositions. With this in mind, using synthetically defined and tuneable synthetic materials for 3D cell culture would be advantageous offering a higher level of material control, and understanding of cell behaviour in response to the material. Hydrogels are highly hydrated networks that exhibit promising properties as ECM-mimics, and can be generated from various sources including polymers, proteins, and peptides or mixtures thereof and have been used for a range of cell-based applications. A limiting factor in the development of any biomaterial is the time-consuming nature of its discovery and optimisation. As such, a high-throughput approach where multiple materials of variable compositions are fabricated and screened in parallel offers a powerful approach to the discovery of optimal materials for a specific cell type or application.

In this thesis I present the development and fabrication of a dynamic 3D hydrogel array, based on imine cross-linked polymers and peptides printed using a drop-on-demand inkjet-printer. 250 different hydrogels were initially screened as novel cell matrices. Hits from the array screen were scaled-up for studies with endothelial cells and showed that these dynamic hydrogels had the ability to maintain the endothelial cell phenotype, promote proliferation and allow the generation of 3D cell clusters.

Furthermore, a mild and enzyme-free passaging system was developed that allowed for the degradation of the hydrogels and cell release by addition of Vitamin B6 derivatives that compete for the imine-linkage. Thus a 3D cell culture matrix allowing for long-term culture and promoting the formation of 3D cell constructs with the capacity to passage in a mild and cell compatible manner was realised.

As a second project a collaborative effort with Tokyo Medical and Dental University aimed to identify novel polymeric substrates that supported pancreatic cancer stem cells and recapitulated the niche environment. Using a polymer microarray of 382 different polyacrylates/acrylamides and polyurethanes, substrates were identified that fulfilled these rules. Subsequently a novel peptide-containing polymer microarray was developed and screened with hits identified that upon scale-up were found to recapitulate the stem cell niche.

Lay Summary

The ability to grow cells in the lab in a controllable, robust and scalable manner is necessary for researchers to be able to make new biomedical discoveries such as identifying new therapeutic targets. Traditionally, cells are grown on 2D plastic surfaces, which although being a straightforward way to grow cells, is a poor model of the actual cell environment within our bodies. Cells grow and reside in a complex 3D environment, known as the extracellular matrix (ECM), which not only provides a support in which cells grow and multiply, but also provides signals and cues that alter cell behaviour. To be able to grow cells in the lab on substrates that can mimic this complex environment would therefore be greatly beneficial. Current materials that offer this to researchers have some serious drawbacks and are poorly defined. Therefore, reproducibility of cell behaviour with these materials is limited.

To address these challenges, the work in this thesis sets out to create new synthetically defined and reproducible materials that can mimic the natural ECM environment. Additionally, the use of an inkjet printing system (similar to the ones used as home) allowed lots of new materials to be made, thus speeding up the process of material identification.

Table of Contents

Declaration of Authorship

The research detailed within this thesis has been accumulated by the author in the duration of her PhD scholarship between the dates of October 2014 and September 2018 under the supervision of Professor Mark Bradley, School of Chemistry, University of Edinburgh.

The work, data and interpretation presented in here is that of the author unless there was a significant collaborative contribution, in which case it has been clearly recognised.

This work has not been submitted for any other degrees of professional qualifications.

Where published work has been consulted or quotations made, the source has been clearly cited.

The work detailed in this thesis has been presented at the following conferences and meetings:

- Bioinspired Materials GRC and GRS, Les Diablerets, 2018
- Biomaterials International, Fukuoka, 2017
- Stem Cell Research in Europe: Status and Prospective, Amsterdam, 2017
- RSC Chemical Biology and Bio-Organic Group Postgraduate Symposium, Glasgow, 2017
- Joseph Black Conference, Edinburgh, 2016 and 2017
- HumEn consortia meeting, Max Planck Institute Bad Nauheim, 2016
- Bioprinting and 3D Printing in the Life Sciences, Cambridge, 2016
- Lab on a chip and microfluidics, Munich, 2016
- Warwick Polymer Conference, University of Warwick, 2016
- RSC Innovations in Encapsulation, Edinburgh, 2016
- Hydra XI Stem Cell School, Hydra, 2015

None of the author's works have been published up until the date of thesis submission.

Signed:

Sara Schmidt

Date:

30th April 2019

Acknowledgements

First and foremost, I must thank Professor Mark Bradley for taking me on as a PhD student and for providing me with such an exciting project. Thank you for all your support and guidance for the past four years, and for the many opportunities you have given me regarding collaborations, visits to other labs and supporting my attendance at international conferences.

Dr Annamaria Lilienkampf – Nanna – I am forever grateful for everything you have done for me during my PhD and the excellent support you have provided with regards to my research, career and everything else. I would also like to thank all other Bradley group members, past and present, for their support and help during my time in the group.

I want to extend a special thanks to Dr Matthew Owens, whom I am sure knows that I consider myself a very lucky gal to have him as a friend and colleague. The past four years would have been significantly less fun and rewarding without you as my intelligent and hilarious partner in crime.

Two former Bradley group members, Dr Jessica Clavadetscher and Dr Andrea Venturato have also been hugely important for me during my PhD and I want to thank them both for their help and friendship. Jess, it was a pleasure to share a fume hood with you and I sure learnt a lot from your professionalism and work ethic in the lab. Andrea, our HumEn trips and discussions about polymers, collaborations and more made me both think, laugh and develop as a researcher. I also want to acknowledge a newer Bradley group member, Sonia Rehman, who is stronger than most, and funnier too. You say I am your spirit animal, but really you are mine.

Also thanks to the student's that I have been fortunate enough to supervise during my PhD, Sarah, Ross, Zuzanna and Charlotte, who have helped with various aspects of my projects.

I must also thank my collaborators at the Tokyo Medical and Dental University for working with me on an exciting project and making the process of working across continents effortless. I particularly want to thank Dr Yoshitaka Murota, it was a pleasure to work with you, both from Tokyo, but particularly during your visit to the Bradley group.

The various support staff that I have worked with during the years – Steve at the SEM facility, Melanie, Lyndsey and Mike at the histology and immunohistochemistry service and Elena who helped me with the rheology measurements – were all immensely helpful and supportive.

On a more personal note, I must thank my parents, Cristina Glad and Olle Schmidt, and brother, Fredrik Schmidt, who always believed in me and was there during both the happy and sad times. Particularly thanks to my mother, I hope you know that you are my role model and the one who inspired me to become a scientist in the first place. I also want to thank my lovely girls, Alex Amon and Anna Brand. Without our chats, laughs, tears, brunches and just generally excellent times together I am not sure where I would be today.

Finally, thanks to David Edwards, the person who makes every day worthwhile. You helped me push through to the end and your actions remind me every day that what we have together is very special. The love we share is just amazing and I cannot wait to see what our next adventure will be like. I love you and I like you.

Abbreviations

Ahx	6-aminohexanoic acid
AIBN	Azobisisobutyronitrile
ALP	Alkaline phosphatase
APTES	(3-aminopropyl)triethoxysilane
BF	Bright-field
BSA	Bovine serum albumin
CD31	Cluster of differentiation 31
cDNA	Complimentary deoxyribonucleic acid
CSC	Cancer stem cell
DAB	3,3-diaminobenzidine
DAPI	4′,6-diamidino-2-phenylindole
DCC	N,N′-dicyclohexylcarbodiimide
DCM	Dichloromethane
DIC	N,N′-diisopropylcarbodiimide
DIPEA	Diisopropylethylamine
DMAP	4-Dimethylaminopyridine
DMEM	Dulbecco's Modified Eagle Medium
DMF	Dimethylformamide
DMSO	Dimethyl sulfoxide
DNA	Deoxyribonucleic acid
ECM	Extracellular matrix
EDC	1-ethyl-3-(3-dimethylaminopropyl)carbodiimide
EGF	Epidermal growth factor
ELP	Elastin-like polypeptide/protein
ESA	Epithelial-specific antigen
FACIT	Fibril associated collagens with interrupted triple helices
FACS	Fluorescence assisted cell sorting
FAK	Focal adhesion kinases
FBS	Foetal bovine serum
FDA	Fluorescein diacetate
FDS	(Tridecafluoro-1,1,2,2-tetrahydrooctyl)-1-dimethylchlorosilane

FGF	Fibroblast growth factor
FITC	Fluorescein isothiocyanate
Fmoc	Fluorenylmethoxycarbonyl
FXIIIa	Transglutaminase factor XIIIa
GAG	Glycosaminoglycan
GF	Growth factor
GPC	Gel permeation chromatography
GSPG	Chondroitin sulphate proteoglycan
H&E	Haemotoxylin and Eosin
HA	Hyaluronic acid
HEK293	Human embryonic kidney cells 293
hESC	Human embryonic stem cell
HRMS	High resolution mass spectrometry
HSPG	Heparan sulphate proteoglycan
HTSS	High-throughput synthesis and screening
HUVEC	Human umbilical vein endothelial cell
IHC	Immunohistological
iPSC	Induced pluripotent stem cells
KOSR	Knock-out serum replacement
MAPK	Mitogen-activated protein kinase
mESC	Mouse embryonic stem cells
MMP	Matrix metalloproteases
mRNA	Messenger ribonucleic acid
MSC	Mesenchymal stem cell
NHS	N-hydroxysuccinimide
NMP	N-Methyl-2-pyrrolidone
NMR	Nuclear magnetic resonance
ODC	Ornithine decarboxylase
PCL	Poly(ε-caprolactone)
PDI	Polydispersity index
PEG	Poly(ethylene glycol)
PEGDA	Poly(ethylene glycol) diacrylate
PET	Poly(ethylene terephthalate)

PFA	Paraformaldehyde
PFOA	Perfluorooctanoic acid
PHEMA	poly(2-hydroxyethyl methacrylate)
pHUVEC	Primary human umbilical vein endothelial cell
PI	Propidium iodide
PLA	Poly(lactic acid)
PLGA	Poly(lactic-co-glycolic acid)
PLP	Pyridoxal 5′-phosphate
PMMA	Poly(methyl methacrylate)
PNIPAAm	Poly(*N*-isopropylacrylamide)
PS	Polystyrene
PVA	Poly(vinyl alcohol)
PyrAm	Pyridoxamine dihydrochloride
PyrHCl	Pyridoxal hydrochloride
qPCR	Quantitative polymerase chain reaction
RGD	Arginine-Glycine-Aspartic acid
RNA	Ribonucleic acid
RP-HPLC	Reverse phase high-performance liquid chromatography
SD	Standard deviation
s.e.m	Standard error of mean
SEM	Scanning electron microscopy
SPAAC	Strain-promoted azide-alkyne cycloaddition
SPPS	Solid phase peptide synthesis
TCPS	Tissue culture plastic polystyrene
TFA	Trifluoroacetic acid
TGF-β	Transforming growth factor β
THF	Tetrahydrofuran
TIS	Triisopropylsilane
VEGF	Vascular endothelial growth factor
vWf	von Willebrand factor
YAP	Yes-associated protein

Chapter 1. Introduction

1.1 Recapitulating the ECM for Cell Culture Applications

1.1.1 From tissue culture to *in vitro* virus culture

Before cell culture was developed as we know it today, scientists developed methods for culturing pieces of tissue *in vitro*. The field of tissue culture developed from the early 1900's onwards, notably by Harrison who developed the first tissue culture technique by growing frog nerve fibres embedded in plasma on a coverslip, which then was inverted to let the plasma form a hanging drop in which the tissue was maintained.[1] Methods similar to this hanging drop technique are used nowadays in spheroid and organoid cultures.[2]

Thereafter Carrell and Burrows demonstrated the growth of tissue from chickens and various mammals, by culturing them in plasma and transferring them to new flasks following sufficient growth (known as passaging).[3,4] Claims were made that cells from a chick embryo heart were passaged over 100 times and kept alive over the span of 33 years, although today it is questioned whether this actually was the original culture or a contaminated version.[5,6] In parallel with the development of these techniques, Carrell also emphasised the necessity of sterile techniques and work environments when working with biological samples, and was a key player in developing the composition of growth media used for cell culture. Notably, he introduced the use of serum, solving the issue of plasma clotting.[6] Another key player in these early days was the aviator Lindbergh, who together with Carrell in the 1920's developed the Corning Pyrex® tissue culture flasks that due to their heat resistance could be sterilised by autoclaving.[6,7]

Developments in virus growth *in vitro* was a key driving force for cell culture. It was shown that viruses could be replicated *in vitro* by adding them to chick embryonic tissue and incubating for 24 h with virus activity maintained after 2 weeks storage at

– 20 °C. Viruses including polio, influenza and chickenpox were cultured using this technique, thus beginning *in vitro* culture of viruses and vaccination strategies.[6,8] The plaque assay was subsequently developed, allowing for virus quantification.[9] Moreover, during these early days, several components ubiquitous to today's cell culture were discovered, including the use of antibiotics and fungicides to cell culture medium to prevent contamination, and the use of the protease trypsin to dissociate tissues and allow single cell isolation.[6]

1.1.2 Establishment of continuous mammalian cell lines

Even with the development of techniques for tissue culture, the ability to culture human cells *in vitro* was unsuccessful, despite many attempts. It was not until 1951 that the first human cell line was established with the isolation of cells from a cervical cancer tumour.[10] The tumour cells came from a woman named Henrietta Lacks, hence the naming of the cell line as HeL. The culture was established in the lab of professor Gay, where they identified cells that grew very rapidly, with seemingly endless proliferation. Gay sent cell samples to scientists around the world and HeLa cells quickly spread and became the staple cell line for cell culture. The success of HeLa was not just in their rapid and aggressive growth, which allowed studies for cell reproduction and division, but also importantly their ability to support the growth of viruses for vaccine production that previously had not been possible to culture *in vitro*.[6]

With the identification of HeLa, several other cells were identified that could grow independently *in vitro*, causing a rapid expansion of the cell culture field. Among these was the development of the mouse fibroblast cell line L292,[11] and of the CHO cell line isolated from Chinese hamsters.[12] CHO cells have been particularly useful to study genetics, due to their near normal chromosome set.[6]

In the 1970's Milstein and Köhler established hybrid cell cultures and the production of monoclonal antibodies.[13] By mixing cultures of myeloma cells (fast growing tumour cells) and antibody-producing B-cells isolated from spleens, hybrids (termed hybridomas) were formed that grew as rapidly as the myeloma cells, but also produced antibodies like the B-cells. In the 1980's further discoveries into growth factors present in serum that could support the culture of lymphocytes and isolation

of stem cells paved the way for the establishment of immune cell culture and stem cell culture.[6] This brings us to cell culture as we know it today, where despite the constant introduction of new discoveries and establishment of more complex cell models, many of the techniques used in the lab today still resemble those established more than 50 years ago.

Despite the numerous developments made with traditional cell culture methods, there are several limitations. Firstly, culturing cells on hard plastic or glass surfaces as a monolayer, although facile, is very different from the natural *in vivo* environment where cells reside in and are part of a complex and dynamic 3D environment called the ECM.[14–16] The function of the ECM is not only to provide a structural support for the cells residing within it, but to organise cells into tissue-specific shapes and provide them with spatially and temporally controlled chemical and mechanical signals. In this environment, a dynamic interplay of cell-cell and cell-matrix interactions as well as the secretion of soluble signals e.g. growth factors and cytokines and metabolic signals, e.g. hormones and ions, direct cell behaviour such as proliferation, differentiation, adhesion, spreading, and survival while maintaining tissue homeostasis (the maintenance of tissue structure and function).[14–19] Cell behaviour and signalling affects the composition of the ECM, which is produced by cells themselves, with its formation and degradation dictated by the surrounding and infiltrating cells.[20] This reciprocal relationship between the ECM and cells result in a dynamic environment where spatial and temporal control over its composition and remodelling directs tissue formation and function.

Culturing cells as a monolayer means that important aspects of the natural environment are lost, including 3D cell-cell and cell-matrix interactions, mechanical cues from the ECM to cells and vice versa, as well as the interplay between different cell types within a tissue.[15] The lack of these aspects leads to dramatically altered cell behaviour with 2D culture of cells leading to cell flattening, rearrangement of the actin cytoskeleton and a flattened nucleus. It also leads to numerous changes in gene expression and subsequent protein expression levels that alter cell behaviour and give rise to a different phenotypes.[21,22] Thus conclusions from *in vitro* experiments do not reflect the real *in vivo* environment which they are supposed to model. As such cells

in a monolayer culture respond very differently to drugs compared to those in a 3D environment, representing a great challenge for preclinical drug discovery.[22]

Thus, recent years have seen an increased attention paid to the development and use of 3D cell culture models, wherein crucial cell-cell and cell-matrix interactions are maintained or at the very least mimicked based on their natural *in vivo* setting.[15,16] The use of 3D cell culture and matrices promises to bridge the gap between 2D cell culture and animal models,[16] but before detailing the usefulness and options for 3D cell culture it is important to understand the composition and attributes of the natural ECM.

1.1.3 The composition and function of the ECM

i) Components of the ECM

Two main types of macromolecules, in combination with water, make up the ECM: fibrous proteins such as collagen, elastin, fibronectin and laminin and glycoproteins such as proteoglycans and hyaluronic acid.[17,23] The major structural elements of the ECM are collagen, proteoglycans and hyaluronic acid that provide cells with a structural framework, while proteins like laminin and fibronectin aid in connecting cells to the other ECM components and soluble molecules such as growth factors and hormones.[23]

Collagen

Collagen is the most abundant protein of the ECM, with over 20 different types found in humans. It is composed of trimeric polypeptides (α-chains) assembled into helices, with the repeating Gly-X-Y motif, where X and Y can be any amino acid, but frequently are proline or hydroxyproline as they aid in helical stability.[23] The trimeric assembly of the α-chains results in different types of collagen with one of the most common being fibrillary collagen or Collagen type I, whose assembly consist of four main steps (Figure 1.1). Propeptides are first intracellularly synthesised and assembled into triple helices initiated by the C-terminal domain, followed by removal of N- and C-termin, resulting in collagen formation.[23] The enzyme lysyl oxidase subsequently catalyses oxidative deamination of lysine residues to form inter- and intramolecular cross-links between the chains. Fibrillar collagen is found in multiple

tissues, including skin, tendon and ligaments where it imparts high tensile tissue strength.[24]

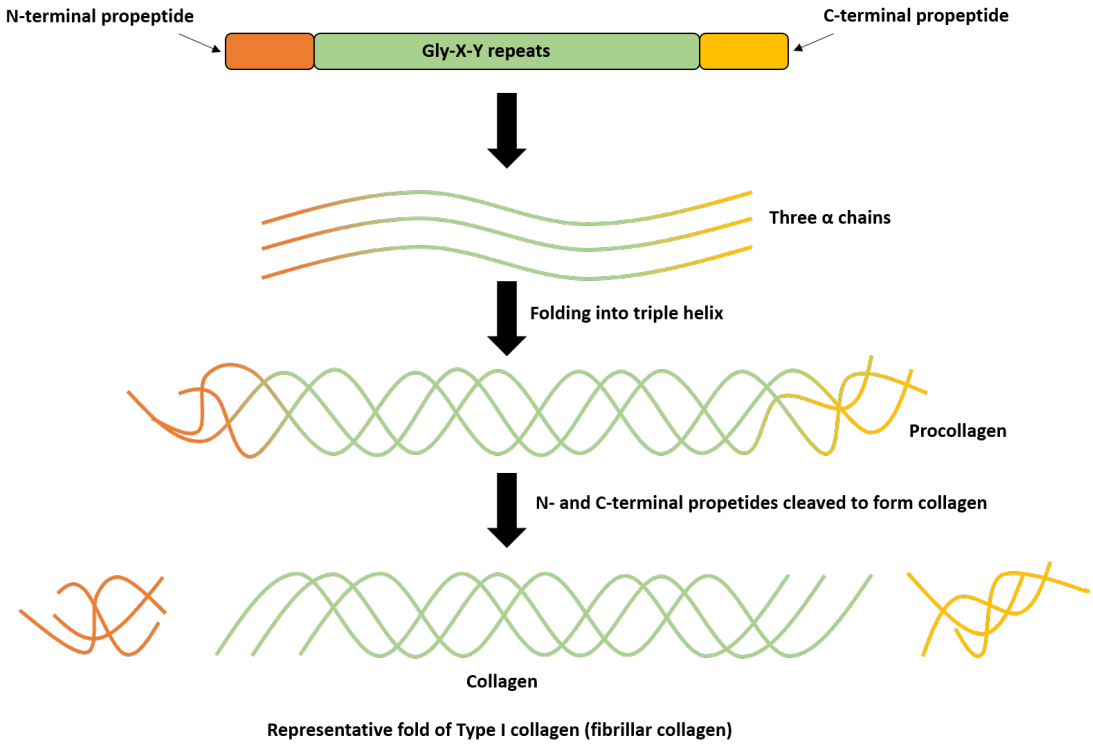

Figure 1.1: Structure and folding of collagen e.g. Type I. Collagen fibrils are composed of three α chains, characterised by Gly-X-Y repeats (where X and Y are frequently proline or hydroxyproline) flanked by N- and C-terminal propeptides, and undergo folding into procollagen triple helices. The so-called called N- and C-terminal propeptides are enzymatically cleaved to form mature collagen that self-assembles into larger fibrils composed of multiple collagen molecules.[23]

Another type of collagen are fibril associated collagens, which has interrupted triple helices (FACIT) where regions intersperse the collagen triple helix (due to Gly-X-Y interruption), leading to kinks in the final structure that straighten upon strain. FACITs integrate into fibrillary collagen and display altered surface properties, which enable binding of other ECM components such as proteoglycans or cell surface receptors.[23]

Elastin and elastic fibres

Elastin proteins form the core of elastic fibres, surrounded by a sheath of microfibrillar glycoproteins such as fibrillin and fibrulin.[25] Elastic fibres line blood

vessels and are a major component of the skin and connective tissue, where it provides extensibility to allow for e.g. the stretching of skin. Elastic fibres are only assembled during development and any redevelopment, degradation or damage during adulthood is irreversible and the loss of elastic fibres is partly responsible for wrinkling of skin or artery stiffening.[26]

Laminin

Laminins consist of three polypeptide chains, α, β and γ that combine to form triple-helical coiled coils with Y-shaped structures.[27] Several different isoforms of α, β and γ-chains have been identified, and the naming of laminins is according to the combined chains and their composition, e.g. $\alpha_1\beta_1\gamma_1$ is referred to as Laminin 111. Laminins are mainly found in the basal lamina, a component of the basement membrane, but are also an intermediary between cells and other ECM-components since it binds to cell surface integrins.[23]

Fibronectin

Fibronectin forms fibrillary structures that surround cells and act as a main connecting protein between cells and other ECM components, e.g. collagen, thus acting to regulate cell adhesion and migration. Three modules (Type I, II and III) make up fibronectin, each containing specific binding motifs for other ECM components and cell surface receptors. Di-sulphide bonds between the modules results in dimer formation.[28]

Proteoglycans and glycosaminoglycans

Proteoglycans are glycoproteins are ECM components attached to a protein core that also are attached to one or more glycosaminoglycans (GAGs), which are negatively charged polysaccharides compromised of repeating disaccharide units.[23] Common ECM proteoglycans include heparan sulphate proteoglycan (HSPG) and chondroitin sulphate proteoglycan (GSPG). The GAG heparan sulphate is composed of highly sulphated disaccharide repeats of N-acetylated or N-sulphated glucosamine (N-acetylglucosamine or N-sulphoglucosamine) and uronic acids (glucuronic acid or iduronic acid) (Figure 1.2A), and HSPGs are a major component of the basement membrane.[23,29] Its negative charge enables binding to other ECM components such as

fibroblast growth factors (FGF), laminin and fibronectin and to some cell surface receptors.[29]

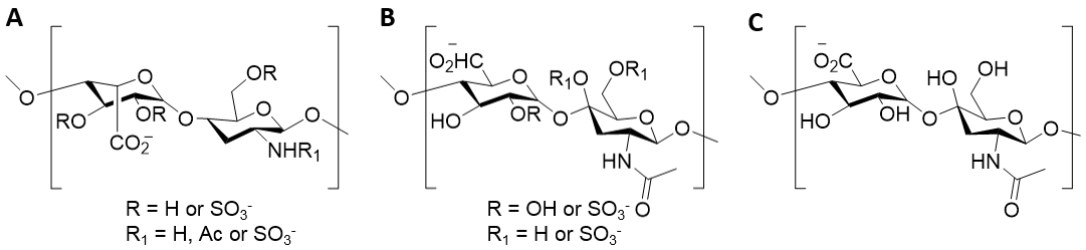

Figure 1.2: Structures of common GAGs found in the ECM. **A.** Heparan sulphate. **B.** Chondroitin sulphate. **C.** Hyaluronic acid.

Chondroitin sulphate is composed of sulphated disaccharide repeats of glucuronic acid and *N*-acetylgalactosamine (Figure 1.2B) and GSPGs are mainly found in neural and cartilage tissue.[23] A family of chondroitin sulphates, the lecticans, contain binding sites for hyaluronic acid (HA), a negatively charged GAG composed of dimers of glucoronate and *N*-acetyl glucosamine (Figure 1.2C). Since HA is not attached to a protein core it is not considered a proteoglycan, but it is a major component of the ECM and is capable of retaining large amounts of water, making it a major component of soft tissues e.g. neuronal and ocular.[23,30] HA is known to bind several cell surface receptors including CD44 and CD168.[22]

ii) Organisation and mechanical properties of the ECM

It is the specific organisation and combinations of the ECM components that result in the varied environments and functions observed in tissues. Broadly speaking, the ECM can be divided in two parts; the interstitial matrix rich in collagen I and fibronectin and the basal lamina, rich in proteoglycans, laminin and collagen IV.[31] As already mentioned, collagen I is abundant in tissues capable of withstanding high mechanical loads, such as the tendon which is 65-80 % collagen I. The fibrillar collagen fibres align to form bundles that together with tendon fibroblast cells connect bone to muscle. The fibroblasts also produce a matrix rich in proteoglycans that surround the collagen and other ECM proteins, e.g. elastin that makes up 1-2 % of the tendon ECM.[32]

The fibrillar structure is almost entirely absent in the basal lamina, which is one of the components that makes up the so-called "basement membrane", a thin layer of ECM proteins that separates endothelial and epithelial cells from adjacent connective tissues (Figure 1.3). The basal lamina is connected to the epithelial cells and is rich in collagen IV and VII and laminin that is connected to HSPGs and the glycoprotein entactin.[23] Laminin binds to the epithelial cells through integrins and entactin, forming a sheet of ECM that is further stabilised by collagen IV. It is this direct interaction between cells and laminin that connects the ECM with intracellular signalling pathways, which helps drive cell behaviour such as the establishment of polarity of the epithelial cell.[23] The other component, the reticular lamina, is rich in collagen I, III and V and connected to the connective cells layer.

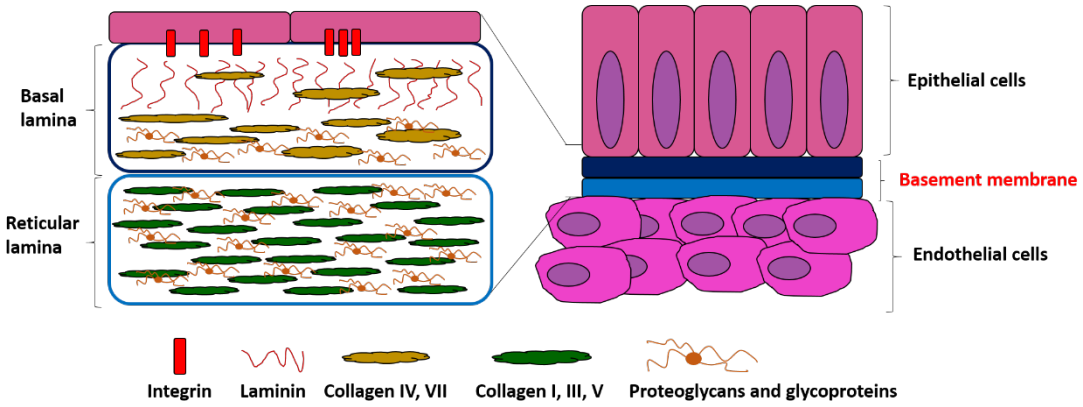

Figure 1.3: Structure of the basement membrane, which forms a sheet of ECM connecting epithelial to endothelial cells. The basement membrane is composed of two parts, the basal lamina, mainly composed of laminin, collagen IV and VII connected to proteoglycans and glycoproteins and the reticular lamina, mainly composed of collagen I, II and II as well as proteoglycans.[23]

As the ECM composition changes so does its mechanical properties, and a common way of measuring these properties is through the elastic modulus (the stress applied to the material divided by the amount of strain the material is subjected to).[20] The elastic moduli (or stiffness) of the majority of human tissues range from 1-100 kPa, although tissue stiffness ranging from 167 Pa in mammary tissue and 54 GPa in cortical bone have been reported.[17,33] Mechanical properties are closely linked to ECM composition, for example the high collagen content of tendons results in a high elastic

modulus (1.2 GPa),[34] while the ECM of the inner eye is mainly composed of hyaluronic acid, which gives a much lower elastic modulus.[30]

iii) ECM-cell interactions and mechanotransduction

ECM-cell interactions are predominantly mediated by cell surface membrane receptors, and an important family of these are the integrins with several examples of ECM proteins binding to them already mentioned.[35] One of the most commonly used integrin-binding motifs added to ECM-mimicking materials to improve cell-binding capacity is the tripeptide Arginine-Glycine-Aspartic acid (RGD), which is found in many ECM-proteins, including fibronectin, and vitronectin.[36]

Integrins are heterodimeric transmembrane proteins that bind to specific amino acid sequences found within some ECM proteins e.g. RGD, while internally being connected to intracellular signalling molecules e.g. the focal adhesion kinase (FAK). These are in turn linked to the actomyosin cytoskeleton and to intracellular signalling pathways e.g. the Rho and mitogen–activated protein kinase (MAPK) through linker proteins such as vinculin and talin (Figure 1.4).[17,26,35] Through these links the mechanical properties of the ECM are able to generate biochemical signals intracellularly, resulting in changes to cell behaviour, a process known as mechanotransduction.[26]

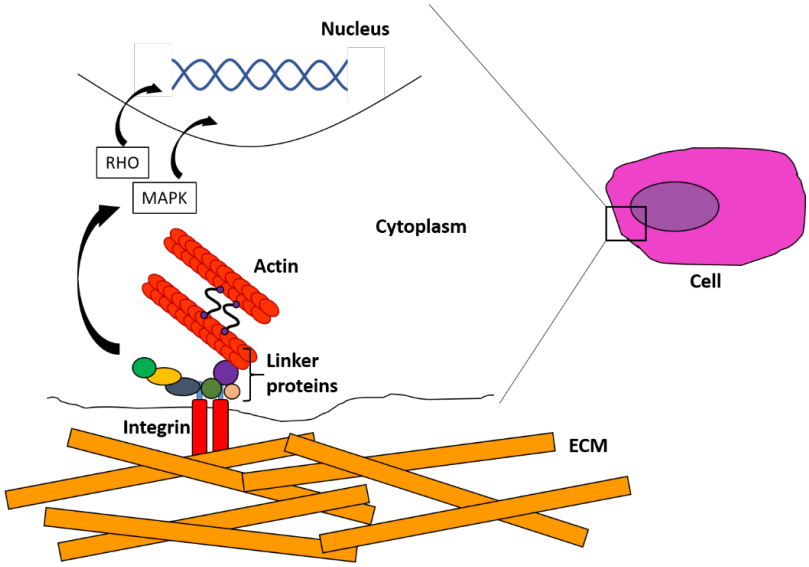

Figure 1.4: Representation of mechanotransduction process converting a mechanical signal from the ECM to a biochemical signal within a cell. Cells are connected to the ECM via integrins that intracellularly binds to linker proteins (e.g. vinculin and talin) connected to the actin cytoskeleton and intracellular signalling molecules that activates signalling pathways (e.g. Rho and MAPK). These in turn relay the original signal from the ECM to the nucleus and can result in a change in gene expression and thereby cell behaviour.[26]

An example of mechanotransduction is how ECM stiffness regulates the cell cycle in mammalian epithelial cells and vascular smooth muscles.[37] When these cells were cultured on fibronectin-coated acrylamide gels with higher stiffness (2.4 kPa), formation of ECM-integrin connections caused the phosphorylation (activation) of FAK, which in turn activated the extracellular signalling-regulated kinase pathway, leading to the production of cyclin D1, a cell cycle regulator that promotes the transition from the G_1 to the S-phase of the cell cycle. When cultured on lower stiffness surfaces however (2 kPa), low levels of cyclin D1 were observed, resulting in cell cycle arrest. This has implications for disease progression such as breast cancer where overexpression of cyclin D1 is observed, suggesting that tissue stiffening, a hallmark of the disease, is partly responsible for oncogenic events such as increased cell proliferation.[37,38]

iv) Remodelling of the ECM

The ECM is constantly degraded and remodelled by its surrounding cells to control tissue homeostasis.[26,31] Degradation of ECM components are mainly carried out by

proteases, with three main families; matrix metalloproteinases (MMPs), meprins and adamalysins. MMPs are the main proteases for ECM degradation with 20 different types having been identified in humans, each with specific ECM targets that collectively are able to cleave all ECM proteins.[31] Meprins are dimeric complexes with α and β units known to cleave collagen IV and fibronectin, as well as activating collagen by cleaving the procollagen chains, or activation of MMPs, thus regulating ECM remodelling.[31] Adamalysins are so-called "sheddases", meaning they cleave domains from transmembranes that connect them to the cell surface, releasing the extracellular part of the protein.[39]

1.1.4 Current approaches to 3D cell culture

The modulus of tissue culture plastic polystyrene (TCPS) is about 3 GPa, higher than the stiffness of many human tissues and organs.[17] Using materials and methods that allow for 3D cell culture, which try to recapitulate the natural ECM environment by allowing for cell-cell and cell-matrix interactions, but which simultaneously are cheap and easy to manufacture, would be highly advantageous.[16]

One of the first studies that looked at the benefits of 3D cell culture was published in 1975 and used floating collagen gels to culture rat hepatocytes.[40] Increased cell viability (> 20 days) was observed for the 3D culture compared to monolayer cultures on collagen-coated plates (6 days viability), with the formation of 3D cell constructs observed such as bile canaliculi. A landmark study in 1997 showed that T4-2 cells (a cell model for breast cancer) grown in 3D (in Matrigel) or in 2D (on collagen-coated surfaces) coupled with blocking the overexpressed cell surface β_1-integrin resulted in different cell phenotypes.[41] Integrin blocking in 3D reversed the cells' malignant phenotype, something that was not observed for 2D cultures with the phenotype reversal coupled with cyclin D1 downregulation and cell cycle arrest.

Following these findings, the area of 3D cell culture has grown rapidly, but although promising to be better cell models, they also present challenges. The optical analysis of 3D cell culture models is more complex, requiring imaging through the depth of the 3D structure, which requires confocal microscopy or multi-photon microscopy.[16] Materials need to be optically transparent to allow for imaging in the 3D plane,

although sectioning and 2D reconstruction is possible but time consuming. Moreover, passaging will be more complex and the ability to do so will depend on the chemical composition of the material, and its inherent degradability.

Several methods have been developed for 3D cell culture, and broadly speaking these can be divided into scaffold-free or scaffold-based methods. Some of the most commonly used methods of each are detailed below.

i) Scaffold-free methods for 3D cell culture

For scaffold-free methods, the propensity for cells to form 3D clusters, also known as spheroids, under certain conditions is utilised. Two of the most commonly used techniques to achieve this are the hanging drop method and low-adherence plates.[2,15,21] In the hanging drop method cells are suspended in a small drop of media that is placed on a flat surface and then inverted, resulting in a so-called "hanging drop", and because of gravitational forces the cells are promoted to form clusters. Coating the surface of the plates with cell-repellent solutions that promotes cell cluster formation is also widely used.

In a recent study, spheroids of several different human tumour cell lines (breast, prostate, head and neck and colorectal) were generated using a polydimethylsiloxane substrate fabricated into hanging drop arrays.[42] It was demonstrated that these spheroids were easily manufactured and could be used to better mimic the tumour microenvironment for drug screening, cell co-cultures and tumour invasion assays.

A drawback of these methods, however, is the difficulty in generating more complex 3D cell models, since the larger the spheroid, the larger its necrotic core, because of lack of nutrient and oxygen supply.[15] To create larger and more complex 3D cell models some form of supporting material, or scaffold, is needed.

ii) Scaffold-based methods for 3D cell culture

In scaffold-based 3D cell culture a material is used to support and confine the cells. Several different materials have been used for this, including polymers, proteins, peptides, ceramics, metals and glass.[14,15] Benefits include their tuneable properties and their capacity to incorporate specific cell adhesion groups (e.g. integrin binding

sequences).[15] Despite the usefulness of the materials mentioned above, another scaffold-based material has emerged as one of the most promising for 3D cell culture, namely hydrogels.[22] Hydrogels are highly hydrated polymeric networks that can be designed to have similar mechanical properties to the ECM. Most of the work in this thesis relates to the development and use of hydrogels, and therefore the following section details the types of hydrogels available, their design and examples of use their use in 3D cell culture.

1.2 Hydrogels for 3D cell culture

Hydrogels are networks with high water content that can be good ECM-mimics due to their soft mechanics and capacity for diffusion and transport of nutrients and oxygen.[18,20,43,44] The natural ECM can be considered a hydrogel and many components of it are routinely used as 3D cell culture matrices due to their usually cell-compatible formation and tuneable biochemical and biophysical properties such as chemical composition, adhesive ligand and growth factor presentation and substrate stiffness or topography.[19,20,33] Several aspects of hydrogel design must be considered in order to create materials that mimic the spatial and temporal control of the ECM and aspects discussed in further detail in this section include (Figure 1.5):

- The material used for hydrogel formation, i.e. natural or synthetic source.
- The hydrogel cross-linking method, which will impart specific properties to the hydrogel and the 3D cell culture.
- The hydrogel functionalisation with cell-binding ligands or growth factors to induce desired cell behaviour.
- The control of concentration and composition of the hydrogel components, which allows their mechanical properties to be tuned.
- The tuning of hydrogel topography at the nano- and micro-scale to mimic the ECM environment of specific organs and tissues.
- The development of degradable hydrogels to allow for cell migration and spreading.

In addition, by tailoring their chemical composition, responsive hydrogels can be generated, for example in response to temperature,[45] pH[46] or light.[47] Other factors to tune apart from the hydrogel material, is the introduction of gradients e.g. of growth factors or material stiffness and the introduction of vascularisation within the hydrogel to provide oxygenation.[48–50] *In vivo*, all cells are <100 µm from a blood vessel with cells further away turning necrotic due to lack of oxygen supply and larger hydrogel structures must be able to recapitulate this.[17]

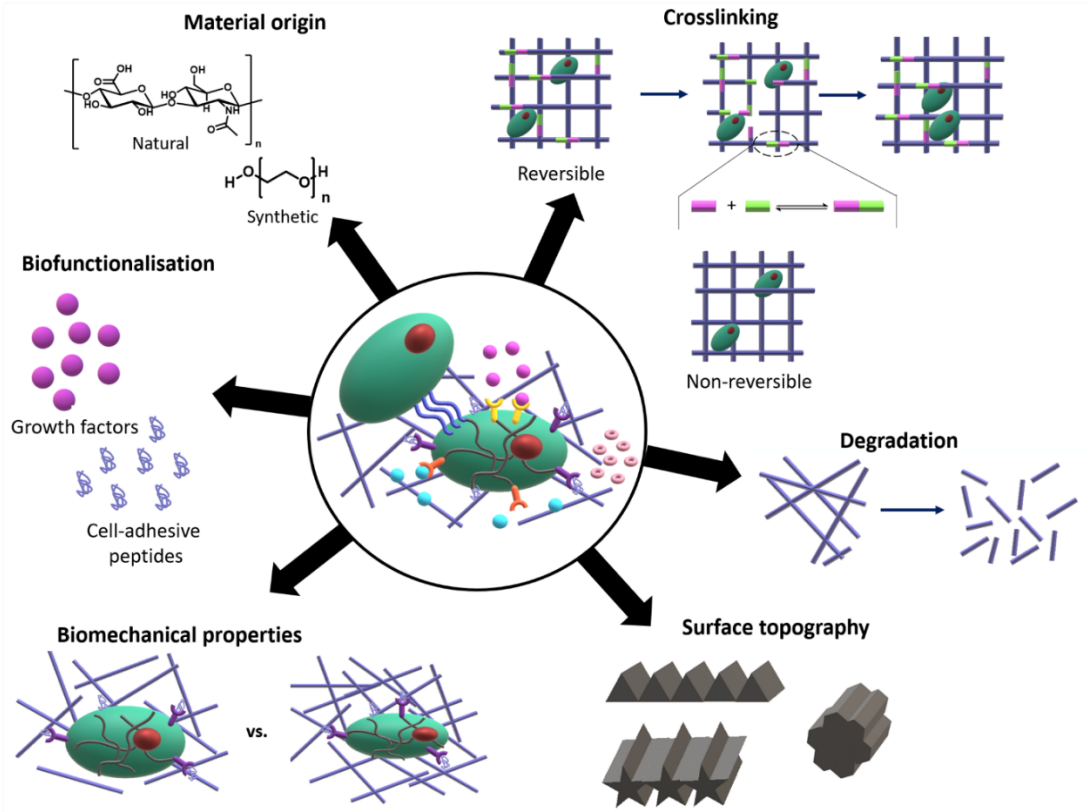

Figure 1.5: Hydrogel properties to consider that recapitulates the dynamic and complex *in vivo* ECM environment. These properties range from material origin consideration and cross-linking methods, the biofunctionalisation of hydrogels with biochemical motifs and tuning the hydrogel biomechanical properties, surface topography and degradation characteristics.

1.2.1 Natural hydrogels for 3D cell culture

Natural materials used for hydrogel formation include ECM-derived proteins such as collagen, laminin, fibrin, and fibronectin or proteoglycans like HA and chondroitin sulphate.[33,51] Other non-ECM derived natural materials are also used, for example the polysaccharides chitosan and alginate (Figure 1.6).[33]

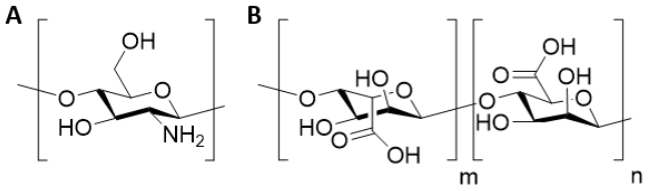

Figure 1.6: Structure of non-ECM polysaccharides used for hydrogel formation. **A.** Chitosan. **B.** Alginate.

Natural-based hydrogels are advantageous due to their inherent biological activity, but several disadvantages are associated with their use such as their usually exogenous source, imparting batch-to-batch variability and introducing poor reproducibility of experimental results.[21,51,52] Furthermore, their poorly defined structure and limited ability for precise modification makes the tuning of biomechanical and biochemical properties difficult.[21,52,53] Nonetheless, the use of natural hydrogels for 3D cell culture is common and a good starting point.

i) Collagen

Collagen type I (Figure 1.1) has commonly been used for hydrogel formation, although Type II and III have also been reported. The rat-tail tendon, bovine skin and human placenta are common sources of collagen type I, usually sold as a low pH solutions that require low temperature storage to prevent spontaneous gelling.[54] The need for low temperatures during preparation is one of the main disadvantages of collagen hydrogels, along with its relatively poor mechanical stability. Collagen type I gels were used to create a 3D model of breast cancer model using MDA-MB-231 cells that compared to monolayer culture were able to recapitulate the tumour necrotic core by upregulation of hypoxia-inducible factor (HIF)-1α as well as increase of vascular endothelial growth factor (VEGF)-A expression.[55]

Methacrylate-functionalised monomeric collagen type I were developed in order to increase the gel mechanical properties with cross-linking carried out using visible light (50 mW/cm^2, 30-60 min) and in the presence of rat aortic smooth muscle cells.[56] High cell viability (> 70 %) was observed and the elastic modulus increased from 13.5 kPa of unmodified collagen type I to 162 kPa of the cross-linked hydrogel that also showed improved temperature stability (denatured at 45 °C compared to 39 °C of unmodified collagen).

ii) Hyaluronic acid

HA (Figure 1.2C) used for 3D hydrogel formation is usually isolated from bacteria cultures, and is beneficial due to its ease of functionalisation of its hydroxyl and carboxyl groups to generate cross-linkable groups, e.g. thiols, aldehydes and (meth)acrylate.[57] Commercially available HyStem™ hydrogels (BioTime Inc.) are composed of thiol-modified HA and cross linker PEG-diacrylate (PEGDA) with other thiol-modified components added e.g. thiol-gelatin and thiol-heparin. Thiol-HA, thiol-gelatin and PEGDA were used together to form a multi-layered co-culture of prostate cancer (C2-4B) and bone marrow stromal (HS27a) cells (Figure 1.7A).[58] C2-4B's cultured in the HyStem hydrogel containing HA and PEGDA assembled into 3D organoids, while the HS27a cells grew on a layer of gel composed of HA, gelatin and PEGDA with the system utilised for high throughput (384-well plate) drug screening.

Periodate oxidation is a straightforward way to produce aldehyde functionalised HA that can be cross-linked with amines, hydroxylamines or hydrazides to form imine, oxime and hydrazine cross-linked hydrogels respectively (Figure 1.7B).[57] Aldehyde-modified HA was cross-linked with chitosan to produce imine cross-linked hydrogels that supported the encapsulation and growth of L929 fibroblasts over 48 h and demonstrated abdominal tissue regeneration in a rat model, facilitated by the deposition of ECM matrix as well as initiation of vascularisation.[59]

Clinical applications of HA include wound healing and dermis regeneration as it directs fibroblast behaviour, the cells responsible for collagen deposition during wound healing. The application of long HA chains to these areas have been shown to increase the order of collagen deposition, thus contributing to control over the wound healing process. HA also improves keratinocyte proliferation and can be used to improve their proliferation motility in synergy with other ECM components e.g. fibronectin and epidermal growth factor (EGF).[60]

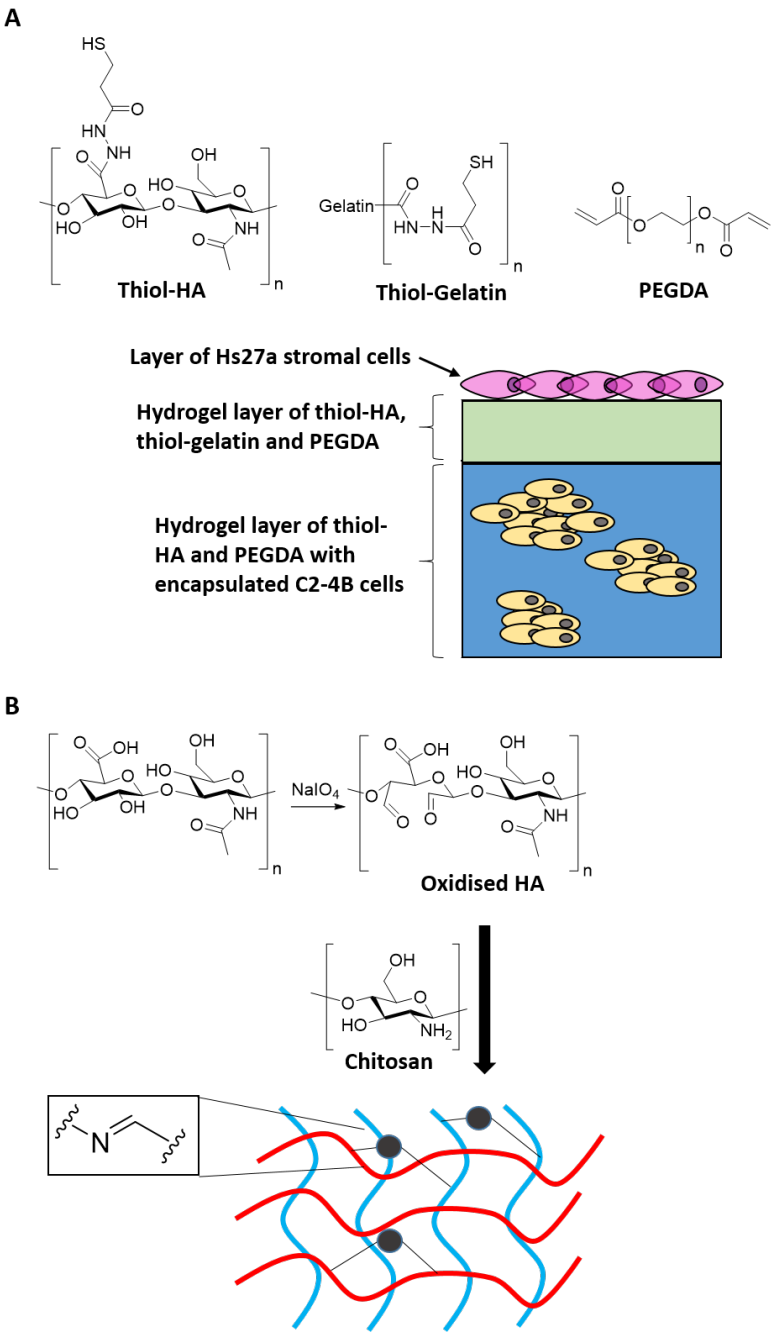

Figure 1.7: Hydrogels formed from hyaluronic acid (HA). **A.** Thiol-modified HA and gelatin are cross-linked by PEG-diacrylate (PEGDA) to form HyStem™ hydrogels. A co-culture was created where C2-4B cancer prostate cancer cells were encapsulated in a HA/Gelatin/PEGDA hydrogel with an overlaying layer of HA/PEGDA hydrogel on which bone marrow stromal cells Hs27a were seeded.[58] **B.** HA-chitosan hydrogel cross-linked through imine bonds. Aldehyde-modified HA was formed by oxidation of HA with $NaIO_4$, and reacted with amines on chitosan to form the hydrogel network.[59]

iii) Matrigel®/GelTrex™

One of the most commonly used matrices for 3D cell culture is a mouse-derived gelatinous protein mixture sold under different names such as Matrigel® (BD Biosciences) and GelTrex™ (ThermoFisher). This mixture is secreted by Engelbreth-Holm-Swarm mouse sarcoma cells, making up a basement membrane extract mainly composed of collagen type IV, laminin, entactin and various growth factors including FGF, EGF and transforming growth factor-β.[21] The stiffness can be tuned with concentration, where gels ranging from 3 to 19.1 mg/mL result in elastic moduli increase of 9.1 ± 0.3 Pa to 288.2 ± 9 Pa.[61]

The tumour-derived origin, poorly defined composition and the requirement of low temperature handling to avoid spontaneous gelation are some of the major drawbacks of these gels,[22] but they are popular materials for 3D cell culture. The generation of organoids have frequently been reported by growing cells in basement membrane extract matrices with one of the earliest examples being the formation of intestinal organoids from $Lgr5^+$ stem cells that formed crypts without the need of mesenchymal niche-cells to induce this formation.[62]

Another common use of basement membrane matrices are for stem cell maintenance and differentiation where the encapsulation of human induced pluripotent stem cells (iPSCs) resulted in differentiation to ureteric-bud-committed renal progenitor-like cells to create a cell model of kidney disease.[63] The directed differentiation was achieved over a 4-day culture and the subsequent co-culture of the differentiated cells with mouse embryonic kidney cells resulted in the formation of complex 3D chimeric structures, useful for studying kidney development and ureteric bud morphogenesis.

1.2.2 Synthetic and hybrid hydrogels for 3D cell culture

Using synthetic materials to produce hydrogels enables the engineering of structurally defined materials, unlike their natural counterparts, and commonly used building blocks include polymers and peptides.[21,53] Poly(ethylene glycol) (PEG), poly(*N*-isopropylacrylamide) (PNIPAAm), poly(methylmethacrylate) (PMMA), poly(vinyl alcohol) (PVA), poly(lactic acid) (PLA) and poly(lactic-co-glycolic acid) (PLGA) are frequently used polymers for hydrogel formation (Figure 1.8).[51]

Combinations of acrylate/acrylamide/vinyl-based monomers have also been used to form a range of different polymers that can be cross-linked into hydrogels.[45]

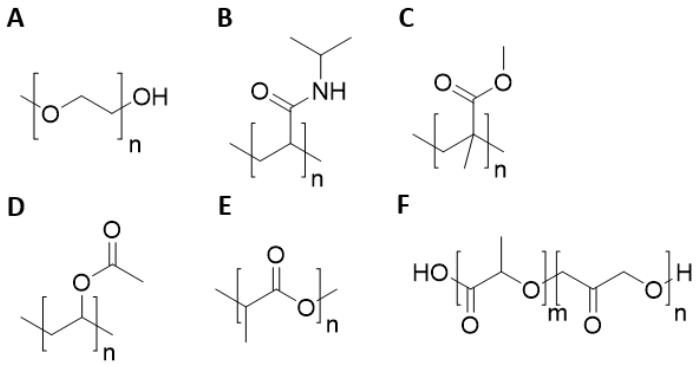

Figure 1.8: Structures of polymers used to form scaffolds for cell culture-based applications. **A.** Poly(ethylene glycol) (PEG) **B.** Poly(*N*-isopropylacrylamide) (PNIPAAm) **C.** Poly(methylmethacrylate) (PMMA) **D.** Poly(vinyl alcohol) (PVA) **E.** Poly(lactic acid) (PLA) **F.** poly(lactic-co-glycolic acid) (PLGA).

The defined chemical composition and tuneable biochemical and biomechanical properties are some of the main advantages of using synthetic-based hydrogels.[21] By tuning the chemistry of the hydrogel components, a wide variety of hydrogels of different cross-linking methods, mechanical properties, bio-functionalisation, degradation characteristics and topography have been generated and used for 3D cell culture.[18,21]

i) PEG for hydrogel formation

Although many kinds of synthetic polymers may be used to form hydrogels, PEG has emerged as one of the most frequently used in the field of 3D cell culture, primarily because of its cytocompatible nature and high water content.[18] Another major advantage of PEG is the facile modification of its terminal hydroxyl groups, for example to alkenes, alkynes, azides, thiols, activated esters, norbornenes, maleimides and more, which enables variation in cross-linking methods to form PEG-based hydrogels.[18] In addition, the commercial availability of multi-branched PEGs is another advantage for hydrogel formation.

8-arm PEGs were functionalised with lysine and glutamine-containing peptides responsive to activated enzyme transglutaminase factor XIII (FXIIIa) that through formation of ε-(α-glutamyl)lysine isopeptide side-chain bridges between the peptides resulted in hydrogel formation (Figure 1.9).[64] These hydrogels were utilised to encapsulate and expand intestinal stem cells and with the addition of laminin 111 to the hydrogel, formation of intestinal organoids was achieved.

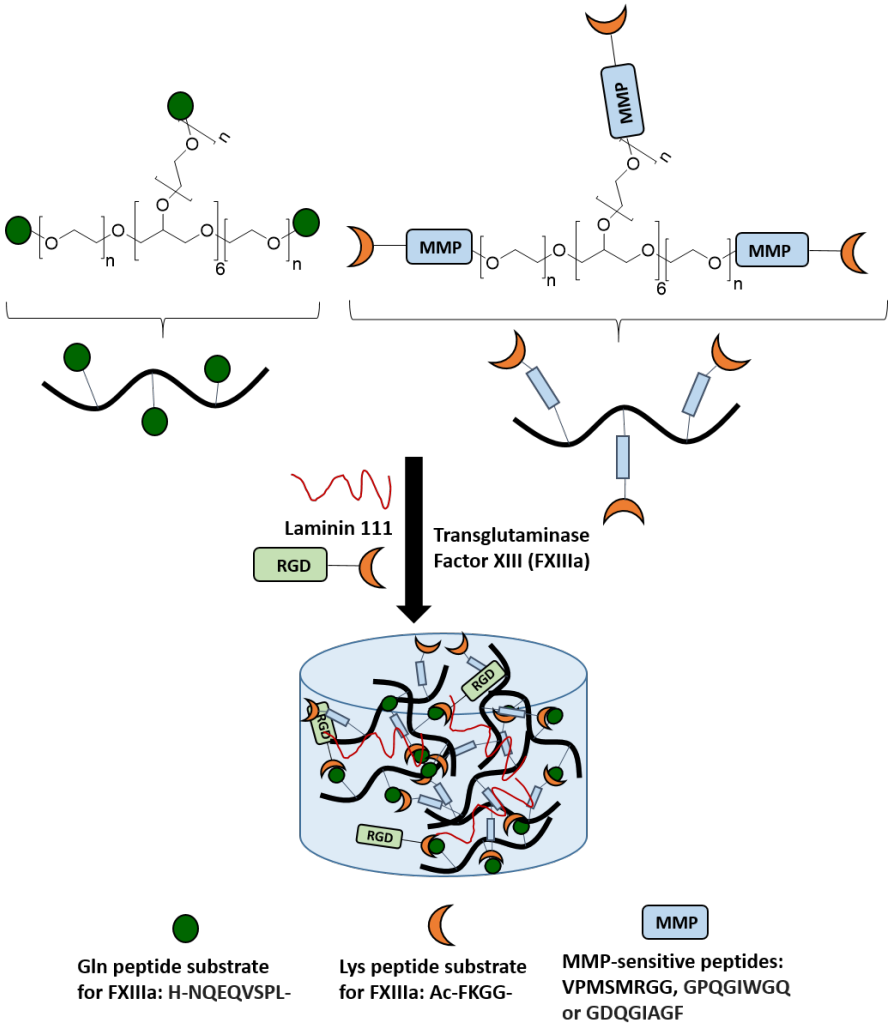

Figure 1.9: Hydrogel formation of 8-arm PEG chains functionalised with Lysine (Lys) and Glutamine (Gln) peptides that undergo enzymatic cross-linking by transglutaminase Factor XIII (FXIIIa). MMP-sensitive peptides were tethered to the lysine sequences to afford degradable hydrogel while RGD peptides and laminin 111 were included for improved cell attachment.[64]

Using PEGDA and thiol-modifed gelatin (as in Figure 1.7A) a UV cross-linked hydrogel was generated allowing 28-day encapsulation of human dermal fibroblasts resulting in increased cytoplasmic spreading and formation of cell networks. Compared to a control gel where the gelatin was physically encapsulated into a UV cross-linked PEGDA hydrogel, high hydrogel swelling and water content as well as a lower stiffness was observed.[65]

ii) Synthetic peptides for hydrogel formation

Using small peptides for hydrogel formation is beneficial due to the biological relevance of their amino acid component, and the cost-efficient synthesis through solid-phase peptide synthesis (SPPS) or recombinant technology.[14,66] Peptides are often attached to other types of components e.g. polymers, to form hydrogels, but their self-assembly also enables the formation of peptide-based hydrogels.[22] Self-assembly behaviours of peptides exploited for hydrogel formation, include the α-helical coiled coil motif of certain peptide chains containing both hydrophobic and charged residues,[66] or the β-sheets resulting from alternating hydrophobic and hydrophilic amino acid combinations, for example the 16-residue peptide $(FEFEFKFK)_2$.[67]

Polypeptides made up of repeating units of the pentapeptide VPGXG, where X can be any natural amino acid apart from proline, derived from the ECM protein elastin have been used to form thermally responsive elastin-like polypeptide/protein (ELP) hydrogels.[68] ELPs display temperature dependent gelation where at low temperatures the hydrophobic residues are surrounded by organised water molecules, but above a transition temperature the water molecule ordering decreases, leading to collapse of the polymer structure and gelation by self-assembly and folding of the ELP chains.[66] ELPs modified hydrazine residues and with a RGD sequence to improve cell attachment were cross-linked with aldehyde-modified HA to form double network hydrogels with both thermosresponsive (due to the ELP motif) and dynamic properties (due to the semi-reversible hydrazone bond) (Figure 1.10), in which mesenchymal stem cells (MSCs) were encapsulated and ejected through a 28G needle. Cells maintained viability and capacity for multiple lineage differentiation including osteogenic, adiopogenic and chondrogenic (by gene expression) over 7 days.[69]

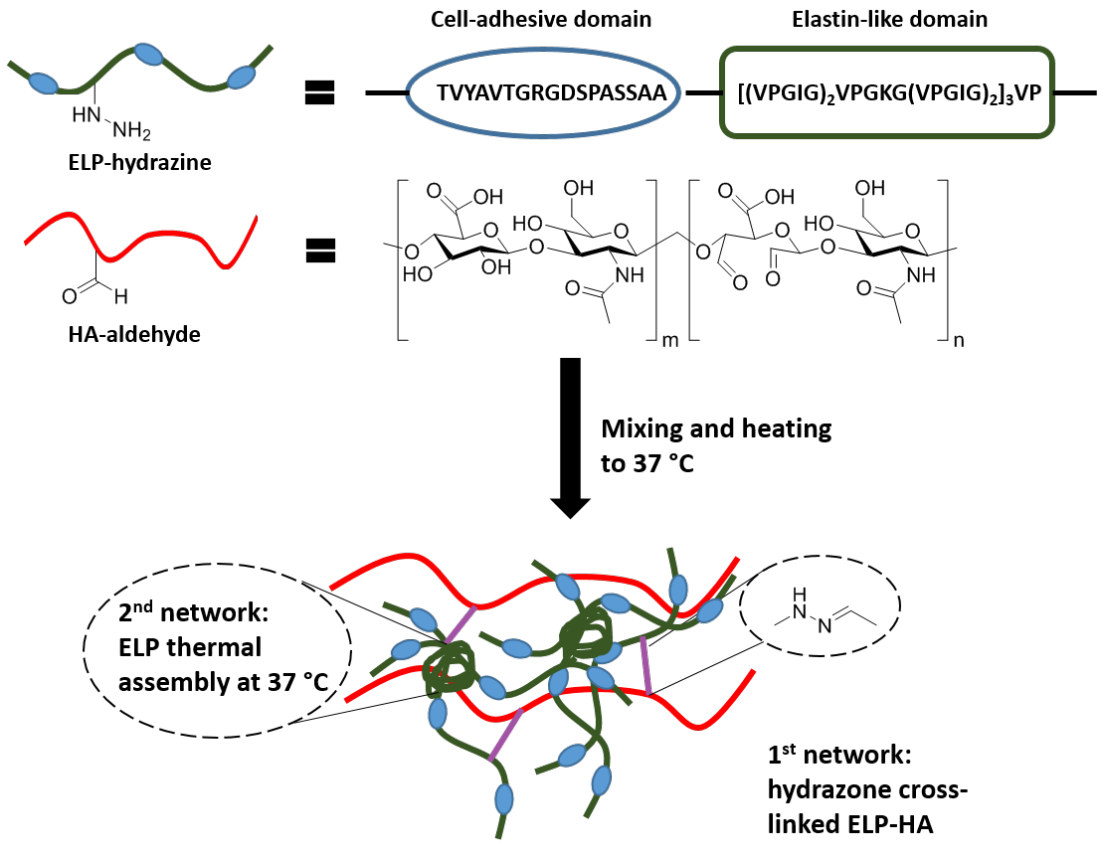

Figure 1.10: Formation of double network Elastin-like peptide/protein (ELP):Hyaluronic acid (HA) hydrogels. ELP-hydrazine and HA-aldehyde form hydrazone cross-linked hydrogels upon mixing and with heating to 37 °C the ELP-domain (-VPGIG/VPGKG-) self-assembles to form the second hydrogel network.[69]

Short aromatic fluorenylmethoxycarbonyl (Fmoc) peptides have also been used to form hydrogels, self-assembled through the π-π stacking and hydrogen bonding of the Fmoc moieties.[70] By mixing the dipeptide Fmoc-Phe-Phe-OH with Fmoc-Ser-OH (Figure 1.11A), hydrogels have been formed that support the growth and maintenance of chondrocytes, human dermal fibroblasts, 3T3 fibroblasts and pericyte chondrogenesis.[70–72]

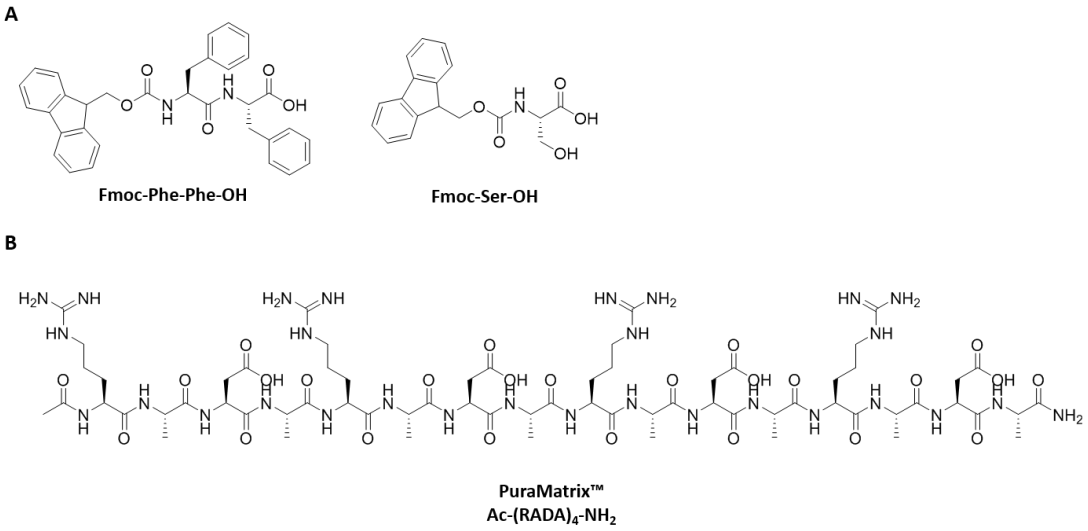

Figure 1.11: Peptide-based hydrogels. **A.** Hydrogels formed by the self-assebly of Fmoc-$(Phe)_2$-OH and Fmoc-Ser-OH have been used in several cell culture-based applications.[70–72] **B.** The peptide Ac-$(RADA)_4$-NH_2 self-assembles to form hydrogels marketed as PuraMatrix™.

PuraMatrix™ is a commercially available peptide hydrogel formed by the self-assembly of Ac-$(RADA)_4$-NH_2 into nanofibers (Figure 1.12b). Human brain-derived neurotrophic factor-engineered human bone marrow MSCs underwent neuronal differentiation when gown on RGD-functionalsied PuraMatrix™ gels.[73] Neuron specific enolase and glial fibrillary acidic protein levels, cell proliferation and growth were increased compared to culture within the unmodified PuraMatrix™.

1.2.3 Hydrogel cross-linking methods

i) Non-reversible covalent cross-linking

Examples of non-reversible covalent bond formation used to form hydrogels include carbon-carbon bond formation during polymerisation of acrylate/acrylamide/vinyl-based monomers, e.g. PEGDA, amide and ester bond formation, thiol-ene reactions, copper catalysed or strain-promoted azide-alkyne cycloaddition and tetrazine-based cycloaddition (Figure 1.12-1.14).

Hydrogels were formed in PBS under physiological conditions by the thiol-ene reaction between cysteine-containing peptides (MMP and RGD sequences) and a norbornene-functionalised 4-arm PEG in the presence of initiator (Igracure D-2959 or

lithium phenyl-2,4,6-trimethylbenzoylphosphinate) and irradiation (365 nm, 10 mW/cm², 5 min) (Figure 1.12).[74] *In situ* encapsulation of hMSCs was afforded by pre-mixing with the monomer solutions and high cell viability 30 min after hydrogel formation was observed. Similar hydrogels have also been used for the encapsulation of β-cells,[75] to investigate the migration of human fibrosarcoma cells (HT-1080)[76] and to afford specific patterning of peptides, e.g. MMPs.[77]

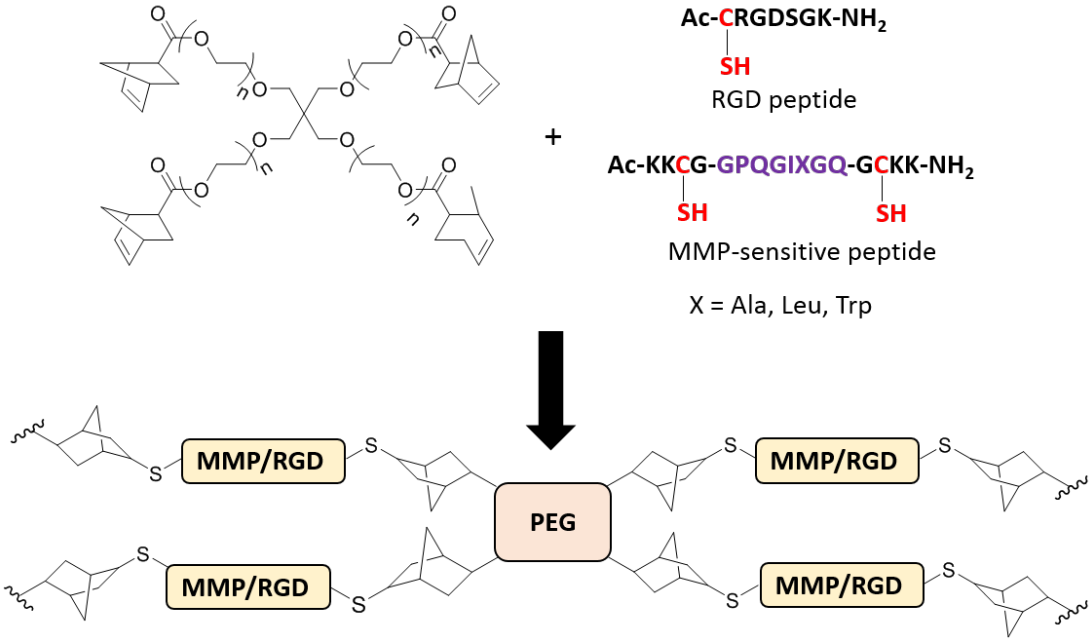

Figure 1.12: Use of thiol-ene chemistry between norbornene-functionalised 4-arm PEG and cysteine-containing peptides to form hydrogels.[74]

Strain-promoted azide-alkyne cycloadditon (SPAAC) between azide-modified 4- or 8-arm PEG and bi-functionalised cyclooctyne PEG formed hydrogels within minutes in PBS at 37 °C (Figure 1.13).[78] Three variants of the hydrogel with different wt % PEG (4.8, 7.2 or 9.6 wt %) were prepared and encapsulated with MSCs. Over 2 weeks, the 4.8 wt % hydrogels degraded, but the 7.2 and 9.6 wt % remained intact and demonstrated high MSC viability.

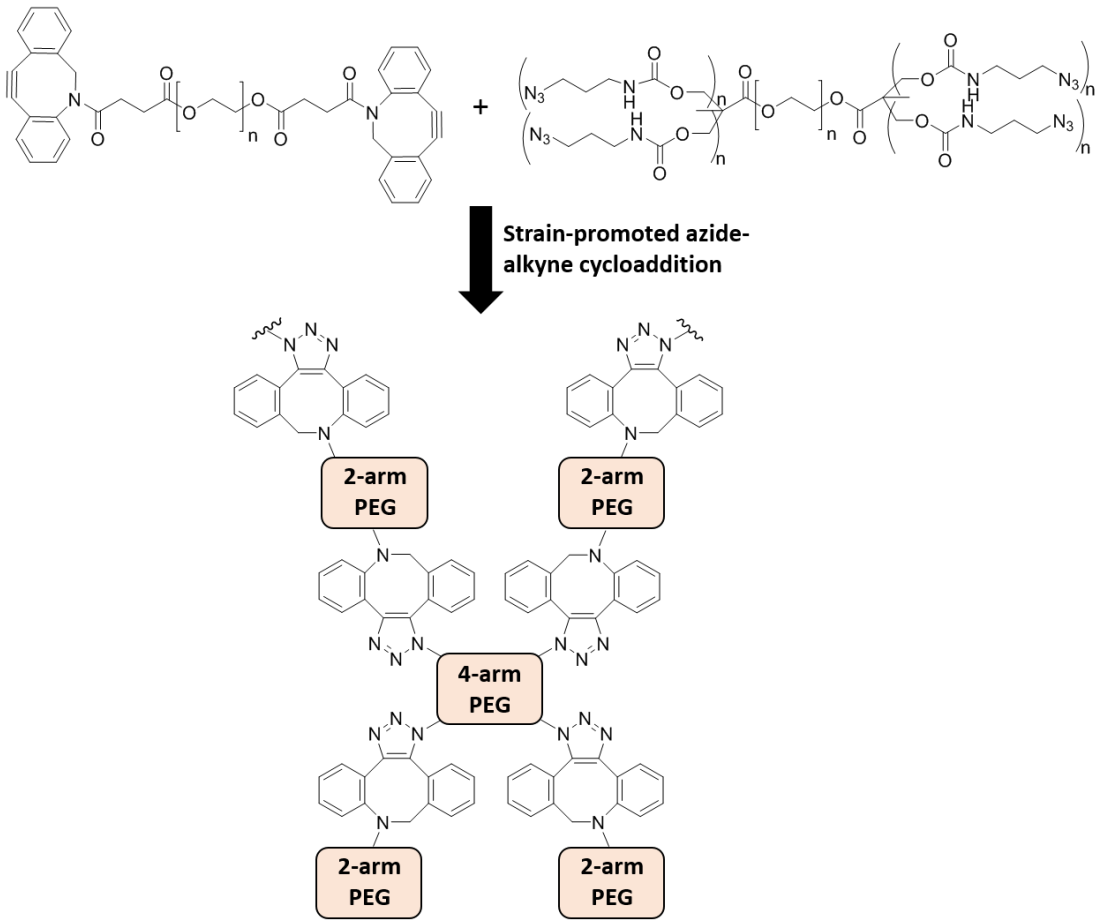

Figure 1.13: Use of strain-promoted azide-alkyne cycloaddition between bis-cyclooctyne PEG and 4- or 8-arm PEG-azide to form hydrogels.[78]

Tetrazine or norbornene-modified alginate-chains have been used to form hydrogels that subsequently were functionalised with RGD peptides by reaction of remaining norbornene groups with cysteine-containing peptides (Figure 1.14).[79] 3D cell encapsulation of 3T3 fibroblasts over 3 days showed high cell viability, and injection of the hydrogels into mice demonstrated low inflammatory response at the injection site over 2 months making these hydrogels promising injectable materials.

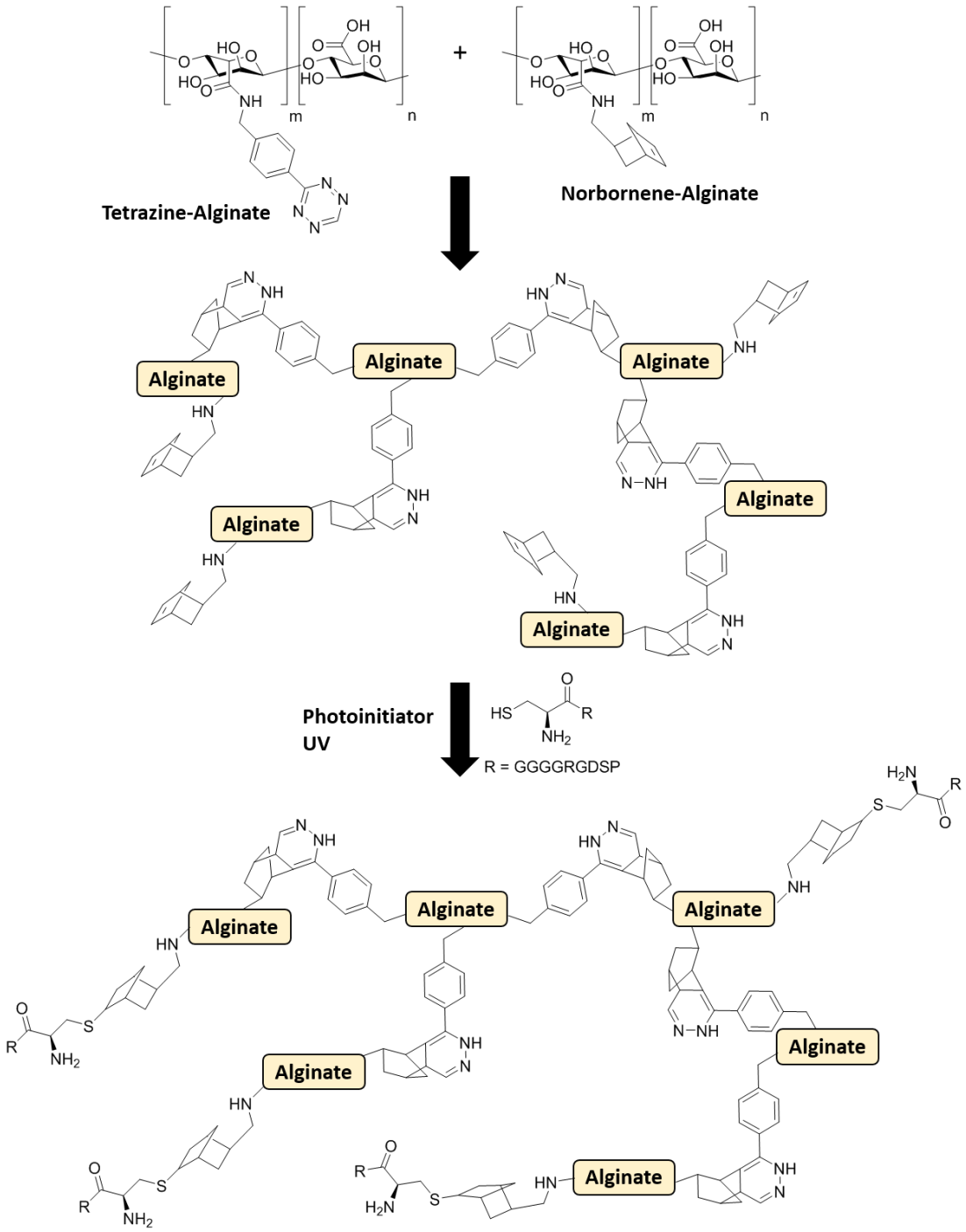

Figure 1.14: Use of tetrazine-based cycloaddition between tetrazine-functionalised alginate and norbornene-functionalised alginate to form hydrogels that subsequently were functionalised with cysteine-containing RGD sequences.[79]

Although non-reversible covalent cross-linking methods are useful for creating strong and stable hydrogels, these materials are very different from the highly dynamic nature of the ECM. Cell spreading and migration is limited in these non-

adaptable hydrogels, and the introduction of degradation within the scaffold is usually necessary to allow for cell movement and growth in 3D.[43] This has been done by using hydrolytically sensitive polymers/building blocks that degrade over time, or by introducing MMP-sensitive peptide sequences that allow for enzymatic cell-mediated degradation[44] (for more on this see Section 1.2.7). Although both are useful to improve cell migration and spreading, these methods result in irreversible hydrogel degradation, which over time will lead to its collapse.[43]

ii) Reversible covalent cross-linking

Using reversible covalent cross-linking results in hydrogels with highly adaptable properties, due to the reversible and dynamic nature of the bonds.[44] The equilibrium of formation and breakage of the bonds allows cells to move and spread through these materials, just like in their natural ECM environment and unlike the irreversible degradation of MMP sensitive sequences, reversibly cross-linked hydrogels do not erode over time.[44] In addition, if the cross-linking is cell-compatible it can take place in the presence of cells, allowing for *in situ* cell encapsulation. Examples of reversible covalent bonds used for hydrogel formation include imines (Schiff base), hydrazones, oximes and disulphide bonds (Figure 1.15).[43]

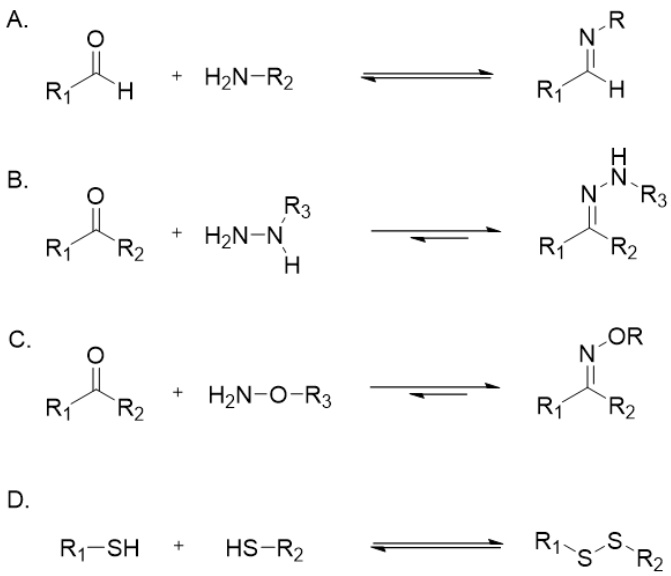

Figure 1.15: Examples of reversible covalent bonds used to form hydrogels. **A.** Imine formation from an aldehyde and primary amine **B.** Hydrazone formation from a ketone/aldehyde and hydrazine **C.** Oxime formation from a ketone/aldehyde and hydroxylamine **D.** Di-sulphide formation from two thiols (e.g. cysteine side chains).

The imine bond formation between a primary amine and an aldehyde has been used to form hydrogels between chitosan and 4-formylbenzoic acid-functionalised PEG (Figure 1.16).[80,81] HeLa cells showed good viability when encapsulated within the resulting hydrogels that formed under physiologically relevant conditions. Degradation was afforded by the addition of acid, with reformation of the hydrogel network achieved when the pH was re-adjusted to physiological conditions.

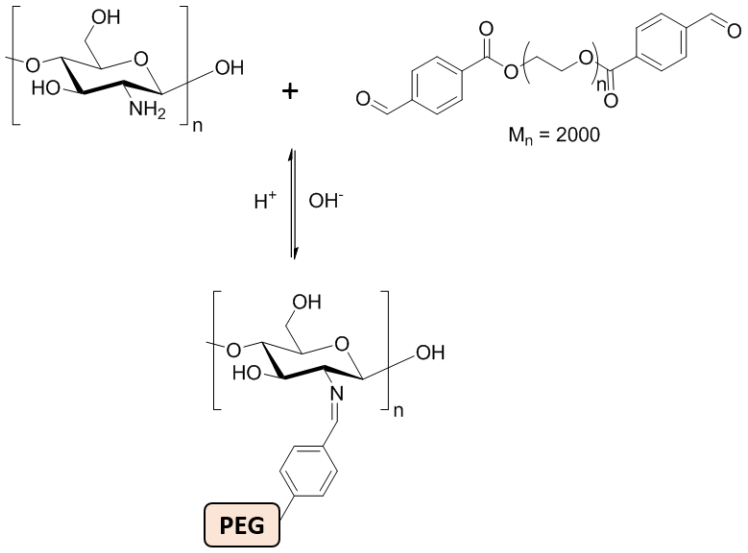

Figure 1.16: Use of imine-bond formation between chitosan and 4-formylbenzaldehye-functionalised PEG to form hydrogels.[80,81]

Aldehydes have also been used to react with hydrazines or hydroxylamines to form hydrazone and oxime cross-linked hydrogels respectively, but due to the electronegativity of the heteroatom (NH for hydrazone and O for oxime bonds) next to the C=N bond, the propensity for nitrogen protonation required for bond hydrolysis, is decreased compared to imine bonds. Thus, oxime and hydrazone bonds are more stable and less reversible under physiological conditions.[82] Cross-linked hydrogels from hydrazine and aldehyde-modified multi-arm PEG (4 or 8-arm) resulted in hydrogel formation with the gels made solely of the 4-arm PEG having a shear modulus of 600 Pa, which increased to 9 kPa for the gels with only 8-arm PEGs (Figure 1.17). C2C12 myoblasts and motor neurons encapsulated within these gels displayed high cell viability.[83,84]

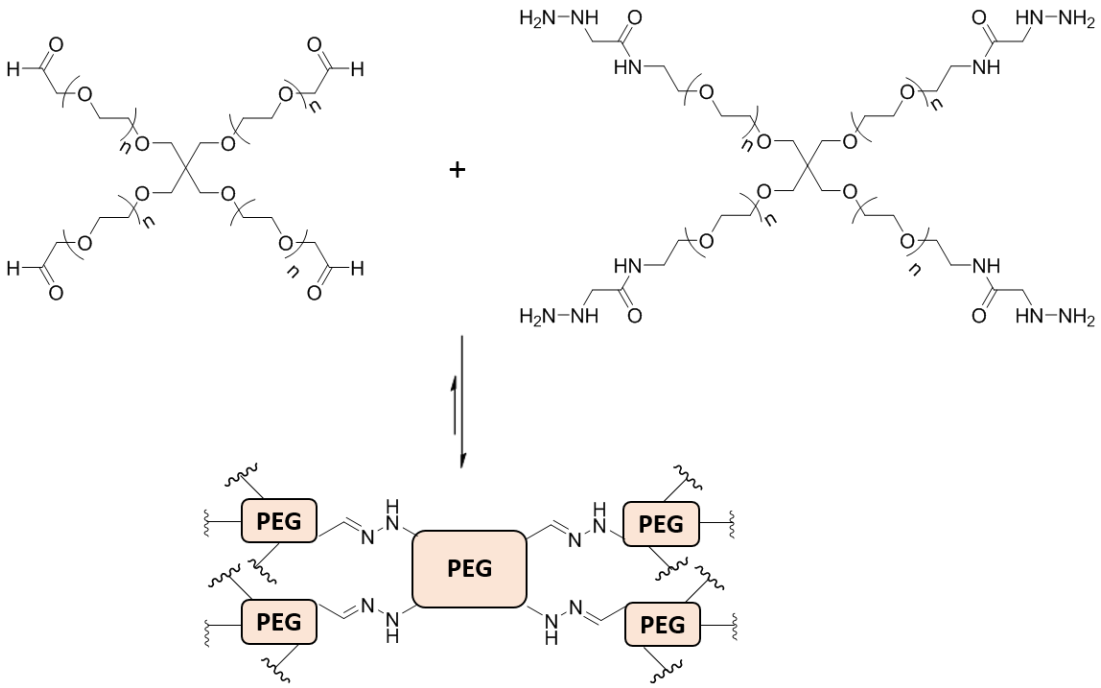

Figure 1.17: Use of hydrazone-bond formation between 4- or 8-arm PEG (only 4-arm shown) functionalised with either aldehydes or hydrazines to form hydrogels.[83,84]

The usually rapid gelation time of imine, oxime and hydrozone cross-linked gels is an advantage for *in situ* cell encapsulation allowing homogenous cell encapsulation within the gel. An added advantage of these hydrogels is the potential to cross-link the aldehyde-bearing components with primary amines naturally present in the biological environment e.g. in the cell media or on cell surfaces and on ECM components produced by the cells in culture, which aid in anchoring the hydrogel to the biological environment. The reaction of aldehydes to biomolecules such as proteins, however, could also pose a risk of inhibiting protein bioactivity.

Thiol-disulphide exchange has been used to form injectable HA-based hydrogels by reacting pyridyl disulphide-functionalised HA with PEG dithiol (3400 g/mol) (Figure 1.18).[85] Hydrogel formation was monitored in real-time by measuring the UV absorption increase as an effect of released pyridine-2-thione from the thiol-disulphide exchange. High viability of Human umbilical vein endothelial cells (HUVEC), MSCs and normal human dermal fibroblasts was observed within the gels. A drawback of disulphide cross-linked hydrogels, however, is the high concentration of reducing agents such as glutathione found within some tissues that can result in bond cleavage and hydrogel collapse.[43]

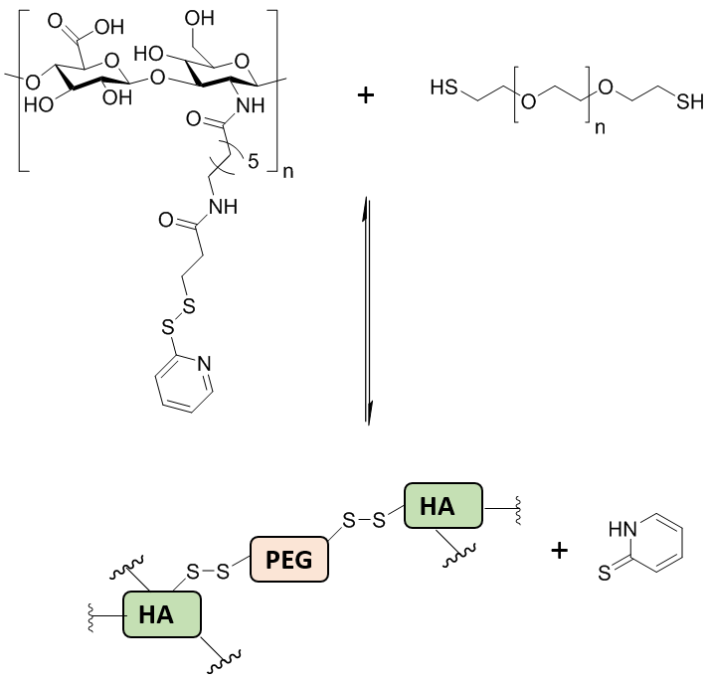

Figure 1.18: Usage of thiol-exchange to form hydrogels between pyridyl disulphide-functionalised hyaluronic acid (HA) and di-thiol PEG with the release of pyridine-2-thione.[85]

iii) Non-covalent cross-linking

In non-covalent cross-linked hydrogels interactions such as hydrogen bonding, electrostatic interactions or ionic coordination, van der Waals forces, hydrophobic interactions or specific molecular recognition such as host-guest interactions are utilised to form the networks.[33,43,44] For example, most peptide-based hydrogels form via non-covalent interactions such as the π-π stacking and H-bonding of Fmoc-Phe-Phe/Fmoc-Ser hydrogels[70–72] as discussed in section 1.2.2.

Due to its low cost and low toxicity, alginate (Figure 1.6B) has become a popular material to use for 3D cell culture. Alginate forms ionically cross-linked hydrogels via the coordination of the alginate chains with positive ions (e.g. Ca^{2+}, Mg^{2+}) with its mechanical properties easily tuned by changing the ion concentration.[43] Alginate hydrogels with varied stiffness (2.5-30 kPa) have been used to direct MSC differentiation, with softer hydrogels (2.5-5 kPa) directing adipogenic lineage commitment according to gene and protein expression analysis, while osteogenic commitment occurred in stiffer hydrogels (11-30 kPa).[86]

Protein-protein interactions have been utilised to form hydrogels by the molecular recognition of a recombinant protein with a WW domain and proline-rich peptides (Figure 1.19).[87] The WW domain can be found in many intracellular proteins and gets its name from conserved tryptophans. By letting recombinant WW domains flanked by hydrophilic spacers bearing RGD peptides (to improve cell attachment) react with a 13-amino acid peptide with seven proline residues, non-covalently cross-linked hydrogels were afforded that have been utilised for several cell-based applications.[88-91] Their assembly was shown to support the encapsulation and viability of adipose-derived stem cells injected into mice.[88] In addition, when functionalised with multi-branched PEGs hybrid doubly cross-linked hydrogels formed in which human iPSCs were encapsulated and injected into an ischemia injury mouse model.[89] Reduced inflammation and muscle tissue regeneration was observed at the injection site compared to PBS control.

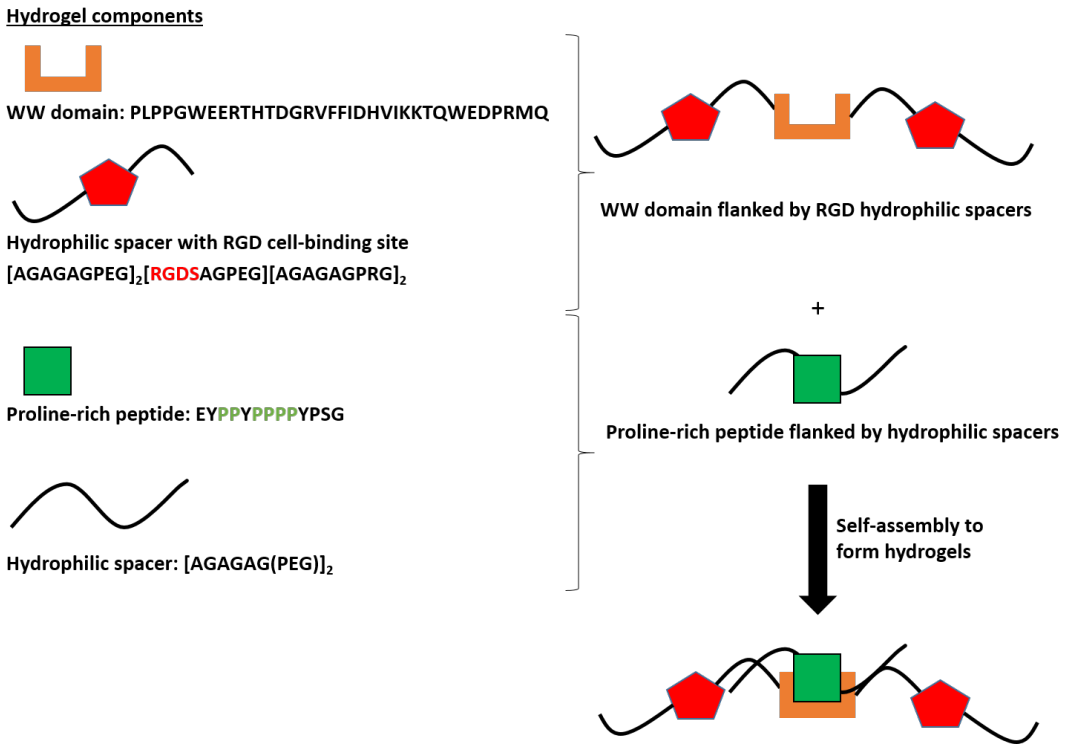

Figure 1.19: Formation of hydrogels via non-covalent self-assembly of the recombinant protein WW domain and a proline-rich peptide. The WW domain is flanked by hydrophilic spacers bearing a RGD sequence for improved cell binding. The proline-rich peptide is flanked by a hydrophilic spacer.[87]

1.2.4 Bio-functionalisation of hydrogels

i) Incorporation of cell adhesive peptides in hydrogels

Cell adhesive peptides can be added to hydrogels to help mimic ECM-integrin interactions with RGD being a common motif. The addition of RGD to photopolymerised PEGDA hydrogels improved cell adhesion and spreading of human-derived MCS with cell viability increasing from 15 % to 75 % compared to the non-modified hydrogel.[92] Studies have shown cell adhesion on RGD-functionalised biomaterials occurs in a concentration-dependent manner with an increased concentration of RGD leading to higher levels of cell attachment and spreading, but if the levels are too high, it can hinder cell detachment and thus migration.[93]

The ability to mimic the spatial and temporal control of ECM-cell adhesion can greatly improve the performance of hydrogels and can be mimicked by using patterned hydrogels, with specific presentation of cell adhesion ligands to promote local attachment and spreading. 3D hydrogels formed via the reaction between a 4-arm PEG-azide and a bis-cyclooctyne peptide containing both an MMP-sensitive sequence and a vinyl-modified lysine were formed in the presence of 3T3 cells allowing for *in situ* cell encapsulation (Figure 1.20).[94] RGD-patterning within the hydrogel was achieved by reacting the vinyl groups in the hydrogel backbone with thiol-functionalised RGD sequences via UV exposure (λ = 365 nm) and use of photomasks to spatially control the functionalisation. Over 10 days culture, improved cell spreading was observed in the RGD patterned areas compared to those without peptide-functionalisation. This type of patterning also allows for the local clustering of RGD ligands, a mimic of the ligand clustering of integrins (also known as focal adhesions) observed *in vivo* and crucial for forming stable ECM-cell adhesions.[20]

Although RGD is a common motif, its selectivity is poor as it binds many different cell receptors and cell types.[17] As such, more selective cell adhesion peptides can be used to improve the adhesion of specific cell types. Cell-adhesive peptides have been identified from several ECM-proteins, including REDV and LDV from fibronectin, DGEA and GFOGER (O = hydroxyproline) from collagen and IKLLI and YIGSR from laminin.[17] Although these peptides can promote cell adhesion on their own, it has

been reported that their combination with RGD is necessary to give the desired cell-binding.[20]

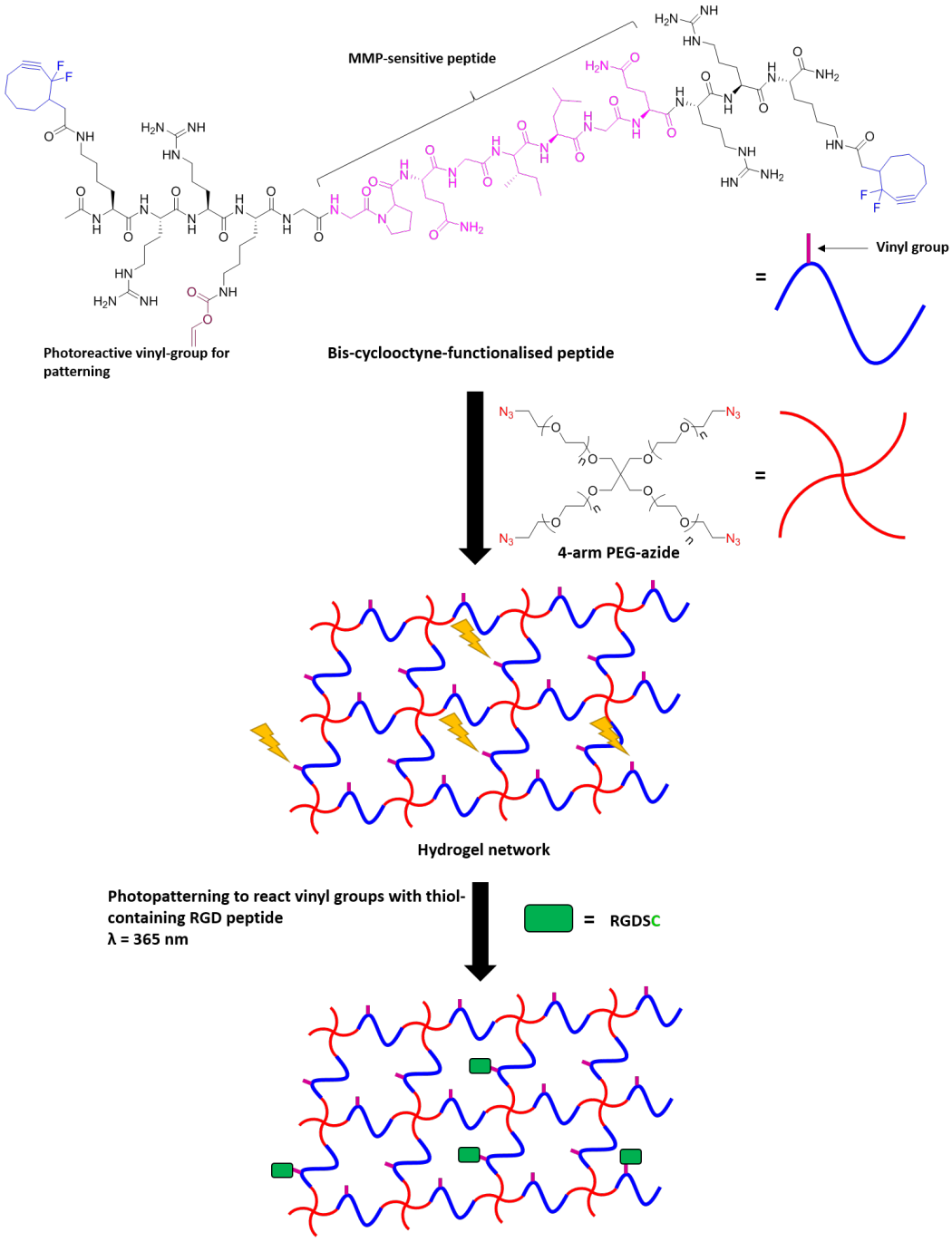

Figure 1.20: Formation of hydrogels by cross-linking 4-arm PEG-azide and a bis-cyclooctyne-functionalised peptide with an MMP-sequence and an alkene-functionalised lysine. The two components undergo strain-promoted azide-alkyne cycloaddition to form hydrogels. By selectively irradiating areas of the hydrogel (λ = 365 nm) and adding a cysteine-containing RGD-sequence selective RGD-patterning was afforded.[94]

ii) Incorporation of growth factors in hydrogels

To mimic the secretion of soluble factors from cells and/or the ECM to direct cell communication and behaviour, growth factors (GFs) can be included in the hydrogel structure. GFs modulate cell behaviour, including proliferation rates, differentiation, cell adhesion, migration and gene expression profiles.[95]

A challenge of GFs inclusion is to recapitulate their local concentration profiles and controlled release as observed *in vivo*.[18,44] One strategy for achieving this is to use light-based strategies and a common approach involves the use of an ortho-nitrobenzyl moiety, which upon irradiation forms an aromatic nitrosocarbonyl (Figure 1.21A).[96] The release of the functional group at the benzylic position allows specific release of GFs/peptides/targeting moieties etc. or selective functional group unmasking can be achieved. Using this strategy, a cysteine-containing peptide derivatised with a 2-nitrobenzyl-modified lysine and a 4-arm PEG-thiol were cross-linked with an 8-arm PEG-vinylsulphone to form thiol-ene cross-linked hydrogels (Figure 1.21B).[97] The 2-nitrobenzyl residues were then cleaved upon irradiation (λ = 405 nm), which led to the exposure of the primary amine on the lysine side chain. The lysine motif was enzymatically linked to a glutamine-containing peptide conjugated to VEGF by using FXIII (as in Figure 1.9). The use of laser-scanning lithography to control the 2-nitrobenzyl decaging enabled the spatial patterning of VEGF within the hydrogel.

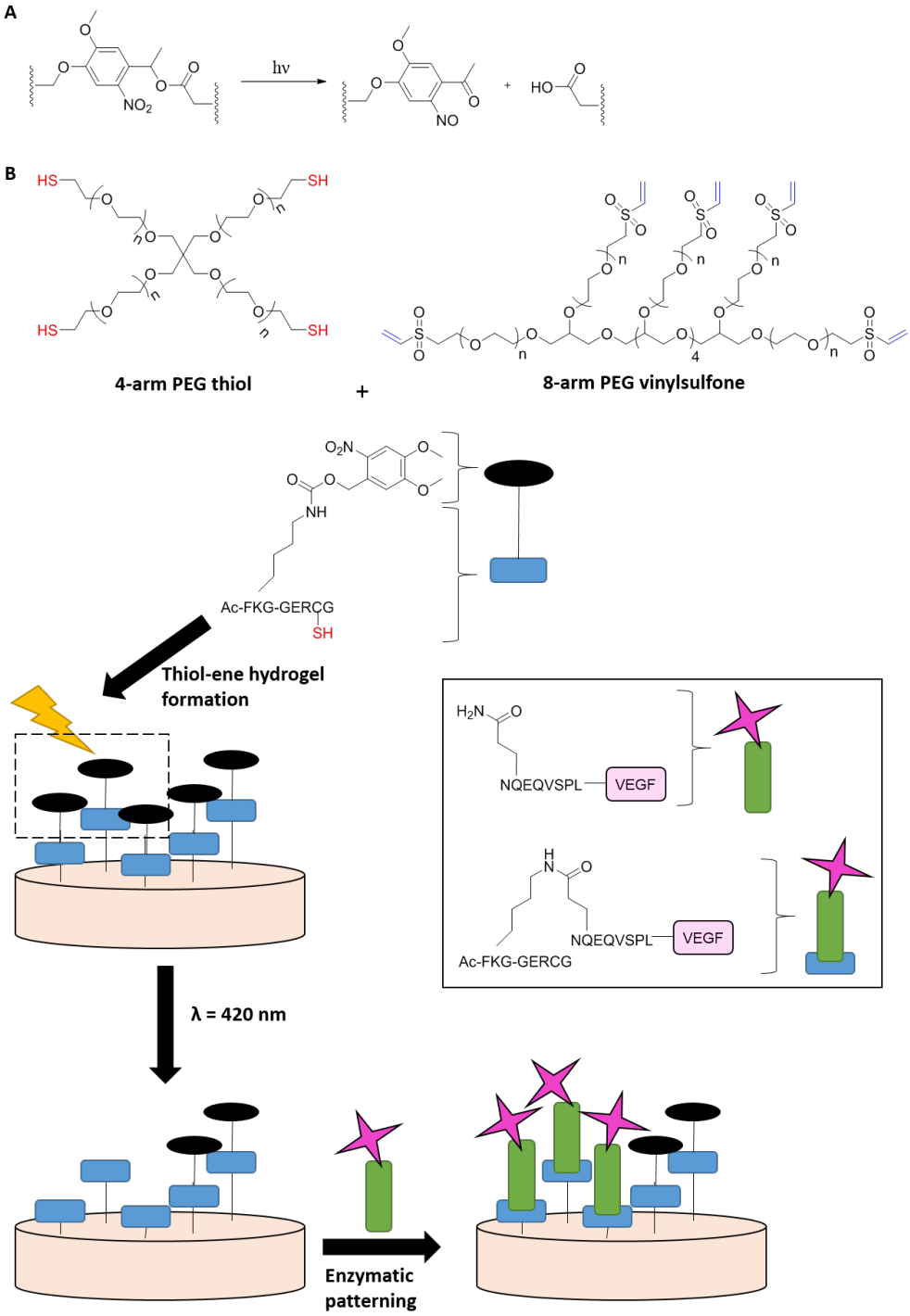

Figure 1.21: A. Photocleavage of nitrobenzyl as used for patterning of hydrogels. **B.** Formation of thiol-ene cross-linked hydrogels by mixing an 8-arm PEG vinyl-sulphone with 4-arm PEG-thiol and a cysteine-containing peptide that contain a FXIIIa sensitive peptide with a 2-nitrobenzyl-capped lysine residue. After hydrogel formation, irradiation (λ = 420 nm) led to the cleavage of the 2-nitrobenzyl moiety, thereby unmasking the lysine residue. Addition of FXIIIa and a VEGF-conjugated glutamine-containing peptide resulted in the VEGF-patterning within the hydrogel by virtue of the FXIIIa mediated lysine-glutamine linkage.[97]

1.2.5 Tailoring hydrogel biomechanical properties

As discussed above cells respond to the mechanical properties of the surrounding ECM through mechnotransduction and by altering the hydrogel stiffness and elasticity this can be tuned. A method of increasing hydrogel stiffness is to simply increase the component concentrations and/or introduce higher cross-linking levels.[33,51] Seminal experiments in this field were done in 2D using collagen-coated polyacrylamide hydrogels, where hMSC lineage commitment was shown to be dependent on substrate stiffness.[98] When cultured on surfaces with low (1 kPa), medium (11 kPa) or high (34 kPa) elastic modulus, gene expression profiles showed neural, myogenic and osteogenic lineage commitment respectively, in line with the observed stiffness of these tissues *in vivo*.

In recent years, several studies have introduced the concept of spatial control over hydrogel mechanics, usually through photochemistry. PEGDA-based hydrogels with a nitrobenzyl ether photodegradable unit were formed with 10 kPa elastic modulus.[99] Upon spatially controlled irradiation (λ = 365 nm, 5 mW/cm^2, 6 min) patterned hydrogels with mechanically softer and stiffer regions were afforded (from 2-10 kPa) with both regular and randomly patterned gels fabricated (Figure 1.22). Higher levels of cell spreading and Yes-associated protein (YAP) activation (gene known to regulate cell behaviour in response to mechanical stimulus) were observed when hMSCs were grown on regularly patterned hydrogels with osteogenic lineage commitment as assessed by upregulation of the osteogenic marker alkaline phosphatase (ALP). By irradiating the hydrogel to afford a randomly patterned hydrogel cells became more rounded and showed lower levels of ALP and YAP activation. Furthermore, expression of the stem cell marker CD105 increased, indicating low levels of differentiation and demonstrated that the spatial control of hydrogel mechanical properties could direct stem cell fate.

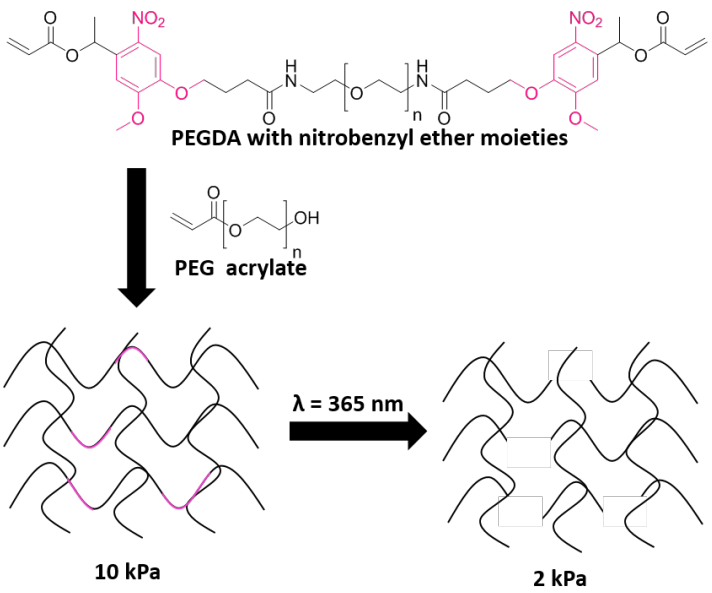

Figure 1.22: Hydrogels with patterned stiffness by inclusion of a 2-nitrobenzyl moiety in a PEG-based hydrogel. Initial hydrogels had a stiffness of 10 kPa, which after irradiation (λ = 365 nm) led to hydrogel network breakage (due to the bond-cleavage of 2-nitrobenzyl) and stiffness decrease down to 2 kPa. By controlling the irradiation time and position hydrogels with patterned stiffnesses were created.[99]

1.2.6 Modifying the hydrogel topography and microstructure

The micro and nanostructure of the ECM varies across tissues and organs with integrin-ECM interactions occuring at the nanoscale and controlling hydrogel topography at this scale can be used to mimic such properties.[17,20] Most studies for cell culture have involved the fabrication of a flat 2D surface, or a stiff and rigid 3D scaffold with nanostructure,[33] such as the nanopatterning of PMMA surfaces with 120 nm diameter and 100 nm deep nanopits using electron beam lithography.[100] The nanopits were arranged into either square, hexagonal or disordered arrays and seeded with hMSCs to monitor osteogenic differentiation by analysing the expression of bone-specific proteins osteopontin and osteocalcin. Higher levels of osteogensis was observed with hMSCs cultured on the square-patterned polymers for 21 days, compared to both unmodified PMMA and the hexagonal or randomly patterned surfaces, demonstrating the control specific nanotopography has on stem cell fate.

1.2.7 Introducing degradation properties into hydrogels

The remodelling of the ECM by cells through its degradation and production is an important aspect to try to mimic within a synthetic ECM matrix. The use of reversible cross-linking methods is one way of introducing a dynamic environment in which cells can spread, proliferate and migrate, as with the imine cross-linked hydrogels used within this thesis.

Many studies for 3D cell culture have used hydrogels with MMP-sensitive peptide sequences functionalised into the hydrogel network to allow for enzymatic degradation, with several such examples already given. The rate of hydrogel degradation can be tuned by altering the peptide motifs to have different affinities for specific MMPs.[20] Initial work in this field used vinylsulfone-functionalised 4-arm PEG cross-linked with a cysteine-modified MMP-sensitive peptide to form hydrogels (Figure 1.23) in which human foreskin fibroblasts were encapsulated and showed improved matrix invasion over time because of cell-mediated MMP secretion and resultant hydrogel degradation.[101]

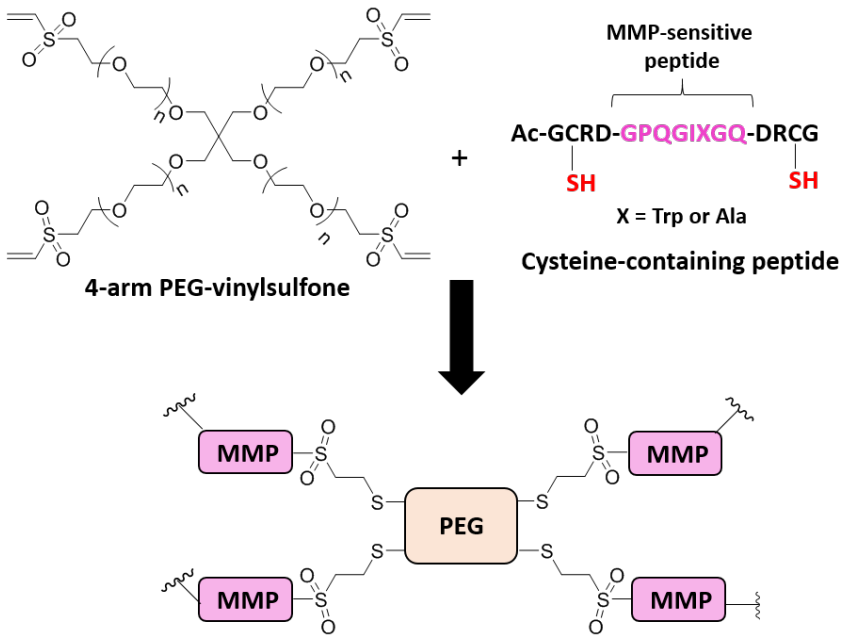

Figure 1.23: Formation of hydrogels by cross-linking 4-arm PEG-vinylsulfone with a MMP-sensitive peptide modified with a cysteine to afford the thiol-ene linkage.[101]

Current work in the area of hydrogel degradation, as in many more regarding hydrogel properties, looks to afford spatial and temporal control over the process. Several studies have accomplished this by encapsulating 2-nitrobenzyl in the hydrogels,[102–105] similar to the techniques used above for controlling hydrogel biofunctionalisation or biomechanical properties. The reaction between a 4-arm PEG functionalised with 2-nitrobezyl linked to a cyclooctyne moiety and azide-modified gelatin formed SPAAC cross-linked hydrogels that could be degraded in a spatial manner by irradiation (λ = 365 nm, 156 mW/cm^2, 30 s) (similar to Figure 1.23) and showed high viability of encapsulated HeLa over 24 h.[105] Although 2-nitrobenzyl-based photopatterning has been successful, care must be taken with any photo-based method, as short wavelengths can be toxic to cells and the use of external triggers adds a layer of complexity to the 3D cell culture platform, which may hinder its transition to widespread use.

1.3 High-throughput synthesis, screening and microarrays

Although the hydrogels and other biomaterials discussed so far have been beneficial in advancing the field of materials for 3D cell culture, their low throughput fabrication with the assessment of only one or a few similar variants of the same material at a time is a disadvantage. The utilisation of high-throughput synthesis and screening (HTSS) is a powerful method to rapidly assess a large number of materials at once, thereby reducing the time, cost and amount of material used.[106] HTSS can be particularly useful for biomaterials identification since the complex and poorly understood relationship between a biomaterial and its cellular response makes prediction of material/cell performance difficult. HT methods have been utilised for biomolecule identification, with microarray technology being particularly advanced for DNA and protein microarrays aimed at understanding gene and protein levels with specific targets of interest e.g. cell or tissue.[106]

A microarray is a solid substrate, most commonly a glass slide, but other materials have also been used e.g. polymers and nitrocellulose membranes or paper, on which probes such as biomolecules e.g. DNA or proteins, or other materials e.g. polymers,

are printed or synthesised and immobilised in a defined pattern. Thousands of features per cm^2 can be afforded with their identification being defined by their position. Incubating a microarray with a target e.g cDNA, the relative binding levels to the different features can be quantified, commonly through fluorescent labelling.[106–108] Different types of printers for deposition of biological materials to produce microarrays exists and within this thesis two robotic-type printing techniques have been used: contact and ink-jet printing.

1.3.1 Printing techniques

i) Contact printing

In contact printing the printing head carrying the sample to be printed and the substrate come in direct contact during the printing process. For pin-based contact printing, multiple pins (usually 16, 64 or 96) are attached to a robotic arm with high X-Y-Z precision and dipped into a sample-reservoir, usually a 394- or 96-well plate. Sample is transferred from the pins to the substrate via physical contact with typically 400-10,000 spots/cm^2 printed per array.[106] Printing quality is affected by the viscosity of the sample, the pin contact area and its surface properties as well as the surface properties of the substrate. Additionally, external factors such as temperature, and humidity will also affect the precision and quality printing.[106,107] Two main types of pins are used for contact printing: solid and split pins (Figure 1.24).

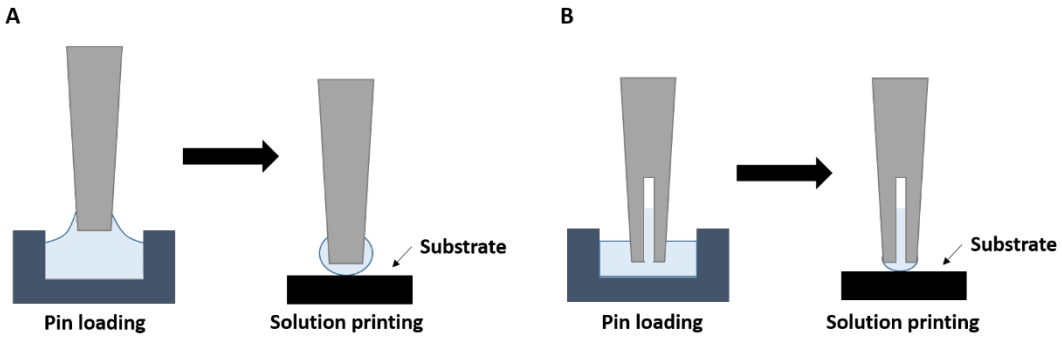

Figure 1.24: Types of pins used for contact printing with their associated pin loading and solution printing. **A.** Solid pins. **B.** Split pins.

Solid pins

Solid pins are usually fabricated out of metals such as stainless steel, titanium or tungsten and dipped into the sample reservoir to load the tip of the pin with ink (Figure 1.24A). Following pick-up, the sample is deposited onto the substrate with the spot size tuned by changing the pin size. Solid pins are particularly useful for samples containing particulates as there is no risk of clogging the interior of the pin, but a disadvantage is the regular need for washing and reloading with new sample during printing since only a few spots can be printed with each load.[106,107]

Split pins

In split pins a narrow microchannel (10-100 μm) is located at the tip of each pin in which the sample is loaded through capillary force action (Figure 1.24B). Upon contact with the substrate, the sample is deposited in the pico- to nanoliter range. An advantage of these pins is the increased throughput compared to solid pins since spots can be printed serially without the need for frequent reloading and washing, but pre-printing is necessary to remove excess sample on the pin walls and ensure uniform printing. Another disadvantage is the risk of pin clogging and precipitation with material getting stuck in the pin microchannel, a problem for protein and polymer solutions. Although the size of the microchannel can be increased to limit this, such pins are subjected to lower printing uniformity.[106,107]

iii) Ink-jet printing

In contrast to contact printing, no physical contact takes place between the printer nozzle and substrate during ink-jet printing with the advantage of reduced risk of contamination and gentler deposition of the sample.[106] Ink-jet nozzles have a small opening into which the sample is drawn and the high printing precision of the printers enables the printing of specific patterns and geometries on the target substrate.[106,109] Two types of nozzles are commonly used for drop-on-demand ink-jet printers: thermal and piezo (Figure 1.25).

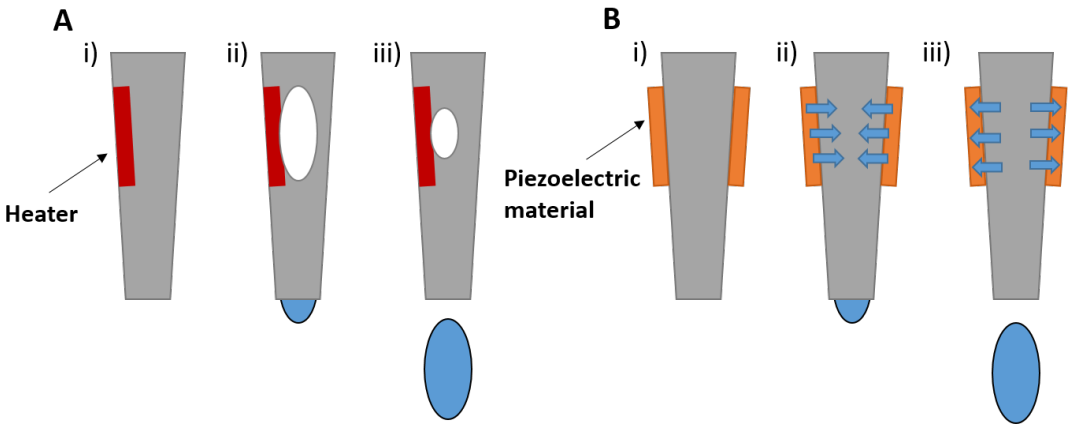

Figure 1.25: Types of nozzles used for ink-jet printing **A.** (i) Thermal jet nozzle, equipped with heater that upon (ii) heating result in the formation of a vapour bubble. (iii) As the heat resistor cools down the vapour bubble shrinks and collapses, resulting in droplet formation. **B.** (i) Piezo jet nozzle equipped with a piezoelectric material that (ii) deforms as a voltage is applied. (iii) When the voltage is turned off and the piezoelectric material relaxes back to its original state pressure builds up inside the nozzle, resulting in droplet formation.

Thermal jet

In thermal jet, the nozzle is equipped with a heater capable of temperatures up to 300 °C. Upon heating a vapour bubble is produced that results in a droplet forming at the end of the nozzle. As the nozzle cools the vapour bubble collapses, resulting in droplet ejection from the nozzle and replacement fluid filling the empty space created from the bubble collapse (Figure 1.25A).[106,109] Although many commercial desktop printers use thermal jet methods, the technique has seen limited use in biomolecule printing due to the high temperatures required.

Piezo jet

For piezo jet printing a deformable (piezoelectric) material e.g. lead zirconium titanate is bound to the nozzle that upon application of a voltage pulse shrinks and thus restricts the nozzle inner diameter. When the voltage if turned off the piezoelectric material relaxes back to its original state, creating a pressure wave inside the nozzle that causes droplet ejection (Figure 1.25B).[109] The droplet size can be tuned depending on the strength (voltage amount) and time (pulse length) applied to the piezoelectric material. Piezo jet techniques are compatible with printing of sensitive biomolecules, but due to their high cost and fragility of the nozzles it is considered a high-cost technique.

1.3.2 Types of microarrays

i) DNA microarrays

DNA microarrays enables the parallel analysis of thousands of genes, by immobilising oligo-DNA probes on a substrate, with the main application being gene expression analysis, although DNA microarrays also are used for transcription factor binding analysis or the detection of single nucleotide polymorphisms.[110] In a typical DNA microarray assay the messenger RNA (mRNA) isolated from the target e.g. cells or tissue is converted to its complementary DNA (cDNA) and amplified, usually with fluorescent labelling. Incubation with the microarray slide allows for DNA hybridisation with the immobilised probes. The level of binding per feature is analysed by fluorescence and relative gene expression levels determined.[108,110]

The probes are typically synthesised directly onto the slide, for example via ink-jet printing by sequential spotting of nucleotides (≤ 60 per probe) in the desired order. The printing substrate is typically functionalised with amines such a polylysine or silylamine-coating to ensure immobilisation of the probes to the surface.[108,111] Photolithography is another method of DNA microarray fabrication wherein oligonucleotides bearing photolabile blocking groups are deposited onto a substrate in a spatially controlled manner with the use of masks. After the first round of nucleotides are attached on the substrate, masks are applied that allow for the light-initiated cleavage of the blocking groups, thus rendering them capable to react with a second nucleotide. A solution of either A, T, C or G conjugated with blocking groups are then added to the chip, allowing for their reaction with the previously unmasked nucleotides. This process in repeated for several rounds with a specific mask each time to spatially control the nucleotide incorporation. Millions of probes can be incorporated per microarray using this technology with up to 25 nucelotides in length.[111] The need for custom-made masks is a limitation of this method however, but is overcome in so-called mask less photolithography where digital micromirror devices guide the position of the light on the array, thus controlling on which probes the photolabile blocks are cleaved to allow for further nucleotide incorporation generating arrays with millions of probes and of longer nucleotide chains (≤ 85) compared to the other methods.[111]

ii) Protein microarrays

For protein microarrays, the immobilised probes are typically antibodies (typically IgG-based libraries), aptamers or short peptides, and are used to investigate protein expression levels found in samples of interest.[108] These "analytical" protein microarrays are used for profiling protein expressions in certain disease states and compared to healthy samples. Recombinant proteins (full-length or fragments) can also be printed, immobilised and screened with proteins, drugs or antibodies to assess protein-protein, protein-drug and antigen-antibody interactions for so-called "functional" protein microarrays.[108]

Drawbacks of protein microarrays include the limited protein stability once printed and the limited bioactivity of printed fragments compared to DNA, as well as the lack of protein amplification methods, which means it is difficult to detect low concentration proteins. In biological samples protein concentrations range from nanomolar (nM) to zeptomolar (zM, 10^{-21}) concentrations, and in biological environments these low concentration proteins typically co-exist with abundant non-target proteins e.g. serum, which can cause antibody cross-reaction and high background signals.[108,112]

iii) Polymer microarrays

For the high-throughput screening of biomaterials polymer microarrays have emerged as a powerful tool to screen polymeric materials, with notable developments within the Bradely[113] and Langer[114] groups for the past 15 years. Libraries of polymers are printed via contact or ink-jet printing onto glass slides and screened with a biological target, typically cells, to rapidly identify promising materials that are scaled-up for further interrogation (Figure 1.26). Polymers can both be printed as pre-made polymer solutions or polymerised *in situ* by the sequential printing of monomers, cross-linker and initiator onto the slide followed by polymerisation.

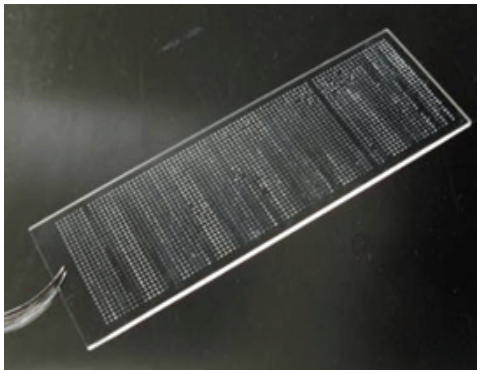

Figure 1.26: A polymer microarray printed with over 1000 different polymer features.

Within the Bradley group several polymer libraries have been synthesised and screened in this manner. For the purpose of contact printing and the deposition of pre-made polymers, libraries of polyacrylate/acrylamide/vinyl and polyurethanes have been utilised.[115–118] Applications of these libraries in array format have included identification of substrates that support skeletal progenitor cells (STRO+1)[119], bind K562 suspension cells,[120] induce platelet activation,[121] trap or repel water-borne parasites[122,123] and bacteria[124] as well as polymers that support stem cell growth, including mesenchymal stem cells (MSCs)[125] and the identification of polymers that bind proteins able to maintain the rat glioma cancer stem cells (CSCs) niche.[126]

To achieve *in situ* polymer formation on glass slides, ink-jet printing has been the preferred method as it allows for the precise and sequential deposition of monomers, cross-linkers and initiators, enabling huge scope in polymer variation on the microarray slide by simple tweaking of the component composition of each spot. Following *in situ* polymerisation (e.g. UV or redox polymerisation) very large polymer libraries have been fabricated[127–130]. Using this approach with a SciFLEXARRAYER S5 printer over 600 polyacrylate and polyacrylamide-based hydrogels were screened with human embryonic stem cells (hESCs).[45] This led to the identification of a hydrogel composed of the monomers 2-(acryloyloxyethyl) trimethylammonium chloride and 2-(diethylamino)ethyl acrylate and cross-linked with *N*-*N*′-methylenebisacrylamide that supported the long-term growth of hESCs (> 30 passages) and maintained their pluipotency, as measured by the expression of pluripotency markers Oct3/4, Nanog and Sox2. Due to the thermal responsiveness of the hydrogel, thermal detachment of the hESCs was possible by lowering the

temperature to 15 °C. Thereby an enzyme-free passaging system was developed. A similar high-throughput approach identified hydrogels that supported the long-term culture of primary hMSCs[131] and of mouse embryonic stem cells (mESC).[132]

Ink-jet printing and *in situ* polymersiation were also used to form high-density polymer microarrays (> 7000 different features per array) that led to the identification of polymers capable of supporting hESC growth and maintenance.[130] Scaled-up hit polymers were incubated with RH1 cells and passaged over 35 days. Maintained pluripotency was demonstrated by Nanog and Oct4 protein expression, and further confirmed by flow cytometry, qPCR and EB differentiation.

Arrays of double network hydrogels were also fabricated using an ink-jet based bioprinter (PolyPico) equipped with cartridges of 100 μm aperture, loaded with monomers, initiator or cross-linker.[133] In contrast to the costly nozzles used for the SciFLEXARRAYER printer the PolyPico uses disposable, low-cost cartridges, reducing the risk of contamination as well as the cost of printing. The first network was composed of combinations of UV-polymerised polymers made of cross-linked methacrylate, acylate and acrylamide monomers that were printed as an array of 80 different polymers. The second network was made up of polyacrylamide UV-polymerised inside the first network offering improved mechanical properties of the hydrogels as a result of the second network.

Aims

The aim of this thesis was to develop a novel approach to generate a library of new hydrogel-based materials that could be screened in a high-throughput manner for biomedical applications. The hypothesis was that these 3D structures would provide a good mimic of the complex ECM environment surrounding cells and that modulation of the hydrogels chemical structure and composition would allow a hydrogel library to be established. Here a library of 100's of hydrogels was fabricated using ink-jet printing technology, with the aim of making this procedure facile to allow longer-term screening of 1000's of materials simultaneously.

Coupled with the establishment of a hydrogel library fabrication platform, another aim was to enable a cell-compatible was to break the hydrogel structure and thus allow passaging. To this end a mild hydrogel passaging system using Vitamin B6-derivatives to afford hydrogel degradation and cell release was developed, in which the dynamic bonds in the gel were broken with competing external ligands.

Outside this work was a collaboration project that used 2D acrylate/acrylamide/peptide polymers to explore enrichment of pancreatic cancer stem cells (CSCs) with the aim of identifying niche-mimicking substrates.

Chapter 2: Development of a high-throughput screening platform of imine cross-linked hydrogels

2.1. Introduction

A drawback of the microarrays described in 1.3.2 is that the materials screened did not permit a large amount of 3D cell encapsulation, but mainly allowed surface cell attachment. Although subsequent scale-up studies enable their fabrication as 3D substrates, it is attractive to study 3D cell encapsulation in a HTS format. As such, in addition to the previously mentioned microarrays developed within the Bradley group, microarrays of polymer blends have also been produced wherein 3D encapsulation is possible.[134,135]

Microarrays with 3D polymer scaffolds were fabricated by the Bradley group with the contact printing of polymer blends.[134] Seven commercially available and biodegradable polymers (chitosan, PEG, PLA, PVA poly(ethyleneimine) (PEI), poly(ε-caprolactone) (PCL), poly(2-hydroxyethyl methacrylate)) with poor cell-attachment on their own were blended together with certain combinations found to form scaffolds that supported the attachment of two osteosarcoma cell lines (MG63 and SaOs) on the microarray platform. Subsequent scale-up of a hit blend (PLLA/PCL 80/20) demonstrated osteogenic differentiation of STRO-+1 skeletal stem cells and bone regeneration in a mouse model implanted with the cell-laden 3D scaffold.

Polymer blends of chitosan and PEI formed hydrogels when mixed at different molar ratios (90:10 to 10:90), which were fabricated as polymer microarrays, and screened with HeLa and primary foetal skeletal cells over 28 days, demonstrating 3D cell encapsulation within the hydrogels and maintained cell proliferation.[135] The skeletal cells remained spherical (a chondrocyte-like morphology) when encapsulated within

the chitosan:PEI hydrogels over the 28-day period as opposed to their fibroblast morphology as monolayer cultures, demonstrating these hydrogels capacity to prevent human skeletal cell fibroblast dedifferentiation. This was confirmed by gene expression analysis with increased expression of the chondrogenic markers Col2a1 (collagen type II) and aggrecan over the 28 days, while the expression of Col1a1, a marker for fibroblasts, remained low over the incubation period.

The Lutolf group produced hydrogel arrays by printing PEG monomers bearing MMP-sensitive peptides and being susceptible to enzymatic cross-linking with FXIIIa (see Figures 1.9 and 1.21) into 1,536-well plates with the use of a liquid handling robot.[136] By changing the amounts of the PEG monomers and varying the amount of MMP-sensitive peptides, ECM components (collagen IV, laminin or fibronectin), cell–cell interaction mediating molecules (E-cadherin, jagged or EpCAM) and soluble factors (fibroblast growth factor 4, bone morphogenic protein 4 or leukaemia inhibitory factor) in the PEG hydrogels, plus varying the cell seeding density, over 1000 different materials were created that could undergo HTS to look for 3D encapsulation of mESCs.

The aim of the work presented in this chapter was to develop a library of synthetic hydrogels that could be printed and screened in a high-throughput manner, while simultaneously allowing for 3D cell encapsulation. Here it was desired to form hydrogels simply by mixing the components by using an inkjet-printing approach as it allowed variation in hydrogel compositions by varying the component ratios of each spot. Imine cross-linked hydrogels were chosen, allowing primary amines and aldehyde-bearing components to quickly form hydrogels due to the rapid imine cross-linking. In addition, the dynamic nature of the imine bond should allow for cell movement within the hydrogels. Using this system, a novel family of hydrogels formed from the imine cross-linking of aldehyde-functionalised PEG cross-linkers and ECM-based peptides were developed. Their inkjet-printing onto glass slides enabled the fabrication and screening of 250 different hydrogels as novel cell matrices.

2.2 Hydrogel Library Development

2.2.1 Hydrogel Library Component Synthesis

For imine-mediated hydrogel formation and array fabrication two ECM-based peptides (RGD and LamIII) and three PEG cross-linkers (PEG_{2000}-CL, PEG_{3000}-CL and $(PEG\text{-}NH_2)_4$) were used. The two ECM-based peptides were designed to have free primary amines at both the amino and carboxyl termini (Figure 2.1) and were based on the cell attachment promoting peptide GRGDS (referred to as RGD) and the pentapeptide YIGSR from laminin 111 (referred to as LamIII). RGD is a recognition marker for integrins responsible for cellular adhesion[36] that is found in multiple ECM proteins including fibronectin, collagen and fibrinogen.[137] YIGSR is located within the β_1 arm of laminin 111,[138] and has been shown to increase cell adhesion,[139] improve hepatocyte attachment,[138,140] and decrease tumour growth.[141]

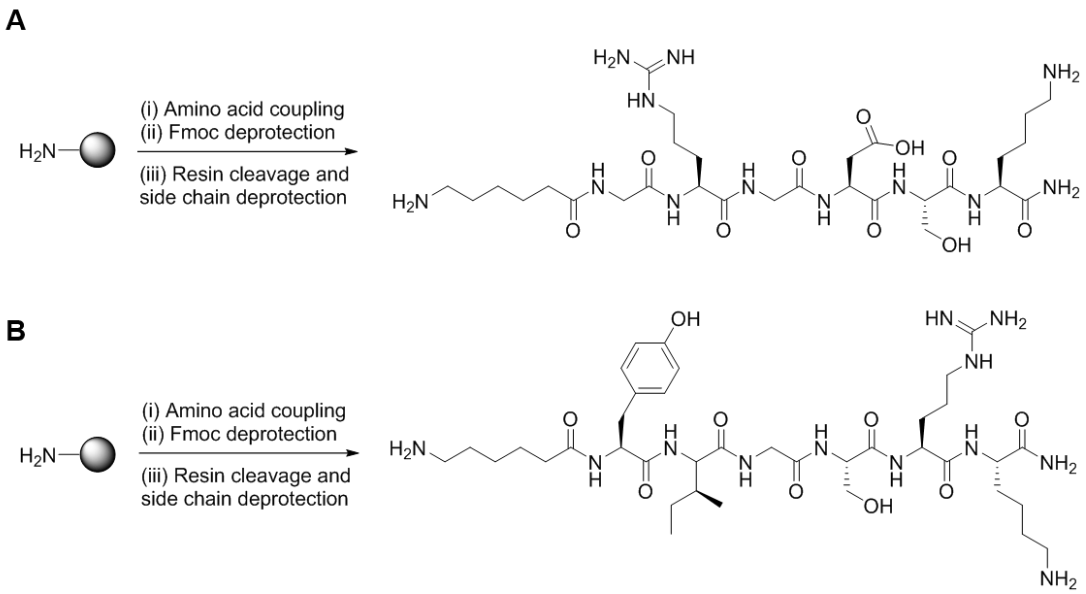

Figure 2.1: Structures and solid phase synthesis of peptides used for hydrogel formation. **A.** RGD (H-Ahx-GRGDSK-NH_2). **B**. LamIII (H-Ahx-YIGSRK-NH_2) (i) Fmoc-AA-OH, oxyma, DIC, DMF, 1 h. (ii) 20 % piperidine/DMF, 2 × 10 min. Steps i and ii repeated with the required Fmoc-AA-OH. (iii) TFA/TIS/H_2O (95:2.5:2.5), 3 h.

To allow crosslinking of the peptides, two linear PEG-based cross-linkers of varying PEG chain length (referred to as PEG_{2000}-CL, M_n = 2000 g/mol and PEG_{3000}-CL, M_n = 3000 g/mol) were bifunctionalised with 4-formylbenzoic acid (Figure 2.2). In

addition, a commercially available 4-armed amino-terminated PEG crosslinker (referred to as $(PEG\text{-}NH_2)_4$, M_n = 10 000 g/mol) was used to improve the rigidity of the hydrogels.

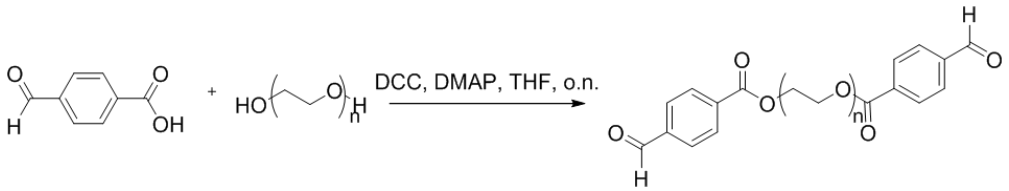

Figure 2.2: Synthesis of PEG cross-linkers used for hydrogel formation. PEG-OH M_n = 2000 g/mol (n = 44) or 3000 g/mol (n = 66)

Hydrogel formation was envisaged to take place via imine-bond formation between the amines on the peptides and $(PEG\text{-}NH_2)_4$ and the aldehydes on the linear PEG cross-linkers (Figure 2.3). Due to the reversibility of the imine bond, the gels would be dynamic, permitting cell migration as bonds make and break over time.

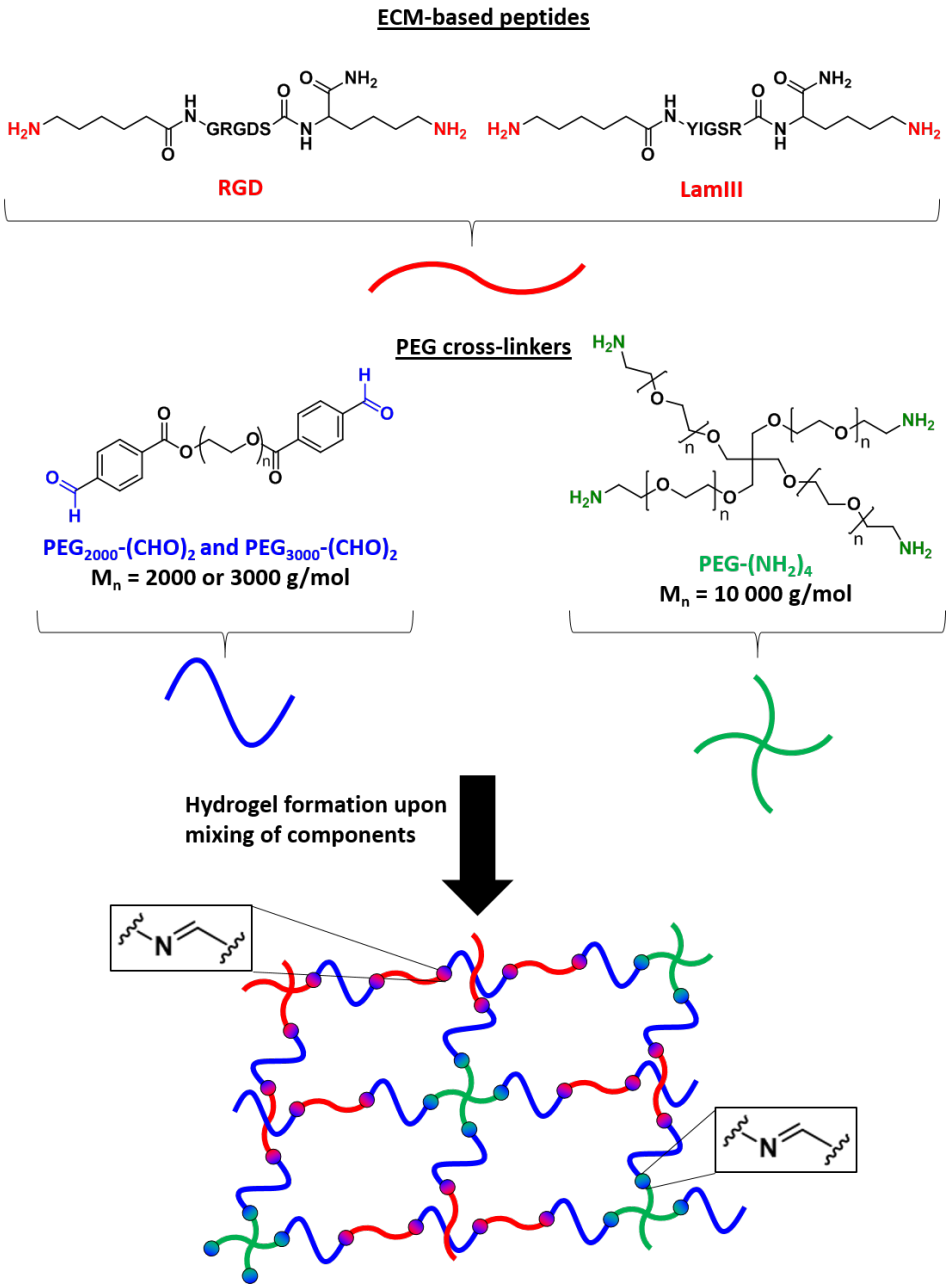

Figure 2.3: The formation of dynamic, imine cross-linked peptide/PEG-based hydrogels with cell encapsulation. Hydrogels form via the combination of ECM-based peptides (RGD and LamIII) with free primary amines at amine and carboxyl termini and bis-aldehyde PEG cross-linkers (PEG_{2000}-CL, PEG_{3000}-CL), as well as a 4-arm amine terminated PEG ($(PEG\text{-}NH_2)_4$).

2.2.2 Bulk Hydrogel Formation and Cell Encapsulation

For hydrogel formation, the five described components (RGD, LamIII, PEG_{2000}-CL, PEG_{3000}-CL and $(PEG\text{-}NH_2)_4$) were dissolved separately in Dulbecco's Modified Eagle Medium (DMEM) cell media. Different combinations of the peptides (RGD, LamIII)

and $(PEG\text{-}NH_2)_4$ were mixed with the cross-linkers (PEG_{2000}-CL, PEG_{3000}-CL), which resulted in gelation for certain combinations (Table 2.1).

Table 2.1: Assessment of hydrogel formation for different combinations of components. Hydrogel formation was assessed at room temperature 30 s after mixing and after 1 h and 24 h incubation at 37 °C. ✓ = hydrogel formed, × = no hydrogel formed, ~ = very soft gel-like structure formed. Hydrogel numbers in red: Components dissolved in DMEM cell media supplemented with 10 % FBS. In all other cases the components were dissolved in DMEM without FBS.

Hydrogel Number	Components	% (w/v)	Hydrogel r.t.	Hydrogel 37 °C, 1 h	Hydrogel 37 °C, 24 h
1	LamIII	2.5	✓	✓	✓
	PEG_{2000}-CL	5			
2	LamIII	2.5	×	×	×
	PEG_{2000}-CL	5			
3	LamIII	1.7	✓	✓	✓
	PEG_{2000}-CL	3.3			
4	LamIII	3.3	✓	✓	✓
	PEG_{2000}-CL	6.7			
5	LamIII	5	×	×	×
	PEG_{2000}-CL	10			
6	LamIII	7.5	~	~	✓
	PEG_{2000}-CL	15			
7	LamIII	3.75	~	~	✓
	PEG_{2000}-CL	15			
	$(PEG\text{-}NH_2)_4$	2.5			
8	LamIII	2.5	~	✓	✓
	RGD	2.5			
	PEG_{2000}-CL	15			
9	RGD	2.5	~	✓	✓
	PEG_{3000}-CL	15			
10	LamIII	1.7	~	✓	✓
	RGD	1.7			
	PEG_{3000}-CL	15			

The hydrogels formed were transparent (Figure 2.4), an important feature for subsequent fluorescence and bright-field imaging. Furthermore, the hydrogels all had a pH of 7, making the hydrogels compatible for cell encapsulation.

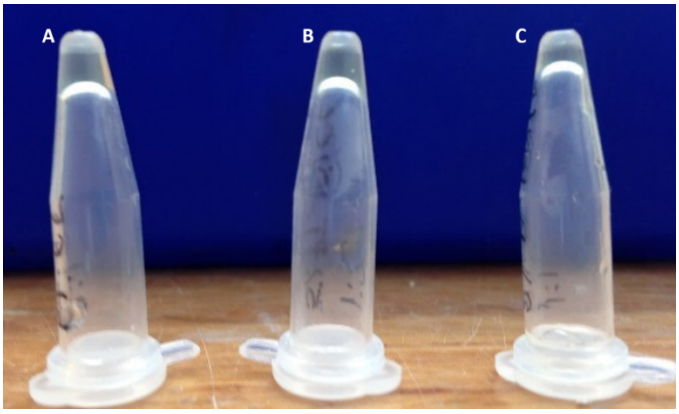

Figure 2.4: Formation of peptide hydrogels made-up of the peptide LamIII and cross-linker PEG_{2000}-CL in DMEM cell media with 10 % FBS. **A**. 2.5 % and 5 %; **B**. 1.7 % and 3.3 %; **C**. 3.3 % and 6.7 % respectively.

Using DMEM supplemented with 10 % foetal bovine serum (FBS) resulted in hydrogel formation at lower component concentrations than when using DMEM without FBS (see Table 2.1). When using DMEM with 10 % FBS, hydrogels composed of LamIII and PEG_{2000}-CL were observed to form at lower concentrations (1.7 %* LamIII and 3.3 % PEG_{2000}-CL). However, when DMEM without FBS was used 7.5 % LamIII and 15 % PEG_{2000}-CL were required to allow hydrogel formation, and these only formed stable features after 24 h incubation at 37 °C. Considering that the globular protein bovine serum albumin (BSA) is a major component of FBS, it is plausible that the BSA aids hydrogel formation due to the many primary amines present in its structure, resulting in increased imine cross-linking and explaining the improved hydrogel formation in FBS-containing media

To assess the capacity for 3D cell encapsulation within the imine hydrogels, HeLa cells were incubated within hydrogel 8 (see Table 2.1 for composition) and stained with Hoechst (nuclei stain) and CellTracker® CMPTX (cytoplasm stain). Good 3D cell encapsulation within the hydrogel to a depth of 75 μm indicated the promising use of these hydrogels as 3D cell matrices (Figure 2.5).

*For this chapter, all % (w/v) solutions are referred to as %

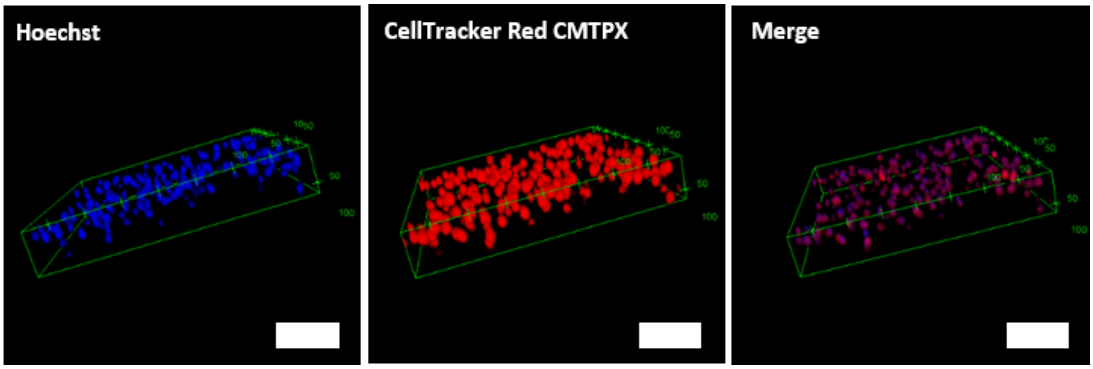

Figure 2.5: HeLa cells stained with Hoechst ($\lambda_{ex/em}$ = 361/497 nm) and CellTracker Red CMTPX ($\lambda_{ex/em}$ = 577/602 nm) were encapsulated within a hydrogel made-up of RGD (2.5 % w/v), LamIII (2.5 % w/v) and PEG_{2000}-CL (15 % w/v) in FBS-free DMEM followed by incubation for 48 h. Merge = merge of Hoechst and CellTracker Red CMTPX images. Scale bar 100 μm.

2.3 Hydrogel Array Fabrication

2.3.1 Initial Hydrogel Printing and Slide Functionalisation

After confirming hydrogel formation using the synthesised components, a strategy for array fabrication was developed. For the first printing trials, combinations of LamIII and PEG_{2000}-CL were used as a model system and printed with a drop-on-demand sciFLEXARRAYER s5 inkjet printer. For printing, each component was dissolved in water and printed layer-by-layer in varying ratios. To determine the optimal ratios/concentration of each component, different % solutions were tested. It was found that concentrations higher than 2.5 % resulted in poor droplet formation for both LamIII and PEG_{2000}-CL.

The optimal printing parameters for the array was investigated, initially with each feature printed as a single spot (Figure 2.6A). Since LamIII and PEG_{2000}-CL were printed at very low concentrations, no hydrogels formed during printing. However, drying and subsequent addition of cell media to spots on the slides where hydrogel components were printed resulted in hydrogel formation, but these small features lifted once the whole glass slide was submerged in cell media. Therefore, a pattern was designed where each feature was made up of "four spots" arranged as a 2×2 square (400 drops/spot, 1600 in total) (Figure 2.6B), with the 2×2 feature merging

into a single feature during printing. After printing of LamIII and PEG_{2000}-CL and drying of the slide, DMEM cell media was printed onto the larger features, resulting in hydrogel formation. However, when the whole slide was submerged in cell media, the hydrogels lifted, and thus a strategy to allow hydrogel attachment to the glass surface was required.

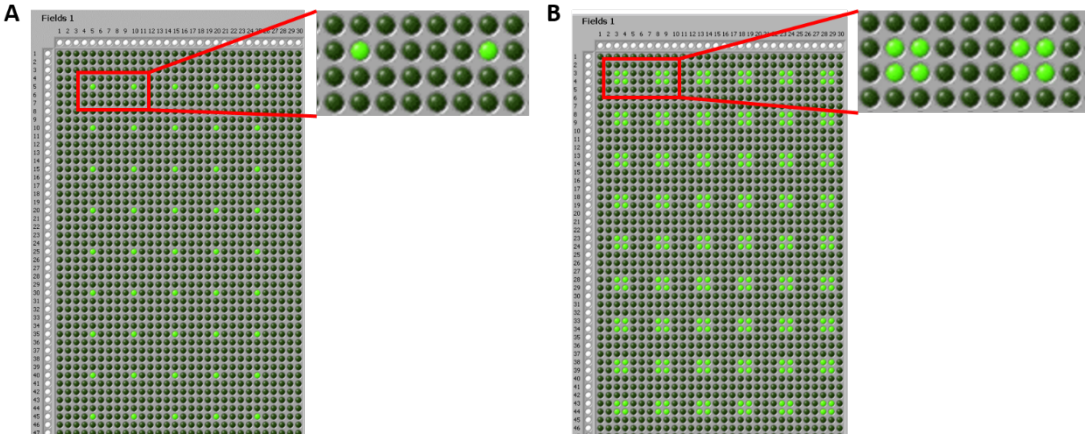

Figure 2.6: Printing patterns used for the hydrogel array using an inkjet printer. **A.** Pattern where each feature is made up of one spot of 1000 drops. **B.** Pattern where each feature is made up of four spots (each 400 drops) that merge upon printing. Pitch distance between adjacent spots was 0.6 × 0.6 mm in both A. and B. Images are screenshots from the sciFLEXARRAYER s5 software.

Several different functional groups on glass slides were tested for their ability to allow hydrogel anchoring (Figure 2.7). Initially printing onto standard microscope glass slides with hydroxyl (OH) functional groups on the surface was investigated. A method developed within the Bradley group was used (Figure 2.7A),[127] where an aqueous sucrose solution was printed in the pattern desired for the final hydrogel array and dried. A fluorous mask across the remaining area was created by treating the glass surface with (tridecafluoro-1,1,2,2-tetrahydrooctyl)-1-dimethylchlorosilane (FDS). Removal of the sugar mask creates confined areas for the hydrogels features, surrounded by a fluorous surface that limit non-specific cell attachment.

Using this masking method, a combination of LamIII and PEG_{2000}-CL were printed, after which the slide was dried at 40 °C overnight, before being submerged in FBS-free DMEM cell media. Although hydrogel formation was observed, all the features

rapidly detached from the slide. This suggested that the hydroxyl-functionalisation on the glass slide was insufficient to keep the hydrogels attached to it. Therefore, primary amine groups on the glass surface were investigated for their ability to provide improved hydrogel anchoring, as imine bond formation with the PEG-CLs and the glass surface would be possible. Two methods of primary amine surface functionalisation were evaluated, using standard microscope glass slides with (3-aminopropyl)triethoxysilane (APTES) or using commercially available aminoalkylsilane-functionalised glass slides.

In the first method, following sucrose patterning, FDS treatment and sucrose removal, APTES was reacted in the exposed areas to afford primary amine functionalisation (Figure 2.7B). Using this method, LamIII/PEG_{2000}-CL features were printed and dried, followed by submerging the slide in DMEM (both with and without 10 % FBS). This resulted in hydrogels forming on the slide, but most of the features had detached after overnight incubation both with and without FBS in the DMEM. In the second method, commercially available primary amine functionalised slides were used (SilanePrep slides, aminoalkylsilane functionalisation) (Figure 2.7C) and printing the same LamIII/ PEG_{2000}-CL features, followed by drying and rehydrating in DMEM without FBS, uniform and stable hydrogels formed that stayed intact on the slide after overnight incubation at 40 °C. When the DMEM was supplemented with 10 % FBS, however, the features immediately lifted. Based on these results, it was decided to continue subsequent array printing using the commercially available aminoalkylsilane-functionalised slides and FBS-free DMEM.

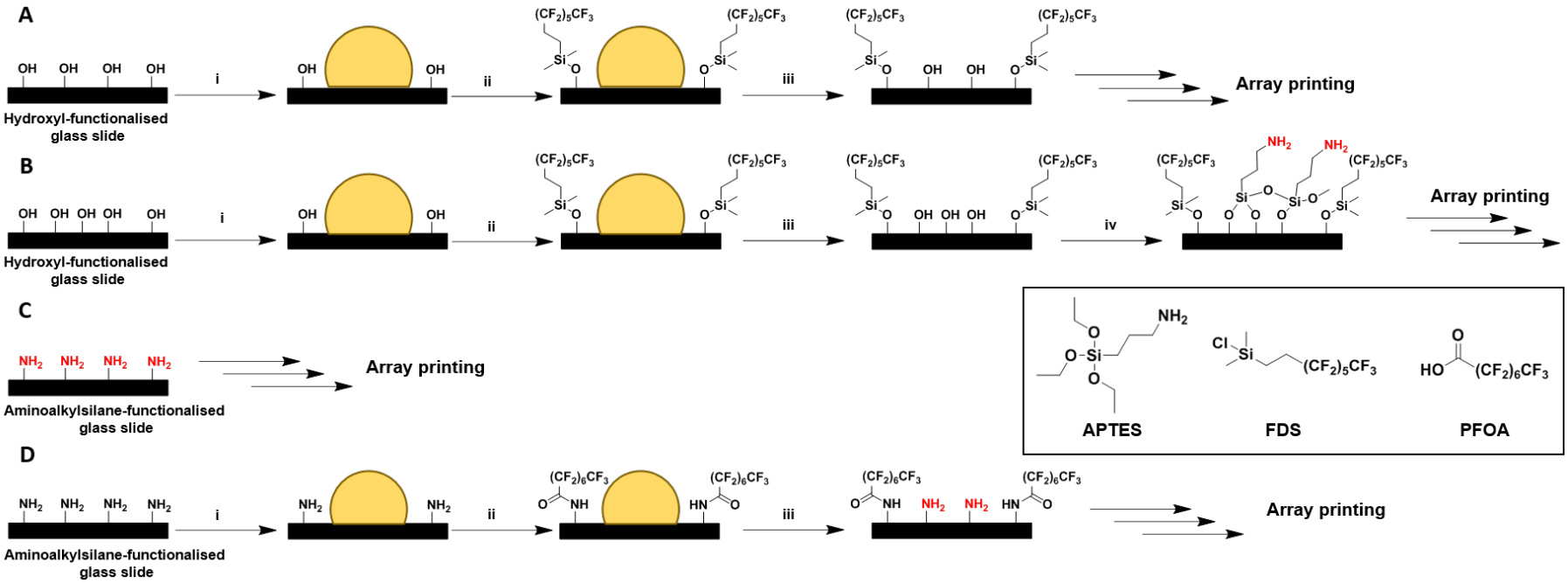

Figure 2.7: Different glass surface functionalisation methods investigated to improve imine hydrogel anchoring to glass slides. **A.** (i) 20 % aqueous sucrose (orange sphere) patterning onto a standard microscope glass slides. (ii) Functionalisation of the remaining areas with FDS, overnight. (iii) Washing with water to remove the sucrose. **B.** (i), (ii) and (iii) as in A. (iv) Functionalisation of the previously sucrose-covered areas with APTES overnight, followed by washing with ethanol and water. **C.** Printing directly onto aminoalkylsilane functionlised slides. **D.** (i) 20 % aqueous sucrose patterning onto aminoalkylsilane functionalised slides. (ii) Functionalisation of the remaining areas with PFOA using EDC, N-hydroxysuccinimide, DIPEA, DCM, 1 hr, r.t. (iii) Washing with water to remove the sucrose. FDS = (tridecafluoro-1,1,2,2-tetrahydrooctyl)-1-dimethylchlorosilane. APTES = (3-aminopropyl)triethoxysilane. PFOA = Perfluorooctanoic acid.

Arrays with 30 features (n = 3) made up of different ratios of RGD, PEG_{2000}-CL and $(PEG\text{-}NH_2)_4$ (see Appendix Table A1.1, HG1-HG30 for compositions) were printed and incubated with HeLa cells overnight to assess the compatibility of the array format with cell encapsulation. Since DMEM containing FBS caused the hydrogels to lift, the DMEM used for cell incubation was supplemented with a serum-alternative, Knock-Out™ Serum Replacement (KOSR, Gibco™). KOSR is a FBS-free and more defined serum supplement that is commonly used for stem cell cultures (e.g. pluripotent stem cells cultured on feeder layers), but can be used for any cell type as a replacement for FBS. Supplementing the DMEM with KOSR did not cause the hydrogel features to lift from the glass slides. After overnight HeLa incubation, cell viability was assessed using fluorescein diacetate/propidium iodide (FDA/PI) staining. Although cell viability was high for most features, a high level of background cell binding to the glass surface was observed (Figure 2.8A). It was therefore decided to develop a capping method to create a fluorous mask analogous to the FDS treatment previously described.

To create a fluorous mask and thus creating confined areas for the hydrogel features, an amide coupling strategy was chosen. On an aminoalkylsilane-functionalised glass slide patterned with sucrose, the N-hydroxysuccinimide (NHS)-ester of perfluorooctanoic acid (PFOA) was reacted with the primary amines in the remaining areas to result in amide bond formation (Figure 2.7D). HeLa cells were then seeded on test arrays printed on either non-functionalised aminoalkylsilane slides (Figure 2.7C) or on the perfluorooctanoic acid-functionalised glass slides (Figure 2.7D). After overnight incubation and viability staining (FDA/PI) a clear reduction in background cell binding was observed on the perfluoroocotanoic acid-functionalised slides compared to the non-functionalised slide (Figure 2.8B). For all subsequent hydrogel arrays the PFOA capping method was therefore used.

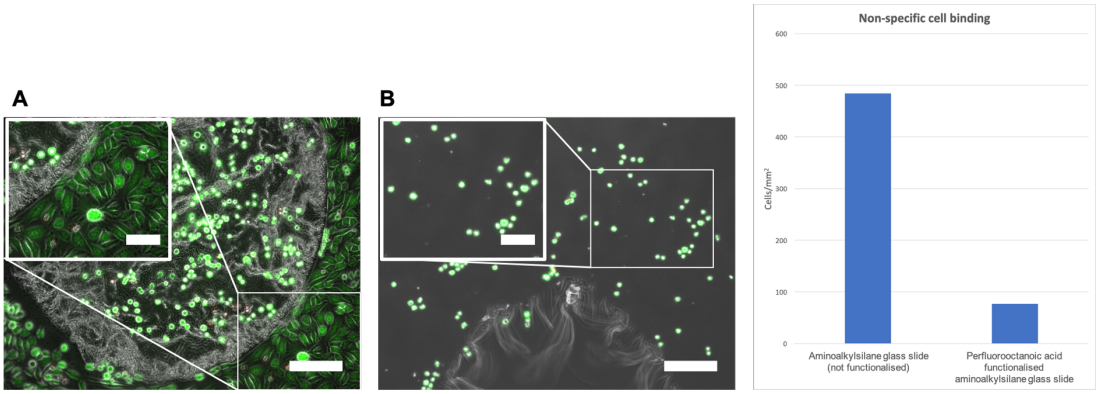

Figure 2.8: Effect of the capping of aminoalkylsilane glass slides with perfluorooctanoic acid on non-specific HeLa cell attachment. **A.** HeLa cell attachment on the hydrogel and on the aminoalkylsilane glass slide, demonstrating high levels of unspecific cell attachment. **B.** Reduction of unspecific HeLa cell attachment on the perflurooctanoic acid functionalised glass slide. Scale bar 200 µm. Scale bar of cut-out 100 µm. Right: Quantification of cells/mm^3 in terms of non-specific cell attachment (cells attached outside hydrogel area) in Image A and B.

2.3.2 Hydrogel library screening

Having developed a method for hydrogel array printing, 250 hydrogels (n = 3) were inkjet fabricated (HG1–HG250, see Appendix Table A1.1) and investigated for their ability to form stable hydrogels and facilitate cell encapsulation. By combining different ratios of the components different hydrogels were generated. Compositions with only RGD or LamIII as the peptide component, as well as the combination of the two peptides (RGD/LamIII) were printed. These were then cross-linked with either PEG_{2000}-CL or PEG_{3000}-CL to form hydrogels. Finally, $(PEG\text{-}NH_2)_4$ was also added to some of the features to promote hydrogel cross-linking and feature stability. Each was printed as 2×2 spots (1600 drops in total, 400 drops/spot, ~300 pL/drop) and on each glass slide a maximum of 96 features could be printed (16 rows × 6 columns) After drying the slide and submerging it in media containing cells, arrays of uniform 3D hydrogel features (0.8-1.5 mm diameter) were generated. (Figure 2.9).

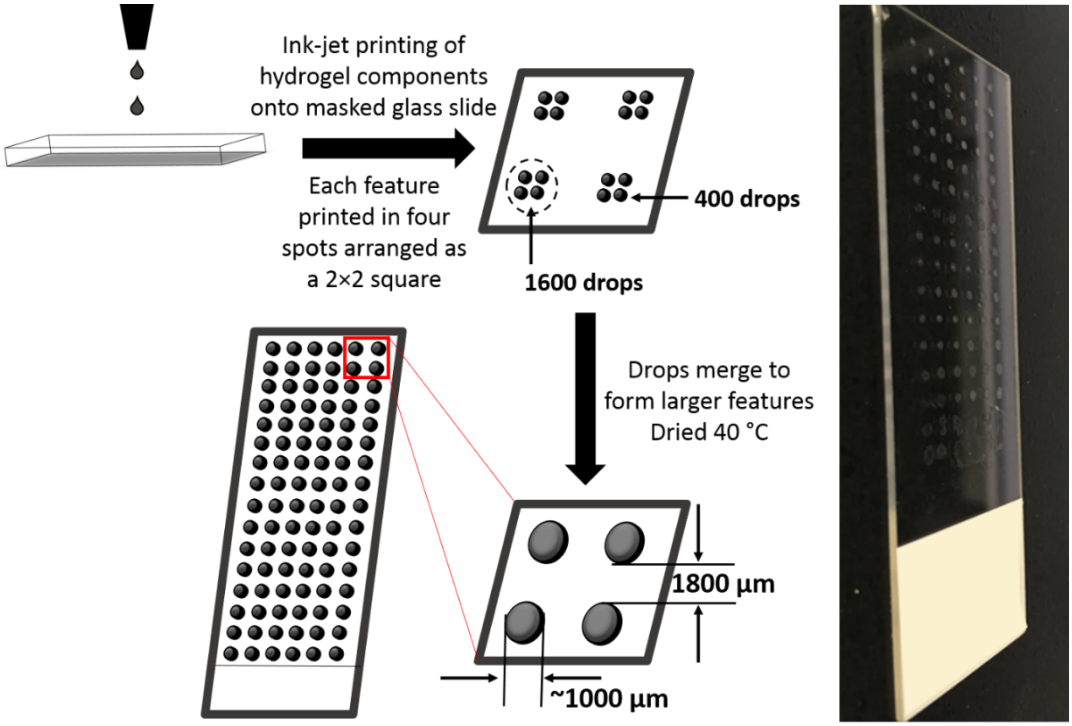

Figure 2.9: Strategy for hydrogel array printing. Hydrogel components were dissolved in water (2.5 % w/v) and printed sequentially onto a masked glass slide to form hydrogel features. Each feature was printed as a 2×2 square composed of four spots that merged together. (400 drops/spot, 1600 drops in total). Feature diameter was around 1000 µm and the distance between features was 1800 µm. On one glass slide a maximum of 96 features were printed. Right: colour image of a dried hydrogel array.

As an initial array, HeLa cells were incubated overnight, which resulted in cell encapsulation with high viability (as analysed by FDA/PI staining) (Figure 2.10, for all features see Appendix Figure A1.1). The number of cells/mm^3 could be calculated by counting the cells per feature and approximating the hydrogel volume to that of a semi-ellipsoid (Figure 2.11). The radii of each feature were measured by analysing their BF images in ImageJ and the height of each hydrogel was estimated to be 200 µm. This was chosen as an average height after measuring the height of features in the z-plane when imaging the hydrogel arrays.

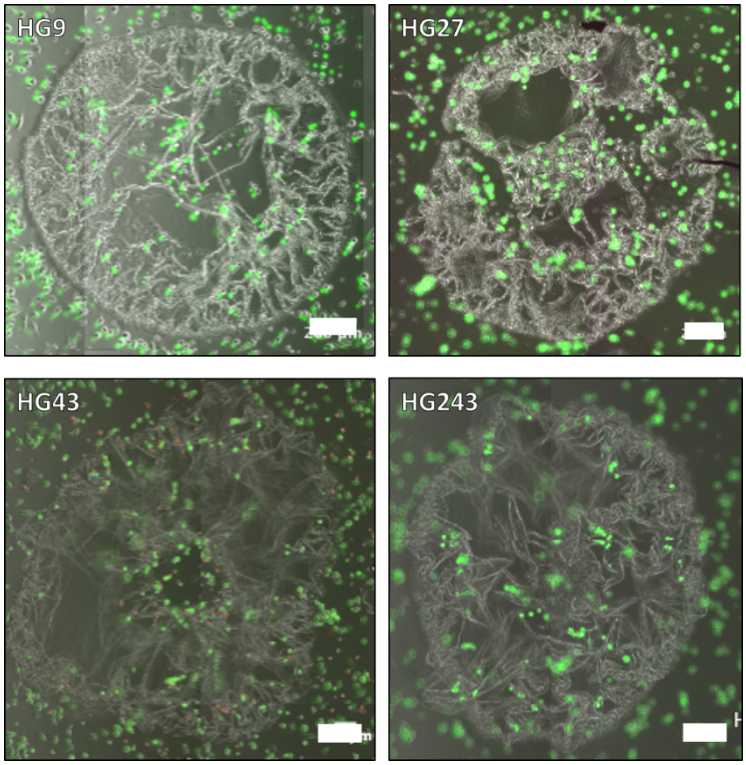

Figure 2.10: Examples of hydrogels from the 250-member hydrogel array screen with HeLa cells incubated on the array for 18 h followed by viability staining with FDA (green, live stain, ($\lambda_{ex/em}$ = 490/514 nm) and PI (red, dead stain, $\lambda_{ex/em}$ = 570/602 nm). The merged images of the FDA, PI and bright field channels are shown. For images of all features see Appendix Figure A1.1.

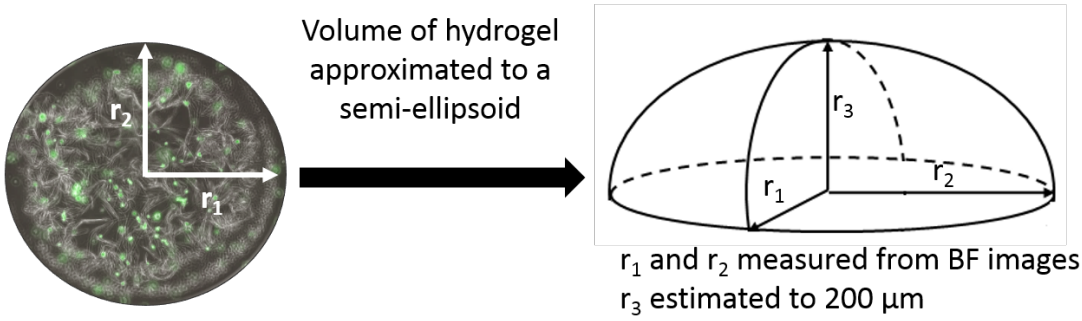

Figure 2.11 Approach to calculate the volume of the hydrogels on the array. The volume of each hydrogel was approximated to that of a semi-ellipsoid, with r_1 and r_2 measured from the microscopy images acquired by hydrogel array analysis. The height (r_3) of each hydrogel was approximated to 200 µm based on imaging in the z-plane.

To rank the hydrogels in terms of physical stability, each feature was given a morphology grade from 0-5 (with 5 being the highest) (see Figure 2.12 for an example of each grade).

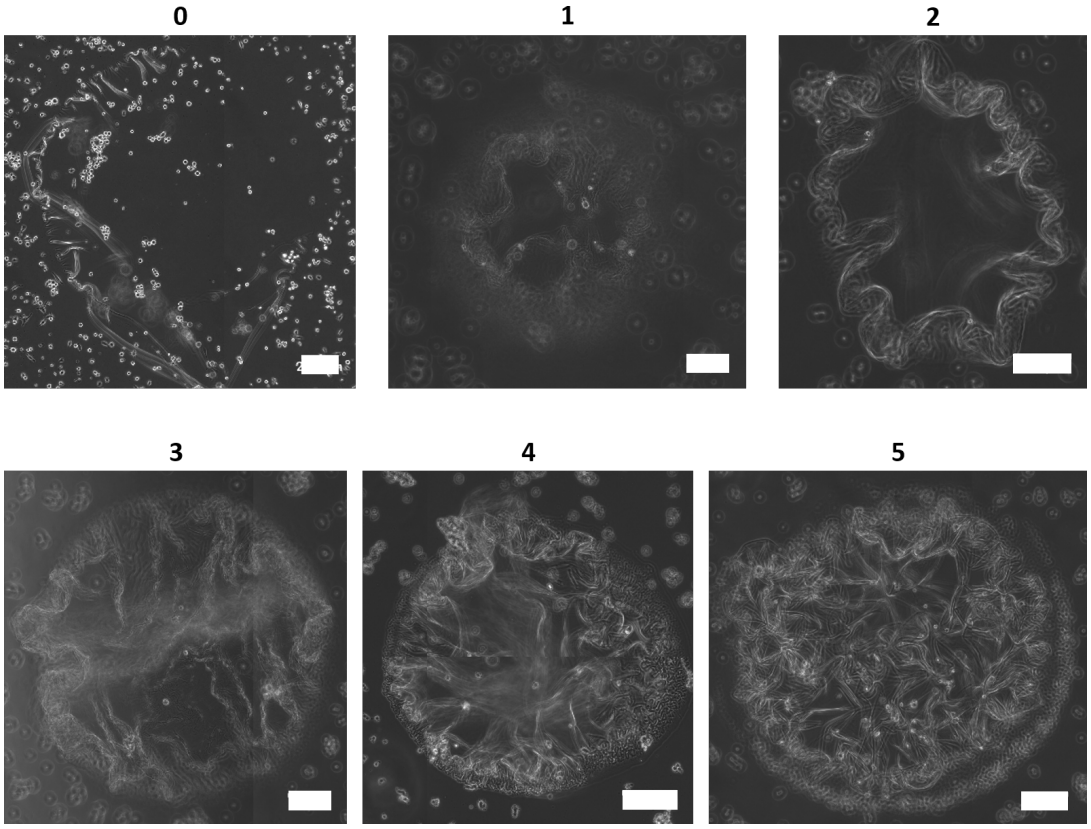

Figure 2.12: Representative bright-field images of each morphology grade assigned to hydrogel features. Grade 0 was given to features that had lifted from the glass slide. Grade 5 was given to the most promising hydrogel features in terms of stability and 3D cell encapsulation capacity. Scale bar 200 μm.

Each feature was then analysed both for cells/mm^3 and morphology grade (see Appendix Figure A1.3 for all combinations individual results). To further understand the factors that drove hydrogel formation between the different components and which of these combinations lead to better morphology and cell attachment several analyses were done (Figure 2.13A-G). Firstly cells/mm^3 was plotted against morphology grade (Figure 2.13A) to examine whether a higher morphology grade equated to higher cell attachment. The effect on morphology and cell attachment of hydrogels containing either RGD or LamIII or a combination of the two peptides was also assessed (2.13B-D). Furthermore, the effect of using either PEG_{2000}-CL or PEG_{3000}-CL as the cross-linker and their optimum molar ratios to the peptides was assessed

(Figure 2.13E-F). Finally, the effect on cell attachment and hydrogel morphology by the addition of $(PEG\text{-}NH_2)_4$ as a component was analysed (Figure 2.13G).

A

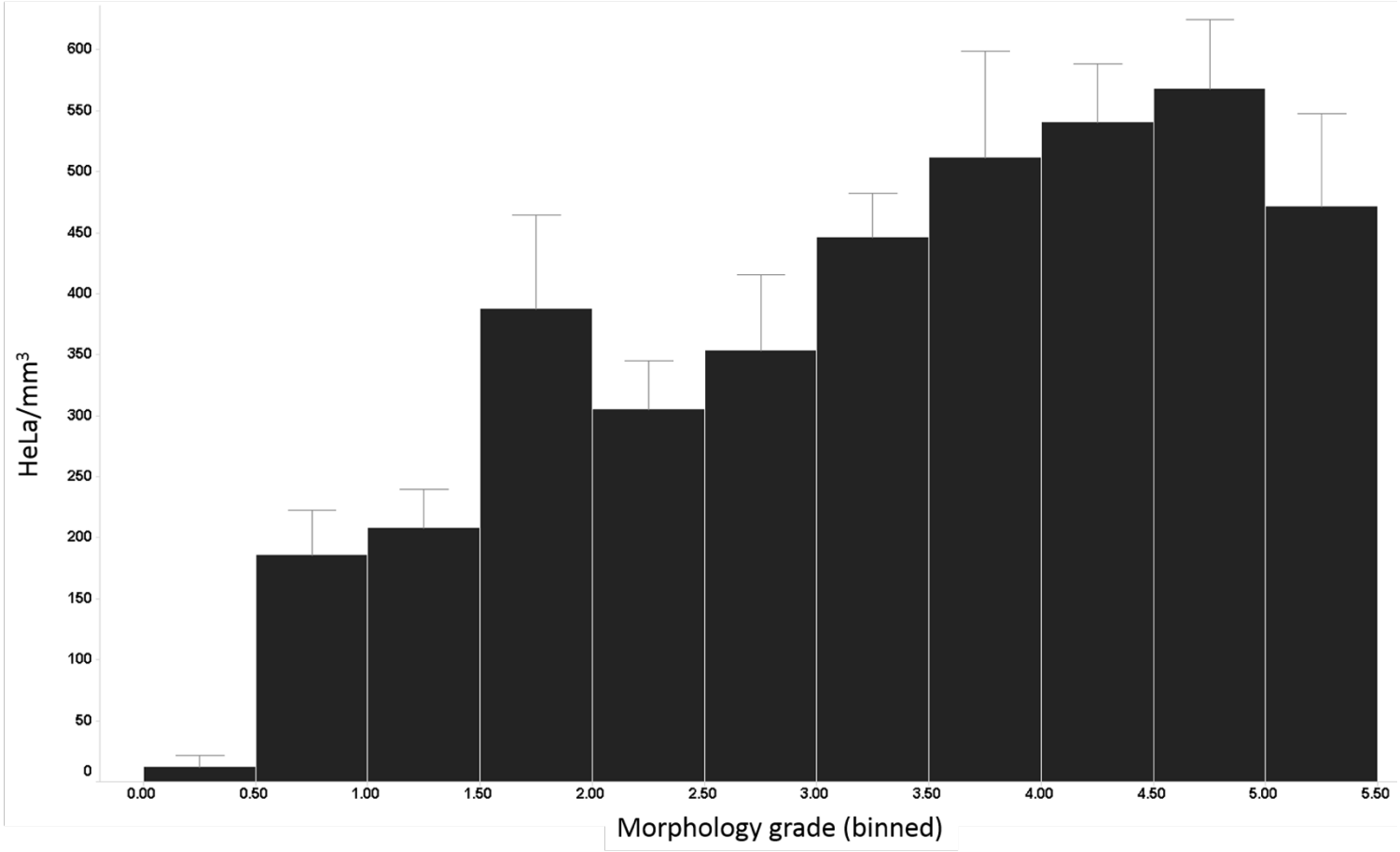
HeLa/mm³
600
550
500
450
400
350
300
250
200
150
100
50
0
0.00
0.50
1.00
1.50
2.00
2.50
3.00
3.50
4.00
4.50
5.00
5.50
Morphology grade (binned)

B

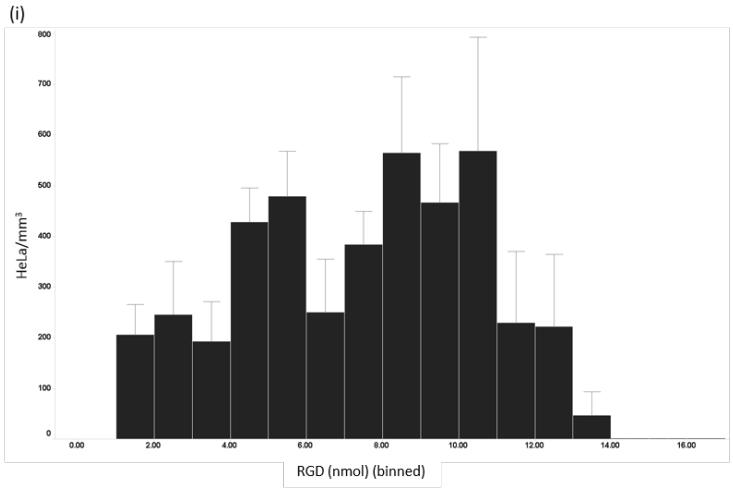
(i)
HeLa/mm³
RGD (nmol) (binned)

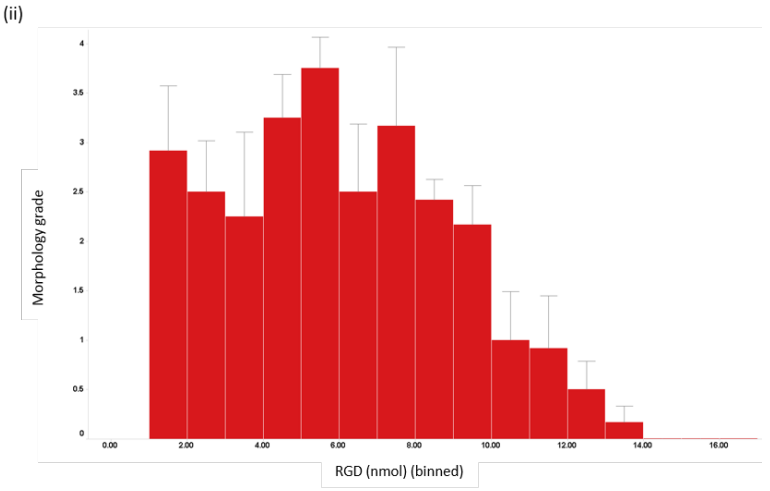
(ii)
Morphology grade
RGD (nmol) (binned)

C

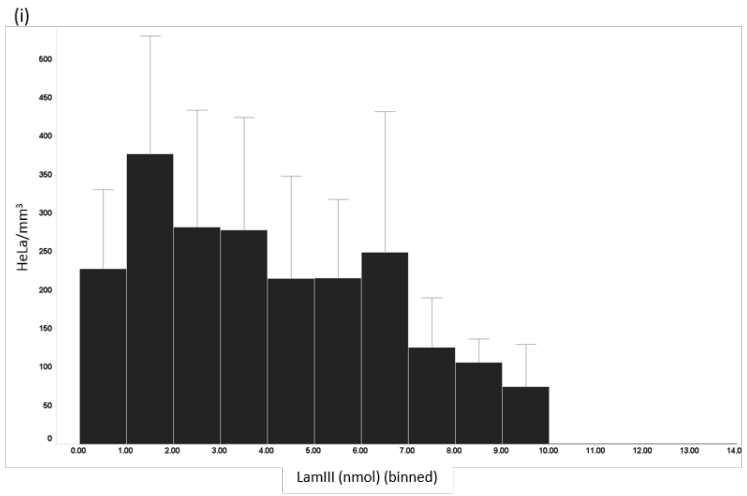
(i)
HeLa/mm³
LamIII (nmol) (binned)

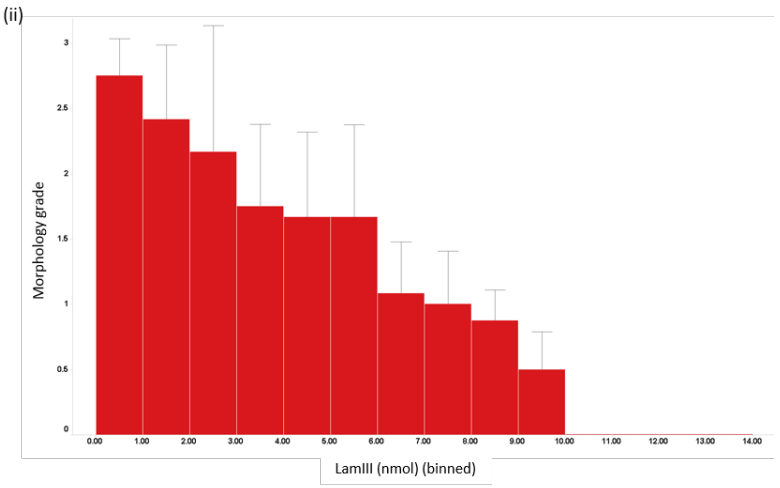
(ii)
Morphology grade
LamIII (nmol) (binned)

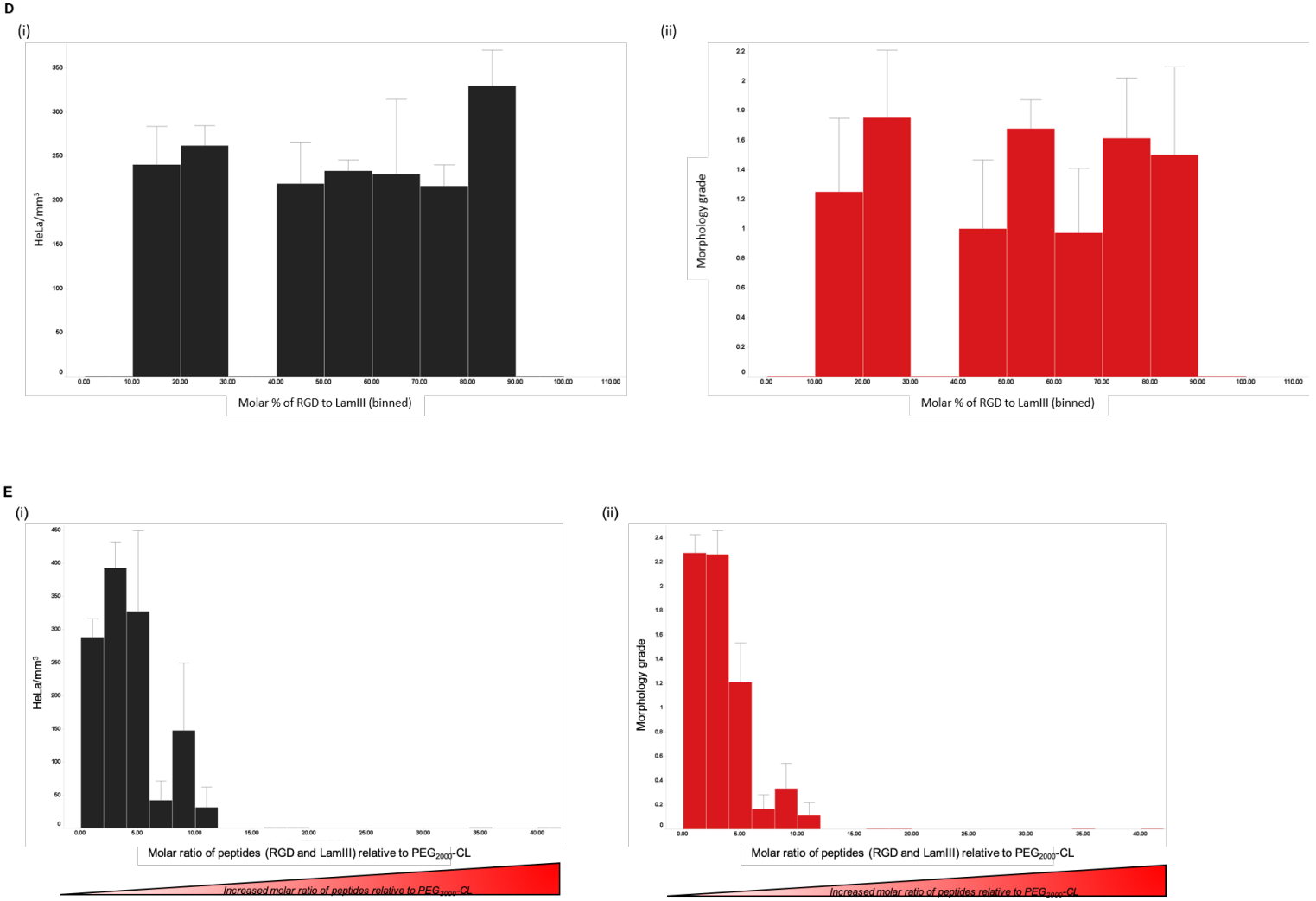
D
(i)
HeLa/mm³
Molar % of RGD to LamIII (binned)
(ii)
Morphology grade
Molar % of RGD to LamIII (binned)
E
(i)
HeLa/mm³
Molar ratio of peptides (RGD and LamIII) relative to PEG2000-CL
Increased molar ratio of peptides relative to PEG2000-CL
(ii)
Morphology grade
Molar ratio of peptides (RGD and LamIII) relative to PEG2000-CL
Increased molar ratio of peptides relative to PEG2000-CL

F

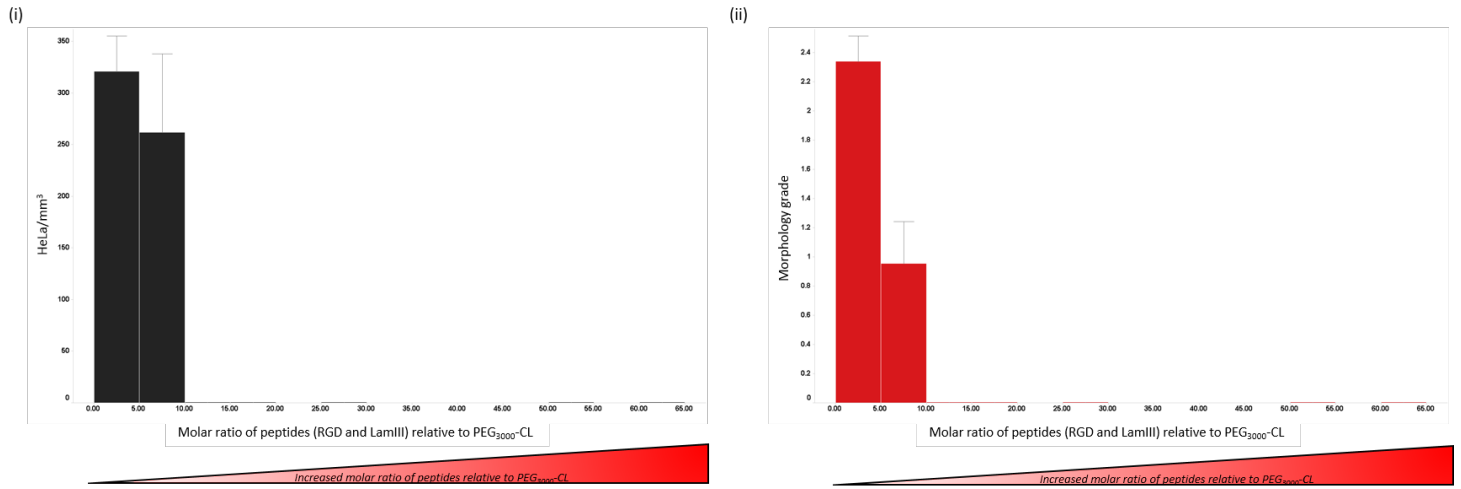
(i)
HeLa/mm³
350
300
250
200
150
100
50
0
0.00
5.00
10.00
15.00
20.00
25.00
30.00
35.00
40.00
45.00
50.00
55.00
60.00
65.00
Molar ratio of peptides (RGD and LamIII) relative to PEG3000-CL
Increased molar ratio of peptides relative to PEG3000-CL
(ii)
Morphology grade
2.4
2.2
2
1.8
1.6
1.4
1.2
1
0.8
0.6
0.4
0.2
0
0.00
5.00
10.00
15.00
20.00
25.00
30.00
35.00
40.00
45.00
50.00
55.00
60.00
65.00
Molar ratio of peptides (RGD and LamIII) relative to PEG3000-CL
Increased molar ratio of peptides relative to PEG3000-CL

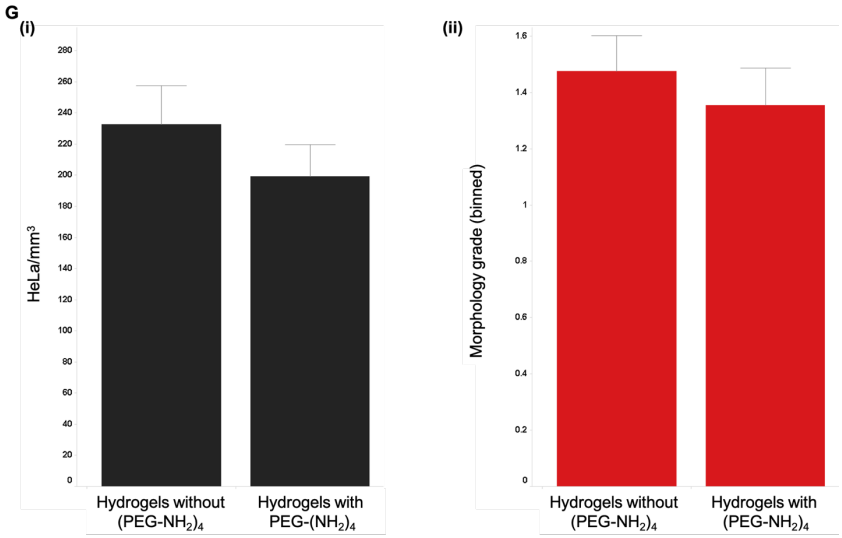

Figure 2.13: Hydrogels from the 250-member hydrogel array screen with HeLa analysed based on their component make-up. **A**. All combinations of hydrogels plotted as HeLa/mm^3 vs morphology grade. **B.** Combinations with RGD as the peptide component (i) HeLa/mm^3 vs RGD (nmol) (ii) morphology grade vs RGD (nmol). **C.** Combinations with LamIII as the peptide component (i) HeLa/mm^3 vs RGD (nmol) (ii) morphology grade vs RGD (nmol). **D.** Combinations with both RGD and LamIII as the peptide component (i) HeLa/mm^3 vs %mol RGD to LamIII (ii) morphology grade vs %mol RGD to LamIII. **E.** Combinations with PEG_{2000}-CL as the cross-linker (i) HeLa/mm^3 vs molar % ratio of peptide (RGD and/or LamIII) to PEG_{2000}-CL (ii) morphology vs molar % ratio of peptide (RGD and/or LamIII) to PEG_{2000}-CL. **F.** Combinations with PEG_{3000}-CL as the cross-linker (i) HeLa/mm^3 vs molar % ratio of peptide (RGD and/or LamIII) to PEG_{3000}-CL (ii) morphology vs molar % ratio of peptide (RGD and/or LamIII) to PEG_{3000}-CL. **G.** (i) HeLa/mm^3 and (ii) Morphology grade both plotted against combinations with or without $(PEG\text{-}NH_2)_4$. For all graphs binning of n = 10 was used and with ± s.e.m. See Appendix Table A1.1 for a full list of hydrogel compositions.

Based on the assessment of cells/mm^3 and hydrogel morphology, 82 hydrogels with a morphology grade ≥ 1 were chosen to fabricate a "hit array" and screened with HUVEC (see Appendix Table A1.2). After 24 h incubation, viability staining (FDA/PI) indicated that high viability was observed on most hydrogels (Figure 2.14, for all hydrogel features see Appendix Figure A1.2) with HUVEC encapsulation within the hydrogels ranging from 0–550 cells/mm^3 (see Appendix Figure A1.4 for individual results of all hydrogels). As with the HeLa array the effect of the different components on hydrogel morphology and cell attachment was analysed (Figure 2.15). Based on these results scale-up studies of identified "hit hydrogels" were carried out using both immortalised and primary HUVEC, as discussed in Chapter 3.

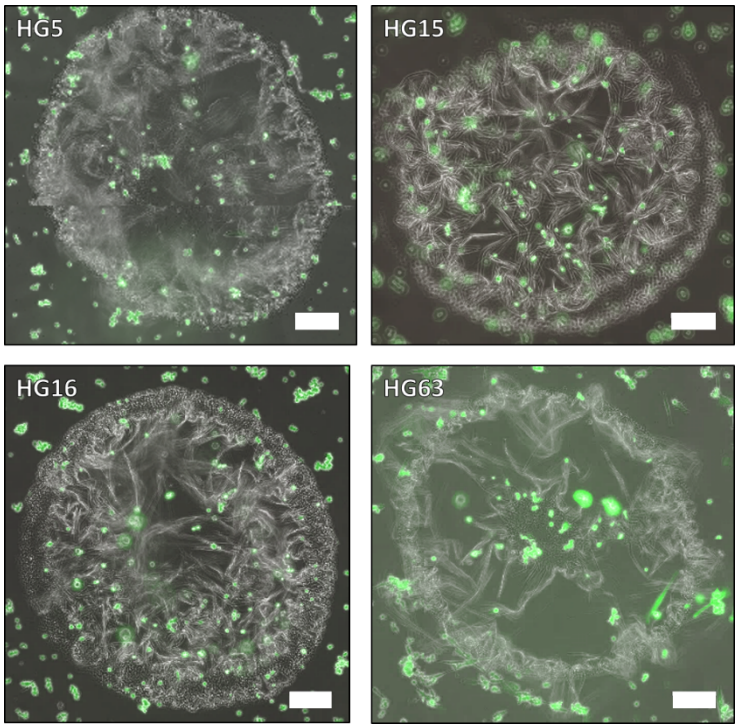

Figure 2.14: Examples of hydrogels from the 82-member hydrogel array screen with HUVEC cells incubated on the array for 18 h followed by viability staining with FDA (green, live stain, ($\lambda_{ex/em}$ = 490/514 nm) and PI (red, dead stain, $\lambda_{ex/em}$ = 570/602 nm). The merged images of the FDA, PI and bright field channels are shown. For images of all features see Appendix Figure A1.2.

A

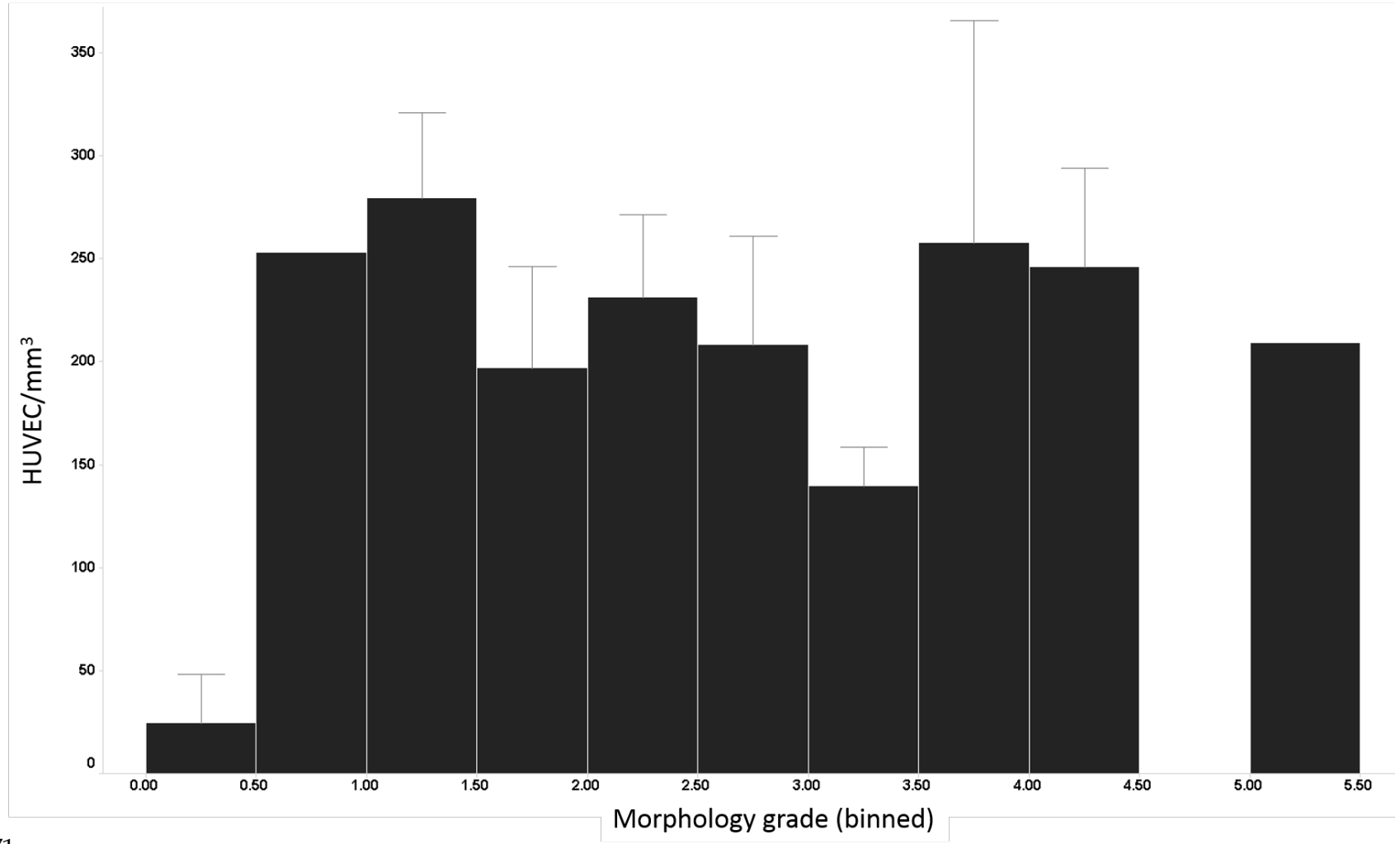
350
300
250
200
150
100
50
0
HUVEC/mm³
0.00
0.50
1.00
1.50
2.00
2.50
3.00
3.50
4.00
4.50
5.00
5.50
Morphology grade (binned)

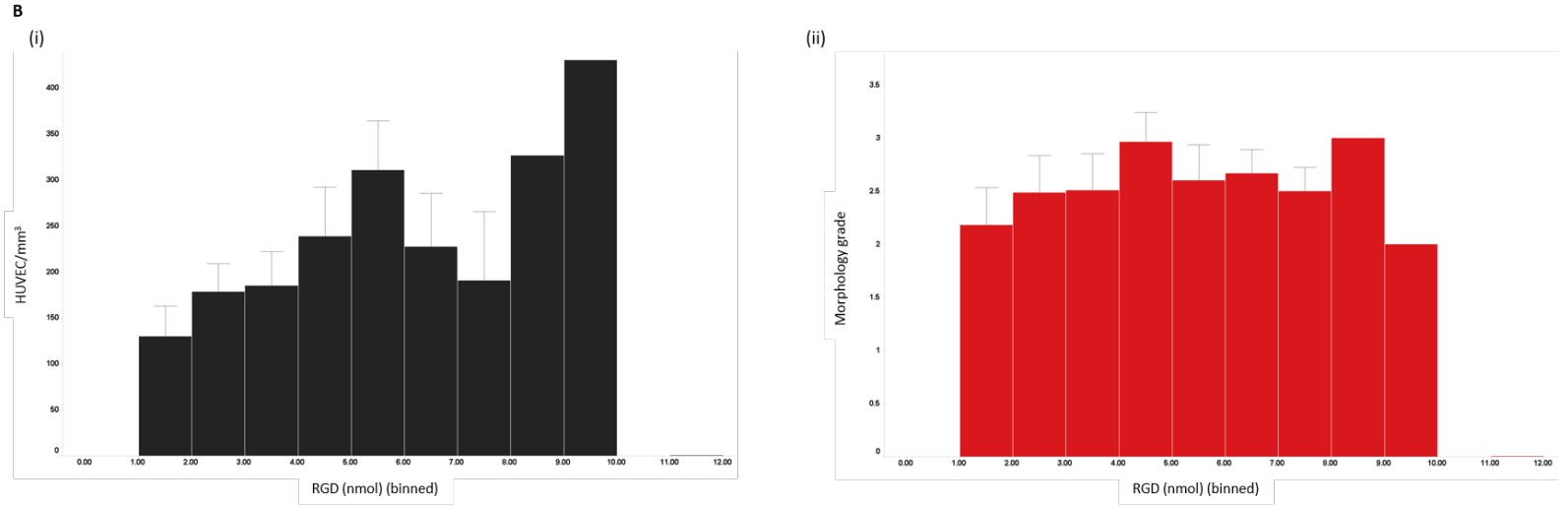
B
(i)
HUVEC/mm³
RGD (nmol) (binned)
(ii)
Morphology grade
RGD (nmol) (binned)

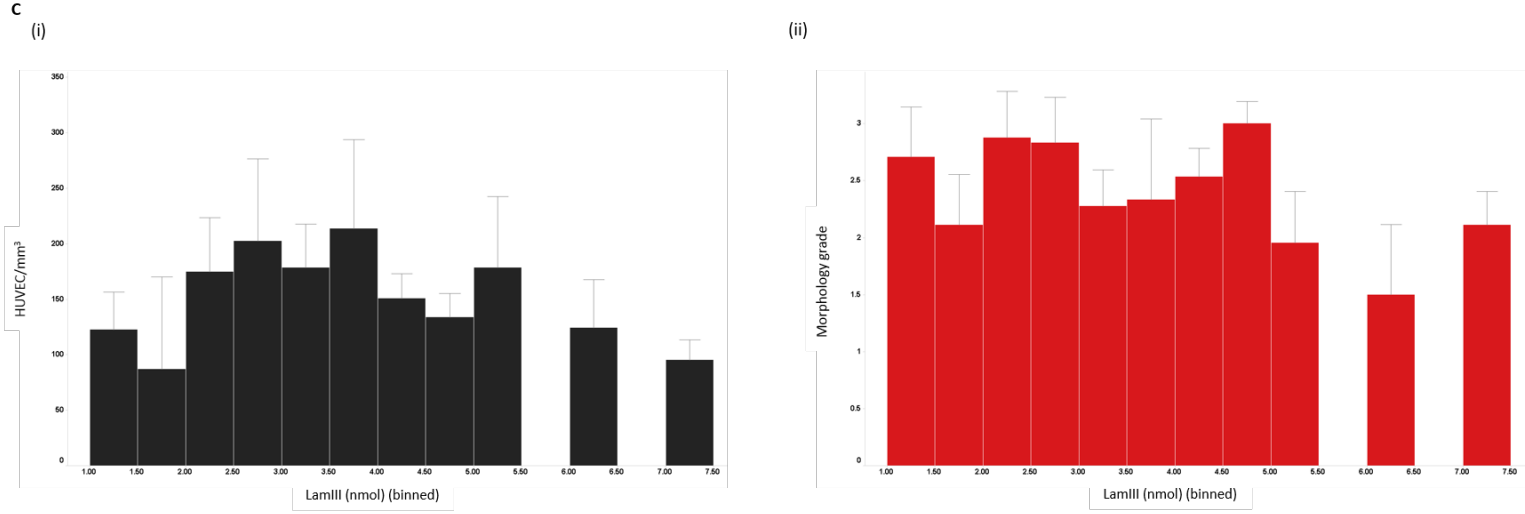
C
(i)
HUVEC/mm³
LamIII (nmol) (binned)
(ii)
Morphology grade
LamIII (nmol) (binned)

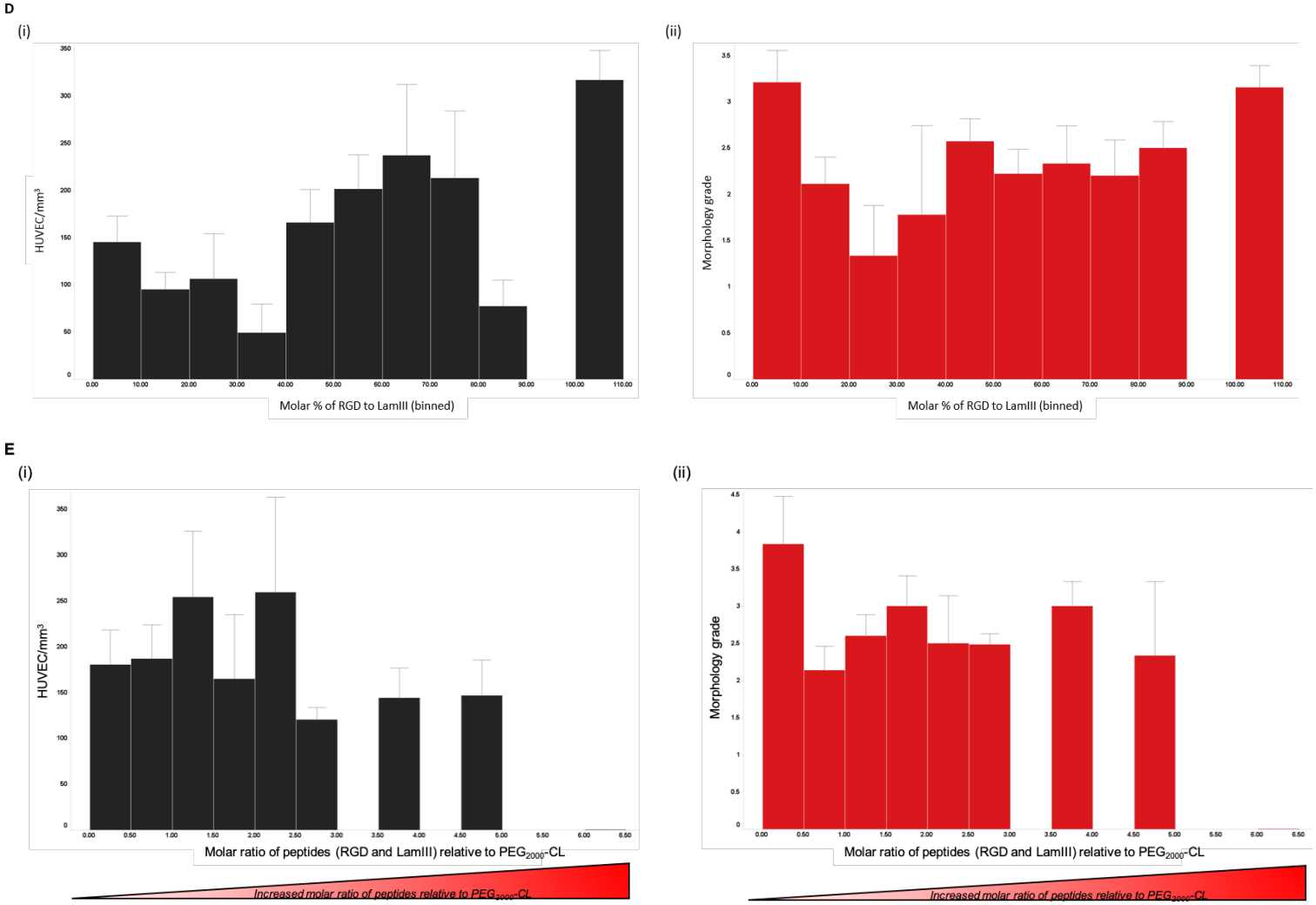
D
(i)
HUVEC/mm³
Molar % of RGD to LamIII (binned)
(ii)
Morphology grade
Molar % of RGD to LamIII (binned)
E
(i)
HUVEC/mm³
Molar ratio of peptides (RGD and LamIII) relative to PEG2000-CL
Increased molar ratio of peptides relative to PEG2000-CL
(ii)
Morphology grade
Molar ratio of peptides (RGD and LamIII) relative to PEG2000-CL
Increased molar ratio of peptides relative to PEG2000-CL

F

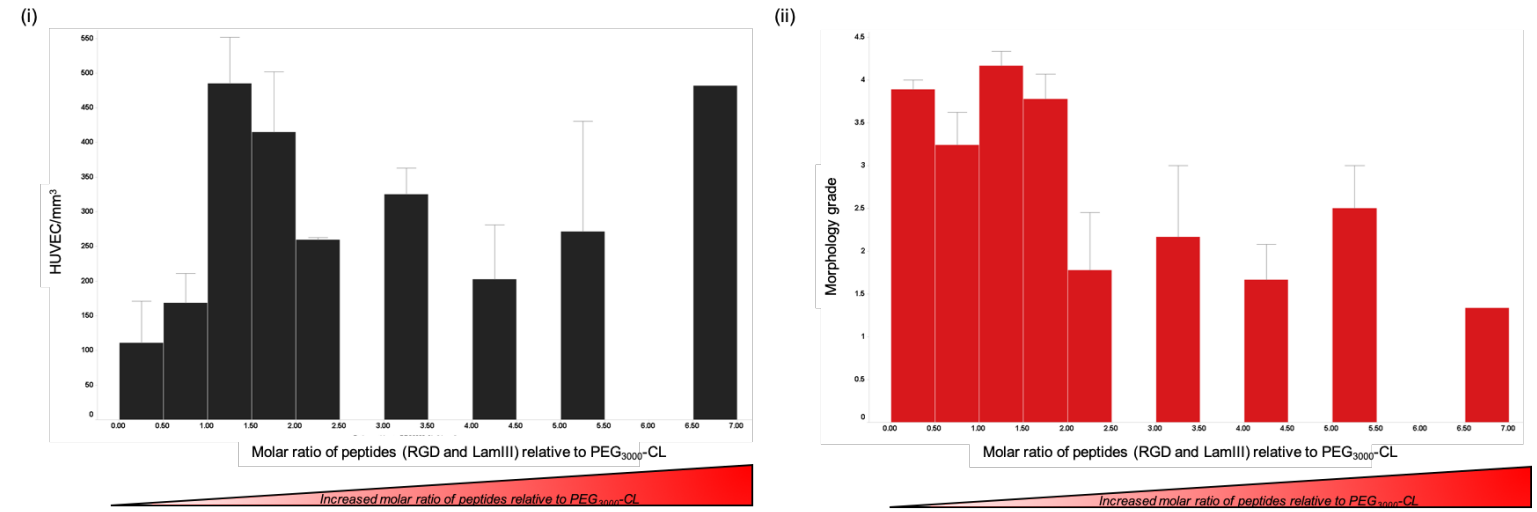
(i)
HUVEC/mm3
Molar ratio of peptides (RGD and LamIII) relative to PEG3000-CL
Increased molar ratio of peptides relative to PEG3000-CL
(ii)
Morphology grade
Molar ratio of peptides (RGD and LamIII) relative to PEG3000-CL
Increased molar ratio of peptides relative to PEG3000-CL

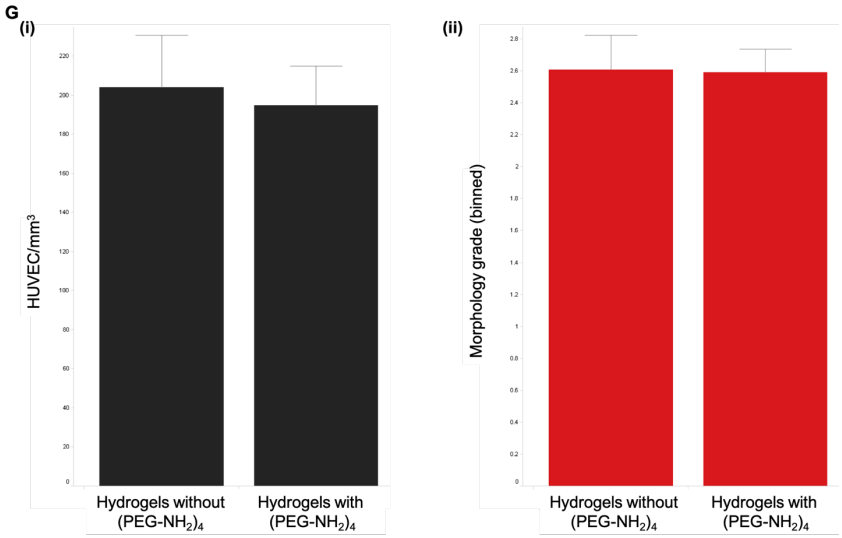

Figure 2.15: Hydrogels from the 82-member hydrogel array screen with HUVEC analysed based on their component make-up. **A.** All combinations of hydrogels plotted as HUVEC/mm^3 vs morphology grade. **B.** Combinations with RGD as the peptide component (i) HUVEC/mm^3 vs RGD (nmol) (ii) morphology grade vs RGD (nmol). **C.** Combinations with LamIII as the peptide component (i) HUVEC/mm^3 vs RGD (nmol) (ii) morphology grade vs RGD (nmol). **D.** Combinations with both RGD and LamIII as the peptide component (i) HUVEC/mm^3 vs %mol RGD to LamIII (ii) morphology grade vs %mol RGD to LamIII. **E.** Combinations with PEG_{2000}-CL as the cross-linker (i) HUVEC/mm^3 vs molar % ratio of peptide (RGD and/or LamIII) to PEG_{2000}-CL (ii) morphology vs molar % ratio of peptide (RGD and/or LamIII) to PEG_{2000}-CL. **F.** Combinations with PEG_{3000}-CL as the cross-linker (i) HUVEC/mm^3 vs molar % ratio of peptide (RGD and/or LamIII) to PEG_{3000}-CL (ii) morphology vs molar % ratio of peptide (RGD and/or LamIII) to PEG_{3000}-CL. **G.** (i) HUVEC/mm^3 and (ii) Morphology grade both plotted against combinations with or without $(PEG\text{-}NH_2)_4$. For all graphs binning of n = 10 was used and with ± s.e.m. See Appendix Table A1.2 for a full list of hydrogel composition

2.4 Discussion

In this chapter, the development of a hydrogel array, using reversible cross-linking, while allowing for 3D cell encapsulation has successfully been demonstrated. Using biologically relevant hydrogel components makes this system highly biocompatible, as indicated by the FDA/PI staining of the cells on the arrays. Hydrogels were formed by inclusion of ECM-based peptides (RGD and LamIII). The use of PEG-based cross-linkers was made because of their current wide use in biomaterials and proven biocompatibility.[142] Using materials already approved by regulatory bodies simplifies the potential future use of these materials for regenerative medicine or *in vivo* applications.

The initial formation of these hydrogels when tested in Eppendorf tubes occurred at quick time-scales (around 30 s, although this was concentration dependent) and formed under physiologically relevant conditions (pH 7, 37 °C). Their formation was also done in cell media, important for *in situ* cell encapsulation where cells can be suspended in one of the component solutions prior to hydrogel formation. Furthermore, the fact that the hydrogels were relatively clear facilitated their imaging. A common hurdle for 3D cell culture, whether using scaffolds or softer hydrogel structures, is the usually opaque nature of materials. This makes imaging in 3D difficult and thus limits their compatibility with methods such as fluorescence microscopy or high-throughput apparatus.

The presence of FBS in the cell media used for component solvation seemed to aid in hydrogel formation. However, it was later found that FBS caused detachment of hydrogel features from the glass slides used for array fabrication. FBS is a necessary supplement for conventional cell culture as it provides molecules necessary for cell growth, proliferation, metabolism and spreading.[143–145] Examples of these molecules include growth factors, hormones, lipids, minerals and transport proteins to name but a few. However, the animal-derived nature along with its poorly defined nature and batch-to-batch variability makes FBS a poor supplement to use for sensitive cell cultures where very little variability in components can be tolerated. In fact, FBS-free alternatives, such as KOSR used here has been, and are routinely, used for advanced

cell cultures such as for pluripotent stem cells.[146,147] Therefore, the incompatibility of FBS with the hydrogel array platform is not a major concern.

Surface functionalisation of the glass slides was necessary to allow for the hydrogels to anchor properly to the surface. The strategy used in this work is similar to the previously deployed strategies within the Bradley group using APTES functionalisation. However, the amide coupling strategy of forming the NHS-ester of perfluorooctanoic acid followed by EDC amide coupling with the primary amines of aminoalkylsilane-functionalised glass slides had not been utilised before. APTES functionalisation is usually done by overnight incubation, but the perflurooctanoic acid amide coupling only required one hour for completion, shortening the overall time for array fabrication.

The pattern designed for fabricating the hydrogel array by ink-jet techniques allowed for the printing of 96 features onto one glass slide. Although this is fewer features than previously reported by the Bradley group for ink-jet printed arrays, the need for printing larger features was necessary for several reasons. Firstly, it was found that printing smaller features (~ 250 μm in diameter) resulted in them detaching upon submerging the slide in cell media. Furthermore, it can be argued that to achieve 3D cell encapsulation larger features are necessary that allows for greater cell numbers per feature, and facilitate cell-cell interaction and communication characteristic for 3D cell environments. The hydrogels formed had diameters ranging from 0.8-1.5 μm and average heights of 200 μm. By assuming semi-ellipsoid geometries, the volume of each feature could be calculated, resulting in a range from around 250-500 nL (for more detail see Figure 3.3).

The hydrogels were very soft in nature, allowing the cells to migrate throughout the materials. To be able to assess the 3D cell behaviour during the array screen is very important when choosing which hydrogels to progress for scale-up and further experiments. Furthermore, the drying of features and rehydrating in cell media with cells eliminates the need for simultaneous array fabrication and cell seeding. This is favourable in terms of handling, storage and transport of the arrays, but would also facilitates future collaboration across labs and universities.

The initial screen of the 250-member hydrogel library with HeLa cells showed good cell compatibility of the majority of combinations of components printed with little to few dead cells. (see Appendix Figure A1.1 for FDA/PI staining of all features). Based on counting the number of viable cells per feature and considering the morphology grade given some conclusions could be made (Figure 2.13A-G, see also Appendix Figure A1.3 for graphs with cells/mm^3 and morphology grades of each feature). Firstly, a trend of combinations with higher morphology grade resulting in increased cell attachment was observed (Figure 2.13A), which was to be expected. Examining combinations only containing RGD (Figure 2.13B) or LamIII (Figure 2.13C) indicated that for combinations with RGD, cell attachment varied stochastically with increased RGD mol content and cell attachment dropping below 100 cells/mm^3 only above 13 nmol (Figure 2.13A-i). In contrast combinations with only LamIII showed cell attachment of ≤ 100 cells/mm^3 already at ≥ 7 nmol LamIII, indicating that higher levels of the LamIII peptide resulted in lower cell attachment compared to higher levels of the RGD peptide. Furthermore, a trend of higher mol content of LamIII resulting in poorer hydrogels was observed (Figure 2.13C-ii), while higher morphology scores were observed for similar levels of RGD content (Figure 2.13B-ii). In fact, out of the 60 compositions containing only RGD, 43 formed hydrogels while 17 combinations washed away upon media addition to the array. Out of the 60 combinations with only LamIII however, only 34 formed hydrogels, further suggesting that RGD facilitated hydrogel formation better than LamIII. The combinations containing both RGD and LamIII showed little variation in both cell attachment and morphology grades as the mol% of RGD to LamIII increased from 0-100 %(Figure 2.13D). The highest cell attachment was observed for combinations with 80-90 mol% RGD to LamIII, indicating higher cell attachment with the RGD peptide, although this was expected considering the integrin-binding motif of RGD (note that no combinations with 90-100 mol% RGD relative to LamIII were printed for this array).

For hydrogel combinations with either PEG_{2000}-CL or PEG_{3000}-CL as the cross-linker, clear cut-offs for hydrogel formation (indicated by morphology grade = 0) were observed (Figure 2.13E-ii and 2.13F-ii). At molar ratios between the cross-linker and peptide(s) (RGD and or LamIII) of ≥ 1:12 and ≥ 1:10 for PEG_{2000}-CL or PEG_{3000}-CL

respectively no hydrogels formed. Consequently, the cell attachment also decreased for both cross-linkers as the molar ratio of peptide to cross-linker increased (Figure 2.13E-i and 2.13F-i). Thus, any further hydrogel formation with these components should use molar ratios between cross-linker and peptide below those identified herein. Combinations with or without $(PEG\text{-}NH_2)_4$ showed similar levels of both cell attachment and morphology (Figure 2.13G), suggesting that increased amount of the tetra-cross-linker would be necessary for future arrays to gain further feature stability.

For the HUVEC screen of 82 hydrogel features identified in the HeLa screen, high levels of viability were also observed (Figure 2.14, see Appendix Figure A1.2 for FDA/PI staining of all features) and doing similar analysis of component effect on cell attachment as for the HeLa screen revealed that cell attachment was similar across morphology grades (Figure 2.15A) apart from those with morphology grade < 0.5. It should also be noted that although the hydrogels for the "hit array" were chosen based on having morphology grade ≥ 1 in the HeLa screen some hydrogels did exhibit lower morphology grades in the HUVEC screen. This could be due to the different media used for this screen (Medium 200) compared to the HeLa screen (DMEM) seeing as a stabilising effect on hydrogels due to the media composition is possible. It could also, however, indicate that hydrogels do not form identical each time on the glass slide, particularly when the structures are relatively poor.

No clear trends to hydrogels with either only RGD or LamIII as the peptide component or those with both peptides (Figure 2.15B-D) was observed in terms of HUVEC attachment or hydrogel morphology. For the "hit array" only hydrogels with a molar ratio of cross-linker to peptide(s) < 1:10 were chosen for both PEG_{2000}-CL and PEG_{3000}-CL (Figure 2.15E-F). The main discernible trend for these combinations was the higher morphology grade of hydrogels with molar ratio of peptide(s) to PEG_{3000}-CL ≤ 1:2. Finally, as with the HeLa screen, no effect on cell attachment or morphology grade was observed for hydrogels containing $(PEG\text{-}NH_2)_4$ compared to those that did not (Figure 2.15G).

Overall, the results in this chapter demonstrated the successful screen of novel imine cross-linked hydrogels and the powerful use of the inkjet printing platform for array

fabrication and HTS to find which combinations of components that formed stable hydrogel features and their capacity for cell encapsulation. The subsequent "hit array" screen with HUVEC identified novel 3D matrices that could support endothelial 3D cell culture (discussed further in Chapter 3).

2.5 Conclusions

A new method for the array fabrication of dynamic imine cross-linked hydrogels as novel cell culture matrices was developed, adding to the already vast family of polymer-based microarrays developed within the Bradley group. Using a combination of ECM-based peptides and PEG-based cross-linkers, 250 different dynamic hydrogels were fabricated (formed via reversible imine bond formation) and screened with HeLa cells to assess the feature stability and cell compatibility. Further screening of a "hit array" of 82 hydrogels with HUVEC enabled the selection of materials to scale-up for further studies (see Chapter 3). Overall, the results demonstrate the capacity of these imine cross-linked hydrogels to form stable 3D cell culture matrices that enable 3D cell encapsulation. Considering their facile high-throughput fabrication, ease of handling and efficient cell encapsulation, this approach is highly attractive for a range of future cell-based applications.

2.6 Materials and Methods

2.6.1 Instruments used for array fabrication

Scienion S5 SciFLEXARRAYER equipped with a Piezo Dispense Capillary PDC 80 with a 50 µm aperture (Scienion AG, Germany)

2.6.2 Instruments for cell experiments and analysis

HERAcell 150 incubator (Heraeus, Germany)

HERAsafe KS 18 class II biosafety cabinet (Heraeus, Germany)

2.6.3 Imaging instruments

Axiovert 200m inverted fluorescence microscope with Axiovision 4.8 software (Carl Zeiss AG, Germany). Filters: DAPI ($\lambda_{ex/em}$ = 300-395/430-505 nm), GPC/FITC ($\lambda_{ex/em}$ = 447-494/500-554 nm), YPF ($\lambda_{ex/em}$ = 490-512/520-554 nm), TRITC/Rhodamine/Cy3 ($\lambda_{ex/em}$ = 527-563/570-650 nm) and Cy5 ($\lambda_{ex/em}$ = 620-659/663-725 nm) filters. Magnification: x10, x20 and x40

Leica SP5 confocal microscope (Leica Camera AG, Germany)

Image analysis was carried out in ImageJ

2.6.4 Instruments for characterisation and purification

Agilent 1100 ChemStation analytical RP-HPLC (Agilent, USA) with a Zorbax Eclipse C18 reverse phase column (4.6 mm × 100 mm, 3.5 µ) with an evaporative light scattering and a multi-wavelength detector eluting with a gradient of water to acetonitrile (5 – 95 %), both with 0.1% formic acid with a flow rate of 1 mL/min

Agilent 1100 GPC equipped with a PLgel MIXED-C columns and a RI detector eluting with DMF containing 0.1M LiBr at 60 °C at 1 ml/min (Agilent, USA)

Isolera One equipped with a Biotage® SNAP HP-BioSphere C18 10 g column detection at 250 nm, eluting with a gradient of water to acetonitrile, both with 0.1 % formic acid with a flow rate of 12 ml/min (Biotage, Sweden)

BenchTop Pro with Omnitronics lyophiliser (SP scientific, USA)

^{1}H NMR at 500 MHz Bruker AVA 500 (Bruker, USA)

Bruker Tensor 27 Standard System FT-IR spectrophotometer (Bruker, USA)

HRMS on a Bruker 3.0 T Apex II spectrometer (Bruker, USA)

2.6.5 Chemicals

All protected amino acids, aminomethyl polystyrene resin, and the Fmoc-Rink amide linker were purchased from GL Biochem Ltd (Shanghai) or NovaBiochem. Poly(ethylene oxide), 4-arm, amine terminated ($(PEG\text{-}NH_2)_4$) (M_n = 10 000 g/mol), was purchased from Sigma Aldrich. All other chemicals were from Sigma Aldrich or Acros, and used as received.

2.6.6 Cells, media and biological equipment

HUVEC were donated by Dr Kate Cameron (University of Edinburgh)

Complete DMEM: DMEM, 10% v/v FBS, 1% v/v penicillin/streptomycin and 1% v/v 200 mM glutamine

Complete Medium 200: Medium 200, Low Serum Growth Supplement (LSGS) kit (Thermo Fisher, USA)

2.6.7 Cell Culture on Tissue Culture Polystyrene

HeLa cells were cultured in complete DMEM. HUVEC were cultured in complete Medium 200. Cells were grown to 70–80% confluency in T25 flasks (37 °C, 5% CO_2) before passaging. HUVEC were used between passage 5–9.

2.6.8 Synthesis of PEG_{2000}-CL

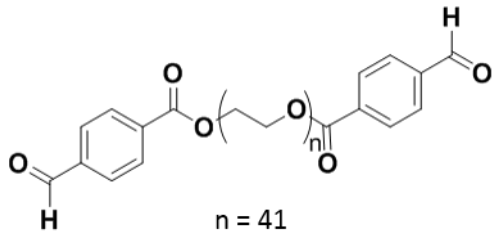

4-Formylbenzoic acid (600 mg, 4 eq.), DCC (1.03 g, 5 eq.) and DMAP (489 mg, 4 eq.) were dissolved in anhydrous THF (140 mL, 0.1 M) and stirred at room temperature under a N_2 stream for 15 min. Poly(ethylene glycol) (M_n = 2000 g/mol) (2.0 g, 1 eq.) was added to the reaction mixture and stirred at room temperature under N_2 overnight. The reaction mixture was concentrated *in vacuo* and the residue was dissolved in MeOH (the minimal volume required). The product was precipitated by the addition of diethyl ether followed by centrifugation and decanting (repeated thrice). The precipitate was dissolved into deionised water (50 mL) and freeze-dried to obtain the product as a white waxy solid (1.53 g, 77 %). ^{1}H NMR (500 MHz, $CDCl_3$) δ 10.13 (s, 2H, CHO), 8.24 (d, *J* = 8.3 Hz, 4H, C<u>H</u>CCHO), 7.98 (d, *J* = 8.0 Hz, 4H, C<u>H</u>CHCCHO), 4.56 – 4.51 (m, 4H, $COOCH_2$), 3.90 – 3.85 (m, 4H, $COOCH_2C\underline{H_2}$), 3.68 – 3.64 (m, 160H, $OC\underline{H_2}C\underline{H_2}O$). IR (neat) ν ($cm^{-1}$) = 2880, 1705, 1466, 1096.

2.6.9 Synthesis of PEG_{3000}-CL

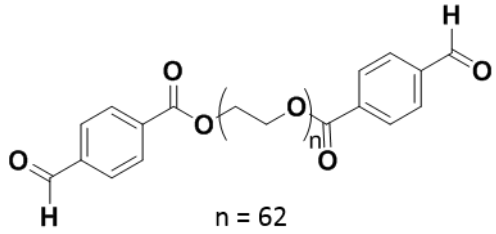

The method was as for PEG_{2000}-CL. Amounts and equivalents used: 4-Formylbenzoic acid (400 mg, 4 eq.), DCC (688 mg, 5 eq.) and DMAP (326 mg, 4 eq.), Poly(ethylene glycol) (M_n = 3000 g/mol) (2.0 g, 1 eq.), anhydrous THF (90 mL, 0.1 M). Yield: 1.41 g, 70 %. ^{1}H NMR (500 MHz, Chloroform-*d*) δ 10.09 (s, 2H, CHO), 8.20 (d, *J* = 7.9 Hz, 4H, C<u>H</u>CCHO), 7.94 (d, *J* = 7.9 Hz, 4H, C<u>H</u>CHCCHO), 4.55 – 4.51 (m, 4H, $COOCH_2$), 3.88 – 3.85 (m, 4H, $COOCH_2C\underline{H_2}$), 3.63 (s, 268H, $OC\underline{H_2}C\underline{H_2}O$). IR (neat) ν ($cm^{-1}$) = 2877, 1701, 1466, 1099.

2.6.10 Solid Phase Peptide Synthesis

H-Ahx-GRGDSK-NH_2 (RGD) and H-Ahx-YIGSRK-NH_2 (LamIII) were synthesised on solid-phase using the Fmoc/^{t}Bu route.[148] The Fmoc-Rink amide linker was coupled to the aminomethyl polystyrene resin (1 g, loading 0.745 mmol/g) prior to peptide synthesis.

Coupling of the protected Rink linker and protected amino acids. Fmoc-Rink or Fmoc-protected amino acids (3 eq.) and Oxyma (3 eq.) were dissolved in DMF (1 M) and stirred for 5 min followed by the addition of DIC (3 eq.) and further stirred for 5 min. The mixture was added to the resin and shaken at room temperature for 1 hour. The resin was washed with DMF, MeOH and DCM.

Fmoc deprotection. The *N*-Fmoc protected peptide on the resin was treated twice with 20 % piperidine in DMF for 10 minutes. The resin was subsequently washed with DMF, MeOH and DCM.

Deprotection of the peptide and cleavage off the resin. TFA/H_2O (95:5) was added to the pre-swollen resin (in DCM) and shaken at room temperature for 3 h. The peptide was precipitated from the filtrate by the addition of cold diethyl ether, collected by centrifugation and washed twice with ether. The peptides were re-dissolved in H_2O (10 mL) and purified by RP-HPLC (Biotage Isolera) (5% to 20 % MeCN/H_2O over 20 min, 20 % to 95 % MeCN/H_2O over 5 min, 95 % MeCN/H_2O over 1 min and 95 % to 5 % MeCN/H_2O over 1 min) followed by lyophilisation. RGD (480 mg, 88 %). LamIII (375 mg, 60 %). The peptides were analysed by RP-HPLC were > 95 % purity and HRMS (RGD $m/z_{\text{calculated}}$ 730.4086, m/z_{found} 730.4127, LamIII $m/z_{\text{calculated}}$ 834.5076, m/z_{found} 835.5146).

2.6.11 Hydrogel bulk formation

Solutions of RGD (5% w/v), LamIII (5 or 15% w/v), PEG_{2000}-CL (10 or 30% w/v), PEG_{3000}-CL (30% w/v) and $(PEG\text{-}NH_2)_4$ (10% w/v) were prepared in complete DMEM or in FBS-free DMEM. The components were gently mixed (see Table 2.1) (total volume 30 or 40 µL), and allowed to stand for 30 s at room temperature to allow hydrogel formation. Hydrogel stability was assessed after 30 s at room temperature

and after 1 h and 24 h incubation at 37 °C. The pHs of the hydrogels were evaluated using pH paper.

2.6.12 HeLa cell encapsulation in an imine cross-linked hydrogel

(2.5 % RGD, 2.5 % LamIII and 15 % PEG_{2000}-CL)

HeLa cells (1.25×10^6) were suspended in 2 mL of CellTracker® Red CMTPX (1 µL of 10 mM stock in DMSO diluted with 2 mL serum-free DMEM) ($\lambda_{ex/em}$ = 577/602 nm) for 10 min (37 °C, 5% CO_2) followed by centrifugation (1500 rpm, 5 min) and removal of staining the solution. The cell pellet was dissolved in 2 mL Hoechst staining solution (1 µL of 10 mg/mL stock diluted into 10 mL PBS) ($\lambda_{ex/em}$ = 361/497 nm) and incubated for 15 min (37 °C, 5% CO_2) followed by centrifugation (1500 rpm, 5 min), removal of the supernatant and resuspension in 2 mL of media. Pre-stained HeLa cells (50 000 cells per hydrogel) were suspended in the LamIII solution (25 µL). Hydrogels (n = 3) prepared in a 96-well plate by mixing RGD (5 % w/v in FBS-free DMEM, 25 µL/well), LamIII (10 % w/v in FBS-free DMEM, 25 µL/well, with 50 000 HeLa cells) and PEG_{2000}-CL (30 % w/v in FBS-free DMEM, 50 µL/well). Following incubation (37 °C, 5% CO_2) for 48 h imaging was carried out on a Leica SP5 confocal microscope.

2.6.13 Inkjet printing with Scienion S5 SciFLEXARRAYER

All printing was carried out in HPLC-grade water using a voltage range of 95-100 V and a pulse range of 45-50 µs, with droplet volumes of ~ 300 pl/drop. The pitch distance between the adjacent spots was 0.6 × 0.6 mm. Glass slides were either microscope glass slides slides (76 × 26 mm) (Menzel GmbH Co. KG, Braunschweig, Germany) or SilanePrep aminoalkylsilane-functionalised glass slides (76 × 26 mm) (SigmaAldrich).

2.6.14 Optimisation of array printing patterns

i) 1×1 printing pattern

Aqueous solutions of LamIII (2.5 or 5 % w/v) and PEG_{2000}-CL (2.5 or 5 % w/v) were printed onto microscope glass slides. The 5 % solutions were too viscous to print so

2.5 % solutions were used. LamIII and PEG_{2000}-CL solutions were printed sequentially at varying ratios (1000 drops total per feature) (n = 3). Following drying at 40 °C overnight, the slides were submerged in FBS-free DMEM.

ii) 2×2 printing pattern

Aqueous solutions of LamIII and PEG_{2000}-CL were printed onto the slides as above in varying ratios. Each feature was made-up of four spots printed as a 2×2 square (400 drops/spot) that merged when printed (see Figure 2.9). Following drying at 40 °C overnight, FBS-free DMEM was printed on top of each feature, resulting in hydrogel formation. The slide was then submerged in FBS-free DMEM.

2.6.15 Optimisation of glass slide surface functionalisation

i) Microscope glass slide with a flurosilane coating

Microscope glass slides were plasma treated with an O_2 plasma for 10 minutes at 1.5 bar oxygen pressure. 20 features of aqueous sucrose (20 % w/v) were printed onto the slides with each feature printed as a 2×2 square (100 drops per spot) that merged when printed (See Figure 2.9). After drying at room temperature, tridecafluoro-1,1,2,2-tetrahydrooctyl-dimethylchlorosilane (FDS) (5 µl/slide) was dropped onto five different areas of the slides (1 µl/drop) and reacted overnight in a sealed Tupperware box followed by washing of the slides with acetone (10 mL) and water (10 mL). The dried slides were coated with (3-aminopropyl)triethoxysilane (APTES) (10 µl/slide) by spreading with a pipette tip, and put into a sealed box, reacted overnight and then washed with water and ethanol before drying under N_2 stream. Aqueous solutions of LamIII (2.5 % w/v) and PEG_{2000}-CL (2.5 % w/v) were printed sequentially in varying ratios in the previously sucrose-masked 2×2 squares (400 drops/spot). Following drying overnight at 40 °C, the slide was submerged in FBS-free DMEM or complete DMEM.

ii) Aminoalkylsilane-functionalised microscope glass slide

Solutions of LamIII and PEG_{2000}-CL were printed onto aminoalkylsilane functionalised glass slides (Sigma Aldrich) as 2×2 square features as described above. Following drying overnight in a 40 °C oven, the slide was submerged in FBS-free DMEM or complete DMEM.

iii) Aminoalkylsilane-functionalised microscope glass slide with perfluorooctanoic acid functionalisation

Features of 20% aqueous sucrose (w/v) were printed on aminoalkylsilane functionalised glass slides as 2×2 square features as explained above, and dried at 40 °C for 2 h. Perfluorooctanoic acid (2.0 g, 4.8 mmol), EDC·HCl (926 mg, 4.8 mmol) and DIPEA (5.1 mL, 29 mmol) were dissolved in DCM (200 mL) and stirred for 5 min. *N*-hydroxysuccinimide (556 mg, 4.8 mmol) was added and the mixture was stirred at room temperature for 45 min (final reaction concentration 0.2 M). The dried glass slides were immersed into this mixture and gently shaken for 1 h. The slides were washed with DCM, water (to remove the sucrose features) and ethanol. Following drying at room temperature, the slides were submerged in FBS-free DMEM or complete DMEM.

2.6.16 HeLa incubation on test array

Aminoalkylsilane glass slides without perfluorooctanoic acid functionalisation

30 features (n = 3) of different ratios of aqueous solutions of RGD, PEG_{2000}-CL and $(PEG\text{-}NH_2)_4$ (all 2.5 %) (see compositions HG1- HG30 in Appendix Table A1.1) were printed on aminoalkylsilane functionalised glass slides. Each feature was printed as a 2×2 square as described above. Following drying at 40 °C overnight, the hydrogel arrays were sterilised under UV light for 45 min using the UV source of a HERAsafe KS 18 class II biosafety cabinet (Heraeus, Germany) and then placed in 4-well slide dish (Nunc™). HeLa cells (525 000 cells/array) in 5 mL of DMEM (supplemented with 10% knock-out serum, 1% penicillin/streptomycin and 1% 200 mM glutamine) were added to each slide, resulting in *in situ* formation of hydrogels with cell encapsulation. Following incubation overnight (37 °C, 5 % CO_2) the DMEM was removed, the slides washed with PBS (1×5 mL) and stained with Fluorescein diacetate (FDA) and propidium iodide (PI). 8 µL of FDA stock solution (5 mg/mL in acetone) and 50 µL of PI stock solution (2 mg/mL in PBS) were added to 5 mL of serum-free DMEM and added to each slide and incubated for five minutes in the dark at room temperature. The solution was removed, the slides washed with PBS (1 × 5 mL) and covered in serum-free DMEM (5 mL). The hydrogels were imaged using a Zeiss

AxioVert 200m fluorescence microscope. Microscope lasers settings were: $\lambda_{ex/em}$ = 447-494/500-554 nm for FDA, $\lambda_{ex/em}$ = 527-563/570-650 nm for PI.

2.6.17 Hydrogel Array fabrication

i) Preparation of masked glass slides

96 features of 20% aqueous sucrose were printed on aminoalkylsilane functionalised glass slides using a sciFLEXARRAYER S5 printer (16 rows × 6 columns). Each feature was printed as a 2×2 square (400 drops/spot) as described above. The slides were dried at 40 °C for 2 h and functionalised with perflurooctanoic acid as described above.

ii) Inkjet-printed hydrogel arrays

2.5% solutions of peptides (RGD and LamIII), cross-linkers (PEG_{2000}-CL, PEG_{3000}-CL) and $(PEG\text{-}NH_2)_4$ were prepared in water and ink-jet printed on the masked glass slides. By varying the ratios of the components 32 different combinations (n = 3) were printed on each slide (96 features per slide). The slides were dried at 40 °C overnight, irradiated under UV light for 1h and stored at room temperature until use. For the hydrogel compositions on each array, see Appendix Tables A1.1 and A1.2.

2.6.18 Encapsulation of cells on hydrogel arrays

The hydrogel arrays were sterilised under UV light for 45 min and placed in 4-well slide dish (Nunc™). HeLa cells (500 000 cells/array) in 5 mL of DMEM (supplemented with 10% knock-out serum, 1% penicillin/streptomycin and 1% 200 mM glutamine) were added to each slide, and incubated for 24 h (37 °C, 5% CO_2) after which media was removed and the slides were stained with fluorescein diacetate (FDA) and propidium iodide (PI) as above and imaged with a Zeiss AxioVert 200m fluorescence microscope. For HUVEC (300 000 cells/slide), the encapsulation, incubation, and staining was carried out in complete Medium 200.

Chapter 3: Identification and scale-up of an imine cross-linked hydrogel that supports endothelial cell maintenance and proliferation

3.1. Introduction

The power of a HTSS platform is only truly realised if the materials used can be scaled-up to allow for larger and long-term studies to confirm and expand upon the results found in the HTSS. Therefore, it was necessary to develop a strategy for scaling some of the "hit" hydrogels from the array screen described in Chapter 2.

When it comes to cell behaviour and hydrogels many parameters must be considered. Importantly, maintenance of cell viability in the presence of the material is crucial, as is demonstrating that the gene and protein expression profiles of the cell of interest displays the desired properties as an effect of hydrogel encapsulation/incubation. Hydrogels can be used to create both cultures to maintain cells in their original state e.g. maintain pluripotency of stem cells, or that causes a desired change in cell phenotype e.g. directed stem cell differentiation. In addition, if 3D cell encapsulation is enabled within the hydrogel, the cellular behaviour and organisation should be considered, to analyse the specific 3D cell construct generated and their differences in gene and protein expression, cell polarity and heterogeneity etc. compared to traditional monolayer culture. [17,51,149,150]

To demonstrate that the imine cross-linked hydrogels developed in this thesis were tuneable for different cell types, both immortalised HUVEC (referred to here as HUVEC) and primary HUVEC sourced from a single donor (referred to here as pHUVEC) were used. HUVEC are routinely used as a model for the angiogenic function of endothelial cells.[151,152] HUVEC and pHUVEC differ in their *in vitro* behaviour however, with HUVEC capable of growing on TCPS over many passages (> 20) and are recognised by their cobble like shape and organisation (Figure 3.1A)[151].

pHUVEC, on the other hand, are directly obtained from human donors. When cultured as a monolayer they are more rounded and less spread out compared to HUVEC (Figure 3.1B), and it is recommended that they are only kept in culture for a few passages (< 5), with their gene and protein expression profile changing due to the 2D *in vitro* culture conditions.[153]

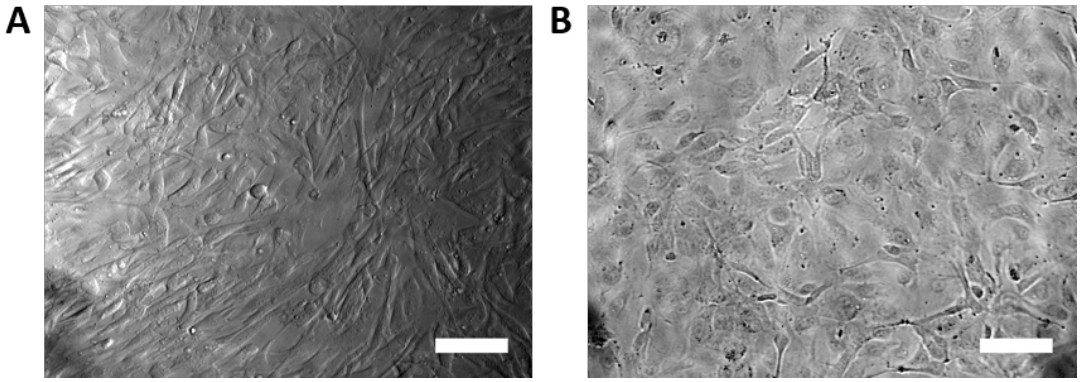

Figure 3.1: Bright-field images of **A.** Immortalised HUVEC. **B.** Primary HUVEC. Scale bar 100 μm.

In this chapter is presented the scale-up studies of identified hit hydrogels from the screen in Chapter 2. After optimisation of the platform in which the hydrogels were formed, several parameters relating to cell behaviour were analysed, including cell viability, protein levels and gene expression and scanning electron microscopy (SEM) characterisation. Furthermore, material characterisation by rheology was carried out.

3.2 Choosing hydrogels for scale-up

After the hit hydrogel array screening with HUVEC (see Chapter 2), it was decided to scale up eight hydrogels (HG2, HG5, HG6, HG7, HG15, HG16, HG63 and HG80, see Appendix Table A1.2 for printing patterns) based on their hydrogel morphology grade and number of cells/mm^3. The eight hydrogels chosen all had morphology grades ≥ 3, apart from HG80 (grade 1.75), which was chosen based on its number of HUVEC/mm^3 (Figure 3.2).

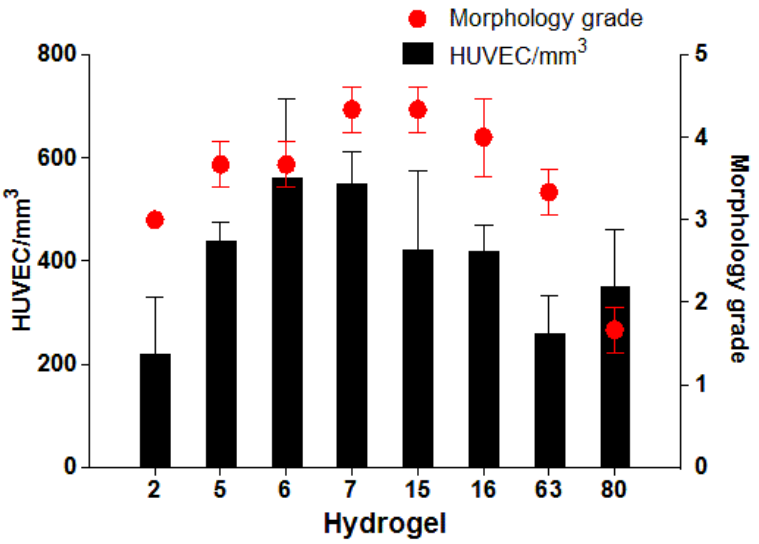

Figure 3.2: Hydrogels chosen for scale-up from the HUVEC hydrogel array screen. Left axis is the number of HUVEC encapsulated per mm^3 on each hydrogel (black bars). Right axis is plotted the morphology score (scale 0-5, with 5 being the highest) (red dots). Mean with ±SEM is plotted in each instance, n = 3.

The five components used for hydrogel array fabrication were all represented in the hits. All hits contained the RGD peptide, and six out of the eight (HG6, HG7, HG15, HG16, HG63 and HG80) contained both RGD and PEG_{3000}-CL, indicating the favourability of the RGD and PEG_{3000}-CL to form hydrogels with good morphology and high level of cell encapsulation. By approximating the hydrogel volume to that of a semi-ellipsoid as in Chapter 2 (see Figure 2.11), the % w/v of each hydrogel could be calculated (Table 3.1). The radii of each feature were measured by analysing their bright field images in ImageJ with the height of each hydrogel was estimated to be 200 μm. This was chosen as an average height after measuring the height of features in the z-plane when imaging the hydrogel arrays.

Table 3.1: Composition of hydrogels chosen for scale up as % w/v. The volume of each feature was estimated as a semi-ellipsoid (see Figure 2.11) The mass printed of each component was known from the number of spots printed (see Appendix Table A1.2, ~300 pl/drop, 2.5 % w/v).

Hydrogel	Composition	
	Component	*% (w/v)*
HG2	RGD	1.1
	PEG_{2000}-CL	1.9
	$(PEG\text{-}NH_2)_4$	0.4
HG5	RGD	1.3
	PEG_{2000}-CL	5.6
	$(PEG\text{-}NH_2)_4$	0.8
HG6	RGD	3.3
	PEG_{3000}-CL	7.2
HG7	RGD	2.5
	PEG_{3000}-CL	7.6
HG15	RGD	2.4
	PEG_{3000}-CL	5.4
	$(PEG\text{-}NH_2)_4$	1.0
HG16	RGD	1.3
	PEG_{3000}-CL	4.0
	$(PEG\text{-}NH_2)_4$	0.7
HG63	RGD	1.0
	LamIII	1.0
	PEG_{3000}-CL	4.3
HG80	RGD	1.3
	LamIII	1.3
	PEG_{3000}-CL	5.8
	$(PEG\text{-}NH_2)_4$	1.0

3.3 Scanning electron microscopy analysis

To investigate the interaction between cells and hydrogels in more detail dry scanning electron microscopy (SEM) was carried out. The eight hit hydrogels were printed onto masked aminoalkylsilane glass slides followed by HUVEC encapsulation over 24 h. For SEM sample preparation, the cells were fixed and thereafter post-fixed with Osmium tetroxide (OsO_4) for improved contrast. The hydrogels were then dehydrated in graded concentrations of acetone followed by critical point drying with liquid CO_2, and finally mounted and sputter coated with gold/palladium before SEM analysis. Imaging showed cell attachment throughout

the gels, cell–cell interactions and formations of cell clusters, although the amounts of this differed across the sections of the different gels that were analysed (Figure 3.3).

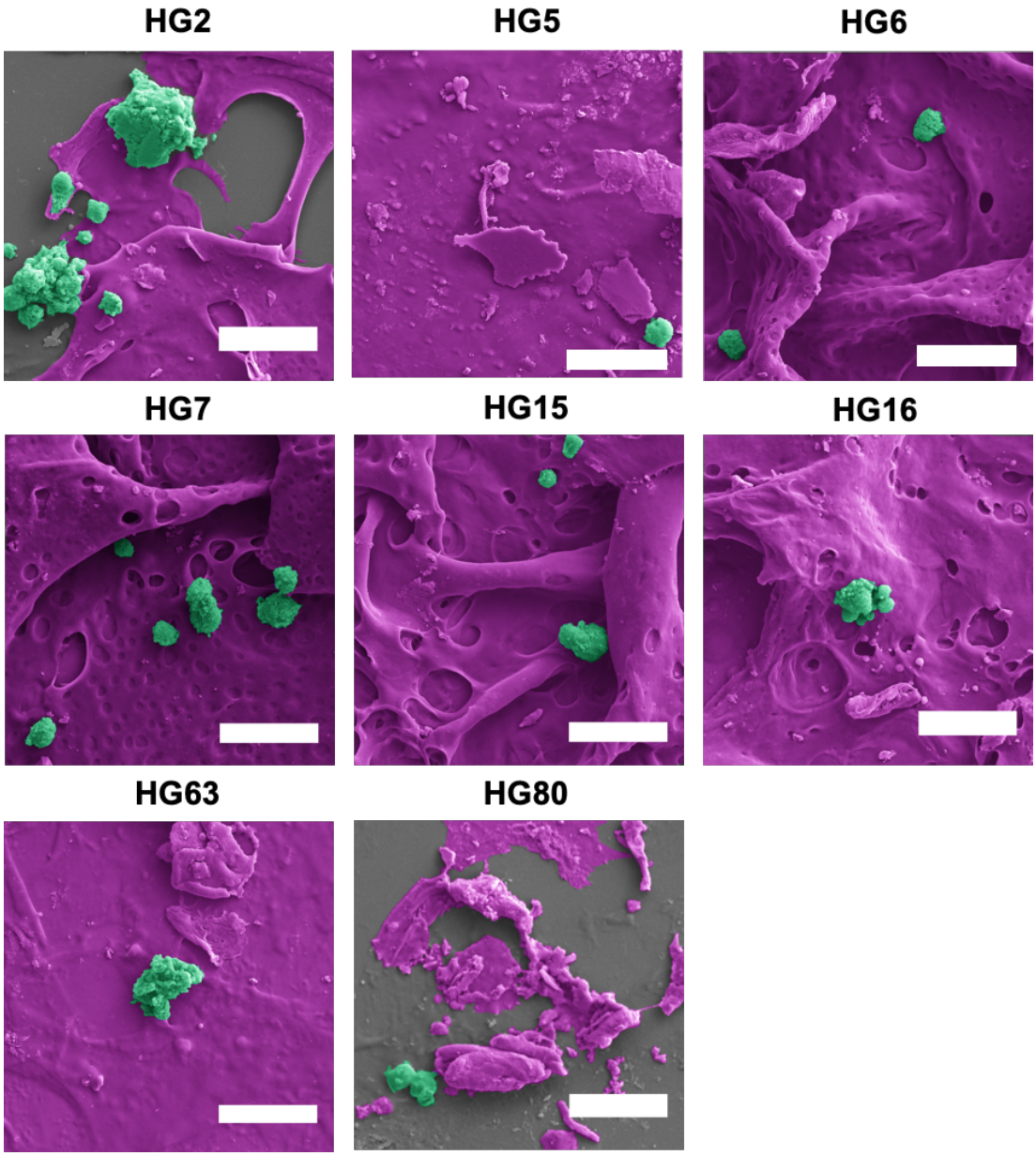

Figure 3.3: SEM image analysis of eight hit hydrogels encapsulated with HUVEC over 24 h. False colouring with cells shown in turquoise and hydrogel in magenta. Scale bar 30 µm.

3.4 Optimising the hydrogel scale-up platform

To scale-up the hydrogels, several different formats were attempted. Firstly, standard 96-well plates or Ibidi μ-slide 8-well chamber slides with "coverslip-like bottoms", useful for high-resolution microscopy and ease of sample preparation. However, these formats were unable to keep the hydrogels stable, and media change or staining caused significant hydrogel disruption. Forming the hydrogels in 96-well plates with amine-functionalised surfaces (Corning® PureCoat™) was also attempted to afford imine-linkage between the plate and the hydrogel, but this was still not sufficient to generate stable hydrogel features. Instead, an approach of scaling up the hydrogels on aminoalkylsilane-functionalised glass slides was attempted.

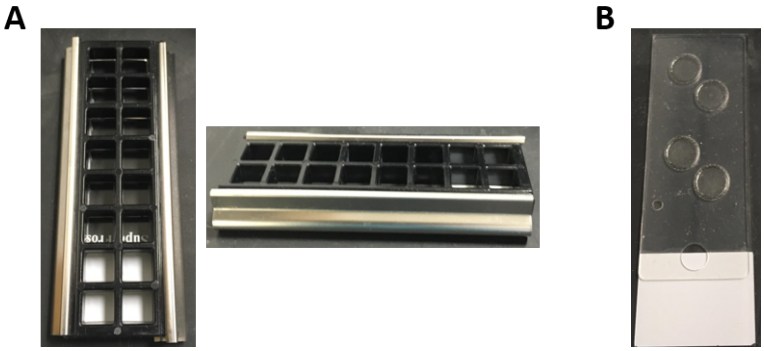

Figure 3.4: Different platforms used for hydrogel formation. **A.** 16-well Pro Plate (Grace Bio-Labs). Top and side view shown. **B.** 4-well silicone gasket (Grace Bio-Labs). Both A and B are fitted on to the top of aminoalkylsilane-functionalised glass slides.

16-well Pro Plates (Figure 3.4A) were fitted on top of aminoalkylsilane slides and the chosen hydrogels formed inside and seeded with HUVEC. After incubation for four days, the cells were fixed and their nuclei stained with 4′,6-diamidino-2-phenylindole (DAPI). It was also attempted to stain with a cluster of differentiation 31 (CD31) antibody conjugated to fluorescein (FITC). CD31 is a cell adhesion protein found on endothelial surfaces and widely used as a endothelial cell marker.[154] The antibody staining was not successful as the many incubation and washing steps required disrupted the hydrogels and cells dislodged from the structure. Based on these results an alternative approach to *in situ* hydrogel antibody labelling was used for future protein expression studies. For all eight hits, cell clusters formed within the hydrogels

(Figure 3.5), a stark contrast to the flat and stretched out shape of HUVEC observed when grown as a monolayer.

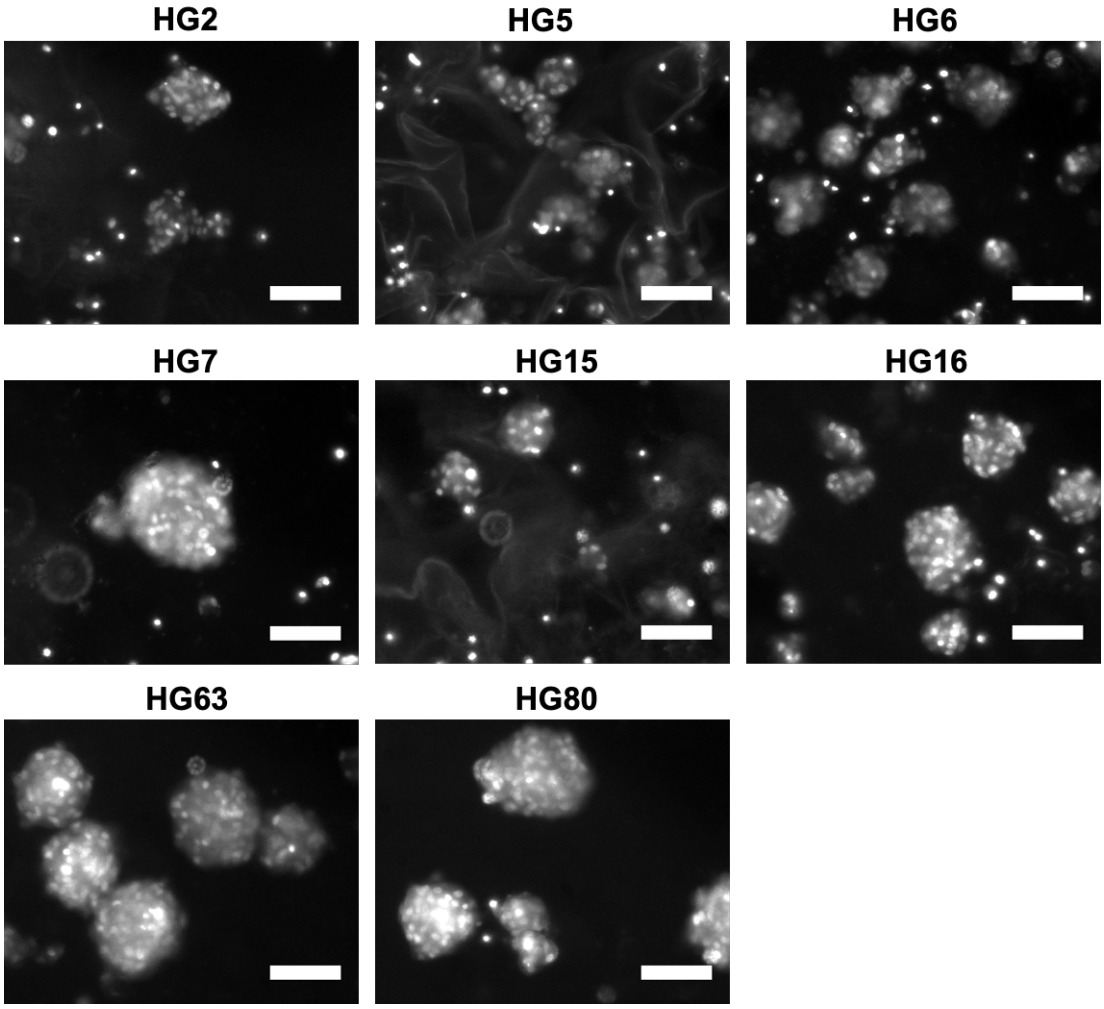

Figure 3.5: Incubation of HUVEC within hydrogels for 4 days. The cell nuclei were stained with DAPI ($\lambda_{ex/em}$ = 358/461 nm). Note a high propensity for cell cluster formation was observed across all hydrogels. Scale bar 100 μm.

After the initial 4-day incubation with HUVEC in the eight hit hydrogels, it was clear that the soft nature of these imine cross-linked hydrogels would require much optimisation for future staining protocols and analysis. As such, one of the eight hydrogels, HG15, was taken forward to optimise the protocols since it had emerged as the most stable hydrogel to handle and showed good 3D cell encapsulation morphology. All the following scale-up experiments in this chapter were thus done with HG15.

3.5 Investigating cell viability in HG15

Firstly, the strategy to form HG15 was modified. Silicone gaskets of 1 mm thickness (Figure 3.4B) were chosen instead of the ProPlates, because the reduced height of the gaskets made it easier for microscope set-up and imaging. Using gaskets with 4 wells fitted on top of the aminoalkylsilane-functionalised glass slides, cell viability within HG15 was evaluated. HUVEC and pHUVEC were encapsulated into HG15, and the cells incubated for 4 and 30 days, after which cell viability was assessed by Calcein AM/PI staining (Figure 3.6).

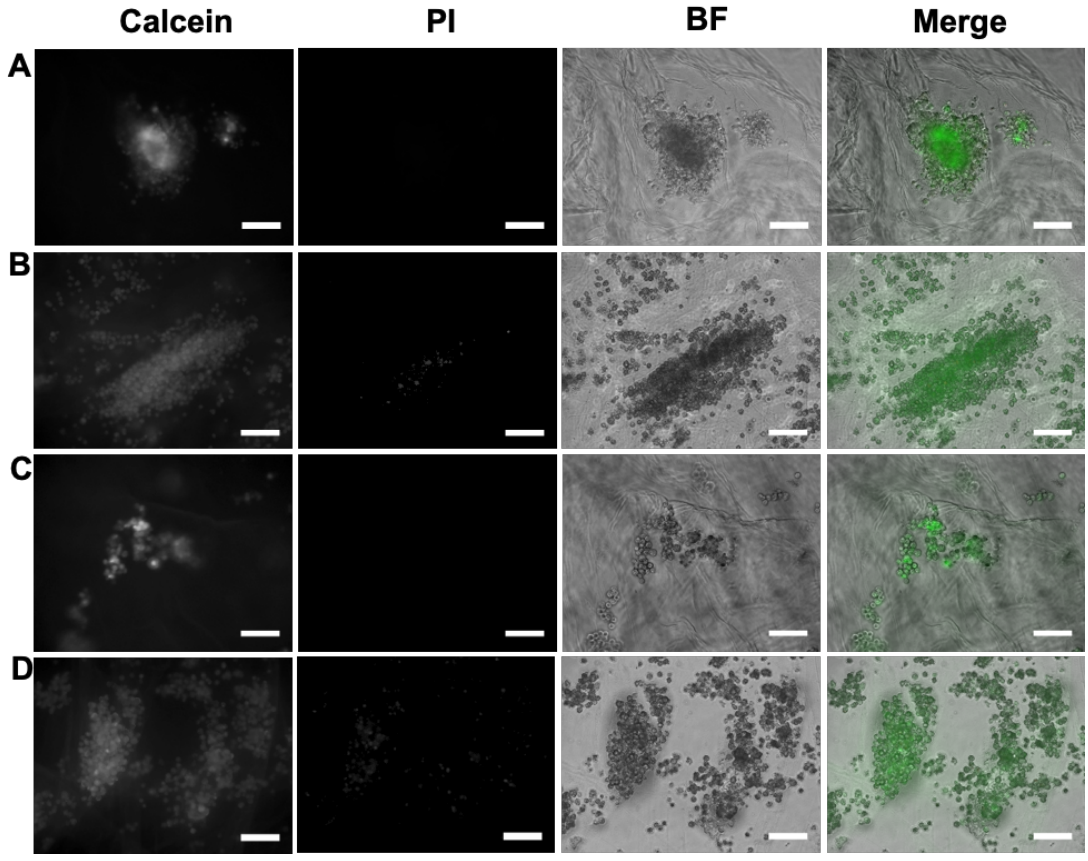

Figure 3.6: HUVEC viability analysis within HG15 with Calcein AM (live stain) ($\lambda_{ex/em}$ = 488/515 nm) and PI (dead stain) ($\lambda_{ex/em}$ = 570/602 nm). **A.** HUVEC after 4-day incubation. **B.** HUVEC after 30-day incubation. **C.** Primary HUVEC after 4-day incubation. **D.** Primary HUVEC after 30-day incubation. PI = propidium iodide. BF = bright field. Merge = merge of Calcein AM (green), PI (red) and BF images. Scale bar 100 µm.

For both incubations and cell types high cell viability was observed, with small numbers of dead cells within the gels. Cell clusters formed within 24 h of culture, indicative of the capacity of cells to move and interact within the 3D matrix. After 4 days, both cell types showed a similar propensity for cluster formation with "ball-like" and "string-like" clusters being formed. Interestingly the string-like clusters were observed to grow along the strands of the hydrogel network structure, showing the interaction between the cells and HG15, presumably via the RGD peptide (see Figure 3.6A and 3.6B).

3.6 Protein expression analysis in HG15

Following the confirmation of cell viability within HG15, protein expression was analysed. After encapsulation of HUVEC and pHUVEC within HG15 for 4 days, the cells were harvested and re-plated onto uncoated TCPS well plates. After 24 h incubation to allow for cell attachment, staining for CD31 was carried out. However, most cells detached from the well plates during the staining protocol. The cells that were still there though were positive for CD31 expression, and maintained the rounded shape as observed within the HG15 despite the 24 h growth on TCPS (Figure 3.7).

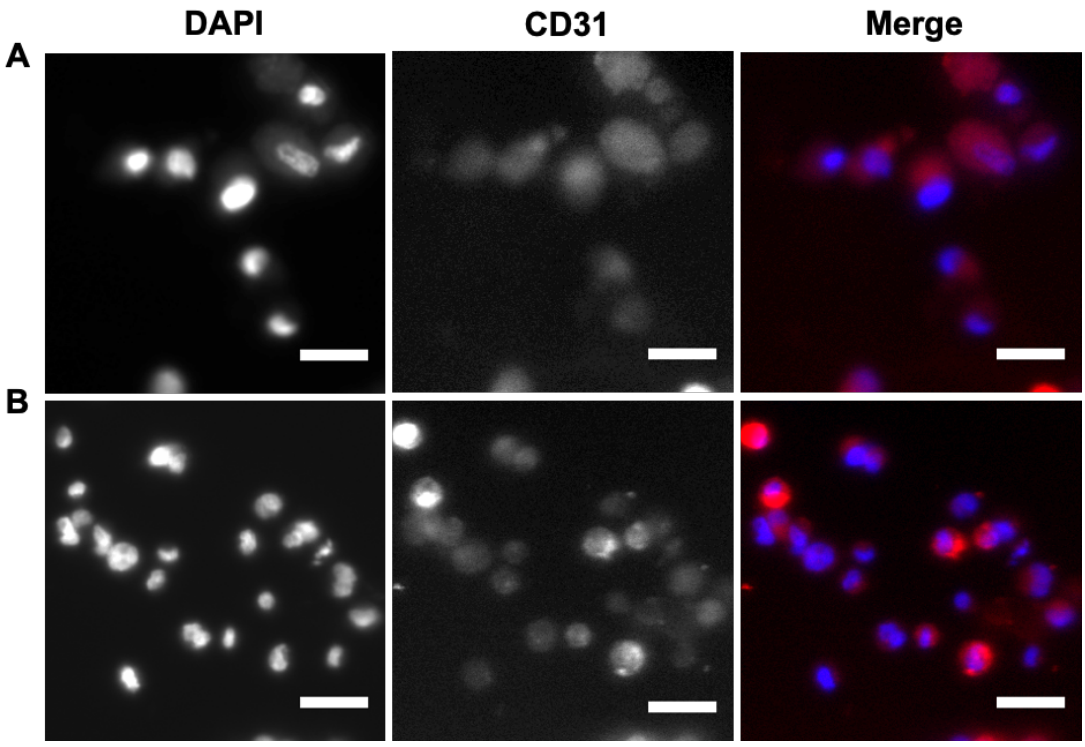

Figure 3.7: Immunofluorescent staining for CD31, a marker of HUVEC and primary HUVEC. Cells were incubated within HG15 for 4 days followed by re-plating on TCPS for 24 h. **A.** HUVEC **B.** primary HUVEC. Cells were stained with a CD31 primary antibody followed by an Alexa Fluor 568 secondary antibody ($\lambda_{ex/em}$ = 578/603 nm) shown in red in merge, and with DAPI nuclei stain ($\lambda_{ex/em}$ = 358/461 nm) shown in bluein merge. Scale bar 30 μm.

Instead of immunofluorescence, immunohistochemistry (IHC) staining of hydrogel slices was attempted to visualise cells within the hydrogel structure and analyse protein expression. For IHC analysis of cells encapsulated within HG15, the hydrogels were incorporated into agarose and paraffin-embedded with subsequent sectioning for IHC analysis. Sections of HUVEC encapsulated in HG15 for four days were stained with haematoxylin and eosin (H&E staining) (Figure 3.8) to visualise the cell nuclei and cytoplasm of the cells respectively. The staining showed the presence of cell clusters within the hydrogel network, and also evidence of hollow areas within the cluster, similar to lumen observed in endothelial cells when developing new blood vessels (angiogenesis).

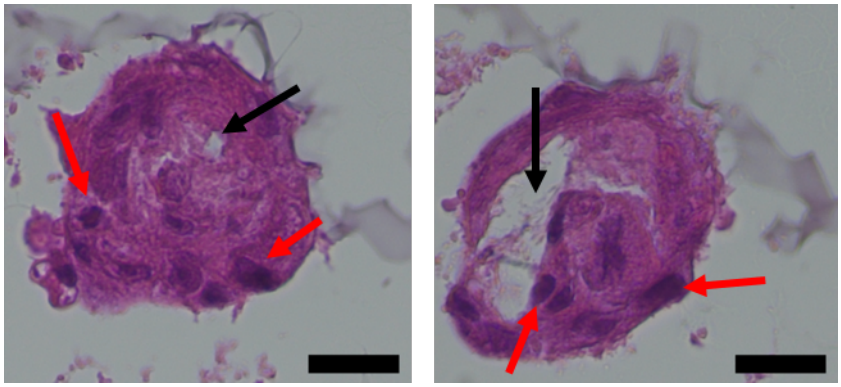

Figure 3.8: Haematoxylin and Eosin (H&E) staining of hydrogel sections. HUVEC were encapsulated in HG15 for four days and then embedded in agarose, paraffin-embedded, cut into slices and stained with Haematoxylin and Eosin Y, staining the cell nuclei and cytoplasm respectively. Two cell clusters are shown, with examples of nuceli indicated with red arrows. Black arrows indicate the presence of empty space, or lumina, in the clusters. Scale bar 20 µm.

Thereafter, gel/cell sections were stained with protein markers for endothelial cells (CD31, VE-cadherin and von Willebrand factor (vWf)), proliferation (Ki-67) and apoptosis (cleaved caspase-3) (Figure 3.9A-D). Semi-quantitative analysis of expression levels was also carried out (Figure 3.9E) (see Appendix Figure A2.1 for negative controls).

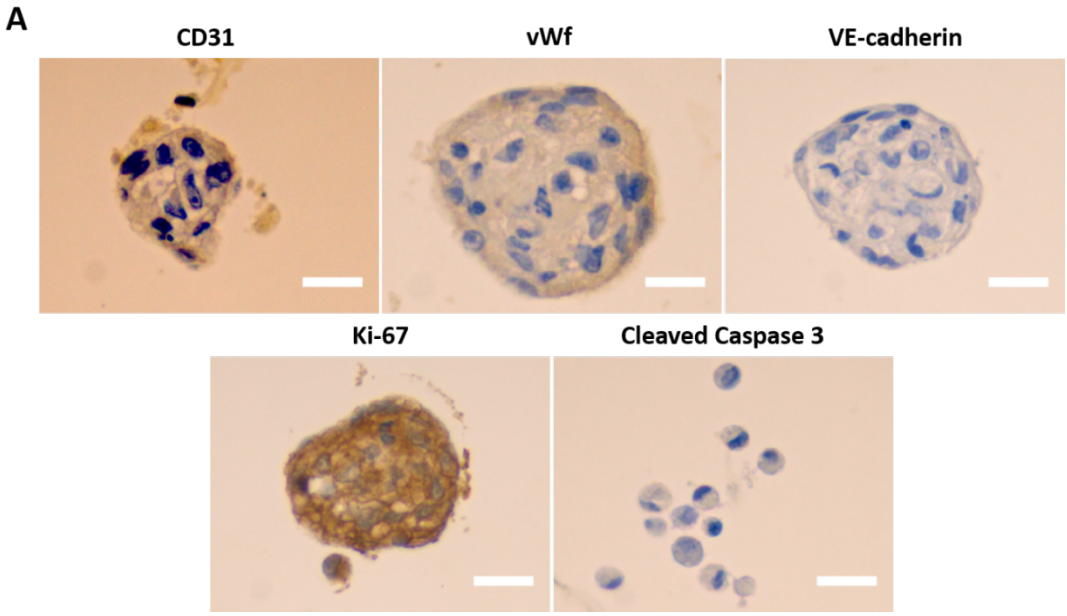

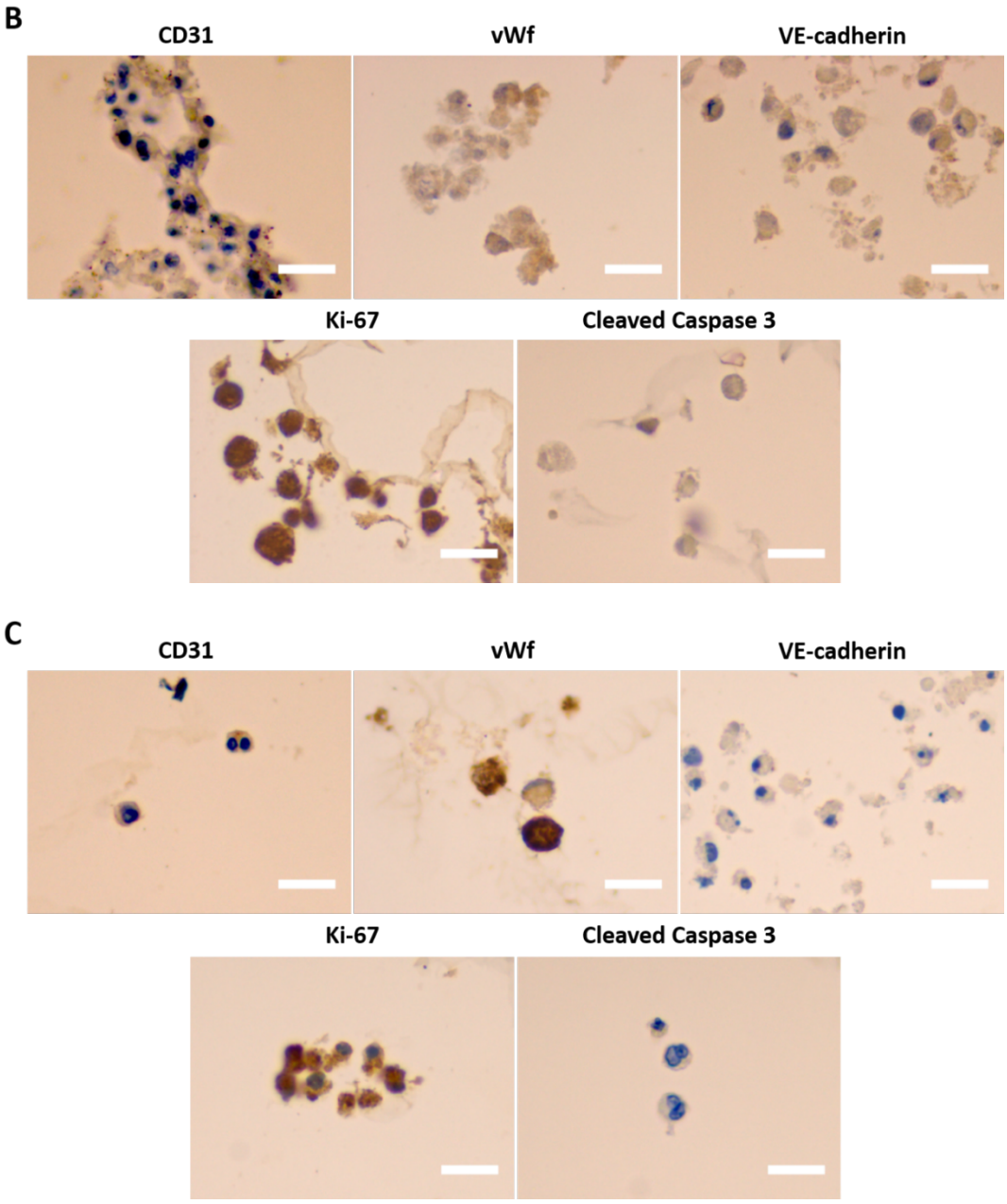
B
CD31
vWf
VE-cadherin
Ki-67
Cleaved Caspase 3
C
CD31
vWf
VE-cadherin
Ki-67
Cleaved Caspase 3

D

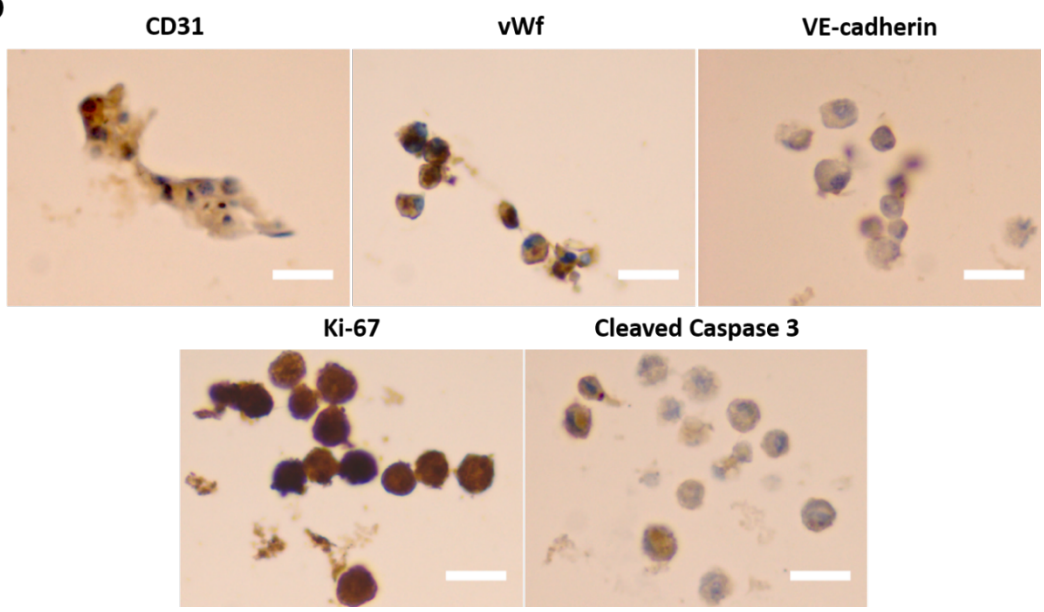

E

HUVEC	4 days	30 days
CD31	+	-
vWf	++	++
VE-Cadherin	-	+
Ki-67	+++	+++
Cleaved Caspase 3	-	+

Primary HUVEC	4 days	30 days
CD31	++	+
vWf	+++	+++
VE-Cadherin	-	+
Ki-67	+++	+++
Cleaved Caspase 3	-	+

Figure 3.9: Immunohistological analysis of endothelial (CD31, VE-cadherin, vWf), proliferation (Ki-67) and apoptosis (cleaved caspase 3) markers in HUVEC and primary HUVEC after incubation in HG15 (4 or 30 days). Following cell incubation for the desired time point and cell fixation, the gels were embedded in agarose, paraffin-embedded, cut into slices, permeabilised and stained with primary and secondary antibodies and haematoxylin. Visualisation was done with 3,3-diaminobenzidine (DAB). Positive DAB staining is shown in brown and the nuclei counterstain in blue with haematoxylin. **A.** HUVEC 4 days. **B.** HUVEC 30 days. **C.** Primary HUVEC 4 days. **D.** Primary HUVEC 30 days. **E.** Semi-quantitative evaluation of marker levels compared to a negative control (= no primary antibody staining with secondary antibody staining only) (images shown in Appendix Figure A2.1). Analysis was carried out in Image J using the colour deconvolution plug-in, H DAB vector. (−) = very low to no expression (+) = low expression, (++) = moderate expression, (+++) = high expression. Scale bar 20 µm.

3.7 Gene expression analysis in HG15

To supplement the protein expression analysis, gene expression was analysed by the quantitative polymerase chain reaction (qPCR). Five genes relevant for endothelial cell expression were investigated (vWf, CDH5, PECAM-1, KDR and TEK). CDH5 is the gene encoding VE-Cadherin, while PECAM-1 encodes CD31. KDR encodes for the vascular endothelial growth factor receptor 2, which is expressed on endothelial cell surfaces. TEK encodes for angiopoietin-1 receptor, a tyrosine kinase receptor for angiopoietin 1 and 2, both growth factors involved in angiogenesis[155]. GAPDH was used as the housekeeping gene.

Both HUVEC and pHUVEC were encapsulated in HG15 for 4 or 30 days. The hydrogels were then degraded with pyridoxal HCl and pyridoxamine 2 HCl (see Chapter 4 for more details and the protocol development) followed by cell harvesting, RNA isolation and qPCR analysis of the cDNA. To isolate enough RNA was a challenge throughout the project, and only results for the 4-day incubation time are presented in here since insufficient quantities of RNA were obtained to give reliable results for the 30-day incubation. Both cell types were compared to cells grown on either TCPS or on a thick layer of collagen (Figure 3.10).

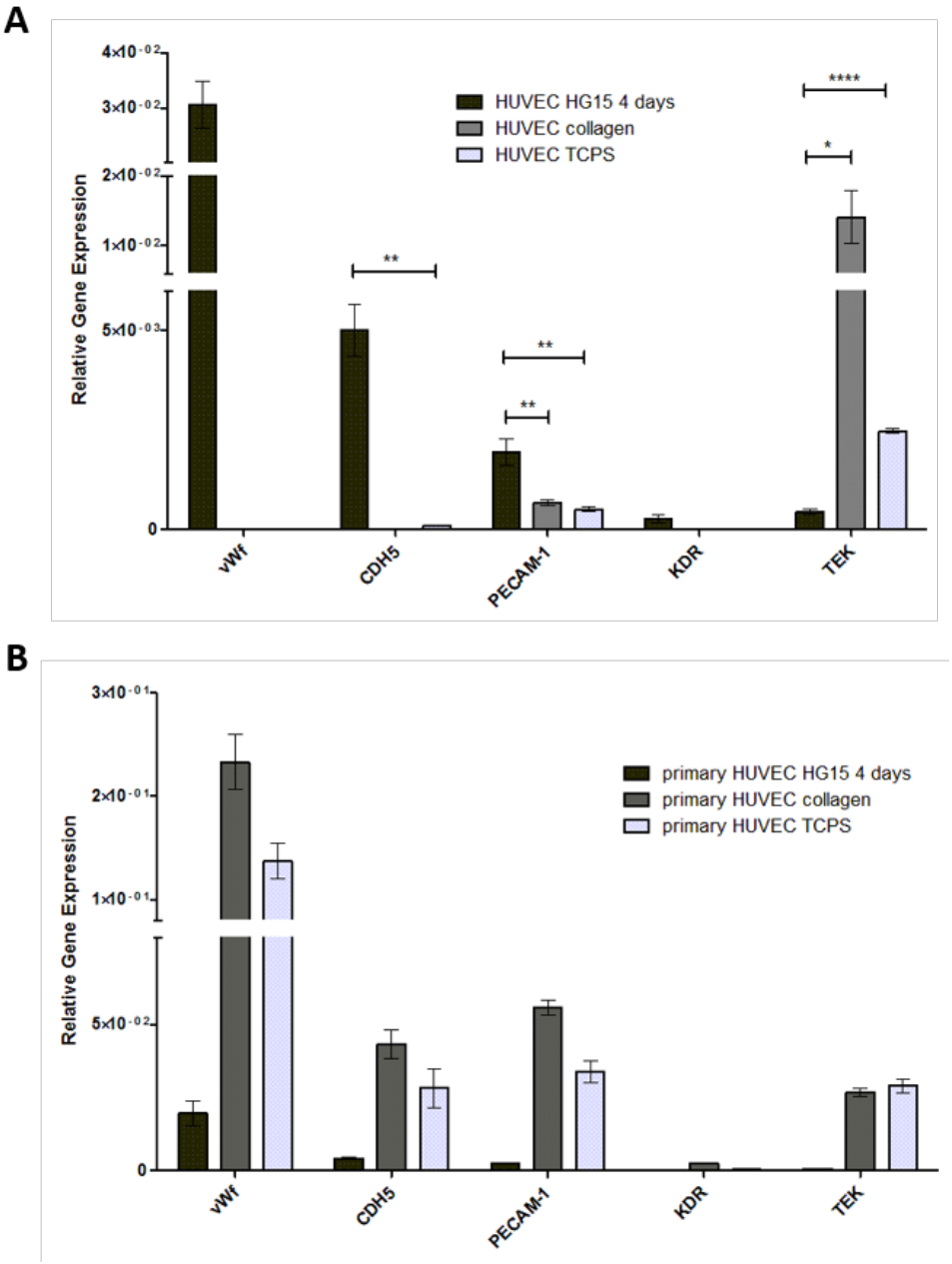

Figure 3.10: qPCR analysis of endothelial markers in A. HUVEC and B. Primary HUVEC cultured in HG15, on TCPS or on a collagen gel. Gene expression relative to GAPDH (quantified as $2^{-(Ct(target\ gene)-Ct(GAPDH))}$). (n = 4, ± s.e.m) (****p ≤ 0.0001; ***p ≤ 0.001; **p ≤ 0.01; *p ≤ 0.05)

For HUVEC in HG15 high expression of vWf factor was observed, while no expression was observed on either TCPS or collagen. Similarly, for CDH5 and PECAM-1, HUVEC encapsulated in HG15 had significantly higher expression of these genes compared to both TCPS and collagen. The expression of KDR was low in

HUVEC encapsulated within HG15, but no expression was observed on TCPS or collagen. TEK was the only gene where expression down-regulated after encapsulation within HG15. For primary HUVEC all genes were downregulated after encapsulation within HG15, and expression of the endothelial markers were upregulated or similarly expressed on collagen compared to TCPS.

3.8 Mechanical properties of HG15

The mechanical properties of HG15 were analysed by oscillatory rheology. The results indicated very low elastic (2.6±0.66 Pa) and viscous (0.6±0.25 Pa) moduli, demonstrating the very soft nature of HG15. When increased concentrations of HG15 were tested (HG15×2, HG15×5, see Figure 3.11 for details) an increase of elastic and viscous moduli was observed, indicating an expected increase in mechanical properties with increased hydrogel component concentration.

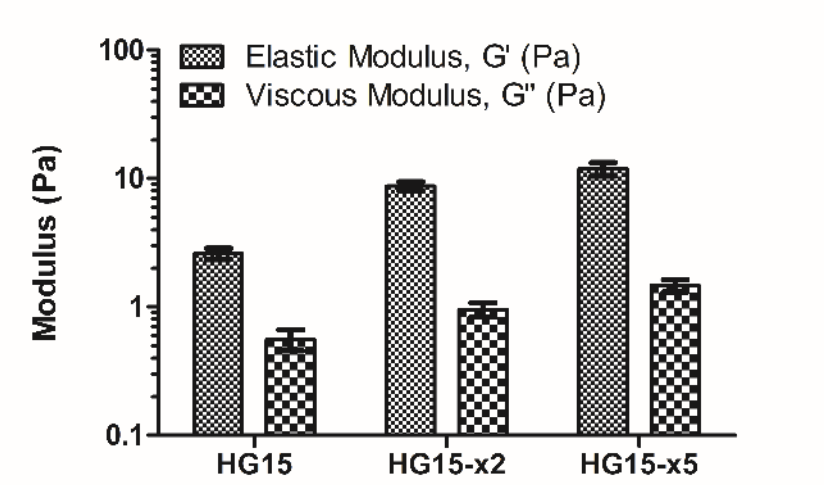

Figure 3.11: Elastic (G') and viscous (G'') moduli of HG15 (2.4% RGD, 5.4% PEG_{3000}-CL, 1.0% $(PEG\text{-}NH_2)_4$), HG15×2 (4.8% RGD, 10.8% PEG_{3000}-CL and 2% $(PEG\text{-}NH_2)_4$) and HG15×5 (12% RGD, 27% PEG_{3000}-CL and 5% $(PEG\text{-}NH_2)_4$) as measured by oscillatory rheology (n = 4). Average values (±s.e.m) over a frequency sweep from 0.1–10 rad/s (1% strain rate) is shown. HG15 had elastic (G') and viscous (G'') moduli of 2.6 ± 0.66 Pa and 0.6 ± 0.25 Pa, respectively. HG15×2 showed an increase of G' to 8.7 ± 1.53 Pa and G'' to 1.0 ± 0.27 Pa, while HG15×5 had a G' of 11.9 ± 2.84 Pa and a G'' of 1.47 ± 0.32 Pa. For full frequency sweep curves see Figure 3.13.

Due to the very low values of moduli measured for HG15, oscillatory rheology of complete Medium 200 was also measured to ensure that the moduli measured were due to the hydrogel network structure and not inherently present in the media used to make up the hydrogels. The elastic and viscous moduli of Medium 200 was lower than that of HG15, indicating that the measured moduli, albeit very low, were due to the network in HG15 (Figure 3.12).

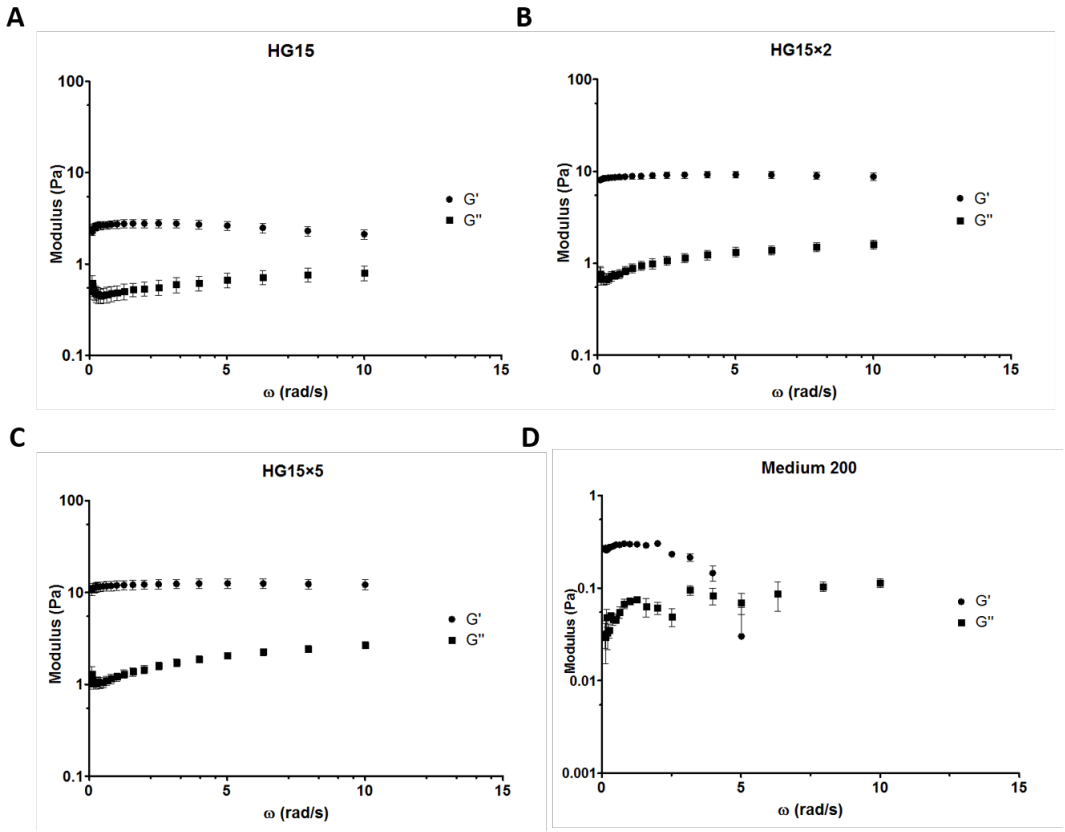

Figure 3.12: Rheological properties of HG15 at different concentrations. **A.** HG15; **B.** HG15×2; **C.** HG15×5; **D.** Complete endothelial Medium 200. Frequency sweep at 0.01–10 Hz at fixed 1 % strain. G′ = elastic, G′′ = viscous modulus (n = 5).

3.9 Discussion

Eight hydrogels were chosen to scale-up to confirm the results from the array screen with HUVEC (Chapter 2) based on the number of cells attached per hydrogel feature, and their morphology grade, with all having ≥ 90 % liquid content. The high water content, combined with the dynamic imine cross-linking used for their formation, explains the very soft nature of the gels. Furthermore, the main components used for

hydrogel formation were both linear (bi-functionalised) and of low molecular weight, both contributing to a loosely cross-linked network. For future applications, it would be interesting to use multi-branched cross-linkers, such as the $(PEG\text{-}NH_2)_4$, to examine its effect on improving rigidity to the structures. Considering the wide variety of commercially available amine-terminated multi-branched PEGs of varied molecular weights, and the ease of synthesising these into their aldehyde-equivalents, this strategy could easily be adopted to the hydrogel platform developed within this thesis.

SEM analysis showed good interactions between the hydrogel structures and cells, and DAPI staining (after 24 h) showed formation of cell clusters. Much effort was put into optimising the platform in which to perform the scale-up studies. The use of silicone gaskets fitted on top of aminoalklysilane-functionalised glass slides worked well, but was not without its own limitations. Due to the very soft nature of the hydrogels, removal of media for media changes was not possible without disrupting the hydrogel network and/or removing cells from the structure. Therefore, a culture method analogous to the "hanging drop" methods used for spheroid formation was adopted, wherein media was added every 48 h, without any media removal.[2] The small volume of each hydrogel feature (100 μL) caused evaporation of media from the features over 48 h, so that their volume was not constantly increased with the media additions. However, not being able to remove old media leads to the build-up of metabolites and waste products from the cells. Thus, this is not a suitable 3D cell culture platform, and further optimisation of the culture is necessary, but increasing the cross-linking concentration to improve the hydrogel mechanical properties would be a potential strategy to solve this. Nonetheless, high cell viability of both HUVEC and pHUVEC was observed over both 4 and 30 days inside one of the hit hydrogels, HG15 (see Figure 3.6).

Protein expression analysis by immunofluorescence of HUVEC and pHUVEC encapsulated in HG15 was unsuccessful when staining was attempted *in situ*, due to hydrogel network breakage and removal of cells with multiple staining and washing steps. Re-plating the cells on TCPS after encapsulation and then staining them for CD31 showed expression of the endothelial cell marker in both HUVEC and pHUVEC, but the large number of cells not attaching to the plastic surface, or which

detached after media change and washing steps suggests that this is a non-optimal method for staining. In addition, 24 h culture on TCPS would alter cell expression levels to those observed in the hydrogel. Considering the fact that both cell types poorly attached to the TCPS suggest that they had adapted to the more natural *in vivo* environment of the soft 3D hydrogel network. Furthermore, by breaking up the hydrogel and releasing the cells, the cell organisation observed within the 3D culture, such as clusters, could not be captured. Therefore, IHC on these structures while simultaneously allowing for analysis of protein expression was needed.

Protein expression analysis by IHC showed that both HUVEC and pHUVEC expressed endothelial markers at 4 and 30 days. Analysis indicated that HUVEC incubated in HG15 for 4 days expressed both CD31, a cell adhesion protein found on endothelial surfaces,[154] and vWf, an important factor for endothelial haemostasis maintenance.[156] Although the expression of VE-cadherin, responsible for endothelial intercellular cohesion and organisation[157] was minimal after 4 days it had increased after 30 days. Moreover, despite the observation that global CD31 expression in HUVEC after 30 days in HG15 was low, it was observed that it was cell specific with some cells still expressing CD31. pHUVEC showed good expression of both CD31 and vWf after 4 days in HG15, which was maintained over 30 days in the hydrogel. In a similar manner to the immortalised HUVEC cells, the pHUVEC had very low expression of VE-cadherin after 4 days, but an increase in the protein levels was observed after 30 days encapsulation. Cell apoptosis levels were low for both HUVEC and pHUVEC at day 4, and this increased slightly after 30 days incubation, which was expected due to the longer incubation time and build-up of waste products due to the limitations of the culture method and media change as discussed above. Overall, this demonstrated the capacity of HG15 to maintain the endothelial profile of both immortalised and primary endothelial cells, which combined with the high proliferation levels and low levels of apoptosis, indicates the promise of HG15 as a 3D endothelial cell culture platform.

The formation of 3D cell clusters within the gels was also observed during the sectioning analysis (Figure 3.8 and 3.9A). These are structures that are not typically seen in 2D cell culture, suggesting that the 3D environment of the gel aids in the cluster formation. Although cell clusters were observed for both cell types and

incubation times when imaging the full hydrogels by light microscopy (see Figure 3.6), these were only observed in the IHC sections for HUVEC after 4 days. This could be due to sections with cell clusters not being cut from the paraffin blocks of the other incubation times, indicating a limitation of the method in that a global picture of protein expression is not given since not all parts of the hydrogel will be cut and stained.

As for the qPCR and gene expression analysis, results for HUVEC after 4 days in HG15 confirmed the results obtained from protein expression analysis. Interestingly, vWf was not expressed at all when HUVEC were cultured on TCPS or collagen. Considering the importance of vWf for endothelial cell maintenance and function, this exemplifies the problem of culturing cell lines on rigid 2D surfaces and its effect on cell phenotype. It should be noted that HUVEC used herein had been cultured on TCPS for several passages before encapsulation within HG15. Four days inside a softer 3D matrix was enough to turn on the gene expression of vWf, and it also led to increase in PECAM-1 (CD31) and CDH5 (VE-Cadherin) gene expression compared to TCPS. Expression of TEK was higher in HUVEC cultured on TCPS or collagen compared to in HG15, and upregulation of TEK has been linked to endothelial cells undergoing hypoxia and pro-inflammatory responses.[155] Overall, this suggests that HUVEC encapsulated in HG15 perform better, or more "naturally", than when cultured on TCPS or collagen.

For pHUVEC, the qPCR data did not match the data seen in the IHC protein expression analysis. Several studies have concluded, however, that the correlation between mRNA and protein expression levels are poor (*ca.* 40 %) and that care should be taken when equating gene expression with cell phenotype and behaviour.[158–162] Since protein expression of vWf and CD31 was observed of pHUVEC encapsulated in HG15 by IHC analysis it is clear that these endothelial markers are present. Furthermore, IHC analysis indicated that these and VE-Cadherin were expressed after 30-day encapsulation. Taken together, the results from qPCR should be noted, but they are not definitive indicators of protein levels, where IHC is the superior method of analysis.

Finally, the mechanical properties analysis of HG15 demonstrated its very soft nature with low elastic and viscous moduli (2.6 ± 0.66 Pa and 0.6 ± 0.25 Pa). Their moduli did increase with increased component concentration, which also is seen with Matrigel. Low concentration Matrigel (4.4 mg/mL) has a reported elastic moduli of 20 Pa,[163] while Collagen 1 (rat tail, 2 mg/mL) has been measured as 9 Pa.[164] As such HG15 is of lower stiffness than these commonly used 3D matrices, but that its moduli can be tuned via alteration of concentration and the very soft nature of HG15 makes it a promising material for studies with cells known to reside within low-moduli *in vivo* environments, e.g. neuronal cells.

3.10 Conclusions

A class of dynamic hydrogels were designed as novel 3D cell culture matrices for endothelial cell maintenance and proliferation. Successful scale-up of hit hydrogels identified from a HTS hydrogel array was achieved, with gels showing cell cluster formation. One hydrogel, HG15, was further studied with both immortalised and primary HUVEC, with incubation over 4 and 30 days, which showed high cell viability for both cell types and immunohistological analysis confirming the expression of endothelial marker proteins, and the maintenance of cell proliferation with low levels of apoptosis. The confirmation of the array results validates the power of the hydrogel array platform for high-throughput screening and the identification of 3D cell culture matrices.

3.11 Materials and Methods

3.11.1 Instruments for cell experiments and analysis

HERAcell 150 incubator (Heraeus, Germany)

HERAsafe KS 18 class II biosafety cabinet (Heraeus, Germany)

Synergy HT Microplate Reader (BioTek, USA)

LightCycler 480 (Roche Holding AG, Switzerland)

3.11.2 Imaging instruments

Axiovert 200m inverted fluorescence microscope with Axiovision 4.8 software (Carl Zeiss AG, Germany). Filters: DAPI ($\lambda_{ex/em}$ = 300-395/430-505 nm), GPC/FITC ($\lambda_{ex/em}$ = 447-494/500-554 nm), YPF ($\lambda_{ex/em}$ = 490-512/520-554 nm), TRITC/Rhodamine/Cy3 ($\lambda_{ex/em}$ = 527-563/570-650 nm) and Cy5 ($\lambda_{ex/em}$ = 620-659/663-725 nm) filters. Magnification: x10, x20 and x40

Zeiss Axio Imager Z1 with ZEN imaging software (Carl Zeiss AG, Germany)

Image analysis was carried out in ImageJ

3.11.3 Instruments for characterisation

Carl Zeiss SIMGA HD VP Field Emission Scanning Electron Microscope (Carl Zeiss AG, Germany)

Discovery Hybrid Rheometer (DHR-2) fitted with a 25 mm rough parallel aluminium plate for oscillatory rheology (TA Instruments, USA)

3.11.4 Cells, media and biological equipment

Primary HUVEC were purchased from ATCC (PCS-100-010™)

HUVEC were donated by Dr Kate Cameron (University of Edinburgh)

Complete Medium 200: Medium 200, Low Serum Growth Supplement (LSGS) kit (Thermo Fisher, USA)

3.11.5 Cell Culture on Tissue Culture Polystyrene

HUVEC and primary HUVEC were cultured in complete Medium 200. Cells were grown to 70–80% confluency in T25 flasks (37 °C, 5% CO_2) before passaging. Immortalised HUVEC were used between passage 5–9 and primary HUVEC from passage 1–4.

3.11.6 Scanning Electron Microscopy

The hit hydrogels were printed (n = 3) on a masked aminoalkylsilane glass slide (See 2.6.15). The slide was UV sterilised for 1 h, seeded with HUVEC (300 000/slide) in complete Medium 200 (5 mL) and incubated (37 °C, 5% CO_2) for 24 h. The media was removed and the samples were fixed with glutaraldehyde (3% in 0.1 M $(CH_3)_2AsO_2Na$, pH 7.3) for 2 h, and washed with Hank's buffer (3 × 10 min). The samples were post-fixed with OsO_4 (1% in 0.1 M $(CH_3)_2AsO_2Na$). Dehydration in graded concentrations of acetone (50%, 70%, 90% and 3 × 100%) for 10 min each was followed by critical point drying with liquid CO_2. After mounting the slide on aluminium stubs with carbon tabs attached, the hydrogels were sputter coated with gold/palladium (Au/Pd, 20 nm) and analysed using SEM. The images were analysed in ImageJ and false coulouring was done with Gimp software.

3.11.7 DAPI staining of HUVEC encapsulated in hit hydrogels

Components of the eight hit hydrogels (n = 3) in water were added to the wells of a 16-well ProPlate microarray system (GraceBioLabs) (100 µL) fitted on top of an aminoalkylsilane-functionalised glass slide. After drying at 40 °C overnight, the slide was sterilised under UV light for 30 min. Each hydrogel was seeded with HUVEC (15000 cells in 100 µL complete Medium 200) and incubated for 1 h (37 °C, 5 % CO_2) before addition of complete Medium 200 (100 µL) to each hydrogel. The hydrogels were incubated for 4 days (37 °C, 5 % CO_2), with media change every 48 h. The cells were fixed with 4 % paraformaldehyde (PFA) (100 µL/hydrogel) for 10 min at room temperature followed by washing with Hank's buffer (1×5 mL). The cells were then stained with DAPI (100 µL/hydrogel) for 10 min at room temperature and imaged

using a Zeiss AxioVert 200m fluorescence microscope with lasers $\lambda_{ex/em}$ = 300-395/430-505 nm.

3.11.8 CD31 staining of HUVEC and pHUVEC encapsulated in HG15 and re-plated onto TCPS

Solutions of HG15 (2.4% RGD, 5.4% PEG_{3000}-CL and 1 % $(PEG\text{-}NH_2)_4$) were added to the wells of a 4-well CultureWell silicone gasket (100 µL/hydrogel, n = 4) (GraceBioLabs) followed by dehydration in 110 °C oven for 10 min and 40 °C overnight. Before cell seeding, the silicone gasket was removed from the glass slide and sterilised with 70 % ethanol. After further sterilisation of the silicone gasket and glass slide under UV light for 1 h, the silicone gasket was re-fitted onto the glass slide to again give wells for each hydrogel feature. Hydrogel formation and *in situ* cell encapsulation was achieved upon addition of cell media with suspended HUVEC or primary HUVEC (40 000 cells in 100 µL complete Medium 200 to each hydrogel) followed by incubation (37 °C, 5% CO_2). After 24 h, pyridoxal HCl (50 µL of 4.9 mM in complete Medium 200) was added to each gel and incubated for 15 min (37 °C, 5 % CO_2) followed by addition of pyridoxamine 2HCl (50 µL of 4.1 mM in complete Medium 200) and further incubated for 15 min (37 °C, 5 % CO_2). The cells were filtered through a cell strainer (40 µm nylon mesh, Fisher Scientific) and each well washed with Hank's buffer (100 µL) before centrifugation (300 g, 10 min). The cells were suspended in complete Medium 200, plated into a 48 well plate (1 mL) and incubated overnight (37 °C, 5 % CO_2). The media was removed, each well washed with Hank's buffer and cells fixed with 4 % PFA for 10 min (200 µL/well) and washed with washing buffer (0.05 % Tween20 in Hank's buffer) (200 µL/well). Blocking (ProteinBlocker) was carried out for 30 min at room temperature (200 µL/well), followed by incubation with a primary CD31 antibody (200 µL/well, 1:99 dilution, AbCam28364 Rabbit primary Ab) at 4 °C overnight. The primary antibody solution was removed and cells washed with Hank's buffer twice (2×200 µL). The cells were incubated with a fluorescent secondary antibody (200 µL/well) (AlexaFluor 568, AbCam175471 Goat primary Ab to Rabbit IgG) with gentle shaking for 1 h at room temperature. The solution was removed and cells washed with Hank's buffer (2×200µL). Nuclei staining with DAPI was done for 10 min at room temperature (200

µL/well) followed by washing with Hank's buffer (200 µL/well). The cells were imaged in Hank's buffer (200 µL/well) using a Zeiss AxioVert 200m fluorescence microscope with lasers $\lambda_{ex/em}$ = 300-395/430-505 nm for DAPI, $\lambda_{ex/em}$ = 527-563/570-650 nm for AlexaFluor 568.

3.11.9 Cell viability of HUVEC and primary HUVEC encapsulated in HG15

HG15 (n = 4) was prepared and sterilised as described above (see 3.11.8). Hydrogel formation and *in situ* cell encapsulation was achieved upon addition of cell media with suspended HUVEC or primary HUVEC (50 000 cells in 100 µL complete Medium 200 to each hydrogel) followed by incubation (37 °C, 5% CO_2). 15–20 µL of fresh media was added to each hydrogel every 48 h. After incubation for the desired time-point, the cells were stained with Calcein AM and PI (488/570 nm, LIVE/DEAD Cell Imaging Kit ThermoFisher) according to manufacturer's protocol and imaged on a Zeiss AxioVert 200m fluorescence microscope with lasers $\lambda_{ex/em}$ = 447-494/500-554 nm for Calcein AM, $\lambda_{ex/em}$ = 527-563/570-650 nm for PI.

3.11.10 Immunohistochemistry of HUVEC and primary HUVEC incubated in HG15

HG15 (n = 4) was prepared and sterilised as described above (see 3.11.8). Hydrogel formation and *in situ* cell encapsulation was achieved upon addition of cell media with suspended HUVEC or primary HUVEC (50 000 cells in 100 µL complete Medium 200 to each hydrogel) followed by incubation (37 °C, 5% CO_2) for 4 or 30 days. 15–20 µL of fresh media was added to each hydrogel every 48 h. After incubation for the desired time point cells were fixed in 10 % neutral-buffered formalin (1 mL concentrated formalin in 9 mL water buffered to pH 6.8 with NaH_2PO_4) overnight followed by washing with PBS and staining with Eosin Y (1% in H_2O) for 30 min at room temperature. The hydrogels were immersed in heated agarose (2 % aq., 5 mL, liquid) (Type 1, low EEO) and the agarose cooled to form gels. Hydrogel slices were cut from the agarose block, dehydrated with industrial methylated spirits (IMS) (70%, 80%, 90%, 5×100% IMS, 1 hour each), infiltrated with xylene (3×100%, 1 hour each)

and finally embedded with paraffin wax (3×1 hour). Following mounting and cooling of the sample, sections (5 μm thickness) were cut using a microtome (Leica). The sections were then dewaxed and rehydrated using xylene (×3), ethanol (100%, 95%, 80%, 70%, 20 s each) followed by washing with water. H&E staining of slices was carried out according to a standard operating procedure at the University of Edinburgh. Immunostaining of slices was done using a Bond Max Automated Immunostainer and a Leica Bond Polymer Refine detection kit (DS9800) according to manufacturer's protocol and imaged on a Zeiss Axio Imager Z1. Primary antibodies: Ki-67 (Abcam Ab15580, 1:500 dilution), Cleaved Caspase 3 (Cell signalling technology 9661, 1:100 dilution), CD31 (Abcam, Ab28364, 1:600 dilution), von Willebrand factor (Dako A0082, 1:1000 dilution), VE-Cadherin (Chemicon International MAB1989, 1:100 dilution). Semi-quantitative analysis of protein expression was determined using the ImageJ colour deconvolution plug-in, H DAB vector.

3.11.11 qPCR analysis of HUVEC and primary HUVEC incubated in HG15

HG15 (n = 4) was made and sterilised as described above (see 6.11.8). HUVEC or primary HUVEC were seeded in each hydrogel (50 000 cell in 100 μL complete medium 200) and incubated at 37 °C with 5 % CO_2 for 4 or 30 days. 20 μL media was added to each hydrogel every 48 h. After incubation for the desired time point, the cells were harvested by addition of pyridoxal hydrochloride (50 μL, 4.9mM in complete Medium 200) to each hydrogel and incubated for 15 minutes (37 °C, 5 % CO_2). Thereafter pyridoxamine dihydrochloride was added (50 μL, 4.1 mM in complete Medium 200) and the gels incubated for another 15 minutes at 37 °C with 5 % CO_2. The resulting solutions were put through a cell strainer (40 μm nylon mesh, Fisher Scientific) to remove hydrogel components followed by washing with media. The cell suspension was pelleted by centrifugation (300g, 2×10 minutes). From the cell pellet RNA was isolated using an RNeasy kit (Qiagen) followed by reverse transcription of 1 μg RNA using TaqMan reverse transcription reagents (Applied Biosystems) according to manufacturer's protocol. qPCR was carried out with TaqMan® Gene Expression Master Mix and TaqMan® primers (Applied Biosystems). Primer details: GAPDH (Hs02758991_g1) KDR (Hs00911700_m1), PECAM1

(Hs01065279_m1), CDH5 (Hs00901465_m1), vWf (Hs01109446_m1), TEK (Hs00945150_m1). Analysis was carried out using a LightCycler with GAPDH as housekeeping gene. Relative gene expression was evaluated using $2^{-(Ct(target\ gene)-Ct(GAPDH))}$.[165]

3.11.12 Characterisation of Mechanical Properties

Solutions of HG15 (2.4% RGD, 5.4% PEG_{3000}-CL and 1 % $(PEG\text{-}NH_2)_4$) and variants (HG15×2: 4.8% RGD, 10.8% PEG_{3000}-CL and 2% $(PEG\text{-}NH_2)_4$); (HG15×5: 12% RGD, 27% PEG_{3000}-CL and 5% $(PEG\text{-}NH_2)_4$) were added to the wells of a 2-well CultureWell silicone gasket (400 µL/hydrogel, n = 3) (GraceBioLabs) followed by drying at 110 °C for 10 min and 40 °C overnight. The hydrogels were formed by rehydrating in complete Medium 200 (400 µL/hydrogel). Frequency sweep measurements were carried out using the constant strain (1 %) mode on a Discovery Hybrid Rheometer. Elastic and viscous moduli were measured over the frequency range 0.1–10 rad/s and from this average elastic and viscous moduli were calculated.

Chapter 4: Development of an enzyme-free hydrogel passaging system for cells

4.1. Introduction

The ability to passage (or subculture) cells is a fundamental aspect of cell culture. Traditional adherent 2D cell culture requires a method of dislodging cells from the substrate when they have grown to confluency, and to separate cells from each other to afford a single cell suspension, of which a subset is "passaged" to a new culture vessel.[6,166] Commonly enzymes, such as trypsin or collagenase, that can cleave the proteins between cells and between cells and the growth surface are employed for this. The most frequently used enzyme in mammalian cell culture is trypsin, a serine protease, that cleaves amide bonds.[6] The first reports of using trypsin for *in vitro* tissue/cell culture were by Rous and Jones in 1916, when they reported the use of trypsin to digest and generate single cell suspensions from embryos and tumours from rat and chicken, as well as from normal rat tissue.[167] Once cell culture was developed in the 1950's, trypsinisation became the method of choice as a passaging method.[6]

Although the trypsin method of cell dissociation is routinely used and relatively quick (5-10 min incubation at 37 °C), the process does not come without issues. A primary concern is that the action of trypsin leads to the cleavage of membrane proteins and growth factors from the cell surface, which can lead to cell dysregulation and damage.[168] In fact, a proteomic study of the effects on MCF-7 cells upon trypsin digestion indicated that the expression of 36 proteins were changed compared to non-trypsinised cells.[168] Furthermore, among the down-regulated proteins were ones regulating cell growth, metabolism, adhesion and electron transport in the mitochondria. Conversely, proteins that control apoptosis were upregulated. Another drawback of trypsin is that prolonged cell exposure leads to significant cell damage and cell death. Because of this, a so-called deactivation step of the enzyme is required after trypsinisation, normally using serum or a serum-free deactivation agent.[166]

Alternative cell-dissociation reagents to trypsin exist, such as Accutase® (Innovative Cell Technologies, Inc.), which is an enzyme mixture with both proteolytic and collagenolytic activities and is recommended for use with sensitive cell types such as hESCs[169] and neuronal SCs[170] because it is active at lower concentrations compared to trypsin or collagenase and does not require a deactivation step. Physical disruption of cell layers and colonies is another method of achieving cell dissociation, whereby mechanical forces with either a thin capillary or a cell scraper are used to dislodge the cells from the surface. This can be particularly useful for ESC cultures since colonies of cells are maintained and not dissociated.[171]

For cell culture within a 3D biomaterial, passaging comes with the added hurdle of releasing the cells from the 3D structure, as opposed to the simple 2D surface of traditional methods. For commonly used naturally derived 3D matrices, such as Matrigel®, GelTrex®, collagen or laminin, combinations of different proteases are used to afford cell dissociation from the material. These combinations are often marketed under different names and with proprietary compositions depending on the vendor, for example Corning™ Cell Recovery Solution for Matrigel® and GelTrex® or collagenase for dissocation of collagen gels. For synthetic 3D matrices, trypsin is often the method reported to afford cell dissociation from the scaffold or hydrogel, but an enzyme-free protocol would be desired considering the issues associated with trypsin digestion. This includes the thermally responsive hydrogels developed in the Bradley group that enabled the long-term passaging of hESCs (> 30 passages) with harvesting by lowering the temperature to 15 °C.[45] In another example, the degradation of imine cross-linked chitosan:PEG hydrogels was reported using aqueous pyridoxal HCl, a derivative of pyridoxal 5′-phosphate (PLP), also known as Vitamin B6.[80] It was envisioned that a similar strategy could be employed for the imine cross-linked hydrogels developed within this thesis.

The aim of this chapter was to develop an enzyme-free protocol that allowed for cell culture and passaging within a 3D imine cross-linked hydrogel. By using vitamin B6 derivatives, a biocompatible protocol was developed that allowed for the gentle and enzyme-free passaging of HUVEC and HEK293 cells over multiple passages.

4.2 pH and cytotoxicity of Vitamin B6 and its derivatives

For hydrogel degradation, three derivatives of vitamin B6 were investigated; PLP, pyridoxal hydrochloride (referred to as Pyr HCl) and pyridoxamine dihydrochloride (referred to as PyrAm). It was desired to carry out the hydrogel degradation using solutions made up in cell media to make the system compatible with cell culture reagents. Moreover, because the incubation time reported in literature of using PyrHCl was 30 min,[80] to use cell media was preferred over buffered solutions such as PBS, as cell viability could be affected over this time if the cells were only incubated in buffer. Initially optimal concentrations of the vitamin B6 derivatives were determined. To develop a passaging protocol, the solutions of all components had to be used at physiologically relevant pHs in order not to cause cell damage. PyrHCl and PyrAm are sold as the HCl salts and therefore it was expected that at higher concentrations the pH would be acidic if unbuffered. Indeed, when dissolved in endothelial cell medium the pHs of PyrHCl (49 mM) and PyrAm (41 mM) were 3 and 4 respectively (Table 4.1). At lower concentrations (≤ 9.8 mM for PyrHCl and ≤ 8.3 mM for PyrAm), the pH was buffered to 7. Although the buffering capacity of the Medium 200 could have been increased by addition of $NaHCO_3$ or HEPES to allow the use of the higher concentrations this was not desired as the aim was to develop a protocol using standard reagents. The highest concentration tested of PLP was 8.1 mM as it was insoluble above this and at this and lower concentrations the pH was 7.

Table 4.1: pH of Vitamin B6 derivatives (Pyridoxal 5'-phosphate, Pyridoxal HCl, Pyridoxamine 2HCl) at different concentrations and their corresponding pH's as measured by pH paper. All solutions were made up in endothelial Medium 200 supplemented with low serum growth supplement.

Molecule	Concentration (mM)	pH
Pyridoxal 5'-phosphate (PLP) 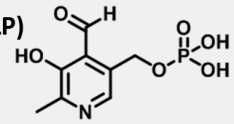	8.1	7
	4.0	7
	0.4	7
	0.04	7
Pyridoxal HCl (PyrHCl) 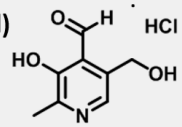	49	3
	9.8	7
	4.9	7
	0.5	7
	0.05	7
Pyridoxamine 2HCl (PyrAm) 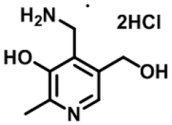	41	4
	8.3	5
	4.1	7
	0.4	7
	0.04	7

The luminescent-based assay, CellTiterGlo (Promega) was used to determine HUVEC viability by measuring levels of ATP from lysed cells following incubation with different concentrations of PyrHCl, PyrAm and PLP for 30 minutes (Figure 4.1). PyrHCl and PyrAm were non-toxic at concentrations ≤ 9.8 mM and ≤ 8.3 mM respectively. High cytotoxicity of PyrHCl and PyrAm was observed at 49 mM and 41 mM respectively, due to the low pH (~ 2) of the solutions. 8.1 mM PLP caused 50 % cytotoxicity and PLP was also more toxic to HUVEC than PyrHCl and PyrAm at lower concentrations showing 70 % cell viability at 4 mM, compared to no toxicity observed for PyrHCl and PyrAm at the similar concentrations.

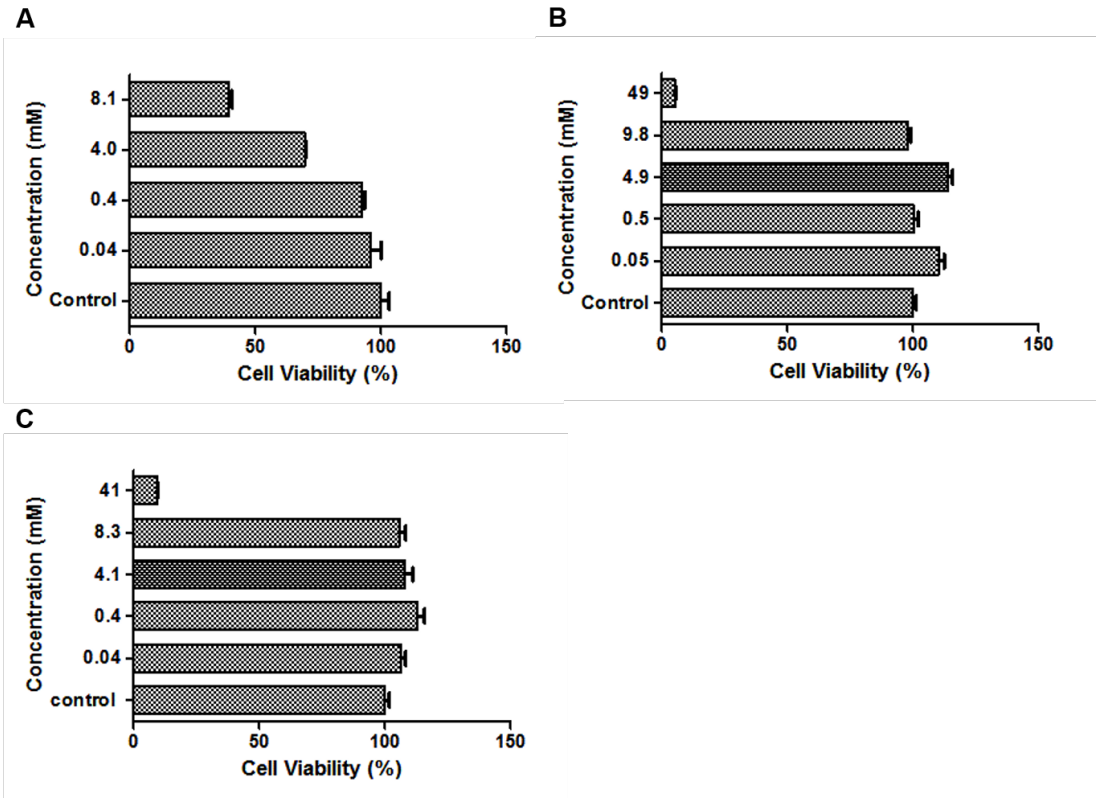

Figure 4.1: Cell viability assay to determine the cytotoxicity of Vitamin B6 and its derivatives to HUVEC. The cell viability was measured using a CellTiter Glo 2.0 assay after 30 min incubation with **A**. Pyridoxal 5'-phophate. **B**. Pyridoxal HCl. **C**. Pyridoxamine 2HCl. All results are normalised to untreated control. Mean ± s.e.m shown for all cases (n = 6).

4.3 Developing a passaging protocol

4.3.1 Pyridoxal 5'-phosphate for hydrogel degradation

The first passaging trials were attempted using PLP (4 mM) to degrade the hydrogels. HG15 had previously been identified as a hit hydrogel from the HUVEC array screen (see Chapter 3) and thus HUVEC were encapsulated in HG15 for 24 h (denoted as passage 0, P0), before the hydrogel was degraded with PLP. The released cells were collected by centrifugation and counted, with only 53 % of the number of cells originally seeded recovered after hydrogel degradation. The released cells were encapsulated into fresh HG15 (denoted as P1) and incubated for 24 h. Cell viability of the passaged cells was then assessed (FDA/PI staining) (Figure 4.2). Although cell viability was found to be high (> 80 % in the cell cluster shown in Figure 4.2), it was

decided to abandon further studies with PLP for hydrogel degradation and cell passaging, due to low cell release and difficulties in pelleting after centrifugation.

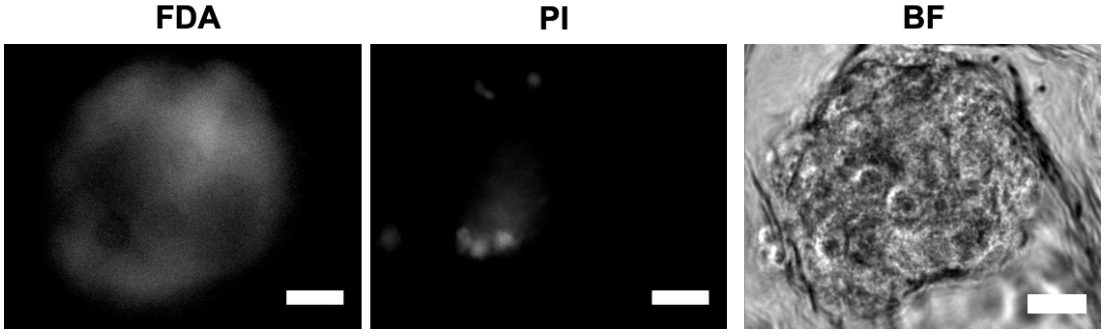

Figure 4.2: Passaging of HUVEC encapsulated in HG15 using pyridoxal 5'-phosphate (PLP). HUVEC were encapsulated in HG15 for 24 h (P0), followed by cell release using PLP (4.0 mM) and encapsulation into fresh HG15 (P1) and incubaion for 24 h. Cell viability was assessed by FDA (live stain) ($\lambda_{ex/em}$ = 490/526 nm) and PI (dead stain) ($\lambda_{ex/em}$ = 570/602 nm). A cell cluster is shown. Scale bar 20 µm. BF = brightfield.

4.3.2 Pyridoxal HCl and Pyridoxamine 2HCl for hydrogel degradation

PyrHCl and PyrAm were used to assess their hydrogel degradation properties, both individually and when combined. 30 min incubation at 37 °C was chosen as the degradation time since early trials of hydrogels in eppendorfs had found that this was the optimal time for complete hydrogel degradation. Solutions of PyrHCl (4.9 mM) and PyrAm (4.1 mM) were tested at different combinations for their capacity to allow hydrogel degradation and cell release (Table 4.2).

Table 4.2: Methods evaluated to afford hydrogel degradation using pyridoxal HCl (PyrHCl) and pyridoxamine 2HCl (PyrAm) with cells seeded, propagated and liberated. PyrHCl (4.9 mM) and PyrAm (4.1 mM) were dissolved in endothelial cell media (Medium 200). Hydrogels (30 µl, n = 2) were seeded with 10,000 HUVEC for each method and the cells were pooled for cell counting.

Method	Hydrogel degradation method	Number of cells seeded	Number of cells pelleted after centrifugation	Cells released as a percentage of cells seeded
A	PyrHCl, 30 min	20,000	29,500	148 %
B	PyrAm, 30 min	20,000	26,500	133 %
C	i) PyrHCl, 15 min ii) PyrAm, 15 min	20,0000	39,000	195 %
D	PyrHCl + PyrAm, 30 min	20,000	26,000	130 %

All combinations resulted in >100 % cell release compared to the number of cells initially seeded (indicating HUVEC proliferation within HG15). It was decided to proceed with method C (Pyr HCl, 15 min + PyrAm 15 min) as it resulted in the highest number of cells recovered after hydrogel degradation and centrifugation (195 %). For the other methods, some cells were found in the supernatant after centrifugation.

During the degradation trials, it was found that some of the hydrogel components were released with the cells after degradation. During centrifugation these fragments pelleted to the bottom before the cells did, thus limiting the centrifugation efficiency for cell collection. Therefore, a "straining step" was added after hydrogel degradation wherein the cell suspension was filtered through a cell strainer that allowed the cells to pass through, but "trapped" the hydrogel network fragments. Cell collection by centrifugation was then found to be more efficient. However, this "cell-hydrogel" material could well be an ideal material to allow subsequent passaging with cell binding to this "semi-synthetic ECM", but this was not explored further.

4.4 3D cell culture and passaging in HG15

4.4.1 Encapsulation and passaging of HUVEC

Once the method for hydrogel degradation was developed, cell viability after passaging within HG15 was investigated. HUVEC were encapsulated in HG15 for nine days (P0), followed by passaging into a new set of HG15 (P1). After 6 days culture cell viability was analysed by Calcein AM/PI staining (Figure 4.3). High viability was observed and cell clusters formed as readily for P1 as they had with P0.

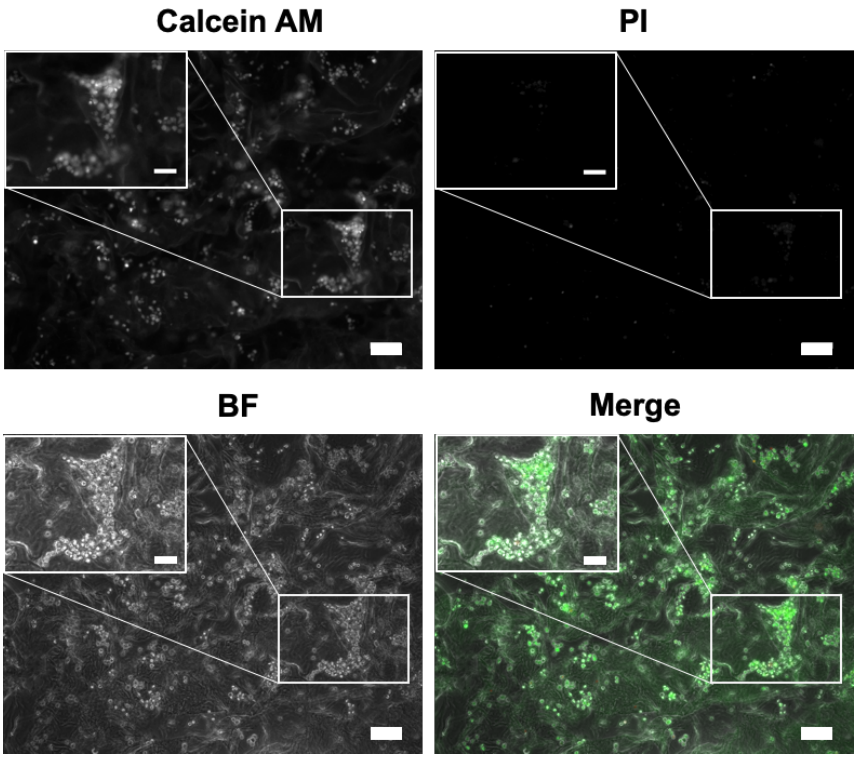

Figure 4.3: Passaging of HUVEC encapsulated in HG15 using pyridoxal HCl (PyrHCl) and pyridoxamine 2HCl (PyrAm). HUVEC were encapsulated in HG15 for nine days (P0), followed by hydrogel degradation and cell release using PyrHCl (4.9 mM) and PyrAm (4.1 mM) and encapsulation into another HG15 (P1) and incubation for six days. Cell viability was assessed by Calcein AM (live stain) ($\lambda_{ex/em}$ = 488/515 nm) and PI (dead stain) ($\lambda_{ex/em}$ = 570/602 nm). BF = brightfield. Merge = merge of Calcein AM (green), PI (red) and BF images. Scale bar of full image 100 µm. Scale bar of cut-out 50 µm.

Passaging over several passages was necessary to demonstrate the usefulness of the passaging method and thus passaging over 3 passages of HUVEC encapsulated in HG15 was attempted (Table 4.3 and Figure 4.4). Both the first (P0 to P1) and second

passaging (P1 to P2) resulted in ≥100 % of the cells seeded being released, but the centrifugation step did not result in all cells being collected, with many still in the supernatant (Table 4.3). Cell viability at P2 was analysed by Calcein AM/PI staining and although all the cells were alive, the lower cell numbers seeded into the hydrogels resulted low levels of cell clustering compared to P0 and P1 (Figure 4.4). The third passage (P2 to P3) allowed few cells to be released, and no cell pellet was observed after centrifugation, which led to the experiment being stopped.

Table 4.3: Passaging of HUVEC encapsulated in HG15 using pyridoxal HCl (PyrHCl, 4.9 mM) and pyridoxamine 2HCl (PyrAm, 4.1 mM) over three passages. Hydrogels (100 µL, n = 8) were seeded with HUVEC for each method, and the cells were pooled for cell counting. The number of cells released after hydrogel degradation and the number of cells pelleted after centrifugation are given. Percentages are based on the numbers of cells seeded (calculated by cell counting).

Passage point	Number of cells seeded	Number of cells released	Number of cells pelleted after centrifugation
P0 → P1	400,000	400,000 (100 %)	350,000 (87 %)
P1 → P2	350,000	420,000 (120 %)	275,000 (65 %)
P2 → P3	275,000	42,000 (15 %)	No pellet

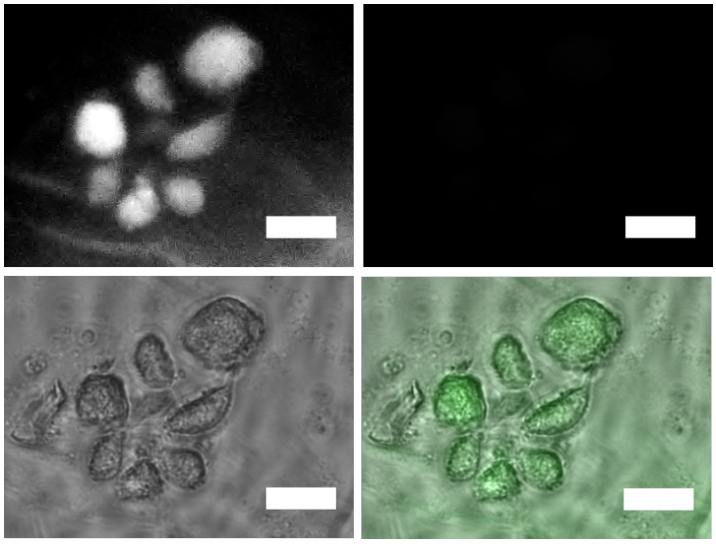

Figure 4.4: Passaging of HUVEC encapsulated in HG15 using pyridoxal HCl (PyrHCl, 4.9 mM) and pyridoxamine 2HCl (PyrAm, 4.1 mM) after 6 days (P0), and encapsulation into another HG15 (P1) and incubation for six days with repeated cell release and passaging (P2). After 24 h incubation of P2, cell viability was assessed using Calcein AM (live stain) ($\lambda_{ex/em}$ = 488/515 nm) and PI (dead stain) ($\lambda_{ex/em}$ = 570/602 nm). BF = brightfield. Merge = merge of Calcein AM (green), PI (red) and BF images. Scale bar 20 µm.

4.4.2 Encapsulation and passaging of HEK293

The problems with poor cell proliferation, limited release from the hydrogel and the low number of cells pelleting after centrifugation as a function of continued passaging were investigated by changing the cell type to HEK293. These cells proliferate faster compared to HUVEC, and do not require specialist cell media, making their culture more time and cost-effective and better suited for problem-shooting experiments. In a similar manner to Section 4.4.1, HEK293 cells were encapsulated into HG15 and passaged with hydrogel release using PyrHCl and PyrAm. Over four passages, good levels of cell release after hydrogel digestion and filtering through a cell strainer was achieved (Table 4.4). Cell proliferation as a measure of the cells released was only observed for P0 → P1 (125 % cell release compared to the amount seeded). As for the number of cells pelleting after centrifugation, the number was around 70 % for both P0 → P1 and P1 → P2, but dropped to 40 % for P2 → P3. For passage P3 → P4 no cell pellet was observed after centrifugation.

Table 4.4: Passaging of HEK293 encapsulated in HG15 using pyridoxal HCl (PyrHCl) and pyridoxamine 2HCl (PyrAm) over four passages. The percentage of cells released after hydrogel degradation and the percentage of cells pelleted after centrifugation based on the cells seeded are given. Hydrogels (100 µl) were seeded with HEK293 and the cells were pooled for cell counting at each passage point (P0 → P1: n= 8, for all other passage points n = 4).

Passage point	Amount of cells seeded	Cells released as a percentage of cells seeded	Cells pelleted as a percentage of cells seeded
P0 → P1	800,000	995,000 (125 %)	703,500 (88 %)
P1 → P2	579,500	537,500 (93 %)	366,500 (63 %)
P2 → P3	366,500	340,000 (93 %)	137,000 (38 %)
P3 → P4	137,000	127,000 (93 %)	No pellet

To assess the cell viability following passaging, the supernatant from centrifugation of the cells suspension was seeded onto TCPS and incubated overnight to allow for cell attachment. Thereafter, the cells were stained with Hoechst and Calcein AM to visualise the nuclei and assess the cell viability respectively (Figure 4.5). High cell viability was observed over all passages.

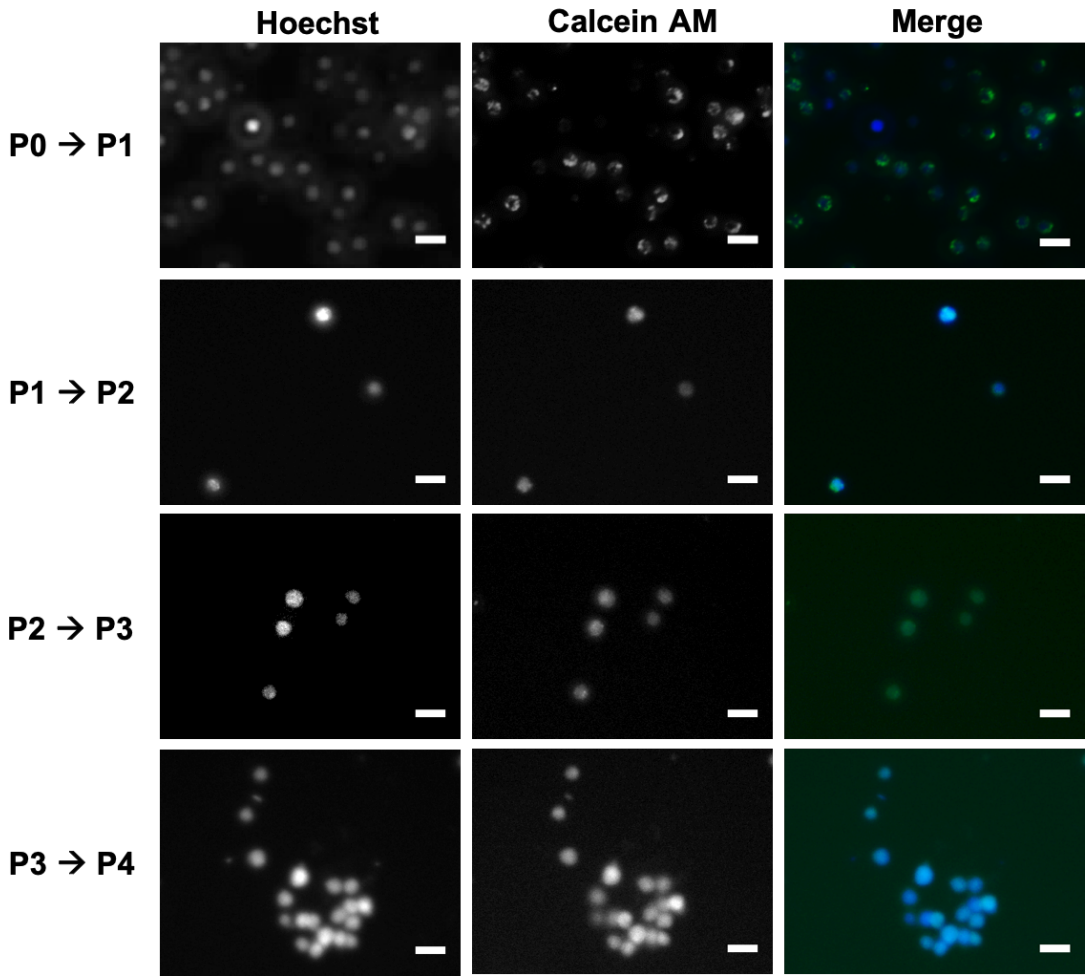

Figure 4.5: Passaging of HEK293 encapsulated in HG15 using pyridoxal HCl (PyrHCl) and pyridoxamine 2HCl (PyrAm). HEK293 were encapsulated in HG15 for 6 days (P0), followed by cell release using PyrHCl (4.9 mM) and PyrAm (4.1 mM) and encapsulation into another HG15 (P1). This procedure was repeated over four passages. The supernatant from cell centrifugation after hydrogel degradation still contained cells, and at each passaging point, the cell supernatant was plated on TCPS and incubated for 48 h. The cell viability of the cells on TCPS was assessed by Calcein AM (live stain) ($\lambda_{ex/em}$ = 488/515 nm). The nuclei were stained with Hoechst ($\lambda_{ex/em}$ = 361/497 nm). BF = brightfield. Merge = merge of Calcein AM (green) and Hoechst (blue) images. Scale bar 20 μm.

4.5 Discussion

The use of enzyme digestion for cell passaging is not ideal for cell culture as the enzymes commonly used (e.g. trypsin, collagenase) can themselves be harmful to the cells, suggesting than an enzyme-free passaging protocol would be beneficial.

Moreover, a common hurdle for the advancement of hydrogels and scaffolds for 3D cell culture is the ability to afford cell release and/or material degradation to enable passaging. To address both these issues, herein was developed a passaging system that is both enzyme-free and allows for degradation of a 3D hydrogel with cell release.

The previously reported use of the PyrHCl to degrade imine cross-linked PEG:chitosan hydrogels[80] did not examine whether the conditions used were biocompatible. Herein we examined both PyrHCl and PLP (aldehyde-bearing) and PyrAm (amine-bearing) for their capacity to compete with the imine-linkage in the hydrogel structures and cause their degradation. After determining the biocompatible pH range of each component, cytotoxicity studies were carried out. These revealed that treatment with all three compounds would be suitable for 30 min incubations when used at ~ 5 mM.

Cell passaging with PLP over one passage was found to be biocompatible, with good cell viability after hydrogel degradation and passaging into another set of HG15. It was found, however, that PLP was less efficient at degrading the hydrogels compared to PyrHCl and PyrAm, reflected by the number of cell released after hydrogel degradation. Therefore, it was decided to use PyrHCl and PyrAm for the passaging system, with the protocol possible with either or both components. Based on the number of cells released after passaging from HG15, the combination of incubating the hydrogel with PyrHCl (4.9 mM) for 15 min and then adding PyrAm (4.1 mM) for another 15 min was optimal. There is no obvious reason why this order and not the opposite (first adding in PyrAm, then PyrHCl) would cause higher levels of hydrogel degradation and thereby cell release. After adding the step of removing hydrogel fragments with a cell strainer, followed by centrifugation, the passaging protocol was complete.

Passaging over one passage with the PyrHCl+PyrAm system showed good cell release and centrifugation and high cell viability of both HUVEC and HEK293 at the P0 → P1 stage. Further passaging, however, was not straightforward due to issues with cell pelleting after centrifugation, which was evident already at the P1 → P2 stage. Several attempts to solve this were attempted, such as longer centrifugation times (20 min) and at lower speed (120 g), as well as repeated centrifugation steps.

None of these improved the results compared to the original method (300g, 2×10 min). Passaging over four passages with HEK293 did confirm, however, that the cells that remained in the supernatant were viable. The use of a cell filter that traps cells rather than letting them through could be a future solution to the issue of poor cell centrifugation, as it removes the need for pelleting.

4.6 Conclusions

A straightforward, enzyme-free and mild passaging system was developed. Although the total time of passaging of 1 hour (30 min hydrogel digestion and around 30 min washings and centrifugation) is longer than the typical 5-10 min trypsin digestion, it is comparable with other 3D matrix digestions protocols, such as collagenase (up to 1 h digestion plus washings and centrifugation). This passaging system and component concentrations used are hypothesised to be compatible with most imine cross-linked hydrogels, independent of hydrogel concentration and rigidity.

4.7 Materials and Methods

4.7.1 Instruments for cell experiments

HERAcell 150 incubator (Heraeus, Germany)

HERAsafe KS 18 class II biosafety cabinet (Heraeus, Germany)

4.7.2 Imaging instruments

Axiovert 200m inverted fluorescence microscope with Axiovision 4.8 software (Carl Zeiss AG, Germany). Filters: DAPI ($\lambda_{ex/em}$ = 300-395/430-505 nm), GPC/FITC ($\lambda_{ex/em}$ = 447-494/500-554 nm), YPF ($\lambda_{ex/em}$ = 490-512/520-554 nm), TRITC/Rhodamine/Cy3 ($\lambda_{ex/em}$ = 527-563/570-650 nm) and Cy5 ($\lambda_{ex/em}$ = 620-659/663-725 nm) filters. Magnification: x10, x20 and x40

Image analysis was carried out in ImageJ

4.7.3 Cells, media and biological equipment

Primary HUVEC were purchased from ATCC (PCS-100-010™)

HUVEC were donated by Dr Kate Cameron (University of Edinburgh)

Complete Medium 200: Medium 200, Low Serum Growth Supplement (LSGS) kit (Thermo Fisher, USA)

Sterile cell strainer (40 μm nylon mesh) (Thermo Fisher, USA)

4.7.4 Cell Culture on Tissue Culture Polystyrene

HEK293T cells were cultured in complete DMEM. HUVEC and primary HUVEC were cultured in complete Medium 200. Cells were grown to 70–80% confluency in T25 flasks (37 °C, 5% CO_2) before passaging. Immortalised HUVEC were used between passage 5–9 and primary HUVEC from passage 1–4.

4.7.5 Cell viability studies and pH measurement of pyridoxal 5'-phosphate, pyridoxal HCl and pyridoxamine 2HCl

HUVEC were plated in 96-well plates (8000 cells/well, n = 6) in 100 μL Medium 200 supplemented with LSGS (Complete Medium 200) and incubated (37 °C, 5 % CO_2) overnight. The media was removed and each well washed with Hank's buffer (1×100 μL). Solutions of pyridoxal 5'-phosphate, pyridoxal hydrochloride and pyridoxamine dihydrochloride (in complete Medium 200) were added to the wells at the desired concentrations (see Figure 4.1) and incubated for 30 min (37 °C, 5 % CO_2). The well plates were allowed to equilibrate at room temperature for 30 min. CellTiter Glo 2.0 (Promega) (100 μL/well) was added to each well and the plates were shaken on an orbital shaker for 2 min to lyse the cells. The plates were left to equilibrate for 10 min. The contents of each well were transferred to a white 96-well plate (Costar 3917) and

the luminescence signal measured using a plate reader. For each compound and concentration controls with no cells were added. The pH of each concentration was measured using pH paper.

4.7.6 Passaging of HUVEC in HG15 with pyridoxal 5'-phosphate

HG15 (n = 3) was prepared and sterilised as described in Chapter 3 (see 3.11.8). Hydrogel formation and *in situ* cell encapsulation was achieved by addition of complete Medium 200 (100 µL) with suspended HUVEC (32,000, n = 3) followed by incubation (37 °C, 5% CO_2) for 48 h. Pyridoxal 5'-phosphate (4 mM, 200 µL) in complete Medium 200 was added to each gel and incubated for 30 min (37 °C, 5 % CO_2). The degraded hydrogels/cell solutions were removed from the wells, and the wells were washed with Hank's buffer (2×100 µL) and the combined solution was centrifuged (300 g, 5 min). After removal of the supernatant the cells were counted (51 000 cells, 53 % of original amount seeded). The cell pellet was re-suspended in complete Medium 200 (300 µL) and seeded into new sets of HG15 (17,000 HUVEC/HG15, n = 3) and incubated (37 °C, 5 % CO_2) for 24 h. Cell viability was analysed by staining with Calcein AM and PI (488/570 nm, LIVE/DEAD Cell Imaging Kit ThermoFisher) according to manufacturer's protocol and imaged on a Zeiss AxioVert 200m fluorescence microscope.

4.7.7 Developing a passaging protocol with pyridoxal HCl and pyridoxamine 2HCl

HG15 (n = 8) was prepared and sterilised as described in above (see 3.11.8). using 8-well CultureWell silicone gaskets (30 µL/hydrogel). Hydrogel formation and *in situ* cell encapsulation was achieved upon addition of complete Medium 200 (30 µL) with suspended HUVEC (10,000, n= 8) followed by incubation (37 °C, 5% CO_2) for 24 h. Hydrogel degradation was attempted using four different methods (See Table 4.2 for methods and cell counting data). Following degradation, and washing with Hank's buffer (1×30 µL) the resulting cell suspension was centrifuged (300 g, 2×10 min), the supernatant removed, the cells suspended in 100 µL of complete Medium 200 and the cells counted.

4.7.8 Passaging of HUVEC in HG15 with pyridoxal HCl and pyridoxamine 2HCl

HG15 (n = 8) was prepared and sterilised as described above (see 3.11.8). Hydrogel formation and *in situ* cell encapsulation was achieved upon addition of complete Medium 200 (100 µL) with suspended HUVEC (50,000, n = 8) followed by incubation (37 °C, 5% CO_2) (P0). After six days, pyridoxal HCl (4.9 mM) in complete Medium 200 was added to each gel and incubated for 15 min (37 °C, 5 % CO_2) followed by addition of pyridoxamine 2HCl (4.1 mM) in complete Medium 200) and further incubated for 15 min (37 °C, 5 % CO_2). The degraded hydrogels and cell solutions were removed from the wells and filtered through a cell strainer (40 µm nylon mesh, Fisher Scientific). Each well was washed with Hanks's buffer (2×100 µL) and the solution was filtered through the cell strainer. The cell number in the combined washings and cell solutions was counted and the solution then centrifuged (300 g, 2×10 min). The number of cells pelleted were counted (For details on cells seeded, released and pelleted see Table 4.3) and suspended in complete Medium 200 and seeded into new sets of HG15 as above and incubated (37 °C, 5 % CO_2) (P1). The same procedure was repeated for subsequent passages. For P2 two out of eight replicates were stained with Calcein AM and PI (488/570 nm, LIVE/DEAD Cell Imaging Kit ThermoFisher) according to the manufacturer's protocol and imaged using a Zeiss AxioVert 200m fluorescence microscope. The remaining five hydrogels were degraded and the cells were used to attempt further passaging (P2 → P3), but no cell pellet was observed upon centrifugation.

4.7.9 Passaging of HEK293 in HG15 with pyridoxal HCl and pyridoxamine 2HCl

Passaging was carried out at described above (see 4.7.8), but at a higher HUVEC density per HG15 (100,000 cells in 100 µL complete Medium 200, n = 8 for P0 → P1, n = 4 for all other passage points). For details on cell seeded, released and pelleted see Table 4.4. At each passage, the supernatant obtained after centrifugation was seeded into 24-well plates and incubated for 72h (37 °C, 5 % CO_2). The cells were then stained

with 1 mL of combined Hoechst (1 μL of 10 mg/mL stock diluted into 10 mL PBS) ($\lambda_{ex/em}$ = 361/497 nm) and Calcein AM (4 μL of 500 μM stock diluted into 1 mL Hoechst staining solution) ($\lambda_{ex/em}$ = 496/596 nm) staining solution by incubation for 15 min at room temperature. Imaging carried out on a Zeiss AxioVert 200m fluorescence microscope.

Chapter 5: Identifying a defined substrate for niche mimicking and trapping of pancreatic cancer stem cells‡

5.1. Introduction

In 2012, the world health organisation estimated that 32.6 million people world-wide lived with cancer, and that 14.1 million new cancer diagnoses were reported.[172] As such, cancer is a very important target for researchers to understand and develop new treatments for. The term cancer, however, composes a wide range of types, e.g. breast, lung, skin or prostate that all differ in their cellular composition and disease progression. Even within a single solid cancer tumour, a large amount of cell heterogeneity is found.[173,174] Between tumour cells differences in, for example, proliferation rate, metastatic propensity and cell-cell interaction makes the tumour cell population very diverse.[173,175]

Tumour cell heterogeneity was originally explained by two models, the stochastic and the hierarchical models.[176,177] In the stochastic model, every tumour cell possesses the same probability of being tumorous. Any variation observed within the tumour population is attributed to stochastic differences in internal and external influences upon the cells. In the past 10-15 years, however, mounting evidence has been found for the hierarchical model[176,178] (Figure 5.1A), where a small subpopulation of tumour cells are capable of initiating and maintaining tumours. This subpopulation is commonly referred to as Cancer Stem Cells (CSCs), because of their stem-like properties, such as self-renewal.[178]

‡Initial polymer microarray printing was performed Dr Christian Mangani (University of Edinburgh) before the start of the author's PhD. Dr Mangani also supervised the initial microarray screen. All biological experiments were performed by Dr Yoshitaka Murota with Assistant Professor Kouichi Tabu and Professor Tetsuya Taga (Tokyo Medical and Dental University). Scale-up polyacrylate/acrylamide synthesis, coverslip coating, peptide monomer synthesis and peptide-containing polymer microarray printing and scale-up was carried out as part of this thesis.

This subpopulation of tumour cells are able to undergo both symmetric (leading to two CSCs or two differentiated cells) and asymmetric cell division (leading to one CSC and one differentiated cell)[179] and are thereby able to both maintain their own population and progress tumour growth. CSCs have been identified in a number of cancers including breast,[180] brain,[181] colon,[182,183] prostate,[184] leukaemia,[185] ovarian,[186,187] and pancreatic cancer,[188] and the hierarchical model is an accepted concept for tumour progression.[178] CSCs have been found to be resistant to many chemotherapeutic drugs and their existence can explain the common recurrence of tumours despite successful chemotherapies that seemingly eradicated the targeted tumour.[189,190] This makes CSCs an attractive drug target for anticancer treatments with the belief that eradicating them would lead to complete tumour eradication. However, despite several discoveries in the field of anti-CSC therapeutics, their eradication is not straightforward. One rationale for this is because CSCs reside in a so-called "CSC niche" that protects the CSCs and substantial efforts have been made to identify the make-up of the niche in different tumours. In the initial hierarchical model, it was proposed that CSCs, similarly to normal stem cells, were rare and/or mainly existed in a dormant (quiescent) state in these niches (Figure 5.1A). Recent findings, however, show that the number of CSCs increase with tumour progression, and that their original dependence on their niche decreases with increased tumour malignancy (Figure 5.1B).[178,191] Moreover, there is evidence that differentiated cells, through their plasticity, are able to revert to CSCs. This suggests that only targeting the CSCs to eradicate tumours may not be enough since the differentiated progeny also may be resistant to chemotherapeutic agents[178].

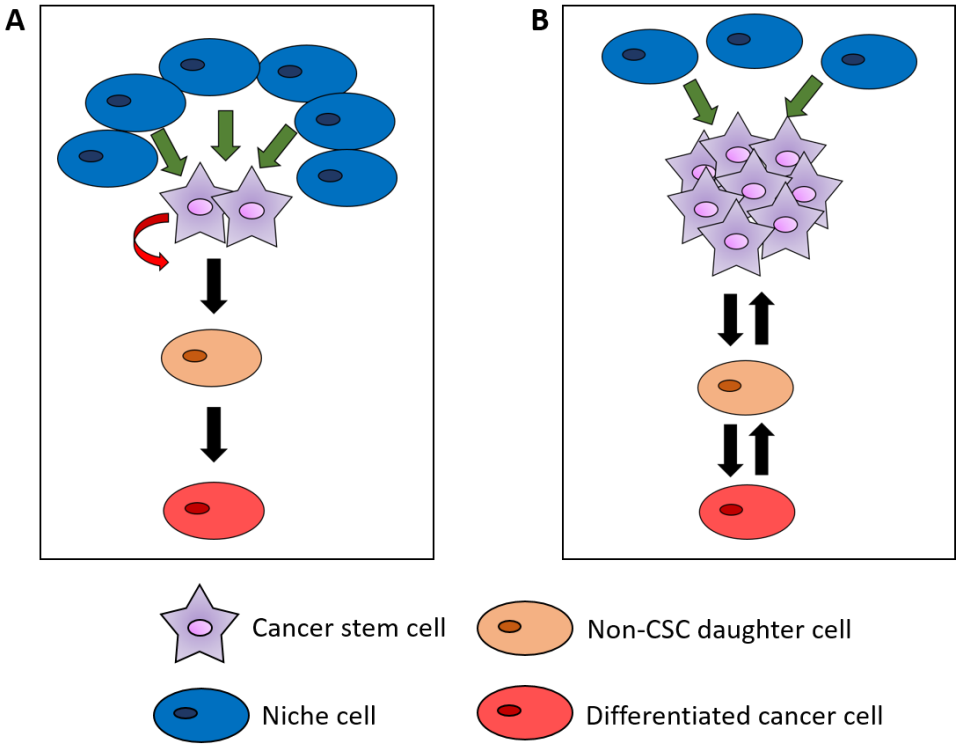

Figure 5.1: Cancer stem cell (CSC) models. **A.** Classic CSC model (also known as hierarchical model). CSCs make up a small subpopulation of the total tumour environment, with a large niche cell presence to guide CSCs. Herein only CSCs are able of self-renewal, while non-CSC daughter cells only are capable of differentiation. **B.** Modified CSC model. CSCs are not rare and/or quiescent and with tumour progression CSCs become less dependent of their niche cells. Both non-CSC daughter cells and differentiated cancer cells have inherent plasticity, capable of reprogramming to CSCs.[178] Green arrows indicate niche signalling. Red arrow indicates self-renewal.

To be able to further understand tumour progression and the role of CSCs, it is necessary to be able to culture CSCs *in vitro* in a scalable manner. It is vital that such culturing conditions maintain the CSC niche, so that the cells maintain their stemness and do not differentiate. To this end, a recent publication between the Taga and Bradley labs identified a polyurethane (PU10), that bound a series of proteins that allowed recapitulation of the glioma CSC niche.[126]

Pancreatic cancer is a very lethal form of cancer, primarily due to its usually late diagnosis with an estimated five-year survival rate of 6.7 %.[192] A hallmark of pancreatic cancer is its highly invasive nature and it has been suggested that pancreatic CSCs are responsible for this and the poor tumour response to current

treatments.[193–195] The isolation of pancreatic CSCs was first described in 2007 when primary human pancreatic adenocarcinomas were implanted in immunocompromised mice, followed by the identification of cell surface markers to identify the pancreatic CSC subpopulation.[188] Cells expressing three markers, CD44, CD24 and epithelial-specific antigen (ESA) (0.2-0.8 % of the cell population), were identified as pancreatic CSCs since they could self-renew and differentiate. Furthermore, injection of 100 pancreatic CSCs into mice was enough to form the same type of tumours as they had originated from. Therefore, using fluorescence assisted cell sorting (FACS) of CD44+/CD24+/ESA+ cells is a useful way of separating pancreatic CSCs from non-CSCs.

The Hoechst 33342 dye exclusion assay is another method for separating CSCs from the non-CSCs. This assay was first developed in the Taga lab to isolate rat glioma C6 CSCs.[196] It is based on the principle that CSCs efflux the DNA binding dye Hoechst 33342 more efficiently than non-CSCs, due to an ATP binding cassette transporter. The CSCs are also known as the side population and the non-CSCs as the main population.

Another method of separating CSCs from non-CSCs utilises the low activity in CSCs of the protein degrading proteasomes.[197] CSCs were separated from non-CSCs (in both glioma and breast cancer cell lines) based on the low activity of proteasome 26S in CSCs.[198] Many proteins require ubiquitination to allow initiation of proteasome degradation, but the protein ornithine decarboxylase (ODC) can be directly degraded by proteasome 26S, avoiding the need for ubiquitination. The recognition site for proteasome 26S in ODC, the so-called degron sequence, is a 37-amino acid sequence at the carboxyl terminus (known as cODC). Using ZsGreen (a fluorescent reporter), fused to the cODC gene a reporter protein (ZsGreen-cODC) was created.[199] In non-CSC cells (with normal activity of proteasome 26S), ZsGreen-cODC was rapidly degraded, conversely, in the CSC subpopulation, low proteasome 26S activity resulted in accumulation of ZsGreen-cODC and thereby stronger ZsGreen fluorescent signal. Using FACS, it was possible to separate the CSC from the non-CSC populations and this method has subsequently been shown to enable the separation of pancreatic CSCs from non-CSCs, and was employed to sort the cells used in this work.

The aim of this chapter was to identify polymeric substrates that could support pancreatic CSCs over longer periods of incubation (> 48 h, referred to as "niche-mimicking"), or that were able to selectively bind CSCs over shorter incubation times (6-24 h, referred to as "trapping"). Using the established polymer microarray techniques of the Bradley group,[115,116,200] 100's of different polymers were screened. In the first instance a library of polyacrylate/acrylamides and polyurethanes were screened, subsequently a novel peptide-incorporating polyacrylate/acrylamide library was developed and screened.

5.2 CSC niche mimicking polymer identification

5.2.1 Polymer microarray screening

To identify pancreatic CSC niche-mimicking substrates, a polymer microarray of polyacrylate/acrylamides and polyurethanes of varied structural properties was printed using an in-house polymer library.[115,116,200] The arrays consisted of 382 polymers (209 polyacrylates/acrylamides, 173 polyurethanes), all in triplicates (1146 features per array) (See Appendix Figure A3.1 for array layout and Table A3.1 and A3.2 for polymer compositions).

As a pancreatic cancer cell model, KLM1 cells (a human pancreatic adenocarcinoma cell line) were used. To allow separation of the subpopulation of CSCs within the cell line the genetically engineered version of the cells (KLM1-ZsGreen-cODC) was established by fusing the ZsGreen gene to the C-terminal part degron of murine cODC[198,199]. The KLM1-ZsGreen-cODC cells were then isolated by FACS with cells with a high ZsGreen intensity (ZsGreen(+)) collected as the CSC fraction, and the rest of the cell population was named the non-CSC fraction (ZsGreen(-)) (Figure 5.2). A 1:1 mixture of the CSC and non-CSC cells were seeded onto the polymer microarrays and analysed for the ability to selectively bind CSCs and maintain and propagate their phenotype over 48 h.

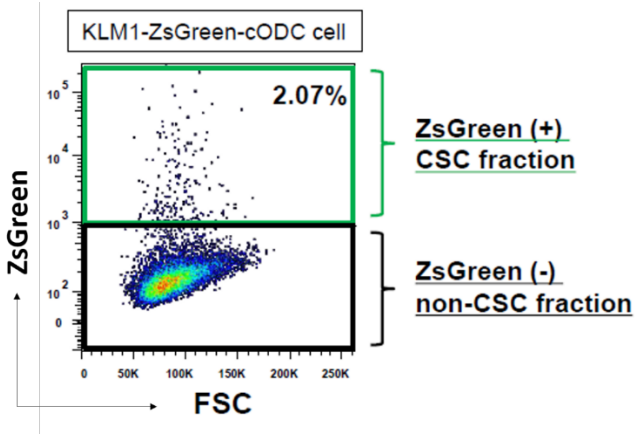

Figure 5.2: Flow cytometry of CSCs of a ZsGreen-cODC transfected KLM1 cell line. CSC were isolated based on their low 26S proteasome activity towards ornithine degradation, and consequently high ZsGreen intensity (ZsGreen(+)). Figure produced by Dr Murota.

Two microarray-printed slides were analysed, with the first seeded with a 1:1 ratio of CSCs and non-CSCs (1×10^6 cells/slide) and incubated for 18 h. The ZSGreen fluorescence intensity was measured for each polymer spot and the slide was incubated for another 30 h. After a total of 48 h incubation the ZsGreen fluorescent intensity was measured again, followed by cell fixing, Hoechst staining and fluorescence intensity measurement at each polymer spot. The second slide was seeded in the same manner, but incubation was stopped after 18 h when ZsGreen fluorescence was measured, the cells were fixed, stained with Hoechst and the fluorescence intensity was measured. The ZsGreen intensity was used as a measure of CSC attachment, while the Hoechst intensity gave the total cell number per spot.

Niche and control polymers for scale-up studies were chosen based on calculated values of 'increasing rate of CSC number' and 'CSC specific support' (see Figure 5.3, Equation 1 and 2). Polymers with high values of both (i.e. polymers that selectively bound CSCs after 18 h and then underwent self-renewal) were considered as putative hit candidates (Figure 5.4). Polymers with low values of 'increasing rate of CSC number', but similar 'increasing rates of total cell number' (see Figure 5.3, Equation 3 and 4) as the niche polymer candidates, were used as putative negative control polymers. Based on this analysis three putative niche-mimicking polymers (PA531, PA419, PA514) and four negative control polymers (PA435, PA418, PA108, PA548) (Figure 5.5 and 5.6) were chosen for scale-up to confirm the microarray results.

$$\text{Increasing rate of CSC number} = \frac{\text{ZsGreen intensity (48 h)}}{\text{ZsGreen intensity (18 h)}} \quad \text{(Eqn. 1)}$$

$$\text{CSC specific support} = \frac{\text{ZsGreen intensity (48 h)/Hoechst intensity (48 h)}}{\text{ZsGreen intensity (18 h)/Hoechst intensity (18 h)}} \quad \text{(Eqn. 2)}$$

$$\text{Predicted Hoechst intensity (48 h)} = \frac{\text{ZsGreen intensity (18 h)}}{\text{ZsGreen intensity (18 h)/Hoechst intensity (18 h)}} \quad \text{(Eqn. 3)}$$

$$\text{Increasing rate of total cell number} = \frac{\text{Hoechst intensity (48 h)}}{\text{Predicted Hoechst intensity (48 h)}} \quad \text{(Eqn. 4)}$$

$$\text{CSC specificity} = \frac{\text{ZsGreen intensity (18h)}}{\text{Hoechst intensity (18 h)}} \quad \text{(Eqn. 5)}$$

Figure 5.3: Equations used to calculate paramters considered for identifying CSC niche-mimicking and trappins polymers

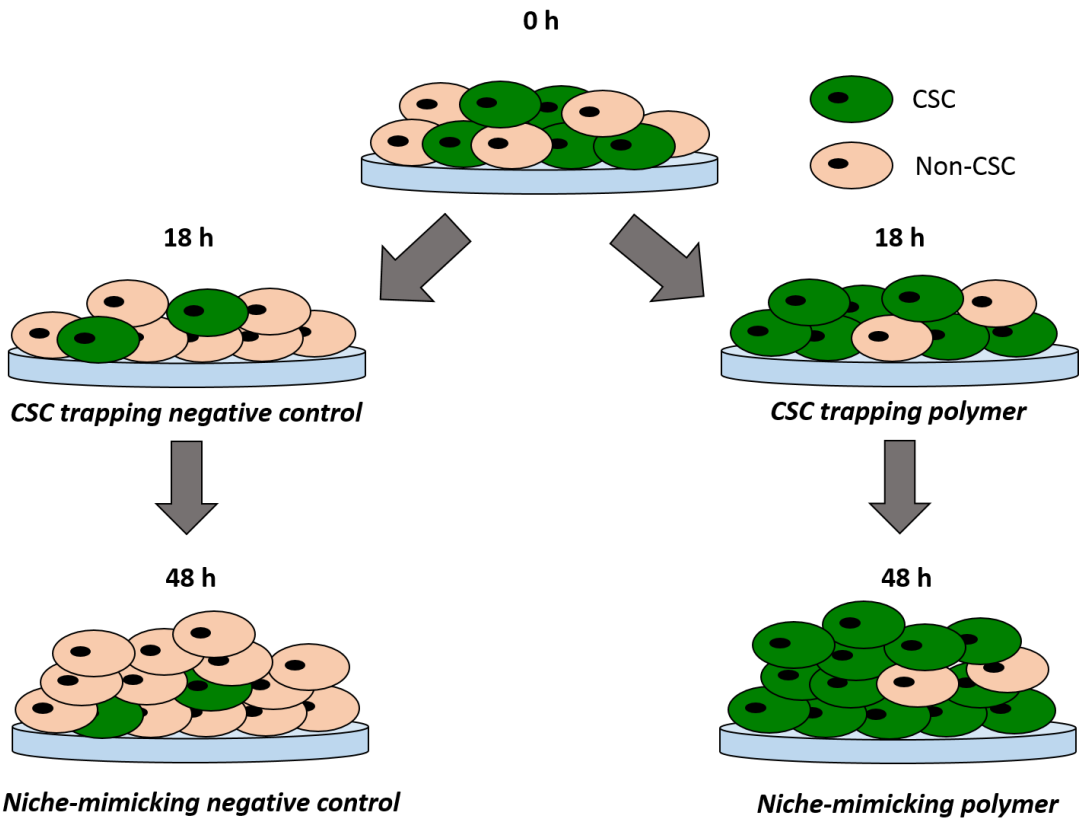

Figure 5.4: Basis of choosing putative CSC niche-mimicking and CSC-trapping polymers and negative controls after polymer microarray seeding. A 1:1 ratio of CSCs (ZsGreen(+)) and non-CSCs (ZsGreen(-)) were seeded on the array. On polymer spots considered as niche mimicking hits, CSCs bind preferentially over non-CSCs at 18 h, and then preferentially undergo self-renewal rather than divide to from non-CSC daughter cells. In contrast, negative control polymers are polymer spots where preferential binding of non-CSCs and differentiation of CSCs to non-CSCs occur. On polymer spots considered as CSC trapping hits, CSCs bind preferentially over non-CSCs at 18 h. In contrast, negative control polymers are polymer spots that show preferential binding of non-CSCs at 18 h.

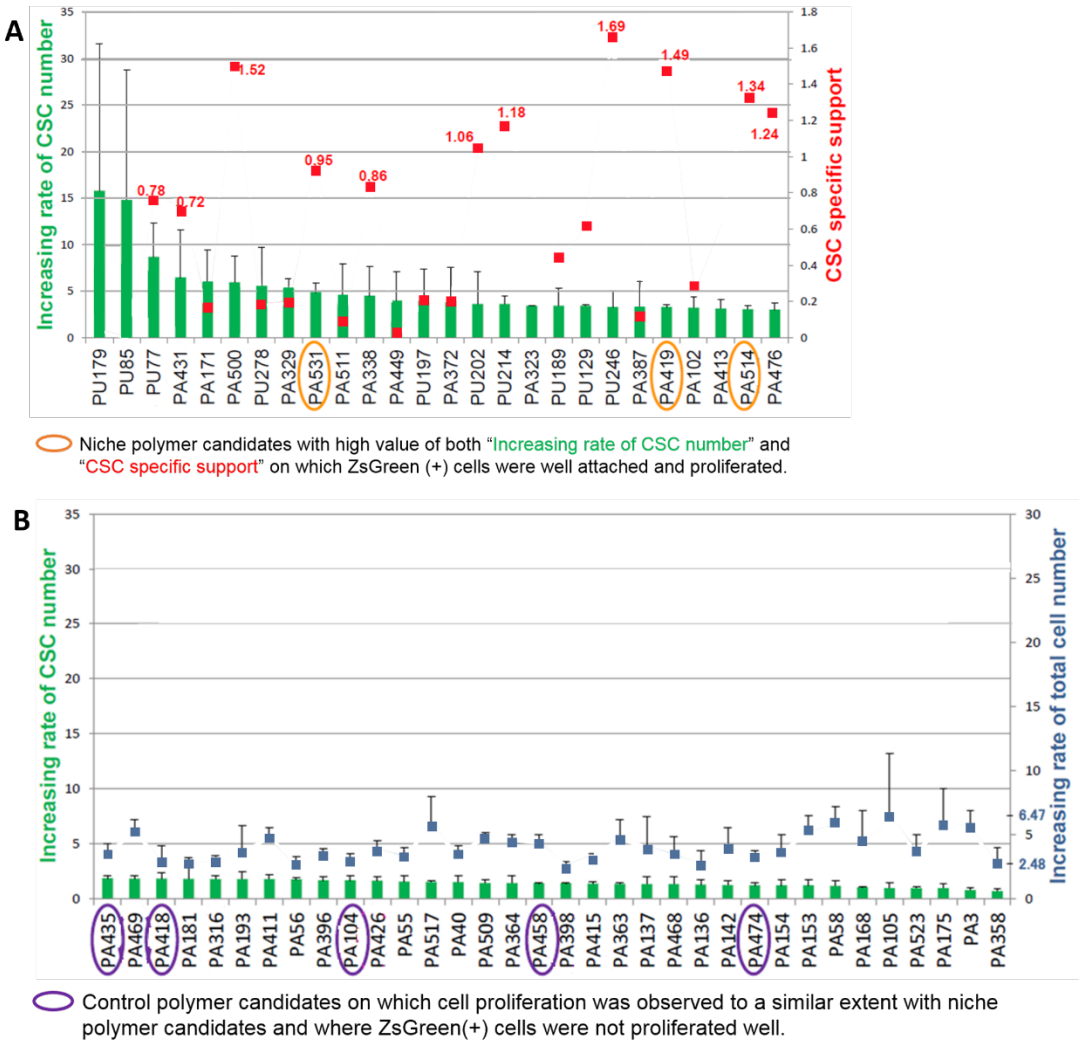

Figure 5.5: Analysis of a 382-polymer microarray to select niche-mimicking polymer candidates for scale-up studies. **A**. 26 polymers with high values of "Increasing rate of CSC Number" (green bars) and "CSC specific support" (red square) were considered as potential niche-mimicking substrates subset. Three polymers, PA531, PA419, PA514 (circled in orange) were chosen to scale-up as putative niche-mimicking hits. **B**. 34 polymers with similar cell proliferation rates as the chosen niche-mimicking hits, calculated as "Increasing rate of total cell number" (blue squares), but with low "Increasing rate of CSC number" were considered as potential negative controls. Four polymers, PA435, PA418, PA104 and PA458 were chosen to scale-up as putative negative controls. Figure produced by Dr Murota and modified. Mean (n = 4) with ± SD is shown in all cases.

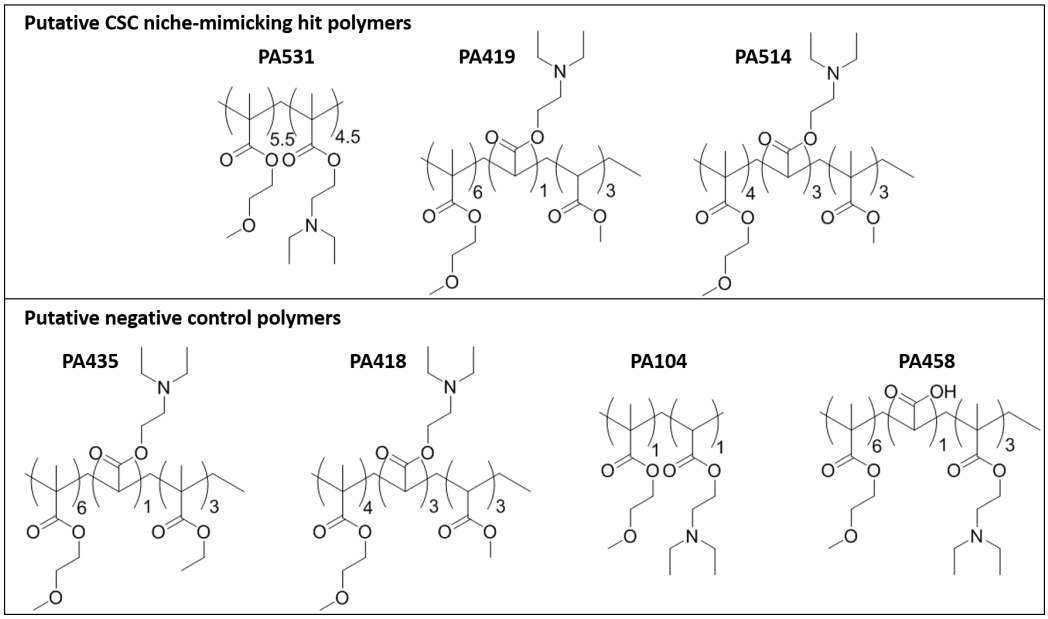

Figure 5.6: Structure of polyacrylates chosen for scale-up for CSC niche-mimicking substrate identification.

5.2.2 Polymer screening

To study the chosen polymers (all polyacrylates/acrylamides) at a larger scale, the polymers were resynthesized via AIBN-initiated random free radical polymerisation and characterised by GPC (for M_n, M_w and PDI of the scaled-up polymers see Table 5.1, for GPC traces see Appendix Figure A3.2).

Table 5.1: M_n, M_w and PDI values of scaled-up polyacrylates/acrylamides as putative niche-mimicking polymers and the negative controls, as determined by GPC.

Polymer Name	**M_n (g/mol)**	**M_w (g/mol)**	**PDI**
Hits			
PA531	59,500	183,500	3.08
PA419	64,100	222,700	3.08
PA514	43,800	133,900	3.05
Negative controls			
PA104	42,800	109,200	2.56
PA435	66,00	210,900	3.20
PA418	38,700	92,800	2.40
PA458	60,200	197,300	3.36

The resulting polymers were spin-coated as solutions (1 % w/v in THF) onto agarose (1 % w/w) coated glass coverslips (32 mm in diameter). A 1:1 ratio of CSCs and non-CSCs were seeded onto the coverslips (1.25×10^5 cells/coverslip) and incubated for 48 or 96 h, followed by cell counting and cell release by trypsinisation for flow cytometry analysis of the number of ZsGreen(+) cells. After 48 h, rounded cells were observed on both the niche and control polymer candidates, suggesting poor cell attachment. After 96 h however, cells started spreading and proliferated well on the polymers. Although this was an improvement compared to conventionally used polystyrene (PS) dishes (results not shown), there was no significant difference observed between the niche and control polymer candidates (Figure 5.7). As such, it was decided to re-analyse the results from the microarray screen to identify a CSC 'trapping' substrate rather than a niche-mimicking material.

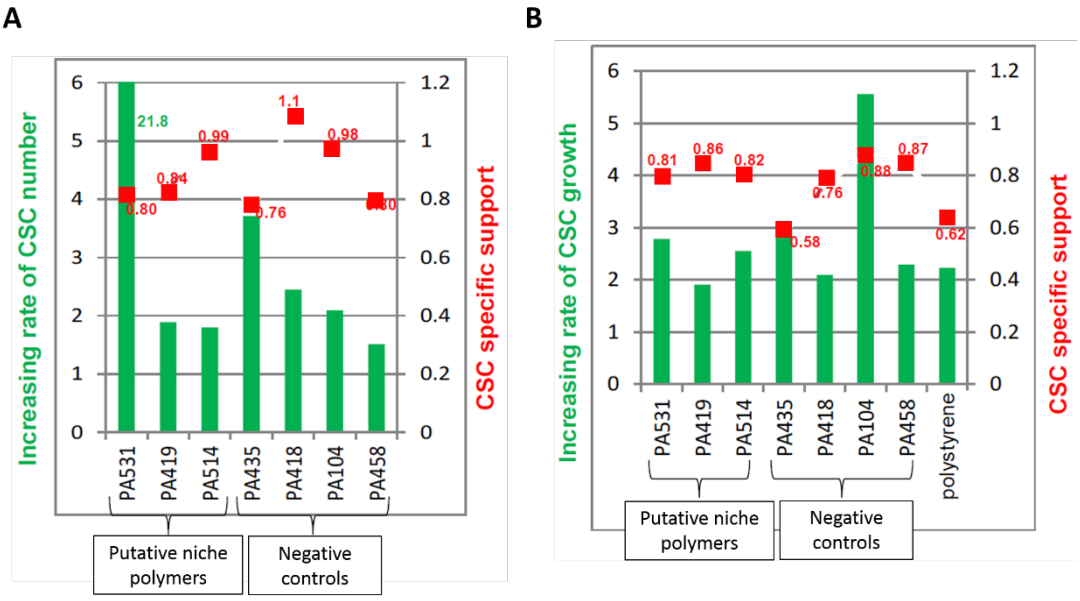

Figure 5.7: Results from the scale-up of the putative hit and control polymer candidates chosen as CSC niche-mimicking substrates after the initial polymer microarray screen. Culture of a 1:1 ratio of CSCs and non-CSCs for **A.** 48 h. **B**. 96 h. No statistically significant difference in "Increasing rate of CSC growth" (green bars) or "CSC specific support" (red squares) were observed between hit and control polymers. Figure produced by Dr Murota and modified.

5.3 CSC trapping polymer identification

5.3.1 Polymer microarray screening

The previously seeded polymer microarray with 18 h incubation was reanalysed to assess trapping capacity (see Figure 5.4, labelled "CSC specificity" in Figure 5.8). Polymers that bound a high number of cells after 18 h and where the majority were CSCs, were considered as CSC trapping hits (see Figure 5.3, Equation 5). Polymers that bound a high number of cells, but where the majority were non-CSCs were considered as negative controls. Based on these results two putative CSC trapping polymers (PA474, PA104) and two putative negative controls (PA450, PA395) were chosen for scale-up studies (Figure 5.9).

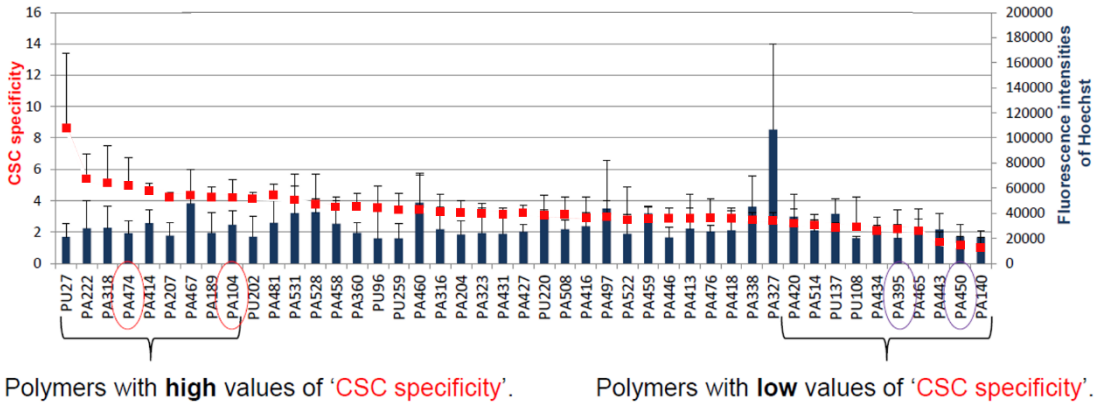

Figure 5.8: Analysis of members of a 382-polymer microarray to select CSC trapping polymer candidates for scale-up studies. 37 polymers with cells showing high hoechst intensity (blue bars) were analysed for their "CSC specificity" (red squares) (see Figure 5.3, Equation 5). Those with high values of "CSC specificity" were considered as potential CSC trapping substrates (on LHS of x-axis). Polymers with low values of "CSC specificity" were considered as potential negative control substrates (on RHS of x-axis). Two polymers (PA474 and PA104) were chosen as putative CSC trapping polymers and two polymers (PA395 and PA450) were chosen as putative negative controls for scale-up studies. Mean (n = 4) with ± SD is shown in all cases. Figure produced by Dr Murota and modified.

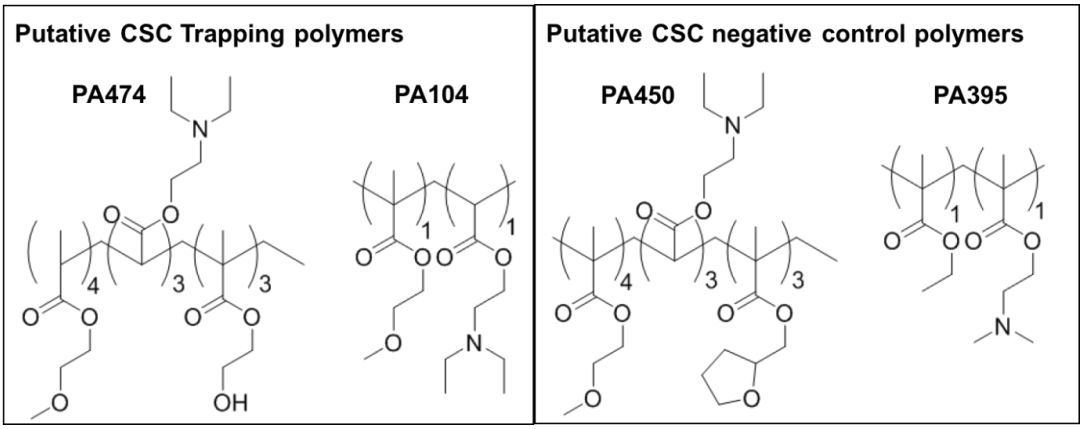

Figure 5.9: Structure of polyacrylates chosen for scale-up studies as CSC trapping substrate identification.

5.3.2 Polymer screening

The chosen polymers were synthesised and coated onto glass coverslips as described in Section 5.2.2 (for M_n, M_w and PDI of the scaled-up polymers see Table 5.2, for GPC traces see Appendix Figure A3.2).

Table 5.2 Molecular weight (M_n) and PDI values of scaled-up polyacrylates/acrylamides as putative CSC trapping polymers and the negative controls, as determined by GPC.

Polymer Name	**M_n (g/mol)**	**M_w (g/mol)**	**PDI**
Hits			
PA474	35,400	71,300	2.01
PA104	42,800	109,200	2.56
Negative controls			
PA395	68,300	222,700	3.26
PA450	47,300	146,500	3.10

A 1:1 ratio of CSCs and non-CSCs (4×10^5 cells/coverslip) were incubated for 18 h. The total number of cells per polymer were counted and the proportion of ZsGreen(+) cells determined by flow cytometry. Unfortunately, no significant difference in CSC trapping between hit and control polymers was observed using these conditions (Figure 5.10). It was hypothesised that the presence of serum in the cell media (10 % FBS) during the incubation was sufficient to allow for cell attachment to the polymer surface, thereby masking the CSC trapping abilities of the polymers. To investigate this, the same experiment was set-up using cell media supplemented with only 1 %

FBS. Unfortunately, the results were similar for all polymers, trapping CSC cells equally well according to ZsGreen fluorescence analysis by flow cytometry (results not shown).

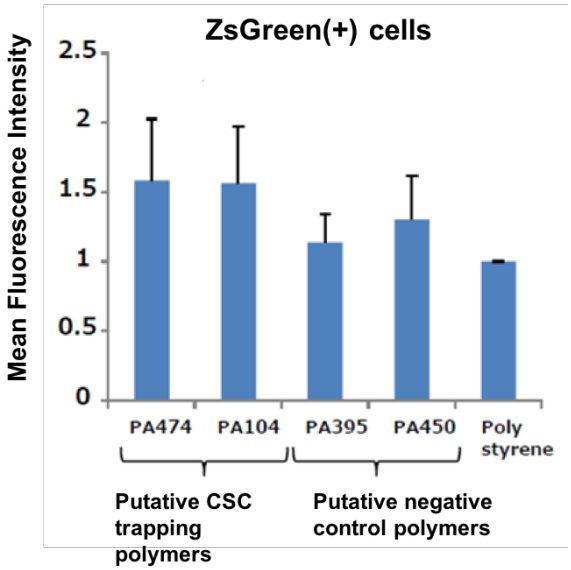

Figure 5.10: Results from the scale-up of putative hit and negative control polymers as CSC trapping substrates. Following incubation of a 1:1 ratio of CSCs and non-CSCs for 18 h and cell release by trypsinisation, the number of ZsGreen(+) cells were analysed by flow cytometry. No statistically significant difference in mean ZsGreen intensity was observed between the putative hit and control polymers. All intensities were normalised to the polystyrene intensity. Figure produced by Dr Murota and modified. Mean (n = 3) with ± SD is shown in all cases.

5.4 Screening of a peptide-containing polymer microarray

To progress the project, it was decided to develop a novel polymer microarray wherein cell-binding peptides were incorporated into the polymers. It was hypothesised that this would aid CSC-binding and provide a better niche-mimicking or trapping substrate. Three peptides were chosen to be included into the polymers, RGD and cyclic RGD (cRGD), both found in fibronectin, as well as a sequence from laminin 111. The linear RGD and laminin 111 peptides had the same cell-binding structures as the peptides used in the Chapter 2. cRGD is known to have increased

integrin affinity compared to its linear version and is potentially more robust.[139,201] The "peptide-containing polymer microarray" was formed by printing monomers, cross-linker and initiator onto glass slides, followed by *in situ* UV polymerisation.

5.4.1 Peptide monomer synthesis

All peptide monomers were synthesised using SPPS methods. The linear RGD (referred to as acrylamide-GRGDS) and laminin 111 (referred to as acrylamide-YIGSR) monomers were designed to bear a 6-aminohexanoic acid linker at the N-terminus to which acryloyl chloride was reacted (Figure 5.11A-B). To afford the cRGD monomer (referred to as acrylamide-c(RGDfK)), Fmoc-Lys-OH was modified with acryloyl chloride to give Fmoc-Lys(acrylamide)-OH. This was used in SPPS to form cRGDfK (Figure 5.11C). All peptides were purified by reverse-phase column chromatography (Biotage, Isolera) and characterisied by reverse-phase high-performance liquid chromatography (RP-HPLC) and high resolution mass spectrometry (HRMS) and isolated at > 95 % purity.

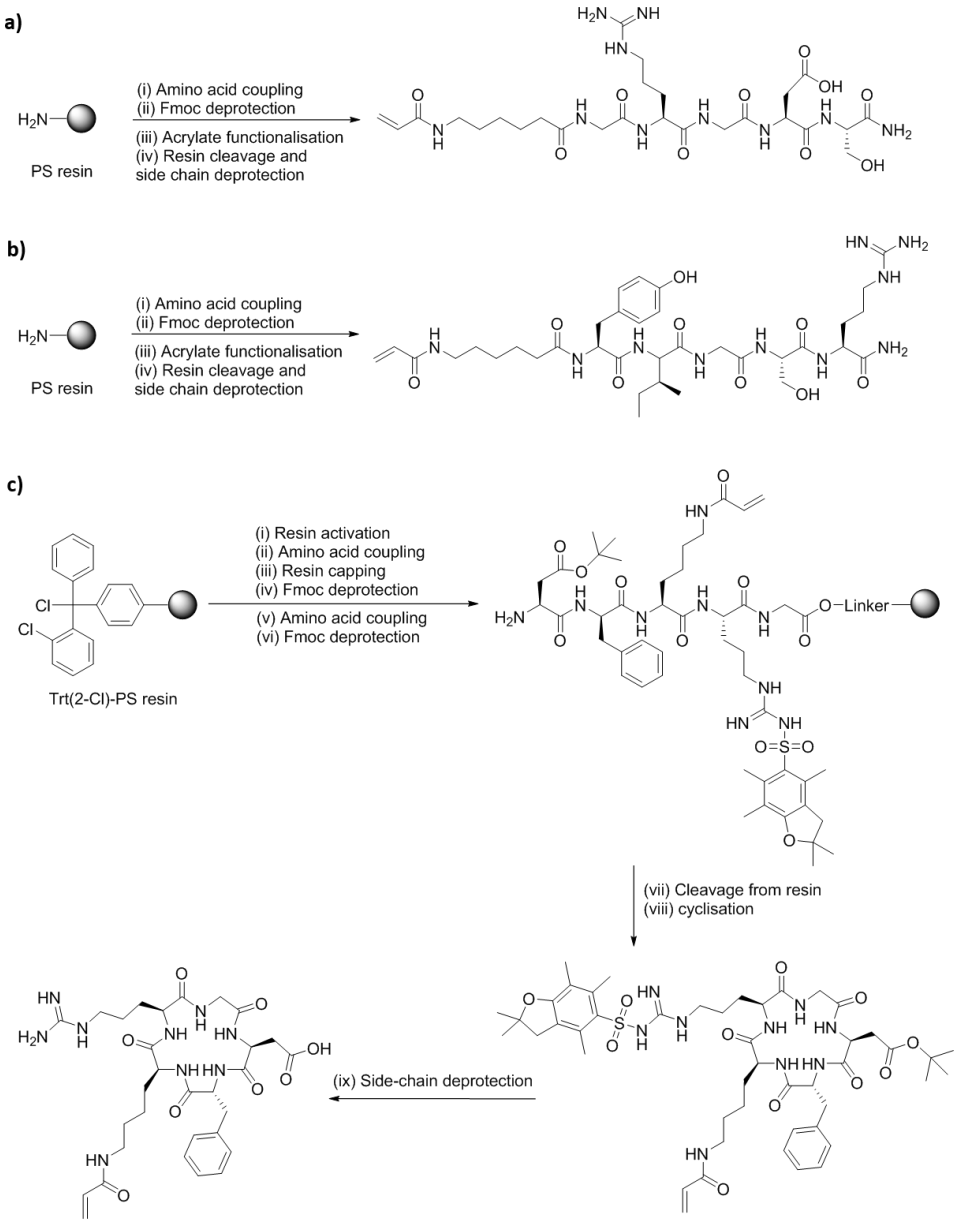

Figure 5.11: Structures and solid phase synthesis of peptide monomers used in peptide-containing polymer microarray. **A.** Acrylamide-Ahx-GRGDS-NH_2 (referred to in main text as Acrylamide-GRGDS) (i) Fmoc-AA-OH, oxyma, DIC, DMF, 1 h. (ii) 20 % piperidine/DMF, 2 × 10 min. Steps i and ii repeated with required Fmoc-AA-OH. (iii) acryloyl chloride, DIPEA, DMF, 1 h. (iv) TFA/TIS/H_2O (95:2.5:2.5), 3 h. **B.** Acrylamide-Ahx-YIGSR-NH_2 (referred to in main text as Acrylamide-YIGSR), same procedure as for Acrylamide-GRGDS. **C.** Acrylamide-c(RGDfK) (i) Thionyl chloride, DMF, N_2, 1 h. (ii) Fmoc-phe-OH, DIPEA, DMF, 1h. (iii) MeOH, DIPEA, DCM, 1 × 20 min, 1 × 30 min. (iv) 20 % piperidine/DMF, 2 × 10 min. (v) Fmoc-AA-OH, oxyma, DIC, DMF, 1 h. (vi) 20 % piperidine/DMF, 2 × 10 min. Steps v and vi repeated with required Fmoc-AA-OH. (vii) HFIP, DCM, 3 h. (viii) PyBOB, HOBt, DIPEA, DCM, o.n. (ix) TFA, DCM, 3 h.

5.4.2 Microarray printing and screening

The microarray was fabricated using a sciFLEXARRAYER S5 printer and consisted of 96 features printed in quadruplicate (384 features in total). 9 monomers divided into three groups (monomer 1, 2 and 3) were used in varying combination and ratios (Figure 5.12 for monomer structures, also see Appendix Figure A3.3 for array layout and Table A3.3 for polymer compositions) with all monomers printed as solutions (20 % w/v in NMP) except for the peptide monomers that due to their limited solubility were printed at 2 % w/v in NMP. 1-Hydroxycyclohexyl phenol ketone (30 % w/v in NMP) was used as the photoinitiator and 1,6-diol diacrylate (30 % w/v in NMP) as the cross-linker. Following printing onto fluorosilane-masked glass slides, the array was polymerised by UV irradiation for 30 minutes (100 mJ/cm^2).

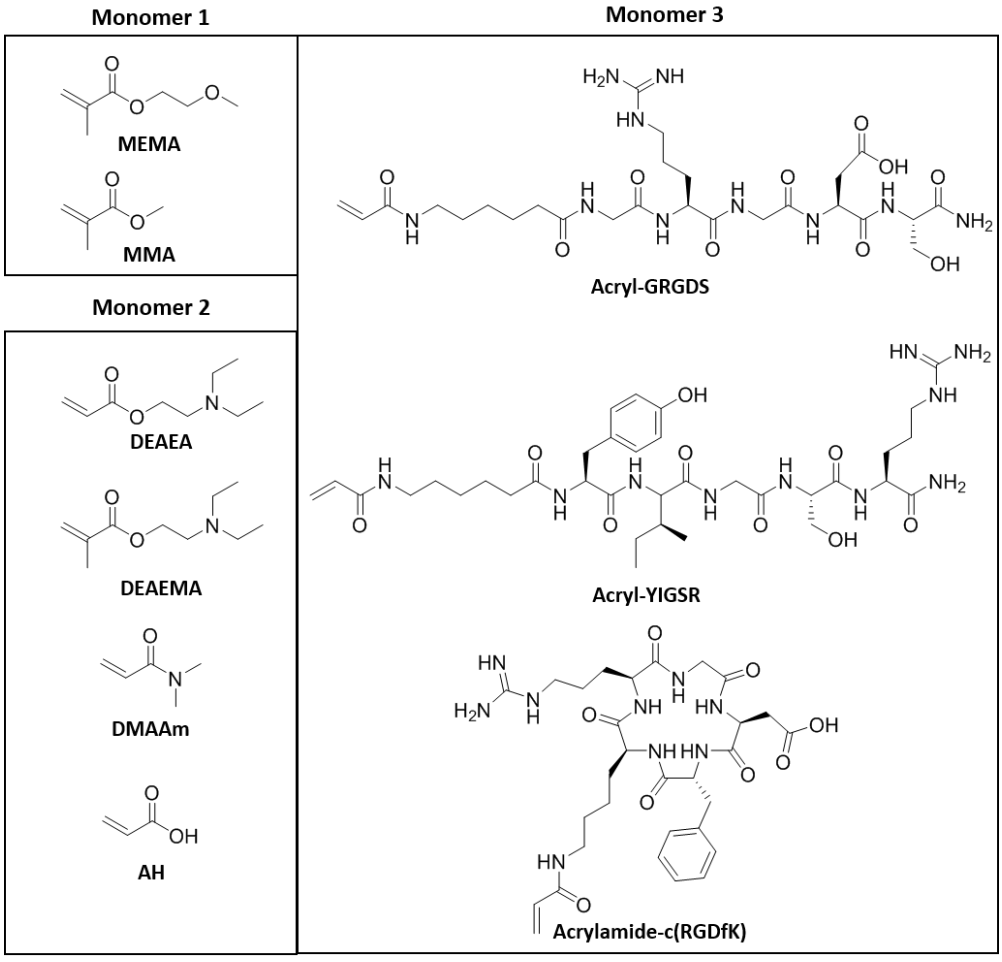

Figure 5.12: Structures of monomers used for the peptide-containing polymer array, divided into three groups Monomer 1, 2 and 3.

For the microarray screening, two slides were screened. On each slide a 1:1 ratio CSCs and non-CSCs (5×10^5 cells/slide) were seeded and incubated for 24 h and ZsGreen intensity was measured. The first slide was incubated for a further 48 h and the ZsGreen intensity measured again followed by cell fixing and staining with hoechst and PI, and fluorescence intensities measured. For the second slide the same procedure was repeated, but with the final incubation time at 24 h. High autofluorescence (particularly in the hoechst channel) of the polymer spots made the fluorescence intensity analysis difficult. Therefore, spot by spot analysis of microscope images was carried out by eye to select CSC trapping, CSC niche-mimicking and their corresponding control polymer candidates. The definition of each was analogous to those explained in Figure 5.4. CSC trapping polymers were selected based on the ratio of ZsGreen(+) cells per PI+ cells (total cell number) after 24 h. CSC niche mimicking cells were selected based on the amount of ZsGreen(+) cells at 48 h and the ratio of ZSGreen(+) cells per PI+ cells at 72 h. From the analysis three putative CSC niche mimicking polymers (PP60, PP62 and PP65) and one negative control were chosen (PP79) (Figure 5.13). For CSC trapping, four putative hit polymers (PP73, PP74, PP77 and PP80) and one negative control polymer (PP61) were chosen (Figure 5.14). All polymers were subsequently scaled-up and used for further cell studies.

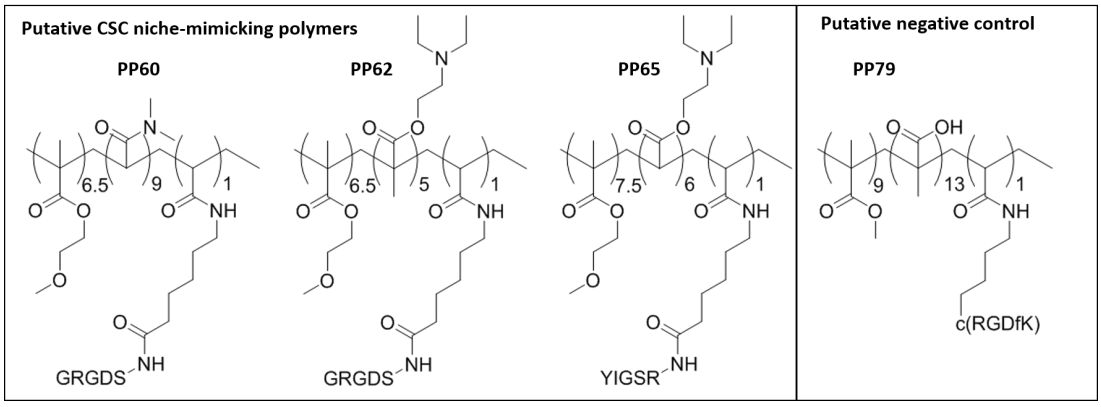

Figure 5.13: Structures of peptide-containing polyacrylate/acrylamides chosen for scale-up for CSC niche-mimicking substrate identification.

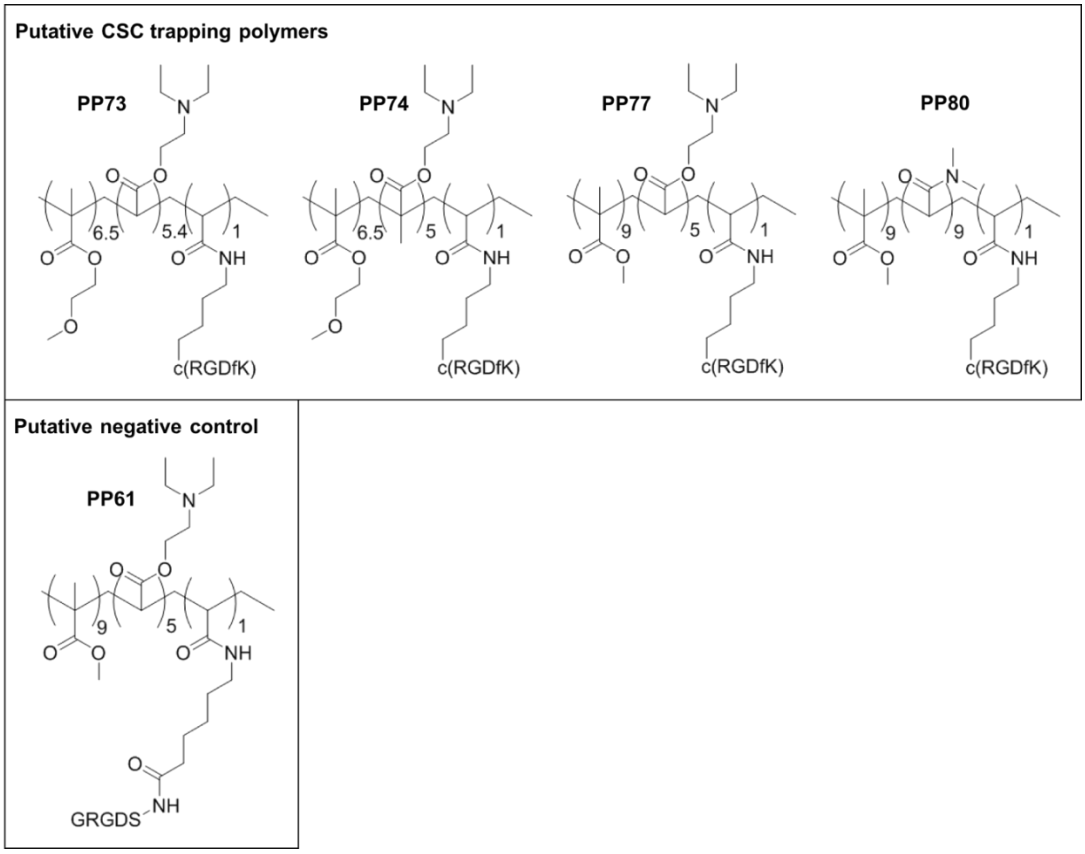

Figure 5.14: Structures of the peptide-containing polyacrylate/acrylamides chosen for scale-up for CSC trapping substrate identification.

5.4.3 Polymer synthesis

For scale-up studies the polymers were polymerised *in situ* on methacrylate-functionalised glass coverslips (13 mm in diameter) (Figure 5.15). The methacrylate group was installed to react with the acrylate/acrylamide monomers to afford anchoring of the polymers onto the glass surface. To ensure that the concentration of monomers was high enough to afford polymers on the glass surface, ×10 increase of monomer concentration was used compared to the array screening. The initiator and crosslinker concentrations were kept the same so as to not generate too heavily cross-linked polymers or very short polymer chains. The pre-polymer solutions of monomers, cross-linker and initiator in NMP were dispensed onto a Poly(ethylene terephthalate) (PET) film, with a functionalised glass coverslip put on top, before UV irradiating to afford polymerisation.[202]

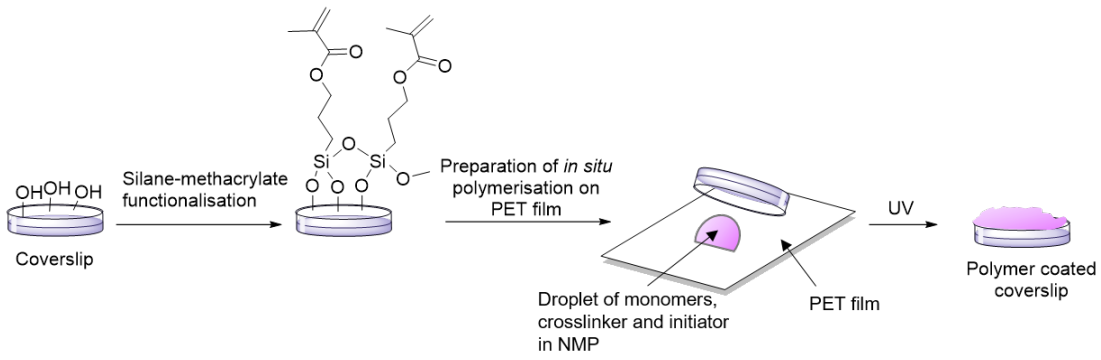

Figure 5.15: Set-up of *in situ* coverslip polymerisation. Hydroxyl-functionalised glass coverslips were functionalised with 3-(trimethoxysilyl)propyl methacrylate. This was followed by UV-initiated polymerisation by depositing a droplet of monomers, crosslinker and initiator on a PET film on top of which the methacrylate-functionalised coverslip was placed. After polymerisation the coverslip was peeled off from the PET film to obtain the polymer-coated coverslip.

5.4.4 Niche-mimicking polymer screening

The polymer-coated coverslips were incubated with a 1:1 mixture of CSCs and non-CSCs (100 000 cells/coverslip) and incubated for 24 and 72 h to assess the ability of the polymers to maintain the CSC population (i.e. mimic the CSC niche). TCPS was used as an additional negative control. Following incubation the cells were released by trypsinisation and the number of ZsGreen(+) cells was determined by flow cytometry (Figure 5.16). The two hit candidates PP62 and PP65 were found to proliferate and maintain the CSC population over time, with 59 % and 49 % CSCs respectively after 72 h incubation. This was an improvement compared to the negative controls PP79 and TCPS where greater level of differentiation of the CSCs was observed (38 % CSCs for both after 72 h incubation). These results were also confirmed by fluorescence microscopy of the coverslips, where a larger proportion of ZsGreen(+) cells were visible on PP62 and PP65 compared to the negative control PP79 (Figure 5.17). To further understand these results, current experiments are underway with the niche-mimicking polymers PP62, PP65 and the negative control PP79 cultured with both mono-CSC cultures and mixed populations of CSCs and non-CSCs.

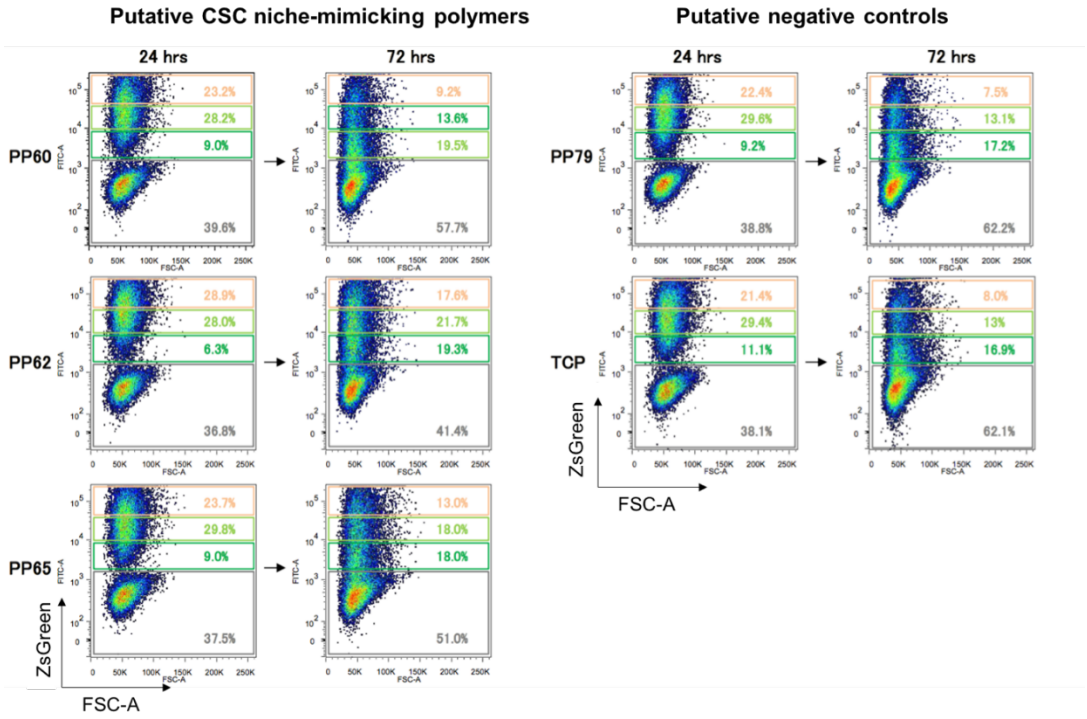

Figure 5.16: Flow cytometry analysis of cells attached to putative niche-mimicking polymers and negative controls (including TCPS) after 24 or 72 h incubation with a 1:1 ratio of CSCs and non-CSCs. ZsGreen(+) cells are considered as CSCs, shown in the three top boxes of each condition. Cells were pooled for flow cytometry analysis (n = 5).

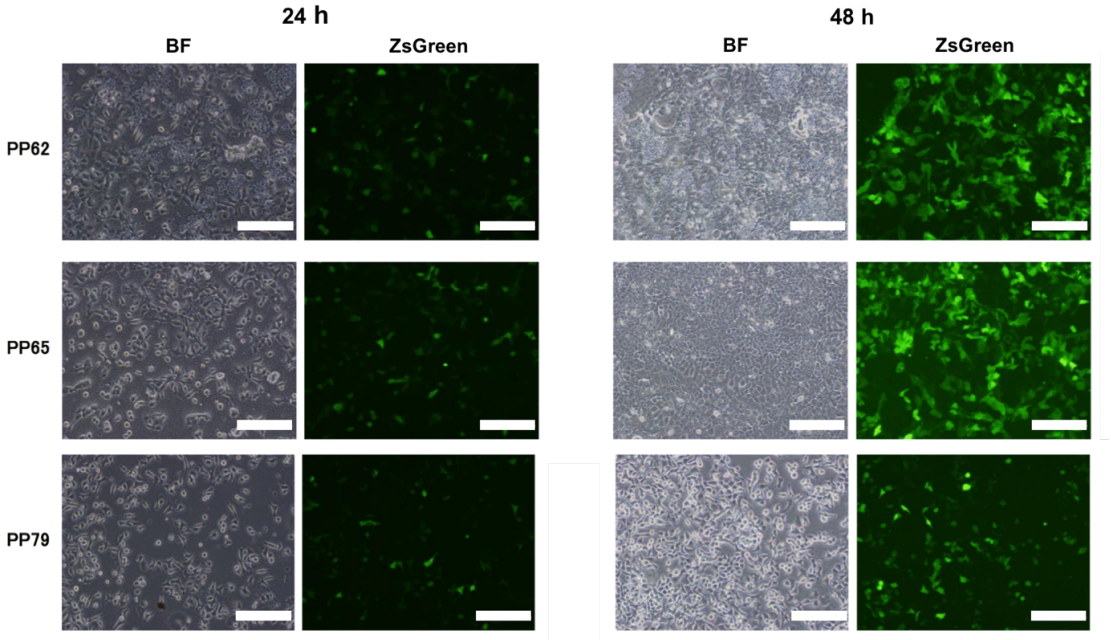

Figure 5.17: Fluorescence and bright-field images of identified niche-mimicking (PP62 and PP65) and negative control (PP79) polymers after 24 and 72 h incubation with a 1:1 ratio of

CSCs and non-CSCs. The proportion of ZsGreen(+) cells (CSCs) over times was maintained better on PP62 and PP65 than on PP79. Scale bar = 200 μm.

5.4.5 CSC trapping polymer screening

The putative CSC trapping polymers and negative control polymer were coated on coverslips and incubated with a 1:1 ratio of CSCs and non-CSCs (100 000 cells/coverslip) for 6 h. This was to assess the capacity of these polymers to preferentially trap CSCs over non-CSCs. Following the incubation and cell release by trypsinisation, the number of ZsGreen(+) cells was determined by flow cytometry. Over this short incubation time, however, no significant difference in CSC to non-CSC binding was observed for the putative hit polymers and the negative controls (Figure 5.18).

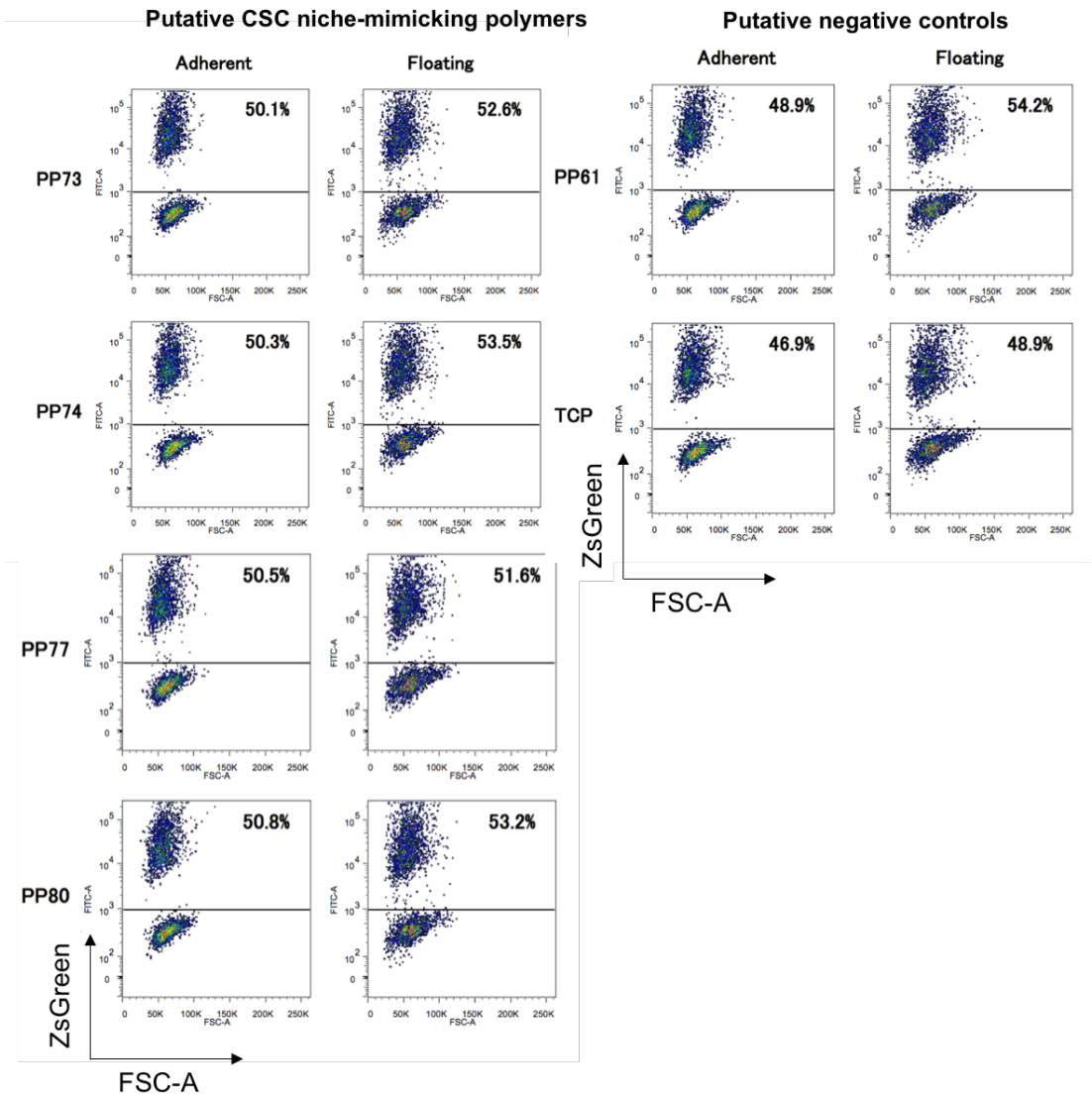

Figure 5.18: Flow cytometry analysis of cells attached to putative CSC trapping polymers and negative controls (including TCPS) after 6 h incubation with a 1:1 ratio of CSCs and non-CSCs. ZsGreen(+) cells are considered as CSCs, shown in the top box of each condition. Cells were pooled for flow cytometry analysis (n = 5).

5.5 Discussion

In current culture methods for pancreatic CSCs, the CSCs make up a very small percentage of the cell population (0.2-0-8 %).[188] Therefore, identifying a substrate that specifically can support their growth and maintenance would be a greatly beneficial.

Screening of a 382-member polymer microarray composed of polyacrylates/acrylamides and polyurethanes enabled the initial identification of polymer substrates that were CSC niche-mimicking, in that they could maintain and increase the amount of CSCs (ZsGreen(+) cells) over 72 h. It also enabled the identification of polymers where preferential attachment, or trapping, of CSCs was seen over non-CSCs (ZsGreen(-) cells). The subsequent scale-up of polymers in both these cases was unfortunately unable to show any significant difference between hit and control polymer candidates. However, for both niche-mimicking and trapping purposes, an improvement was observed compared to the conventional PS culture conditions.

The inclusion of cell-binding peptides was proposed to improve the cell attachment by incorporating acrylamide monomers bearing RGD, a cRGD or a LamIII sequence with commercially available monomers. A new microarray design was developed, with a library of 96 peptide-containing polymers being screened as both niche-mimicking and trapping substrates. Scale-up experiments confirmed the niche-mimicking abilities of two polymers (PP62 and PP65) as they maintained the CSC population over 24 to 72 h incubation, compared with the negative control polymer (PP79), where CSC differentiation was observed. Current efforts are focusing on repeating these experiments to gain further insight into the polymer niche-mimicking properties.

5.6 Conclusions

A high-throughput screening strategy was employed to identify a substrate that could either trap or mimic the pancreatic CSC niche. A 382-member polyacrylate/acylamide library was initially screened, although confirmation of array screening results in scale-up experiments was unsuccessful. A novel peptide-containing polymer microarray was designed and screened with pancreatic CSCs and the subsequent scale-up studies are underway. Looking further ahead, this new microarray design can be used as a screening platform to identify novel substrates for not just other types of CSCs, but in principle for any cell type where novel culture conditions and substrates are desired. Furthermore, the ease of peptide monomer

design makes the facile tailoring of the library to contain certain peptides, such as motifs known to bind the cells of interest or other ECM-derived sequences from e.g. collagen, emphasises the tuneable properties of this platform.

5.7 Materials and Methods

5.7.1 Instruments used for polymer scale-up

Zepto O_2 plasma generator (Diener electronic GmbH, Germany)

CL-1000 Ultraviolet crosslinker (UVP LLC, USA)

Spincoater Model P6700 Series (Specialty Coating Systems, USA)

5.7.2 Instruments for characterisation and purification

Agilent 1100 ChemStation analytical RP-HPLC (Agilent, USA) with a Zorbax Eclipse C18 reverse phase column (4.6 mm × 100 mm, 3.5 µ) with an evaporative light scattering and a multi-wavelength detector eluting with a gradient of water to acetonitrile (5 – 95 %), both with 0.1% formic acid with a flow rate of 1 mL/min

Agilent 1100 GPC equipped with a PLgel MIXED-C columns and a RI detector eluting with DMF containing 0.1M LiBr at 60 °C at 1 ml/min (Agilent, USA)

Isolera One equipped with a Biotage® SNAP HP-BioSphere C18 10 g column detection at 250 nm, eluting with a gradient of water to acetonitrile, both with 0.1 % formic acid with a flow rate of 12 ml/min (Biotage, Sweden)

BenchTop Pro with Omnitronics lyophiliser (SP scientific, USA)

^{1}H NMR at 500 MHz Bruker AVA 500 (Bruker, USA)

Bruker Tensor 27 Standard System FT-IR spectrophotometer (Bruker, USA)

HRMS on a Bruker 3.0 T Apex II spectrometer (Bruker, USA)

5.7.3 Chemicals

All protected amino acids, aminomethyl polystyrene resin, and the Fmoc-Rink amide linker were purchased from GL Biochem Ltd (Shanghai) or NovaBiochem. Poly(ethylene oxide), 4-arm, amine terminated ($(PEG\text{-}NH_2)_4$) (M_n = 10 000 g/mol), was purchased from Sigma Aldrich. All other chemicals were from Sigma Aldrich or Acros, and used as received.

5.7.4 Polymer synthesis

The polymers used for polymer microarray fabrication were part of an in-house library within the Bradley group and their fabrication was according to previously published methods using a Quarray^{mini} contact printer (Genetix, UK).[115,116,200]

For scale-up studies polymers were synthesised using random free-radical polymerisation. Acrylate and acrylamide monomers (see Table 5.3 for compositions) and AIBN (initiator) were dissolved degassed solvent (DMF or toluene) and heated overnight at 60 °C. The resulting polymers were precipitated into cold diethyl ether, centrifuged, decanted and dried under vacuum at 60 °C overnight to afford the final product. Polymer molecular weight and PDI were determined by GPC (Agilent 1100) running with 100 % DMF with 0.1 M LiBr over 25 min.

Table 5.3 Polyacrylates/acrylamide scaled-up as part of Chapter 5. The polymer compositions and molecular weight (M_n and M_w) and PDI values as determined by GPC are given. M1 = Monomer 1, M2 = Monomer 2, M3 = Monomer 3.

Polymer Name	**M1 (%)**	**M2 (%)**	**M3 (%)**	**M_n (g/mol)**	**M_w (g/mol)**	**PDI**
Niche-mimicking						
Hits						
PA531	MEMA (55)	DEAEMA (45)	-	59,500	183,500	3.08
PA419	MEMA (60)	DEAEA (30)	MA (10)	64,100	222,700	3.08
PA514	MEMA (40)	DEAEA (30)	MMA (30)	43,800	133,900	3.05
Negative controls						
PA104	MEMA (50)	DEAEA (10)	-	42,800	109,200	2.56
PA435	MEMA (60)	DEAEA (10)	MEA (30)	66,00	210,900	3.20
PA418	MEMA (40)	DEAEA (30)	MA (10)	38,700	92,800	2.40
PA458	MEMA (40)	DEAEA (30)	THFFMA (30)	60,200	197,300	3.36
CSC trapping						
Hits						
PA474	MEMA (40)	DEAEA (30)	HEMA (30)	35,400	71,300	2.01
PA104	MEMA (50)	DEAEA (10)	-	42,800	109,200	2.56
Negative controls						
PA395	EMA (50)	DMAEMA (50)	-	68,300	222,700	3.26
PA450	MEMA (40)	DEAEA (30)	THFFA (30)	47,300	146,500	3.10

5.7.5 Spin-coating of polymers onto functionalised glass coverslips

Glass coverslips (32 mm in diameter) were lightly shaken in 1M NaOH overnight followed by washing with acetone and water. The coverslips were submerged in 1 % (v/v) APTES in acetonitrile for 1 hour, washed with acetone and dried at 100 °C overnight. Thereafter the coverslips were dip-coated in agarose (1 % w/v) (Type 1, low EEO) in deionised water and dried at room temperature overnight. Polymer solutions (1 % w/v in THF) were spin-coated (200 µl/coverslip) at 2000 rpm for 10 seconds and dried at 40 °C overnight. The polymer-coated coverslips were then sent to Tokyo Medical and Dental University for cell culture experiments.

5.7.6 Synthesis of Fmoc-Lys(acrylamide)-OH[203]

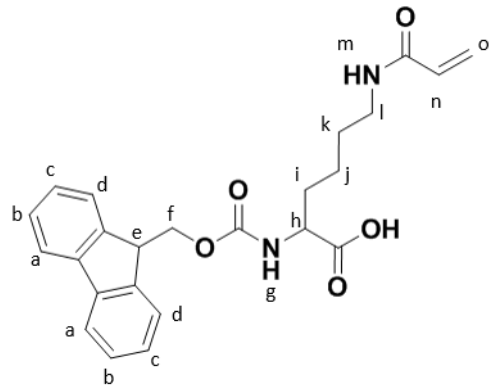

Fmoc-Lys-OH (500 mg, 1.2 mmol, 1 eq.) was dissolved in 1,4-dioxane (5 mL) and cooled on ice. Na_2CO_3 (10 % (w/v), 14 mL) was added dropwise resulting in a white slurry. Acryloyl chloride (123 mg, 1.4 mmol, 1.1 eq.) was added drop-wise and the reaction mixture was allowed to warm to room temperature and stirred overnight. The reaction was concentrated *in vacuo*, the crude product dissolved in water and washed with diethyl ether (3×50 ml). 1M $KHSO_4$ was added to the aqueous layer until pH 2-3 and the product was extracted into ethyl acetate (2×50 ml). The organic layer was dried ($MgSO_4$), filtered and concentrated *in vacuo* and dried under vacuum overnight to afford the final product (325 mg, 62 %). 1H NMR (600 MHz, Chloroform-d) δ 7.74 (d, J = 7.6 Hz, 2H, a), 7.59 (t, J = 7.4 Hz, 2H, b), 7.38 (t, 7.5 Hz, 2H, c), 7.32–7.26 (m, 2H, d), 6.50 (dd, J = 17.3, 1.3 Hz, 1H, o_1) , 6.27 (dd, J = 17.0, 1.3 Hz, 1H, o_2), 6.14 (dd, J = 17.3, 10.4 Hz, 1H, m), 5.95 (dd, J =10.5, 1.3 Hz, 1H, n), 5.76–5.71 (m, 1H, g), 5.63–5.58 (m, 1H, e), 4.42 – 4.34 (m, 2 H, f) 4.15 – 4.10 (m, 1H, h) 3.39 – 3.25 (m, 2H, l), 1.96 – 1.72 (m, 2H, i), 1.62 – 1.53 (m, 2H, j), 1.51 - 1.35 (m, 2H, k). IR (neat) ν (cm^{-1}) = 3300, 2920, 2860, 2360, 1699, 1651 1606. HRMS *m/z* calculated 423.19145, *m/z* found 730.1920.

5.7.7 Synthesis of acrylamide-Ahx-GRDGS-NH_2 and acrylamide-Ahx-YIGSR-NH_2

Acrylamide-Ahx-GRDGS-NH_2 and acrylamide-Ahx-YIGSR-NH_2 were synthesised on solid-phase using the Fmoc/^{t}Bu route.[148] The Fmoc-Rink amide linker was coupled to the aminomethyl polystyrene resin (1 g, loading 0.745 mmol/g) prior to peptide synthesis.

Coupling of the protected Rink linker and protected amino acids. Fmoc-Rink or Fmoc-protected amino acids (3 eq.) and Oxyma (3 eq.) were dissolved in DMF (1 M) and stirred for 5 min followed by the addition of DIC (3 eq.) and further stirred for 5 min. The mixture was added to the resin and shaken at room temperature for 1 hour. The resin was washed with DMF, MeOH and DCM.

Fmoc deprotection. The *N*-Fmoc protected peptide on the resin was treated twice with 20 % piperidine in DMF for 10 minutes. The resin was subsequently washed with DMF, MeOH and DCM.

Coupling of acryloyl chloride. Acryloyl chloride (5 eq.) and DIPEA (10 eq.) were dissolved in DMF (0.1 M) and added to the resin and shaken at room temperature for 1 hour. The resin was washed with DMF, MeOH and DCM.

Deprotection of the peptide and cleavage off the resin. TFA/H_2O (95:5) was added to the pre-swollen resin (in DCM) and shaken at room temperature for 3 h. The peptide was precipitated from the filtrate by the addition of cold diethyl ether, collected by centrifugation and washed twice with ether. The peptides were re-dissolved in H_2O (10 mL) and purified by RP-HPLC (Biotage Isolera) (5% to 60 % MeCN/H_2O over 20 min, 60 % to 95 % MeCN/H_2O over 5 min) followed by lyophilisation. The peptides were characterised by RP-HPLC (> 95 % purity) and HRMS. Acrylamide-Ahx-GRGDS-NH_2 (409 mg, 83 %) $m/z_{calculated}$ 657.33146 m/z_{found} 657.333270. Acrylamide-Ahx-YIGSR-NH_2 (443 mg, 78 %) $m/z_{calculated}$ 761.43045 m/z_{found} 761.42830.

5.7.8 Synthesis of acrylamide-c(RGDfK)

Acrylamide-c(RGDfK) was synthesised on solid phase as above but using a chlorotrityl-linker on a polystyrene resin.

Resin activation. Thionyl chloride (86 µL, 1.2 mmol, 2.5 eq.) dissolved in anhydrous DMF (1.7 mL, 1 mM) was added to the chlorotrityl-linked polystyrene resin (500 mg) and slowly stirred under nitrogen for 1 hour. The resin was washed with anhydrous DMF and anhydrous DCM.

Fmoc-phe-OH coupling. Fmoc-phe-OH (564 mg, 15 mmol, 3 eq.) and DIPEA (507 µl, 15 mmol, 3 eq.) dissolved in anhydrous DMF (5 mL) was added to the resin and stirred at room temperature for 1 hour. The resin was washed with anhydrous DMF and anhydrous DCM.

Resin capping. DIPEA (800 µl) was dissolved in anhydrous DCM (4.3 ml) and dry MeOH (800 µl), and the solution added to the resin and shaken at room temperature for 20 minutes. After removing the reaction solution from the resin by filtration, fresh reaction solution was added and the resin shaken for a further 30 minutes. The resin was washed with DMF, MeOH and DCM.

Fmoc deprotection and coupling of protected amino acids. See 6.5.4

Cleavage off the resin. Hexafluoroisopropanol/DCM (1:4) was added to the resin and shaken at room temperature for 3 h. The protected linear peptide H-K(acrylamide)R(Pbf)GD(OtBu)f-OH was precipitated from the filtrate by the addition of cold diethyl ether, collected by centrifugation and washed twice with ether.

Cyclisation and purification. PyBOP (653 mg, 1.2 mmol, 2 eq.), HOBt (166 mg, 1.2 mmol, 2 eq.) and DIPEA (343 µl, 2.0 mmol, 3.2 eq.) were dissolved in DCM (810 ml). Side-chain protected linear H-K(acrylamide)R(Pbf)GD(OtBu)f-OH (605 mg, 0.6 mmol, 1 eq.) dissolved in DMF (90 mL) was added drop-wise to the reaction solution and stirred at room temperature overnight (final reaction concentration 5.6 mM). The reaction solution was concentrated *in vacuo*, the crude product precipitated into cold diethyl ether, centrifuged and washed twice with ether. The side-chain protected cyclised peptide was dissolved in DCM (3 mL) and TFA (3 mL) and stirred at room temperature for three hours. The reaction solution was concentrated *in vacuo*, the crude product precipitated by the addition of cold diethyl ether, collected by centrifugation and washed twice with ether. The peptide was re-dissolved in H_2O

and purified by RP-HPLC (Isolera One, Biotage) (5% to 60 % MeCN/H_2O over 20 min, 60 % to 95 % MeCN/H_2O over 5 min) followed by lyophilisation.. The peptide was characterised by RP-HPLC (> 95 % purity) and HRMS ($m/z_{calculated}$ 658.33101 m/z_{found} 658.33110).

5.7.9 Peptide-containing polymer microarray fabrication

Microscope glass slides (76 × 26 mm) (Menzel GmbH Co. KG) were treated with an O_2 plasma for 10 minutes at 1.5 bar oxygen pressure. 384 features (12 × 32) of aqueous sucrose (20 % w/v) were printed onto the slides using a sciFLEXARRAYER S5 printer. The pitch between adjacent spots was 0.8 × 0.8 mm. After drying at room temperature, tridecafluoro-1,1,2,2-tetrahydrooctyl-dimethylchlorosilane (5 µl/slide) was dropped onto five different areas of the slides (1 µl/drop) and reacted overnight in a sealed Tupperware box followed by washing of the slides with acetone (10 mL) and water (10 mL) and drying at 40 °. The dried slides were coated with 3-(trimethoxysilyl)propylmethacrylate (10 µl/slide) by spreading the solution with a pipette tip, and put into a sealed box, reacted overnight and then washed with water and ethanol before drying under N_2 stream. For printing, solutions of monomers (20 % w/v in NMP, except for peptide-based monomers, which were 2 % w/v in NMP), 1-hydroxycyclohexyol phenyl ketone (initiator) and 1,6-hexanediol diacrylate (cross-linker) (both 30 % w/v in NMP) were prepared. The solutions were printed in varying ratios (see Appendix Table A3.4) with 125 drops/spot (~ 300 pl/drop). After printing the slide was placed in a UV cross-linker (100 mJ/cm^2, 30 min) followed by drying at 40 °C under vacuum.

5.7.10 *In situ* polymerisation onto functionalised glass coverslips[202]

Glass coverslips (13 mm in diameter) were lightly shaken in 1M NaOH overnight followed by washing with water (2 × 1 hour) and acetone (1 × 1 hour), then drying at 40 °C overnight. The coverslips were submerged and shaken gently in a solution of 3-(trimethoxysilyl)propyl methacrylate (5 % w/v) and triethylamine (0.5 % w/v) in acetonitrile for 48 hours. The coverslips were then washed by shaking in acetone (2 ×

10 min) and allowed to dry at room temperature. Monomers were purified from inhibitor by filtering through a cotton-plugged syringe (2 mL) filled with basic aluminium oxide (1 mL). Solutions of monomers (16 % w/v of M1, 16 % w/v of M2, 11.2 % w/v of M3), 1,6-hexanediol diacrylate (6 % w/v) and 1-hydroxycyclohexyl phenyl ketone (2.4 % w/v) of the identified hit and control polymers were prepared in NMP. These pre-polymer solutions (5 µL) were spotted onto PET films (666-5697, 3M) and a glass coverslip with the functionalised surface facing down was added on top of the liquid spot. To remove trapped air bubbles, the coverslips were gently pushed into the PET. To afford polymerisation, the coverslips on PET films were placed in a UV cross-linker (100 mJ/cm^2, 30 min) irradiated for 30 min. The coverslips (n = 6) were removed from the PET film and dried at 40 °C overnight, washed with ethanol (3 × 10 min) and water (24 h) and dried at room temperature under fume hood ventilation. The polymer-coated coverslips were then sent to Tokyo Medical and Dental University for cell culture experiments.

References

(1) Harrison, R. G. *J. Exp. Zool.* **1910**, *9* (4), 787–846.

(2) Foty, R. *J. Vis. Exp.* **2011**, No. 51.

(3) Carrel, A.; Burrows, M. T. *J. Exp. Med.* **1911**, *13* (3), 387–396.

(4) Carrel, A.; Burrows, M. T. *J. Exp. Med.* **1911**, *14* (3), 244–247.

(5) Carrel, A. *J. Exp. Med.* **1913**, *18* (3), 287–298.

(6) Taylor, M. W. In *Viruses and Man: A History of Interactions*; Springer International Publishing: Cham, 2014; pp 41–52.

(7) Carrel, A.; Lindbergh, C. A. *Science* **1935**, *81* (2112), 621–623.

(8) Enders, J. F.; Weller, T. H.; Robbins, F. C. *Science* **1949**, *109* (2822), 85–87.

(9) Dulbecco, R.; Vogt, M. *J. Exp. Med.* **1954**, *99* (2), 167–182.

(10) Scherer, W. F.; Syverton, J. T.; Gey, G. O. *J. Exp. Med.* **1953**, *97* (5), 695–710.

(11) Evans, V. J.; Shannon, J. E.; Bryant, J. C.; Waltz, H. K.; Earle, W. R.; Sanford, K. K. *J. Natl. Cancer Inst.* **1953**, *13* (4), 773–784.

(12) Kao, F.; Chasin, L.; Puck, T. T. *Proc. Natl. Acad. Sci. U. S. A.* **1969**, *64* (4), 1284–1291.

(13) Köhler, G.; Milstein, C. *Nature* **1975**, *256* (5517), 495–497.

(14) Schmidt, S.; Lilienkampf, A.; Bradley, M. *Philos. Trans. R. Soc. Lond. B. Biol. Sci.* **2018**, *373* (1750), 20170223.

(15) Haycock, J. W. In *3D Cell Culture: A Review of Current Approaches and Techniques*; Haycock, J. W., Ed.; Methods in Molecular Biology; Humana Press: Totowa, NJ, 2011; Vol. 695, pp 1–15.

(16) Koledova, Z. In *Methods in molecular biology (Clifton, N.J.)*; 2017; Vol. 1612, pp 1–11.

(17) Heath, D. E.; Cooper, S. L. *J. Biomater. Sci. Polym. Ed.* **2017**, *28* (10–12), 1051–1069.

(18) Kyburz, K. A.; Anseth, K. S. *Ann. Biomed. Eng.* **2015**, *43* (3), 489–500.

(19) Magin, C. M.; Alge, D. L.; Anseth, K. S. *Biomed. Mater.* **2016**, *11* (2), 022001.

(20) Madl, C. M.; Heilshorn, S. C. *Annu. Rev. Biomed. Eng.* **2018**, *20* (1), 21–47.

(21) Knight, E.; Przyborski, S. *J. Anat.* **2015**, *227* (6), 746–756.

(22) Caliari, S. R.; Burdick, J. A. *Nat. Methods* **2016**, *13* (5), 405–414.

(23) Mouw, J. K.; Ou, G.; Weaver, V. M. *Nat. Rev. Mol. Cell Biol.* **2014**, *15* (12), 771–785.

(24) Fratzl, P. *Collagen: structure and mechanics*; Springer, 2008.

(25) Kielty, C. M.; Sherratt, M. J.; Shuttleworth, C. A. *J. Cell Sci.* **2002**, *115* (Pt 14), 2817–2828.

(26) Humphrey, J. D.; Dufresne, E. R.; Schwartz, M. A. *Nat. Rev. Mol. Cell Biol.* **2014**, *15* (12), 802–812.

(27) Hamill, K. J.; Kligys, K.; Hopkinson, S. B.; Jones, J. C. R. *J. Cell Sci.* **2009**, *122* (Pt 24), 4409–4417.

(28) Singh, P.; Carraher, C.; Schwarzbauer, J. E. *Annu. Rev. Cell Dev. Biol.* **2010**, *26* (1), 397–419.

(29) Bishop, J. R.; Schuksz, M.; Esko, J. D. *Nature* **2007**, *446* (7139), 1030–1037.

(30) Bishop, P. *Eye* **1996**, *10* (6), 664–670.

(31) Bonnans, C.; Chou, J.; Werb, Z. *Nat. Rev. Mol. Cell Biol.* **2014**, *15* (12), 786–801.

(32) Kannus, P. *Scand. J. Med. Sci. Sport.* **2000**, *10* (6), 312–320.

(33) Guan, X.; Avci-Adali, M.; Alarçin, E.; Cheng, H.; Kashaf, S. S.; Li, Y.; Chawla, A.; Jang, H. L.; Khademhosseini, A. *Biotechnol. J.* **2017**, 1600394.

(34) Screen, H. R. C.; Berk, D. E.; Kadler, K. E.; Ramirez, F.; Young, M. F. *J. Orthop. Res.* **2015**, *33* (6), 793–799.

(35) McMurray, R. J.; Dalby, M. J.; Tsimbouri, P. M. *J. Tissue Eng. Regen. Med.* **2015**, *9* (5), 528–539.

(36) Ruoslahti, E. *Annu. Rev. Cell Dev. Biol.* **1996**, *12* (1), 697–715.

(37) Klein, E. A.; Yin, L.; Kothapalli, D.; Castagnino, P.; Byfield, F. J.; Xu, T.; Levental, I.; Hawthorne, E.; Janmey, P. A.; Assoian, R. K. *Curr. Biol.* **2009**, *19* (18), 1511–1518.

(38) Bartkova, J.; Lukas, J.; Müller, H.; Lützhøt, D.; Strauss, M.; Bartek, J. *Int. J. Cancer* **1994**, *57* (3), 353–361.

(39) Murphy, G. *Nat. Rev. Cancer* **2008**, *8* (12), 932–941.

(40) Michalopoulos, G.; Pitot, H. C. *Exp. Cell Res.* **1975**, *94* (1), 70–78.

(41) Weaver, V. M.; Petersen, O. W.; Wang, F.; Larabell, C. A.; Briand, P.; Damsky, C.; Bissell, M. J. *J. Cell Biol.* **1997**, *137* (1), 231–245.

(42) Kuo, C.-T.; Wang, J.-Y.; Lin, Y.-F.; Wo, A. M.; Chen, B. P. C.; Lee, H. *Sci. Rep.* **2017**, *7* (1), 4363.

(43) Wang, H.; Heilshorn, S. C. *Adv. Mater.* **2015**, *27* (25), 3717–3736.

(44) Rosales, A. M.; Anseth, K. S. *Nat. Rev. Mater.* **2016**, *1* (2), 15012.

(45) Zhang, R.; Mjoseng, H. K.; Hoeve, M. A.; Bauer, N. G.; Pells, S.; Besseling, R.;

Velugotla, S.; Tourniaire, G.; Kishen, R. E. B.; Tsenkina, Y.; Armit, C.; Duffy, C. R. E.; Helfen, M.; Edenhofer, F.; de Sousa, P. A.; Bradley, M. *Nat. Commun.* **2013**, *4*, 1335.

(46) Hibbins, A.; Kumar, P.; Choonara, Y.; Kondiah, P.; Marimuthu, T.; Toit, L. du; Pillay, V.; Hibbins, A. R.; Kumar, P.; Choonara, Y. E.; Kondiah, P. P. D.; Marimuthu, T.; du Toit, L. C.; Pillay, V. *Polymers (Basel).* **2017**, *9* (12), 474.

(47) DeForest, C. A.; Tirrell, D. A. *Nat. Mater.* **2015**, *14* (5), 523–531.

(48) Bracaglia, L. G.; Smith, B. T.; Watson, E.; Arumugasaamy, N.; Mikos, A. G.; Fisher, J. P. *Acta Biomater.* **2017**, *56*, 3–13.

(49) Moon, J. J.; West, J. L. *Curr. Top. Med. Chem.* **2008**, *8* (4), 300–310.

(50) Sarker, M.; Chen, X. B.; Schreyer, D. J. *J. Biomater. Sci. Polym. Ed.* **2015**, *26* (12), 683–734.

(51) Ruedinger, F.; Lavrentieva, A.; Blume, C.; Pepelanova, I.; Scheper, T. *Appl. Microbiol. Biotechnol.* **2015**, *99* (2), 623–636.

(52) Kraehenbuehl, T. P.; Langer, R.; Ferreira, L. S. *Nat. Methods* **2011**, *8* (9), 731–736.

(53) Kloxin, A. M.; Kloxin, C. J.; Bowman, C. N.; Anseth, K. S. *Adv. Mater.* **2010**, *22* (31), 3484–3494.

(54) Sanyal, S. *Corning Cult. Assay Syst. Used 3D Cell Cult.* **2014**.

(55) Szot, C. S.; Buchanan, C. F.; Freeman, J. W.; Rylander, M. N. *Biomaterials* **2011**, *32* (31), 7905–7912.

(56) Brinkman, W. T.; Nagapudi, K.; Thomas, B. S.; Chaikof, E. L. *Biomacromolecules* **2003**, *4* (4), 890–895.

(57) Khunmanee, S.; Jeong, Y.; Park, H. *J. Tissue Eng.* **2017**, *8*, 2041731417726464.

(58) Engel, B. J.; Constantinou, P. E.; Sablatura, L. K.; Doty, N. J.; Carson, D. D.; Farach-Carson, M. C.; Harrington, D. A.; Zarembinski, T. I. *Adv. Healthc. Mater.* **2015**, *4* (11), 1664–1674.

(59) Deng, Y.; Ren, J.; Chen, G.; Li, G.; Wu, X.; Wang, G.; Gu, G.; Li, J. *Sci. Rep.* **2017**, *7* (1), 2699.

(60) Price, R. D.; Berry, M. G.; Navsaria, H. A. *J. Plast. Reconstr. Aesthetic Surg.* **2007**, *60* (10), 1110–1119.

(61) Katie Slater, J. P.; Nandivada, and H. *Corning Appl. Note* **2017**.

(62) Sato, T.; Vries, R. G.; Snippert, H. J.; van de Wetering, M.; Barker, N.; Stange, D. E.; van Es, J. H.; Abo, A.; Kujala, P.; Peters, P. J.; Clevers, H. *Nature* **2009**, *459* (7244), 262–265.

(63) Xia, Y.; Nivet, E.; Sancho-Martinez, I.; Gallegos, T.; Suzuki, K.; Okamura, D.; Wu, M.-Z.; Dubova, I.; Esteban, C. R.; Montserrat, N.; Campistol, J. M.; Belmonte, J. C. I. *Nat. Cell Biol.* **2013**, *15* (12), 1507–1515.

(64) Gjorevski, N.; Lutolf, M. P. *Nat. Protoc.* **2017**, *12* (11), 2263–2274.

(65) Fu, Y.; Xu, K.; Zheng, X.; Giacomin, A. J.; Mix, A. W.; Kao, W. J. *Biomaterials* **2012**, *33* (1), 48–58.

(66) Jonker, A. M.; Löwik, D. W. P. M.; van Hest, J. C. M. *Chem. Mater.* **2012**, *24* (5), 759–773.

(67) Collier, J. H.; Hu, B. H.; Ruberti, J. W.; Zhang, J.; Shum, P.; Thompson, D. H.; Messersmith, P. B. *Journal of the American Chemical Society*. American Chemical Society 2001, pp 9463–9464.

(68) Kowalczyk, T.; Hnatuszko-Konka, K.; Gerszberg, A.; Kononowicz, A. K. *World J. Microbiol. Biotechnol.* **2014**, *30* (8), 2141–2152.

(69) Wang, H.; Zhu, D.; Paul, A.; Cai, L.; Enejder, A.; Yang, F.; Heilshorn, S. C. *Adv. Funct. Mater.* **2017**, *27* (28), 1605609.

(70) Jayawarna, V.; Ali, M.; Jowitt, T. A.; Miller, A. F.; Saiani, A.; Gough, J. E.; Ulijn, R. V. *Adv. Mater.* **2006**, *18* (5), 611–614.

(71) Jayawarna, V.; Richardson, S. M.; Hirst, A. R.; Hodson, N. W.; Saiani, A.; Gough, J. E.; Ulijn, R. V. *Acta Biomater.* **2009**, *5* (3), 934–943.

(72) Alakpa, E. V.; Jayawarna, V.; Burgess, K. E. V.; West, C. C.; Péault, B.; Ulijn, R. V.; Dalby, M. J. *Sci. Rep.* **2017**, *7* (1), 6895.

(73) Luo, H.; XU, C.; Liu, Z.; Yang, L.; Hong, Y.; Liu, G.; Zhong, H.; Cai, X.; Lin, X.; Chen, X.; Wang, C.; Zhang, N.; Xu, W. *J. Cell. Biochem.* **2017**, *120* (June 2017), 1–21.

(74) Fairbanks, B. D.; Schwartz, M. P.; Halevi, A. E.; Nuttelman, C. R.; Bowman, C. N.; Anseth, K. S. *Adv. Mater.* **2009**, *21* (48), 5005–5010.

(75) Lin, C.-C.; Anseth, K. S. *Proc. Natl. Acad. Sci. U. S. A.* **2011**, *108* (16), 6380–6385.

(76) Singh, S. P.; Schwartz, M. P.; Lee, J. Y.; Fairbanks, B. D.; Anseth, K. S. *Biomater. Sci.* **2014**, *2* (7), 1024–1034.

(77) Anderson, S. B.; Lin, C.-C.; Kuntzler, D. V.; Anseth, K. S. *Biomaterials* **2011**, *32* (14), 3564–3574.

(78) Hodgson, S. M.; McNelles, S. A.; Abdullahu, L.; Marozas, I. A.; Anseth, K. S.; Adronov, A. *Biomacromolecules* **2017**, *18* (12), 4054–4059.

(79) Desai, R. M.; Koshy, S. T.; Hilderbrand, S. A.; Mooney, D. J.; Joshi, N. S.

Biomaterials **2015**, *50*, 30–37.

(80) Zhang, Y.; Tao, L.; Li, S.; Wei, Y. *Biomacromolecules* **2011**, *12* (8), 2894–2901.

(81) Yang, B.; Zhang, Y.; Zhang, X.; Tao, L.; Li, S.; Wei, Y. *Polym. Chem.* **2012**, *3* (12), 3235.

(82) Kölmel, D. K.; Kool, E. T. *Chem. Rev.* **2017**, *117* (15), 10358–10376.

(83) McKinnon, D. D.; Domaille, D. W.; Brown, T. E.; Kyburz, K. A.; Kiyotake, E.; Cha, J. N.; Anseth, K. S. *Soft Matter* **2014**, *10* (46), 9230–9236.

(84) McKinnon, D. D.; Domaille, D. W.; Cha, J. N.; Anseth, K. S. *Adv. Mater.* **2014**, *26* (6), 865–872.

(85) Choh, S. Y.; Cross, D.; Wang, C. *Biomacromolecules* **2011**, *12* (4), 1126–1136.

(86) Huebsch, N.; Arany, P. R.; Mao, A. S.; Shvartsman, D.; Ali, O. A.; Bencherif, S. A.; Rivera-Feliciano, J.; Mooney, D. J. *Nat. Mater.* **2010**, *9* (6), 518–526.

(87) Wong Po Foo, C. T. S.; Lee, J. S.; Mulyasasmita, W.; Parisi-Amon, A.; Heilshorn, S. C. *Proc. Natl. Acad. Sci. U. S. A.* **2009**, *106* (52), 22067–22072.

(88) Parisi-Amon, A.; Mulyasasmita, W.; Chung, C.; Heilshorn, S. C. *Adv. Healthc. Mater.* **2013**, *2* (3), 428–432.

(89) Mulyasasmita, W.; Cai, L.; Dewi, R. E.; Jha, A.; Ullmann, S. D.; Luong, R. H.; Huang, N. F.; Heilshorn, S. C. *J. Control. Release* **2014**, *191*, 71–81.

(90) Cai, L.; Dewi, R. E.; Heilshorn, S. C. *Adv. Funct. Mater.* **2015**, *25* (9), 1344–1351.

(91) Cai, L.; Dewi, R. E.; Goldstone, A. B.; Cohen, J. E.; Steele, A. N.; Woo, Y. J.; Heilshorn, S. C. *Adv. Healthc. Mater.* **2016**, *5* (21), 2758–2764.

(92) Nuttelman, C. R.; Tripodi, M. C.; Anseth, K. S. *Matrix Biol.* **2005**, *24* (3), 208–218.

(93) Hersel, U.; Dahmen, C.; Kessler, H. *Biomaterials* **2003**, *24* (24), 4385–4415.

(94) DeForest, C. A.; Polizzotti, B. D.; Anseth, K. S. *Nat. Mater.* **2009**, *8* (8), 659–664.

(95) Silva, A. K. A.; Richard, C.; Bessodes, M.; Scherman, D.; Merten, O.-W. *Biomacromolecules* **2009**, *10* (1), 9–18.

(96) Brown, T. E.; Anseth, K. S. *Chem. Soc. Rev.* **2017**, *46* (21), 6532–6552.

(97) Mosiewicz, K. A.; Kolb, L.; van der Vlies, A. J.; Martino, M. M.; Lienemann, P. S.; Hubbell, J. A.; Ehrbar, M.; Lutolf, M. P. *Nat. Mater.* **2013**, *12* (11), 1072–1078.

(98) Engler, A. J.; Sen, S.; Sweeney, H. L.; Discher, D. E. *Cell* **2006**, *126* (4), 677–689.

(99) Yang, C.; DelRio, F. W.; Ma, H.; Killaars, A. R.; Basta, L. P.; Kyburz, K. A.; Anseth, K. S. *Proc. Natl. Acad. Sci.* **2016**, *113* (31), E4439–E4445.

(100) Dalby, M. J.; Gadegaard, N.; Tare, R.; Andar, A.; Riehle, M. O.; Herzyk, P.;

Wilkinson, C. D. W.; Oreffo, R. O. C. *Nat. Mater.* **2007**, *6* (12), 997–1003.

(101) Lutolf, M. P.; Lauer-Fields, J. L.; Schmoekel, H. G.; Metters, A. T.; Weber, F. E.; Fields, G. B.; Hubbell, J. A. *Proc. Natl. Acad. Sci.* **2003**, *100* (9), 5413–5418.

(102) Kloxin, A. M.; Tibbitt, M. W.; Anseth, K. S. *Nat. Protoc.* **2010**, *5* (12), 1867–1887.

(103) Tibbitt, M. W.; Kloxin, A. M.; Sawicki, L. A.; Anseth, K. S. *Macromolecules* **2013**, *46* (7), 2785–2792.

(104) Peng, K.; Tomatsu, I.; van den Broek, B.; Cui, C.; Korobko, A. V.; van Noort, J.; Meijer, A. H.; Spaink, H. P.; Kros, A. *Soft Matter* **2011**, *7* (10), 4881.

(105) Tamura, M.; Yanagawa, F.; Sugiura, S.; Takagi, T.; Sumaru, K.; Kanamori, T. *Sci. Rep.* **2015**, *5*, 15060.

(106) Barbulovic-Nad, I.; Lucente, M.; Sun, Y.; Zhang, M.; Wheeler, A. R.; Bussmann, M. *Crit. Rev. Biotechnol.* **2006**, *26* (4), 237–259.

(107) Müller, U. R.; Nicolau, D. V. In *Microarray Technology and Its Applications*; Müller, U. R., Nicolau, D. V., Eds.; Biological and Medical Physics, Biomedical Engineering; Springer-Verlag: Berlin/Heidelberg, 2005.

(108) Wu, P.; Castner, D. G.; Grainger, D. W. *J. Biomater. Sci. Polym. Ed.* **2008**, *19* (6), 725–753.

(109) Calvert, P. In *Chemistry of Materials*; American Chemical Society, 2001; Vol. 13, pp 3299–3305.

(110) Bumgarner, R. *Overview of DNA microarrays: types, applications, and their future.*; NIH Public Access, 2013; Vol. Chapter 22.

(111) Dufva, M. In *Methods in molecular biology (Clifton, N.J.)*; 2009; Vol. 529, pp 63–79.

(112) Schena, M. *Trends Biotechnol.* **1998**, *16* (7), 301–306.

(113) How, S. E.; Yingyongnarongkul, B.; Fara, M. A.; Díaz-Mochón, J. J.; Mittoo, S.; Bradley, M. *Comb. Chem. High Throughput Screen.* **2004**, *7* (5), 423–430.

(114) Anderson, D. G.; Levenberg, S.; Langer, R. *Nat. Biotechnol.* **2004**, *22* (7), 863–866.

(115) Thaburet, J.-F.; Mizomoto, H.; Bradley, M. *Macromol. Rapid Commun.* **2004**, *25* (1), 366–370.

(116) Tourniaire, G.; Collins, J.; Campbell, S.; Mizomoto, H.; Ogawa, S.; Thaburet, J.-F.; Bradley, M. *Chem. Commun.* **2006**, No. 20, 2118.

(117) Mant, A.; Tourniaire, G.; Diaz-Mochon, J. J.; Elliott, T. J.; Williams, A. P.; Bradley, M. *Biomaterials* **2006**, *27* (30), 5299–5306.

(118) Unciti-Broceta, A.; Díaz-Mochón, J. J.; Mizomoto, H.; Bradley, M. *J. Comb.*

Chem. **2008**, *10* (2), 179–184.

(119) Tare, R. S.; Khan, F.; Tourniaire, G.; Morgan, S. M.; Bradley, M.; Oreffo, R. O. C. *Biomaterials* **2009**, *30* (6), 1045–1055.

(120) Pernagallo, S.; Diaz-Mochon, J. J.; Bradley, M. *Lab Chip* **2009**, *9* (3), 397–403.

(121) Hansen, A.; McMillan, L.; Morrison, A.; Petrik, J.; Bradley, M. *Biomaterials* **2011**, *32* (29), 7034–7041.

(122) Wu, M.; Bridle, H.; Bradley, M. *Water Res.* **2012**, *46* (6), 1715–1722.

(123) Pickering, H.; Wu, M.; Bradley, M.; Bridle, H. *Environ. Sci. Technol.* **2012**, *46* (4), 2179–2186.

(124) Venkateswaran, S.; Gwynne, P. J.; Wu, M.; Hardman, A.; Lilienkampf, A.; Pernagallo, S.; Blakely, G.; Swann, D. G.; Bradley, M.; Gallagher, M. P. *J. Vis. Exp.* **2016**, No. 117, e54382–e54382.

(125) Duffy, C. R. E.; Zhang, R.; How, S. E.; Lilienkampf, A.; Tourniaire, G.; Hu, W.; West, C. C.; De Sousa, P.; Bradley, M. *Biomater. Sci.* **2014**, *2* (11), 1683–1692.

(126) Tabu, K.; Muramatsu, N.; Mangani, C.; Wu, M.; Zhang, R.; Kimura, T.; Terashima, K.; Bizen, N.; Kimura, R.; Wang, W.; Murota, Y.; Kokubu, Y.; Nobuhisa, I.; Kagawa, T.; Kitabayashi, I.; Bradley, M.; Taga, T. *Stem Cells* **2016**, *34* (5), 1151–1162.

(127) Liberski, A. R.; Tizzard, G. J.; Diaz-Mochon, J. J.; Hursthouse, M. B.; Milnes, P.; Bradley, M. *J. Comb. Chem.* **2008**, *10* (1), 24–27.

(128) Zhang, R.; Liberski, A.; Khan, F.; Diaz-Mochon, J. J.; Bradley, M. *Chem. Commun.* **2008**, *0* (11), 1317.

(129) Liberski, A.; Zhang, R.; Bradley, M. *Chem. Commun.* **2009**, *0* (3), 334–336.

(130) Hansen, A.; Mjoseng, H. K.; Zhang, R.; Kalloudis, M.; Koutsos, V.; de Sousa, P. A.; Bradley, M. *Adv. Healthc. Mater.* **2014**, *3* (6), 848–853.

(131) Duffy, C. R. E.; Zhang, R.; How, S.-E.; Lilienkampf, A.; De Sousa, P. A.; Bradley, M. *Biomaterials* **2014**, *35* (23), 5998–6005.

(132) Mangani, C.; Lilienkampf, A.; Roy, M.; De Sousa, P. A.; Bradley, M. *Biomater. Sci.* **2015**, *3* (10), 1371–1375.

(133) Duffy, C.; Venturato, A.; Callanan, A.; Lilienkampf, A.; Bradley, M. *Acta Biomater.* **2016**, *34*, 104–112.

(134) Khan, F.; Tare, R. S.; Kanczler, J. M.; Oreffo, R. O. C.; Bradley, M. *Biomaterials* **2010**, *31* (8), 2216–2228.

(135) Khan, F.; Tare, R. S.; Oreffo, R. O. C.; Bradley, M. *Angew. Chemie Int. Ed.* **2009**,

48 (5), 978–982.

(136) Ranga, A.; Gobaa, S.; Okawa, Y.; Mosiewicz, K.; Negro, A.; Lutolf, M. P. *Nat. Commun.* **2014**, *5*, 4324.

(137) Ruoslahti, E.; Pierschbacher, M. D. *Science* **1987**, *238* (4826), 491–497.

(138) Maeda, T.; Titani, K.; Sekiguchi, K. *J. Biochem.* **1994**, *115* (2), 182–189.

(139) Zhu, J. *Biomaterials* **2010**, *31* (17), 4639–4656.

(140) Clément, B.; Segui-Real, B.; Savagner, P.; Kleinman, H. K.; Yamada, Y. *J. Cell Biol.* **1990**, *110* (1), 185–192.

(141) Yoshida, N.; Ishii, E.; Nomizu, M.; Yamada, Y.; Mohri, S.; Kinukawa, N.; Matsuzaki, A.; Oshima, K.; Hara, T.; Miyazaki, S. *Br. J. Cancer* **1999**, *80* (12), 1898–1904.

(142) Alconcel, S. N. S.; Baas, A. S.; Maynard, H. D. *Polym. Chem.* **2011**, *2* (7), 1442.

(143) Brunner, D. *ALTEX* **2010**, 53–62.

(144) Gstraunthaler, G. *ALTEX* **2003**, *20* (4), 275–281.

(145) van der Valk, J.; Brunner, D.; De Smet, K.; Fex Svenningsen, Å.; Honegger, P.; Knudsen, L. E.; Lindl, T.; Noraberg, J.; Price, A.; Scarino, M. L.; Gstraunthaler, G. *Toxicol. Vitr.* **2010**, *24* (4), 1053–1063.

(146) Xu, C.; Inokuma, M. S.; Denham, J.; Golds, K.; Kundu, P.; Gold, J. D.; Carpenter, M. K. *Nat. Biotechnol.* **2001**, *19* (10), 971–974.

(147) Amit, M.; Carpenter, M. K.; Inokuma, M. S.; Chiu, C.-P.; Harris, C. P.; Waknitz, M. A.; Itskovitz-Eldor, J.; Thomson, J. A. *Dev. Biol.* **2000**, *227* (2), 271–278.

(148) Behrendt, R.; White, P.; Offer, J. *J. Pept. Sci.* **2016**, *22* (1), 4–27.

(149) Kharkar, P. M.; Kiick, K. L.; Kloxin, A. M. *Chem. Soc. Rev.* **2013**, *42* (17), 7335–7372.

(150) Ursu, A.; Schöler, H. R.; Waldmann, H. *Nat. Chem. Biol.* **2017**, *13* (6), 560–563.

(151) Bian, C.; Zhao, K.; Tong, G.; Zhu, Y.; Chen, P. *J. Zhejiang Univ. Sci. B* **2005**, *6* (7), 631–636.

(152) Davis, J.; Crampton, S. P.; Hughes, C. C. W. *J. Vis. Exp.* **2007**, No. 3, e183–e183.

(153) Cheung, A. L. In *Current Protocols in Microbiology*; John Wiley & Sons, Inc.: Hoboken, NJ, USA, 2007; Vol. Appendix 4, p Appendix 4B.

(154) Newman, P. J. *J. Clin. Invest.* **1997**, *99* (1), 3–8.

(155) Willam, C.; Koehne, P.; Jürgensen, J. S.; Gräfe, M.; Wagner, K. D.; Bachmann, S.; Frei, U.; Eckardt, K. U. *Circ. Res.* **2000**, *87* (5), 370–377.

(156) Müller, A. M.; Hermanns, M. I.; Skrzynski, C.; Nesslinger, M.; Müller, K.-M.;

Kirkpatrick, C. J. *Exp. Mol. Pathol.* **2002**, *72* (3), 221–229.

(157) Corada, M.; Mariotti, M.; Thurston, G.; Smith, K.; Kunkel, R.; Brockhaus, M.; Lampugnani, M. G.; Martin-Padura, I.; Stoppacciaro, A.; Ruco, L.; McDonald, D. M.; Ward, P. A.; Dejana, E. *Proc. Natl. Acad. Sci. U. S. A.* **1999**, *96* (17), 9815–9820.

(158) Vogel, C.; de Sousa Abreu, R.; Ko, D.; Le, S.-Y.; Shapiro, B. A.; Burns, S. C.; Sandhu, D.; Boutz, D. R.; Marcotte, E. M.; Penalva, L. O. *Mol. Syst. Biol.* **2010**, *6*, 400.

(159) Tian, Q.; Stepaniants, S. B.; Mao, M.; Weng, L.; Feetham, M. C.; Doyle, M. J.; Yi, E. C.; Dai, H.; Thorsson, V.; Eng, J.; Goodlett, D.; Berger, J. P.; Gunter, B.; Linseley, P. S.; Stoughton, R. B.; Aebersold, R.; Collins, S. J.; Hanlon, W. A.; Hood, L. E. *Mol. Cell. Proteomics* **2004**, *3* (10), 960–969.

(160) Lundberg, E.; Fagerberg, L.; Klevebring, D.; Matic, I.; Geiger, T.; Cox, J.; Älgenäs, C.; Lundeberg, J.; Mann, M.; Uhlen, M. *Mol. Syst. Biol.* **2010**, *6*, 450.

(161) Schwanhäusser, B.; Busse, D.; Li, N.; Dittmar, G.; Schuchhardt, J.; Wolf, J.; Chen, W.; Selbach, M. *Nature* **2011**, *473* (7347), 337–342.

(162) Stark, A. M.; Pfannenschmidt, S.; Tscheslog, H.; Maass, N.; Rösel, F.; Mehdorn, H. M.; Held-Feindt, J. *Neurol. Res.* **2006**, *28* (8), 787–793.

(163) Chaudhuri, O.; Koshy, S. T.; Branco Da Cunha, C.; Shin, J. W.; Verbeke, C. S.; Allison, K. H.; Mooney, D. J. *Nat. Mater.* **2014**, *13* (10), 970–978.

(164) Anguiano, M.; Castilla, C.; Maška, M.; Ederra, C.; Peláez, R.; Morales, X.; Muñoz-Arrieta, G.; Mujika, M.; Kozubek, M.; Muñoz-Barrutia, A.; Rouzaut, A.; Arana, S.; Garcia-Aznar, J. M.; Ortiz-de-Solorzano, C. *PLoS One* **2017**, *12* (2), e0171417.

(165) Livak, K. J.; Schmittgen, T. D. *Methods* **2001**, *25* (4), 402–408.

(166) Phelan, K.; May, K. M. *Curr. Protoc. Mol. Biol.* **2017**, *117* (1), A.3F.1-A.3F.23.

(167) Rous, P.; Jones, F. S. *J. Exp. Med.* **1916**, *23* (4), 549–555.

(168) Huang, H. L.; Hsing, H. W.; Lai, T. C.; Chen, Y. W.; Lee, T. R.; Chan, H. T.; Lyu, P. C.; Wu, C. L.; Lu, Y. C.; Lin, S. T.; Lin, C. W.; Lai, C. H.; Chang, H. T.; Chou, H. C.; Chan, H. L. *J. Biomed. Sci.* **2010**, *17* (1), 36.

(169) Bajpai, R.; Lesperance, J.; Kim, M.; Terskikh, A. V. *Mol. Reprod. Dev.* **2007**, *75* (5), 818–827.

(170) Wachs, F.-P.; Couillard-Despres, S.; Engelhardt, M.; Wilhelm, D.; Ploetz, S.; Vroemen, M.; Kaesbauer, J.; Uyanik, G.; Klucken, J.; Karl, C.; Tebbing, J.;

Svendsen, C.; Weidner, N.; Kuhn, H.-G.; Winkler, J.; Aigner, L. **2003**.

(171) Melton, D. *Essentials of Stem Cell Biology*; Elsevier, 2014.

(172) Ferlay, J.; Soerjomataram, I.; Dikshit, R.; Eser, S.; Mathers, C.; Rebelo, M.; Parkin, D. M.; Forman, D.; Bray, F. *Int. J. Cancer* **2015**, *136* (5), E359–E386.

(173) Shackleton, M.; Quintana, E.; Fearon, E. R.; Morrison, S. J. *Cell*. September 4, 2009, pp 822–829.

(174) Brown, D. V; Mantamadiotis, T. *Front Biosci (Landmark Ed)* **2014**, *19*, 1015–1027.

(175) Visvader, J. E. *Nature* **2011**, *469* (7330), 314–322.

(176) Reya, T.; Morrison, S. J.; Clarke, M. F.; Weissman, I. L. *Nature* **2001**, *414* (6859), 105–111.

(177) Lagasse, E. *Gene Ther.* **2008**, *15* (2), 136–142.

(178) Batlle, E.; Clevers, H. *Nat. Med.* **2017**, *23* (10), 1124–1134.

(179) Shahriyari, L.; Komarova, N. L. *PLoS One* **2013**, *8* (10), e76195.

(180) Al-Hajj, M.; Wicha, M. S.; Benito-Hernandez, A.; Morrison, S. J.; Clarke, M. F. *Proc. Natl. Acad. Sci. U. S. A.* **2003**, *100* (7), 3983–3988.

(181) Singh, S. K.; Hawkins, C.; Clarke, I. D.; Squire, J. A.; Bayani, J.; Hide, T.; Henkelman, R. M.; Cusimano, M. D.; Dirks, P. B. *Nature* **2004**, *432* (7015), 396–401.

(182) O'Brien, C. A.; Pollett, A.; Gallinger, S.; Dick, J. E. *Nature* **2007**, *445* (7123), 106–110.

(183) Ricci-Vitiani, L.; Lombardi, D. G.; Pilozzi, E.; Biffoni, M.; Todaro, M.; Peschle, C.; De Maria, R. *Nature* **2007**, *445* (7123), 111–115.

(184) Maitland, N. J.; Collins, A. T. *J. Clin. Oncol.* **2008**, *26* (17), 2862–2870.

(185) Bonnet, D.; Dick, J. E. *Nat. Med.* **1997**, *3* (7), 730–737.

(186) Alvero, A. B.; Chen, R.; Fu, H.-H.; Montagna, M.; Schwartz, P. E.; Rutherford, T.; Silasi, D.-A.; Steffensen, K. D.; Waldstrom, M.; Visintin, I.; Mor, G. *Cell Cycle* **2009**, *8* (1), 158–166.

(187) Zhang, S.; Balch, C.; Chan, M. W.; Lai, H.-C.; Matei, D.; Schilder, J. M.; Yan, P. S.; Huang, T. H.-M.; Nephew, K. P. *Cancer Res.* **2008**, *68* (11), 4311–4320.

(188) Li, C.; Heidt, D. G.; Dalerba, P.; Burant, C. F.; Zhang, L.; Adsay, V.; Wicha, M.; Clarke, M. F.; Simeone, D. M. *Cancer Res.* **2007**, *67* (3), 1030–1037.

(189) Bao, S.; Wu, Q.; McLendon, R. E.; Hao, Y.; Shi, Q.; Hjelmeland, A. B.; Dewhirst, M. W.; Bigner, D. D.; Rich, J. N. *Nature* **2006**, *444* (7120), 756–760.

(190) Eramo, A.; Ricci-Vitiani, L.; Zeuner, A.; Pallini, R.; Lotti, F.; Sette, G.; Pilozzi,

E.; Larocca, L. M.; Peschle, C.; De Maria, R. *Cell Death Differ.* **2006**, *13* (7), 1238–1241.

(191) Clevers, H. *Science (80-.).* **2015**, *350* (6266), 1319–1320.

(192) Vaz, A. P.; Ponnusamy, M. P.; Seshacharyulu, P.; Batra, S. K. *J. cancer stem cell Res.* **2014**, *2*.

(193) Rasheed, Z. A.; Yang, J.; Wang, Q.; Kowalski, J.; Freed, I.; Murter, C.; Hong, S.-M.; Koorstra, J.-B.; Rajeshkumar, N. V.; He, X.; Goggins, M.; Iacobuzio-Donahue, C.; Berman, D. M.; Laheru, D.; Jimeno, A.; Hidalgo, M.; Maitra, A.; Matsui, W. *JNCI J. Natl. Cancer Inst.* **2010**, *102* (5), 340–351.

(194) Raimondi, S.; Maisonneuve, P.; Lowenfels, A. B. *Nat. Rev. Gastroenterol. Hepatol.* **2009**, *6* (12), 699–708.

(195) Hidalgo, M. *N. Engl. J. Med.* **2010**, *362* (17), 1605–1617.

(196) Kondo, T.; Setoguchi, T.; Taga, T. *Proc. Natl. Acad. Sci. U. S. A.* **2004**, *101* (3), 781–786.

(197) Pan, J.; Zhang, Q.; Wang, Y.; You, M. *PLoS One* **2010**, *5* (10), e13298.

(198) Vlashi, E.; Kim, K.; Lagadec, C.; Donna, L. Della; McDonald, J. T.; Eghbali, M.; Sayre, J. W.; Stefani, E.; McBride, W.; Pajonk, F. *J. Natl. Cancer Inst.* **2009**, *101* (5), 350–359.

(199) Adikrisna, R.; Tanaka, S.; Muramatsu, S.; Aihara, A.; Ban, D.; Ochiai, T.; Irie, T.; Kudo, A.; Nakamura, N.; Yamaoka, S.; Arii, S. *Gastroenterology* **2012**, *143* (1), 234-45.e7.

(200) Mizomoto, H. The Synthesis and Screening of Polymer Libraries using a High Throughput Approach, University of Southampton, 2004.

(201) Zhu, J.; Tang, C.; Kottke-Marchant, K.; Marchant, R. E. *Bioconjug. Chem.* **2009**, *20* (2), 333–339.

(202) Zhang, R.; Liberski, A.; Sanchez-Martin, R.; Bradley, M. *Biomaterials* **2009**, *30* (31), 6193–6201.

(203) Stebbins, J. L.; Santelli, E.; Feng, Y.; De, S. K.; Purves, A.; Motamedchaboki, K.; Wu, B.; Ronai, Z. A.; Liddington, R. C.; Pellecchia, M. *Chem. Biol.* **2013**, *20* (8), 973–982.

Appendix

A.1 Appendix for Chapter 2

Figure A1.1: 250-member hydrogel array screen with HeLa cells. HeLa cells were incubated on the array for 18 h followed by viability staining with fluorescein diacetate (FDA) (green, live stain, ($\lambda_{ex/em}$ = 490/514 nm) and propidium iodide (PI) (red, dead stain, $\lambda_{ex/em}$ = 570/602 nm). The merged images of the FDA, PI and BF channels for each replicate are shown. Images are not shown of combinations where features lifted from the slide. BF = bright field.

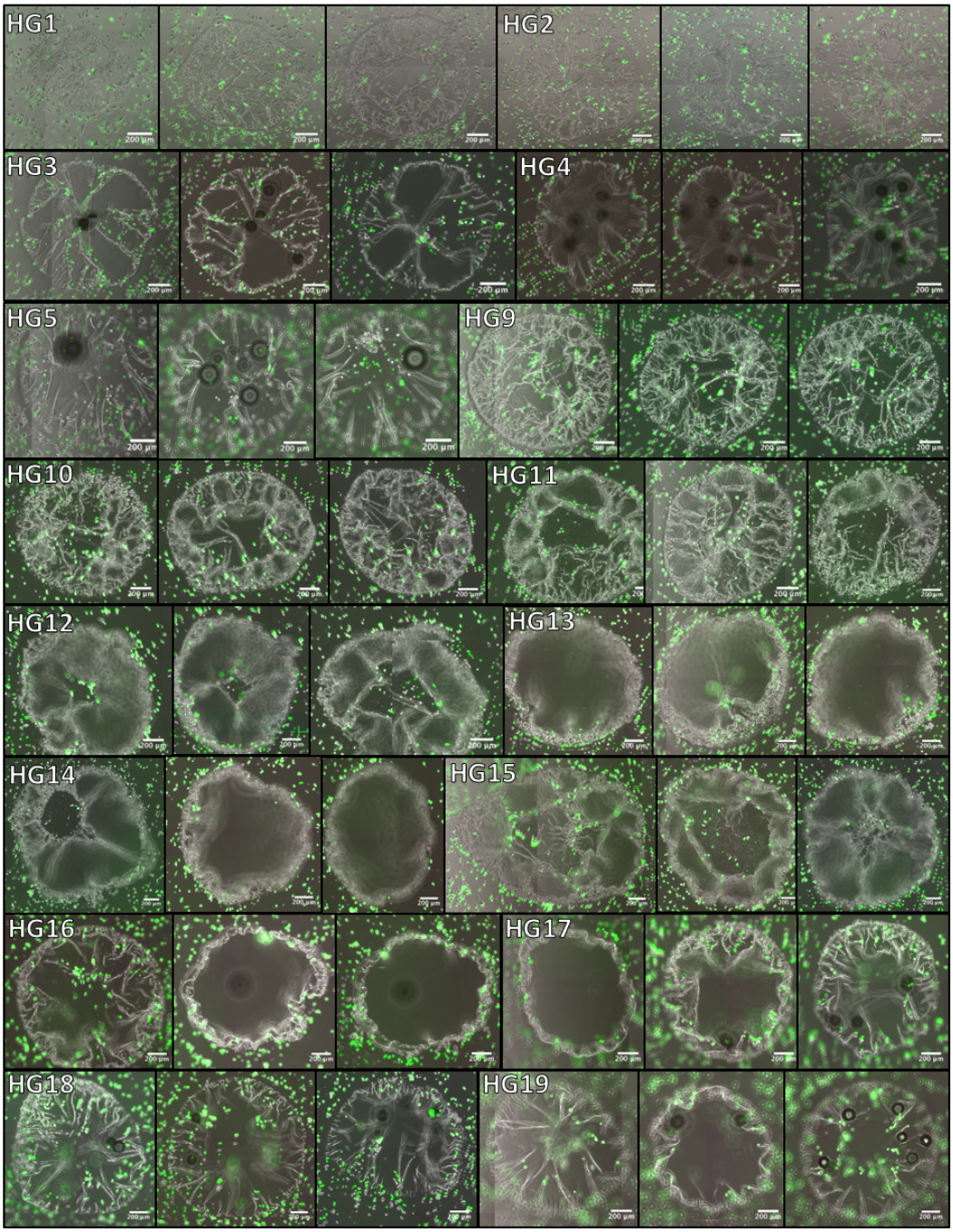

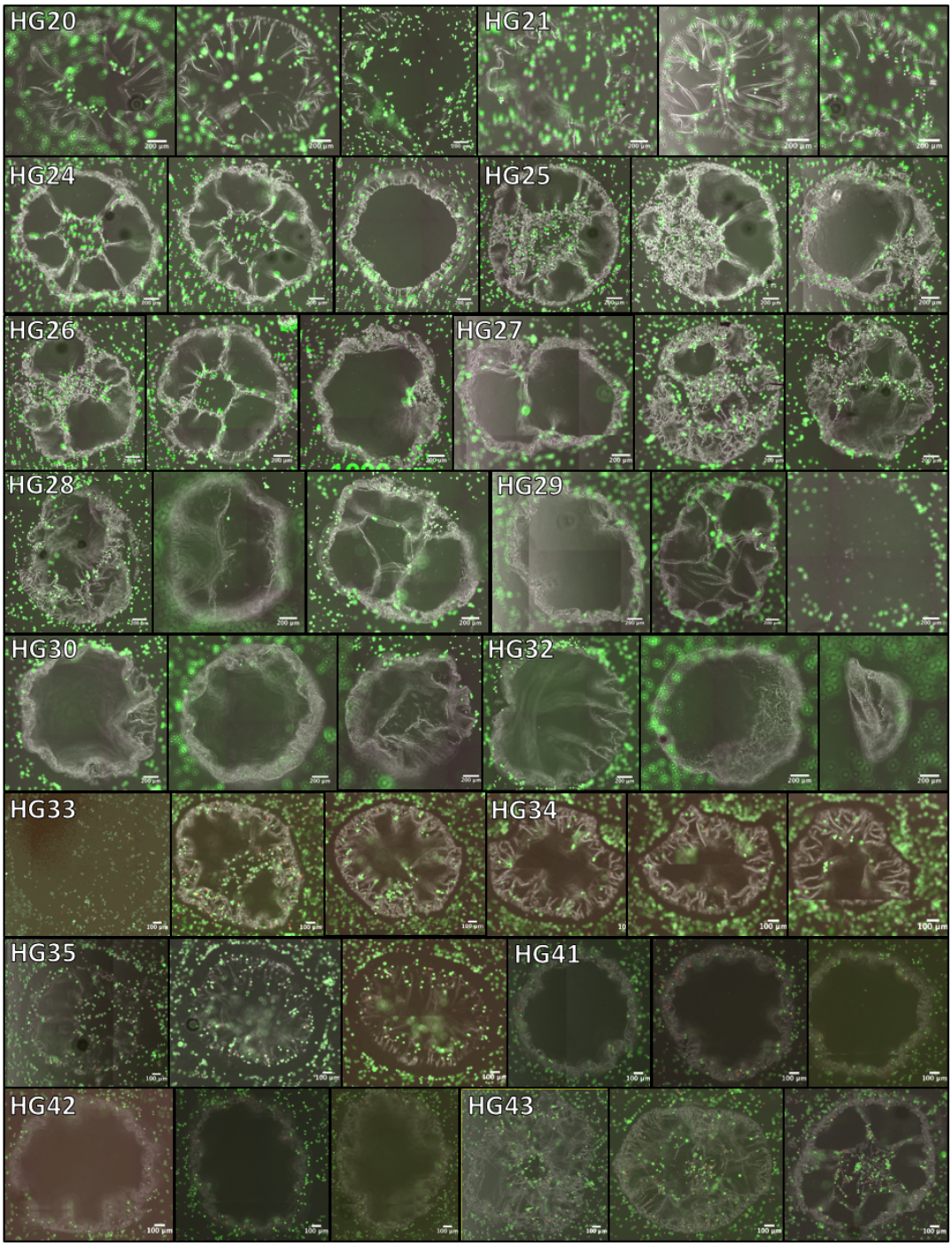
HG20
HG21
HG24
HG25
HG26
HG27
HG28
HG29
HG30
HG32
HG33
HG34
HG35
HG41
HG42
HG43

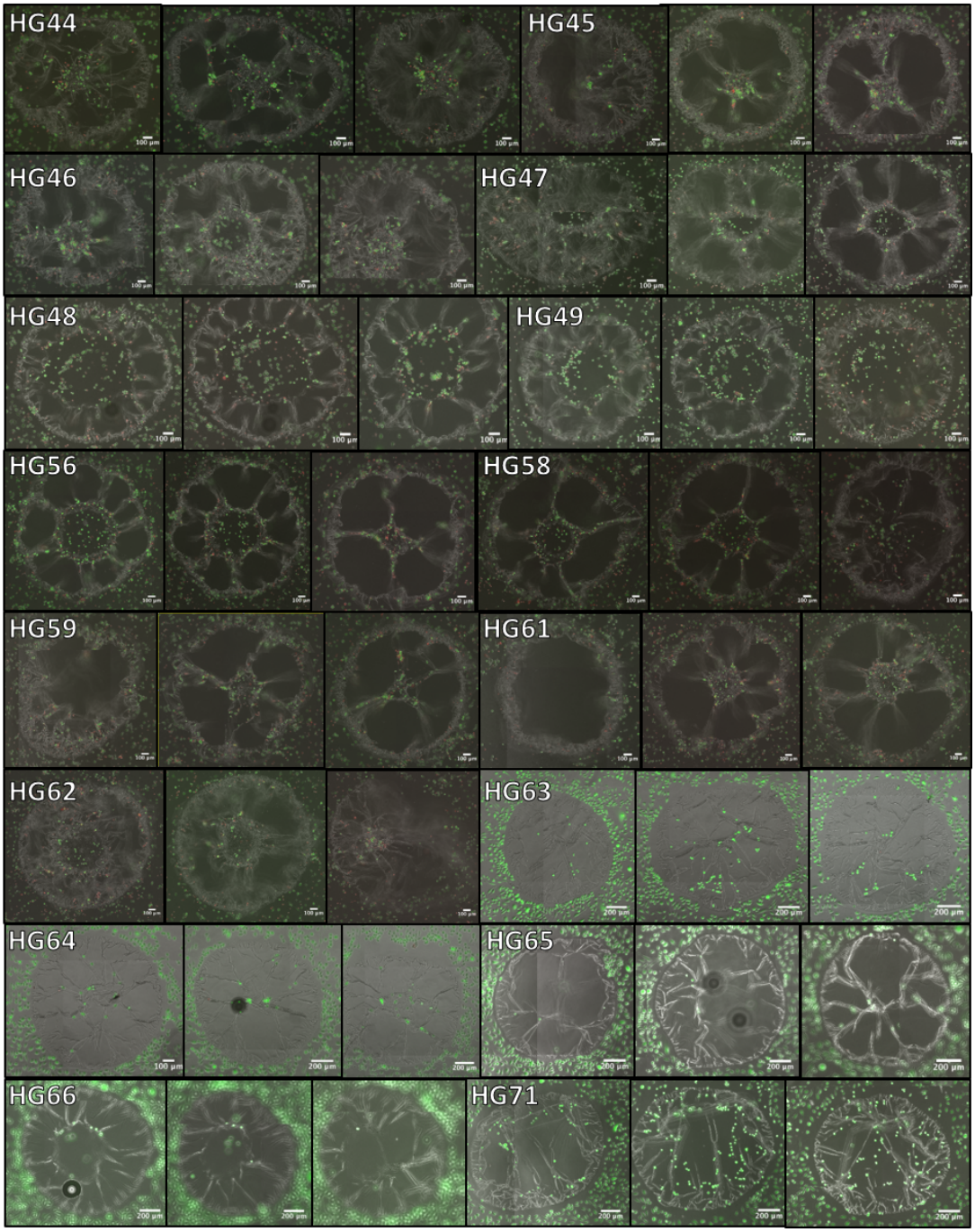
HG44
HG45
HG46
HG47
HG48
HG49
HG56
HG58
HG59
HG61
HG62
HG63
HG64
HG65
HG66
HG71

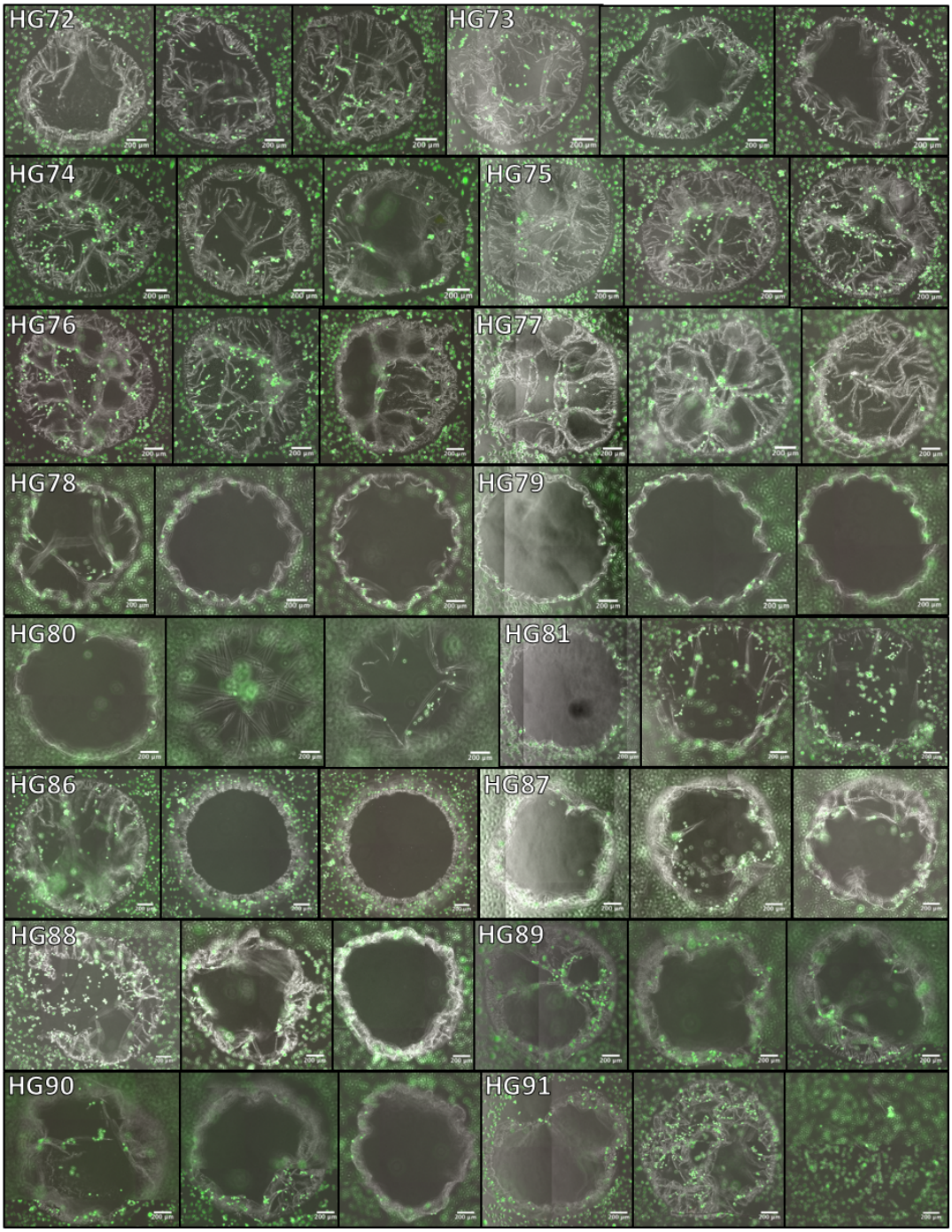
HG72
HG73
HG74
HG75
HG76
HG77
HG78
HG79
HG80
HG81
HG86
HG87
HG88
HG89
HG90
HG91

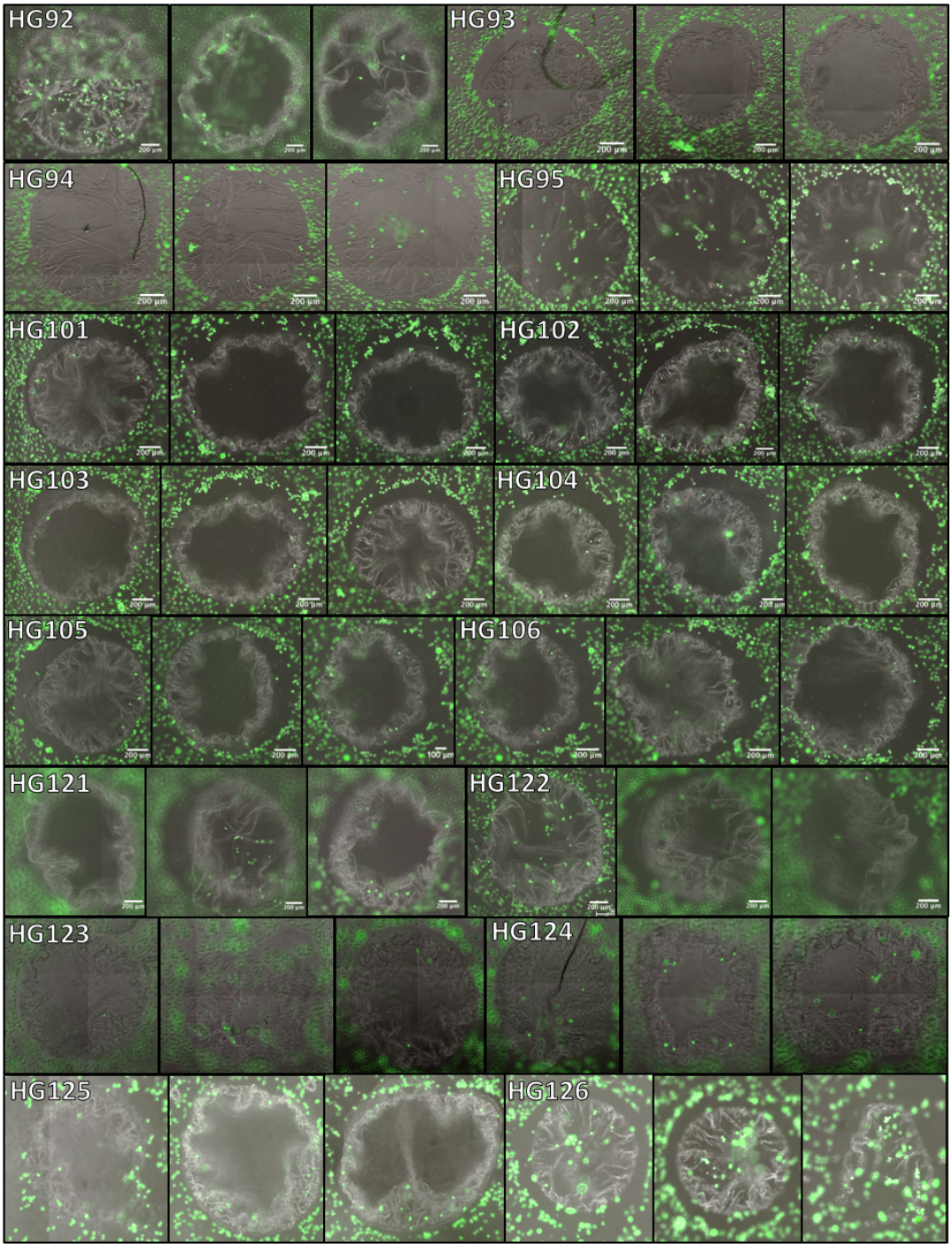
HG92
HG93
HG94
HG95
HG101
HG102
HG103
HG104
HG105
HG106
HG121
HG122
HG123
HG124
HG125
HG126

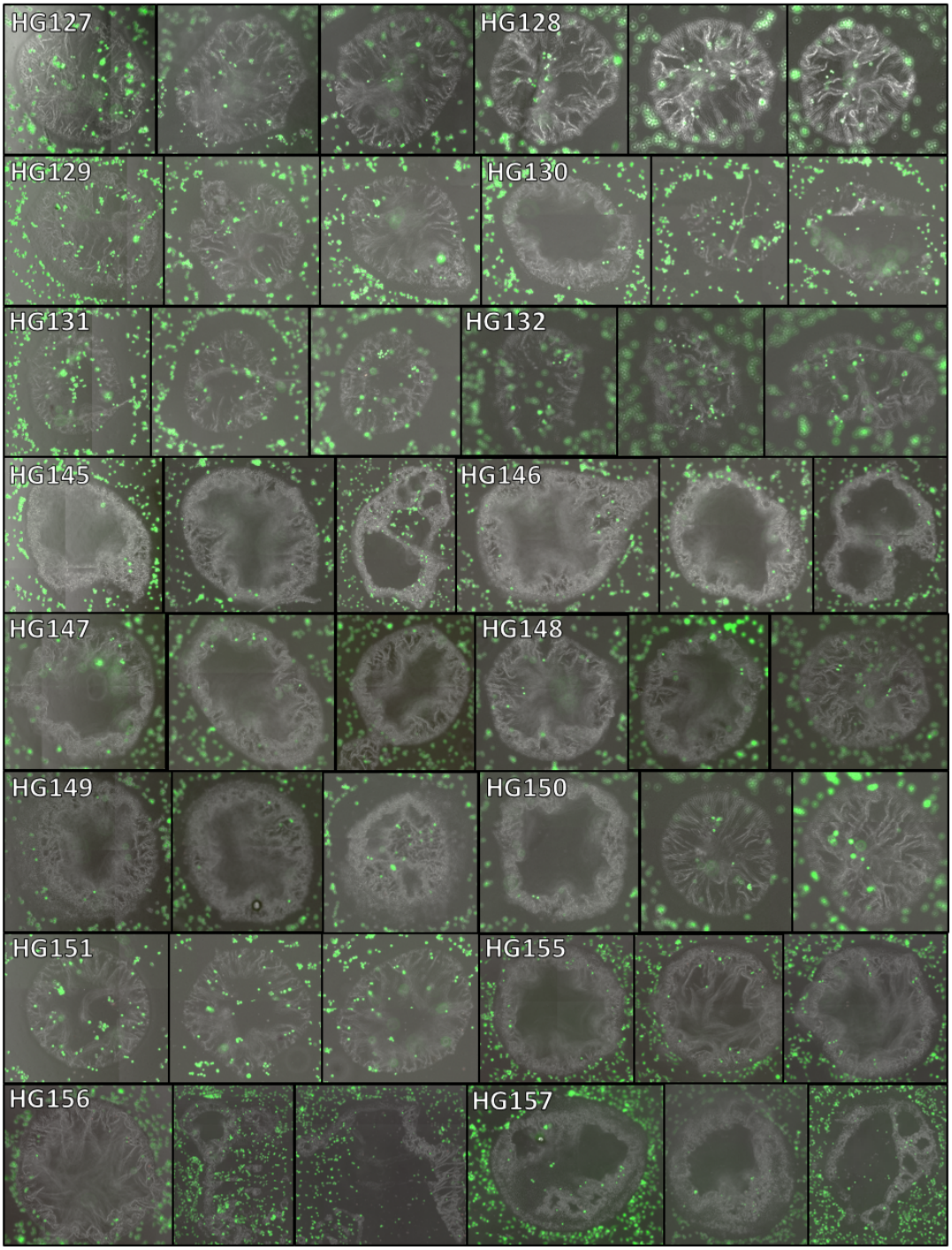
HG127
HG128
HG129
HG130
HG131
HG132
HG145
HG146
HG147
HG148
HG149
HG150
HG151
HG155
HG156
HG157

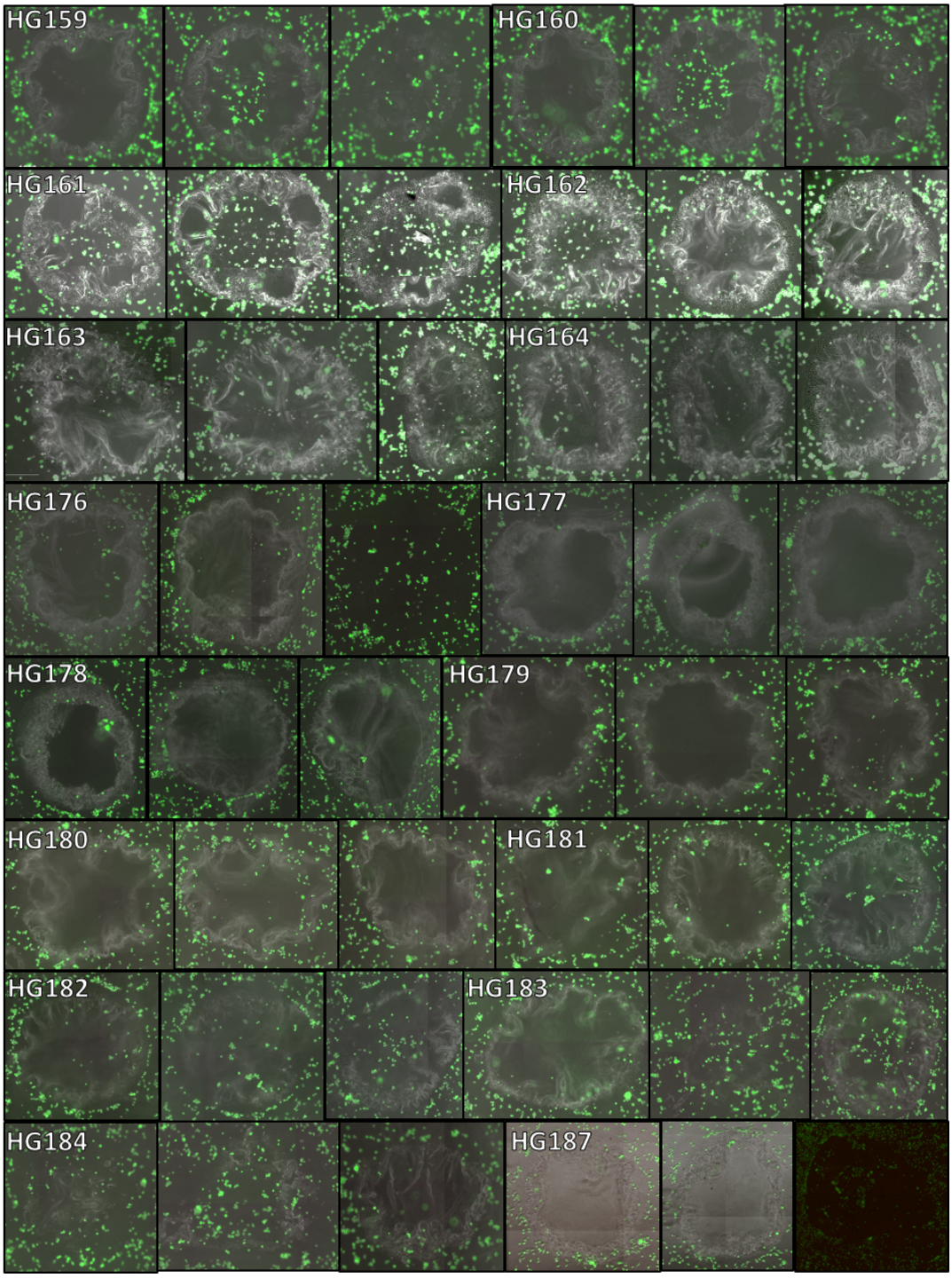
HG159
HG160
HG161
HG162
HG163
HG164
HG176
HG177
HG178
HG179
HG180
HG181
HG182
HG183
HG184
HG187

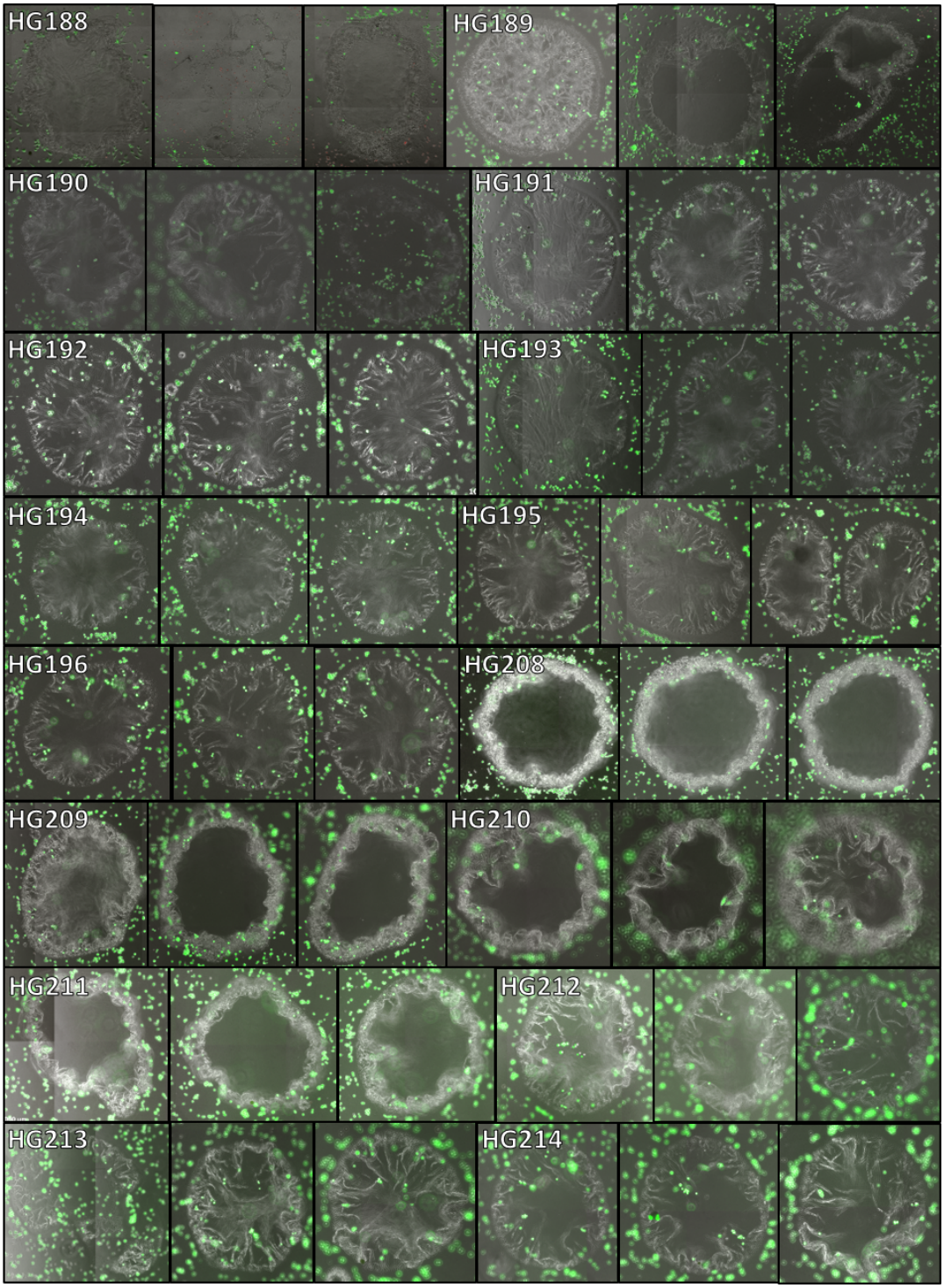
HG188
HG189
HG190
HG191
HG192
HG193
HG194
HG195
HG196
HG208
HG209
HG210
HG211
HG212
HG213
HG214

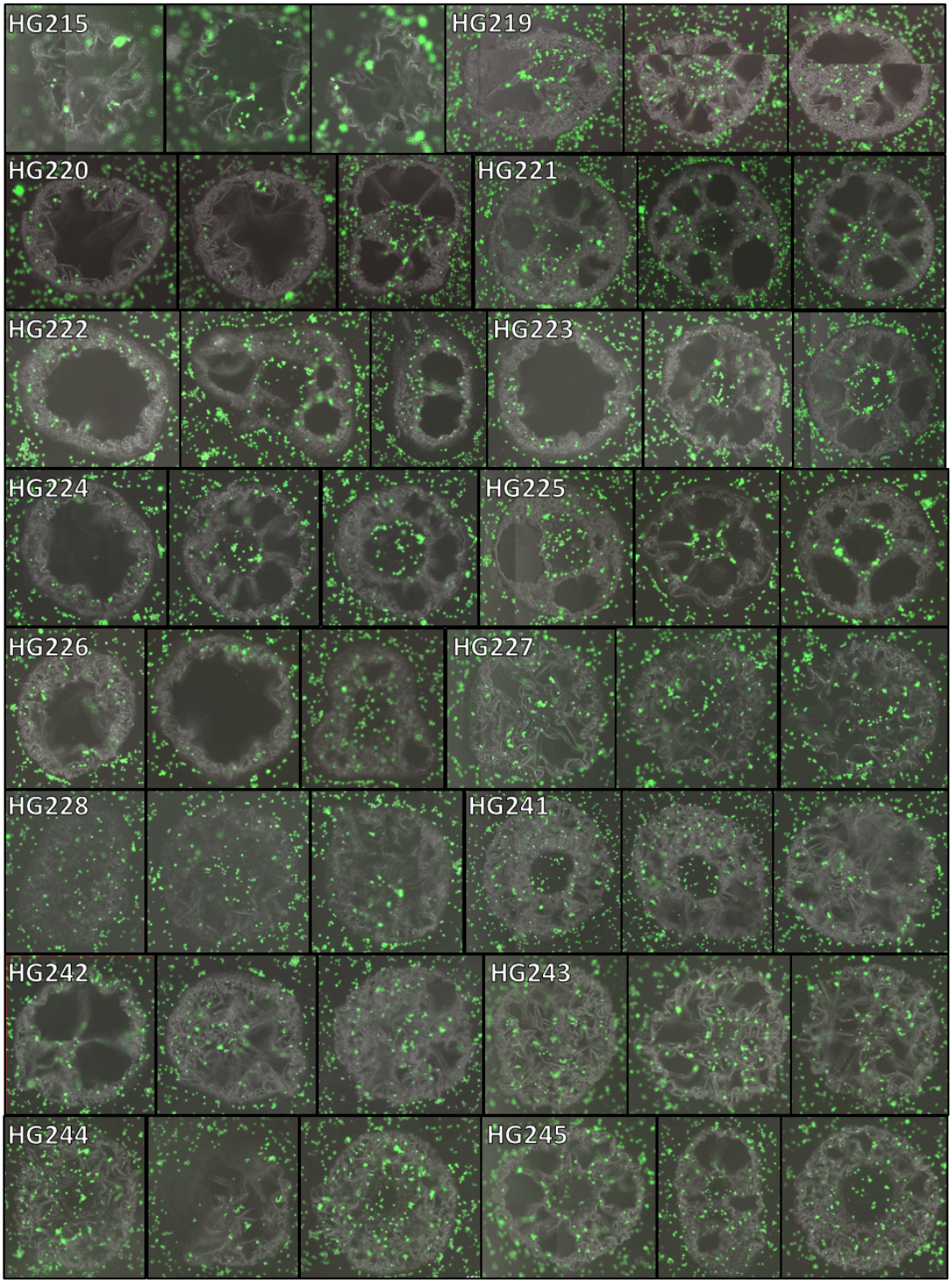
HG215
HG219
HG220
HG221
HG222
HG223
HG224
HG225
HG226
HG227
HG228
HG241
HG242
HG243
HG244
HG245

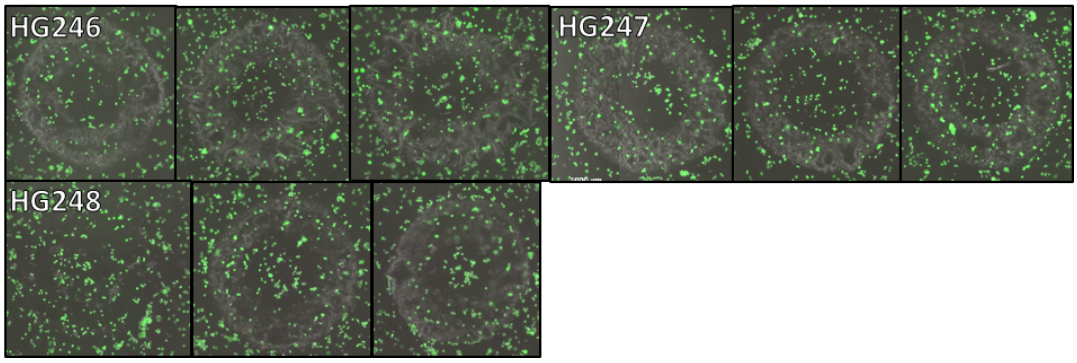
HG246
HG247
HG248

Figure A1.2: 82-member HG "hit array" screen with HUVEC. HUVEC were incubated on the array for 18 h followed by viability staining with fluorescein diacetate (FDA) (green, live stain, ($\lambda_{ex/em}$ = 490/514 nm) and propidium iodide (PI) (red, dead stain, $\lambda_{ex/em}$ = 570/602 nm). The merged images of the FDA, PI and BF channels for each replicate are shown. Images are not shown of combinations where features lifted from the slide. BF = bright field.

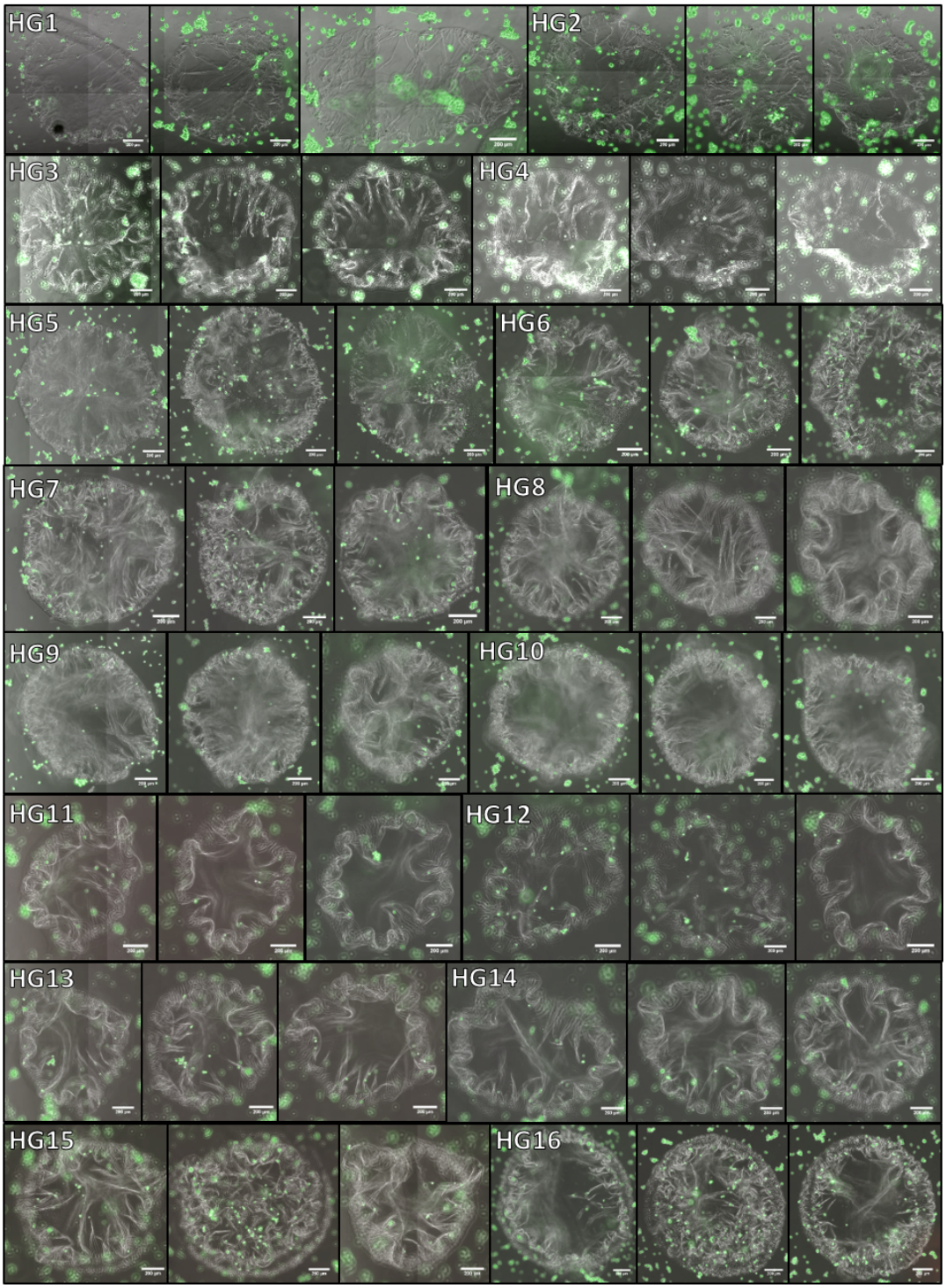

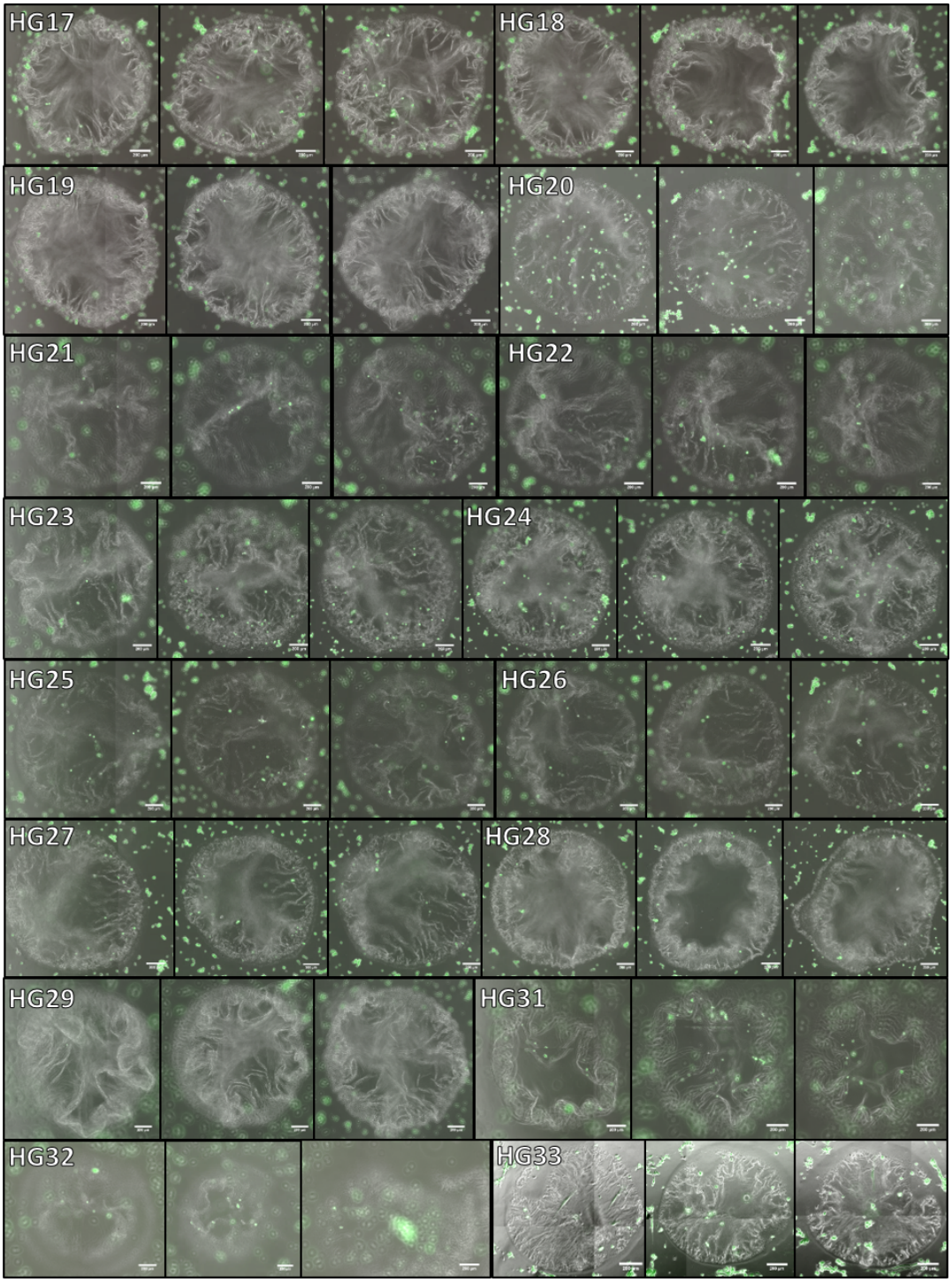
HG17
HG18
HG19
HG20
HG21
HG22
HG23
HG24
HG25
HG26
HG27
HG28
HG29
HG31
HG32
HG33

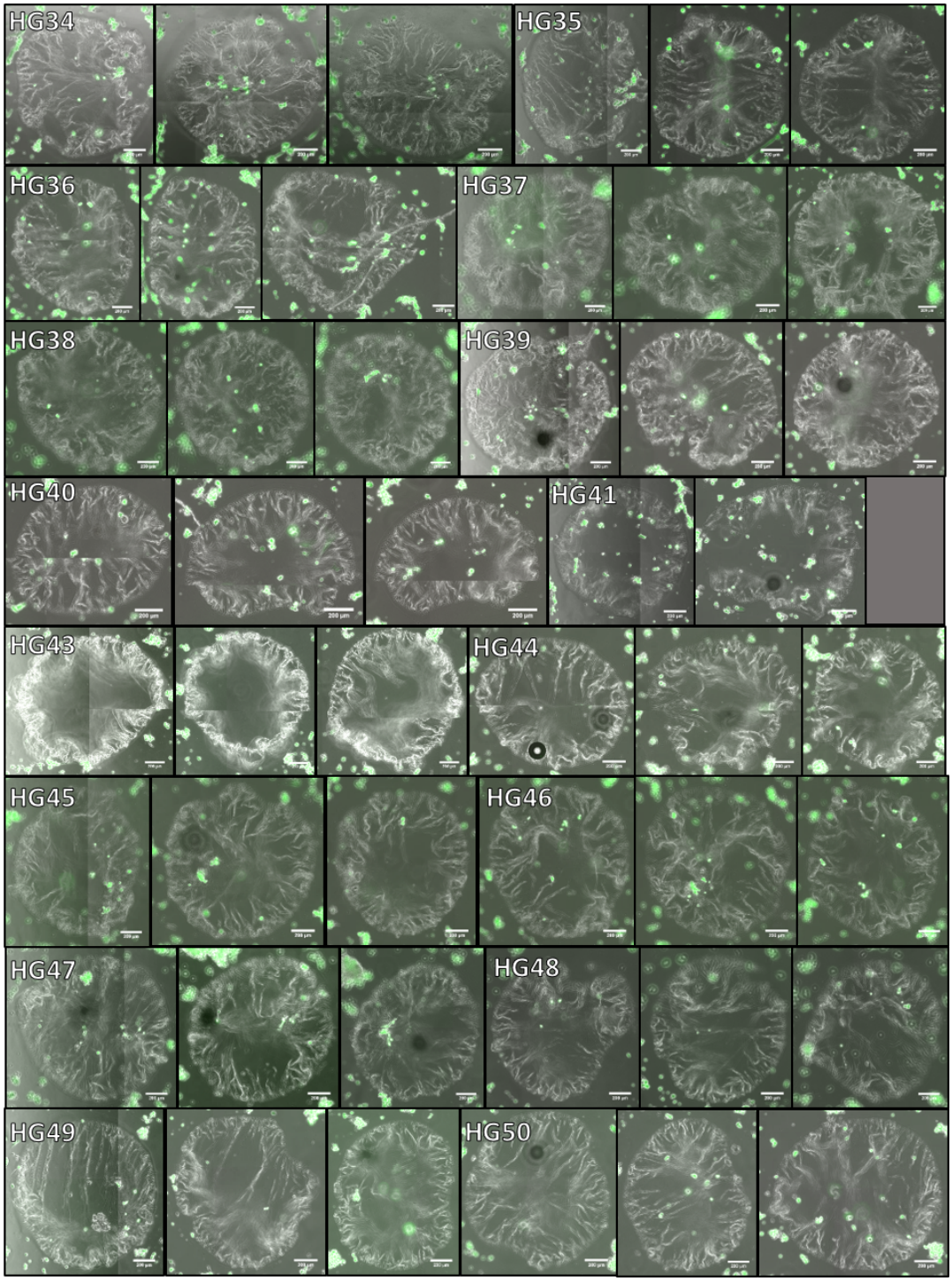
HG34
HG35
HG36
HG37
HG38
HG39
HG40
HG41
HG43
HG44
HG45
HG46
HG47
HG48
HG49
HG50

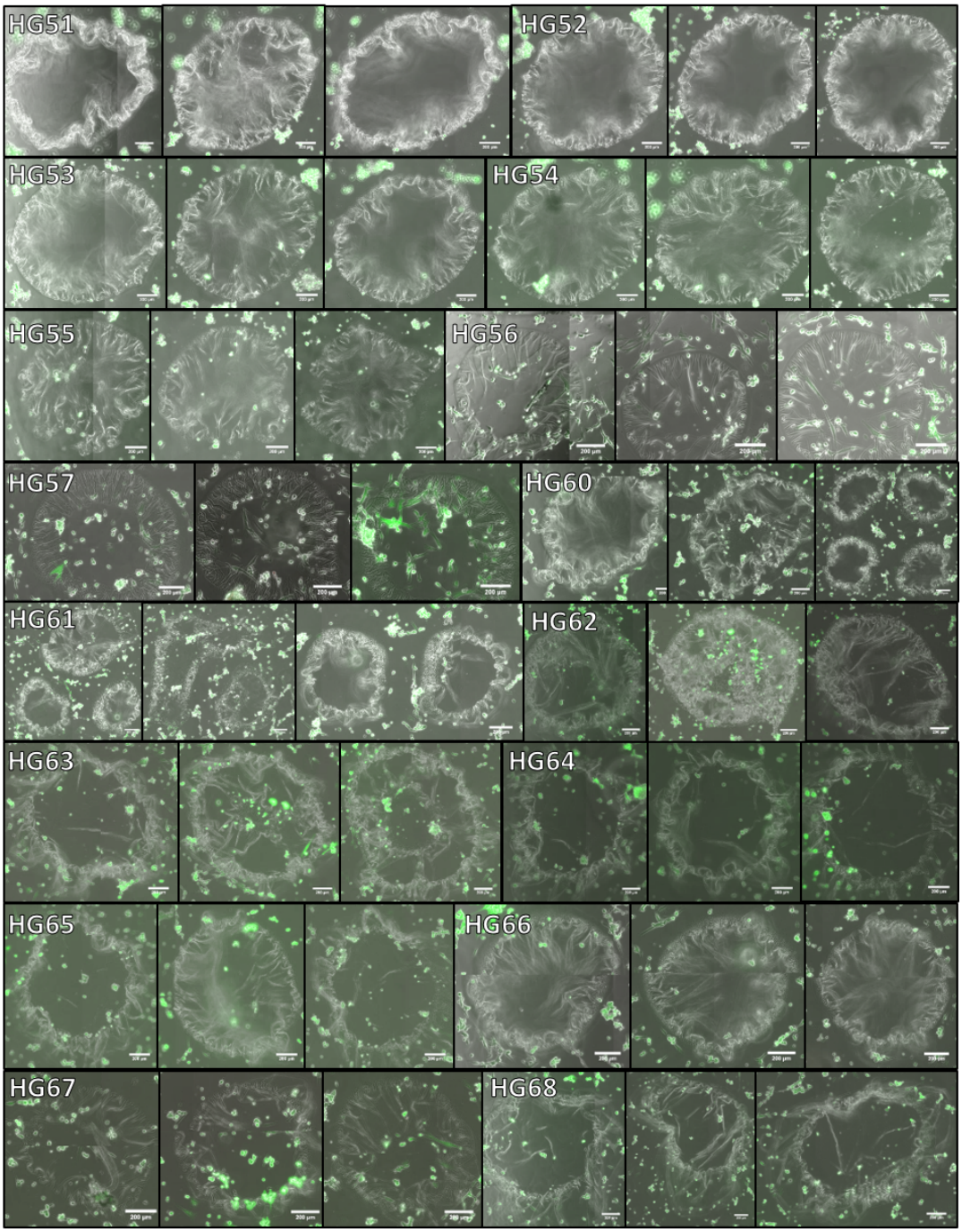
HG51
HG52
HG53
HG54
HG55
HG56
HG57
HG60
HG61
HG62
HG63
HG64
HG65
HG66
HG67
HG68

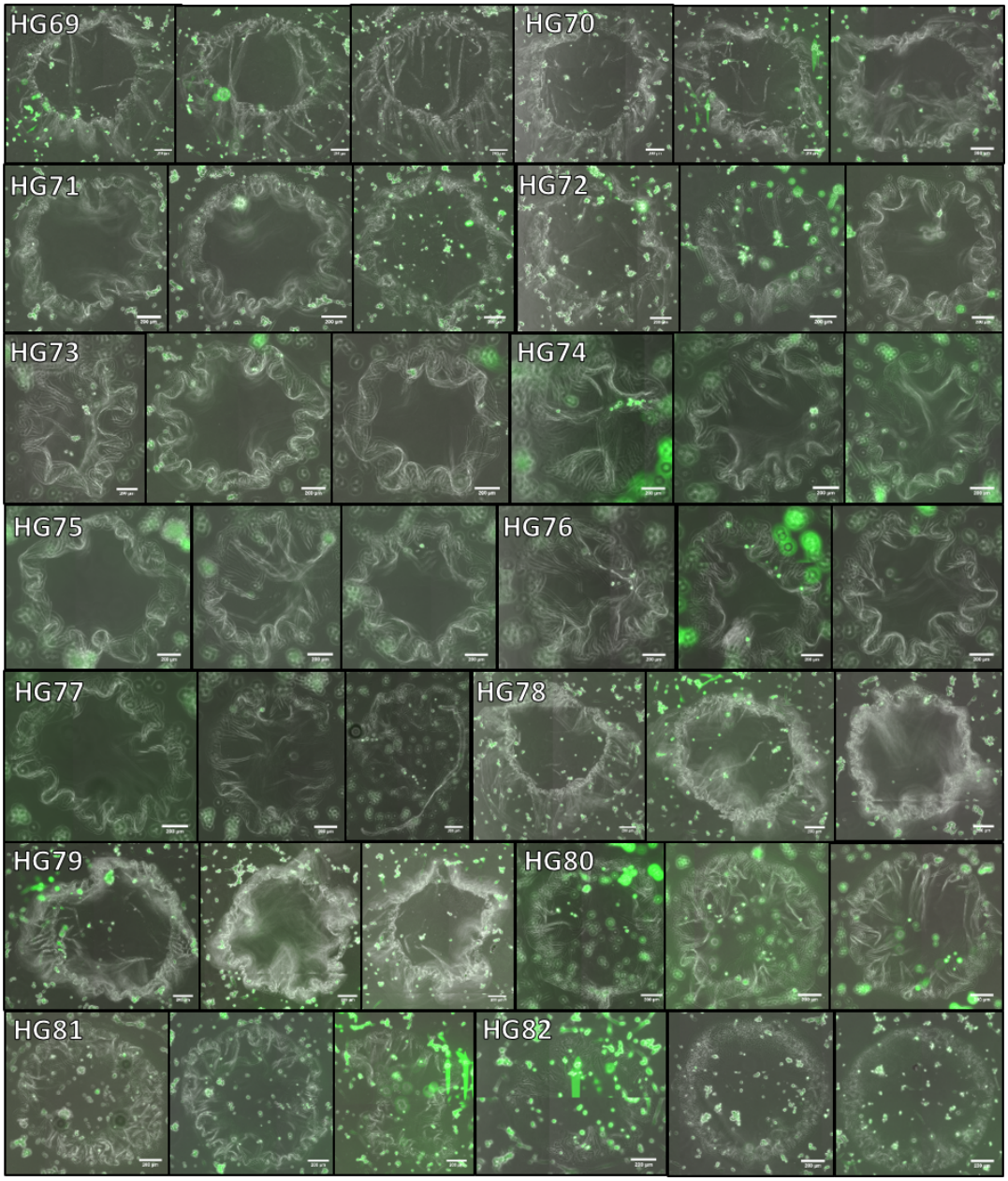
HG69
HG70
HG71
HG72
HG73
HG74
HG75
HG76
HG77
HG78
HG79
HG80
HG81
HG82

Figure A1.3: Analysis of cell encapsulation from an array screen of 250 hydrogels with HeLa cells**. A.** HG1-125. **B.** HG126-250. Cells/mm^3 (± s.e.m, n=3) for each hydrogel feature is given on the left y-axis. On the right y-axis is the morphology grade (0-5, with 5 being the "best morphology"). Gaps with y=0 indicate features where there was no hydrogel formation and/or cell attachment observed. See Table A1.1 for hydrogel compositions.

A

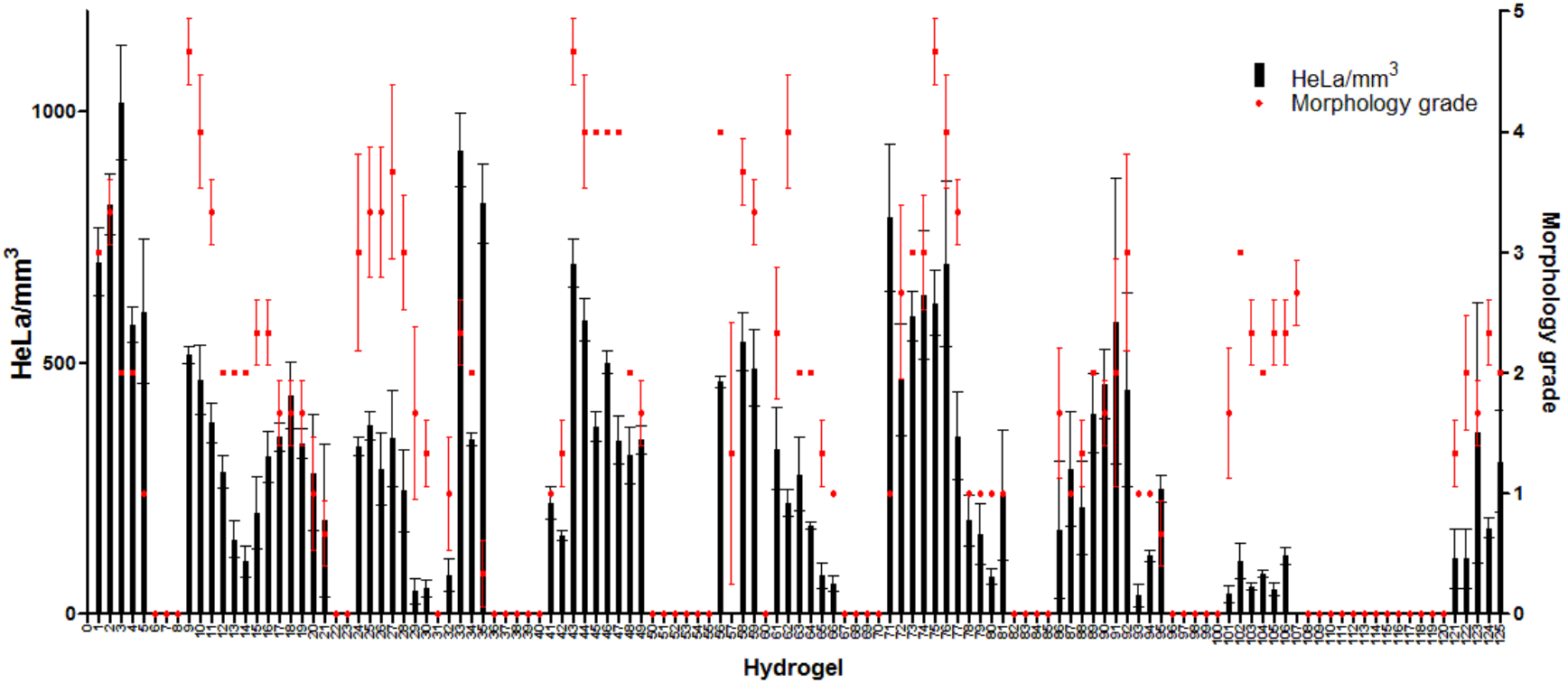

B

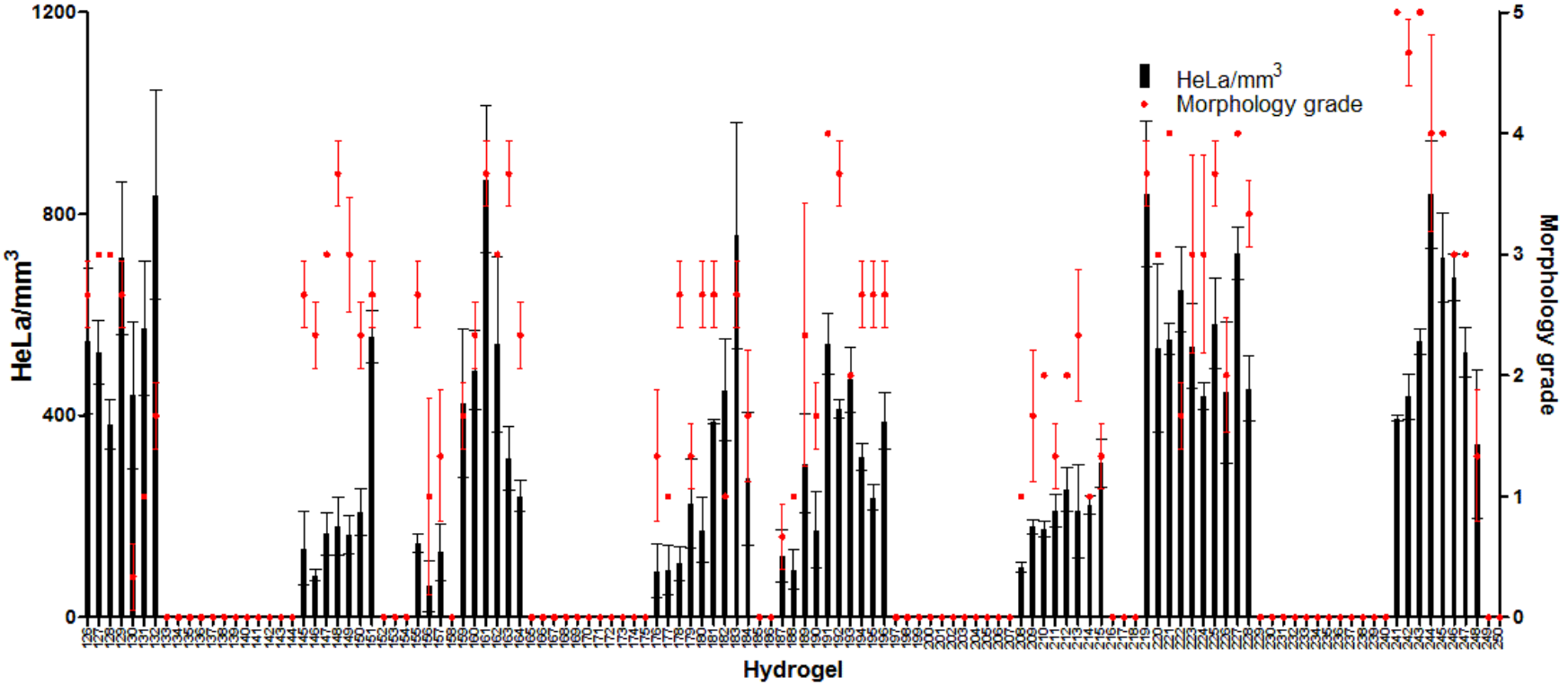
HeLa/mm3
Morphology grade
HeLa/mm3
Morphology grade
Hydrogel
0
400
800
1200
0
1
2
3
4
5

Figure A1.4: Analysis of cell encapsulation from the focused array screen of 82 hydrogels with HUVEC. Cells/mm^3 (± s.e.m, n=3) for each hydrogel feature is given on the left y-axis. On the right y-axis is the morphology grade (0-5, with 5 being the "best morphology"). Gaps with y=0 indicate features where there was no hydrogel formation and/or cell attachment observed. See Table A1.2 for hydrogel compositions.

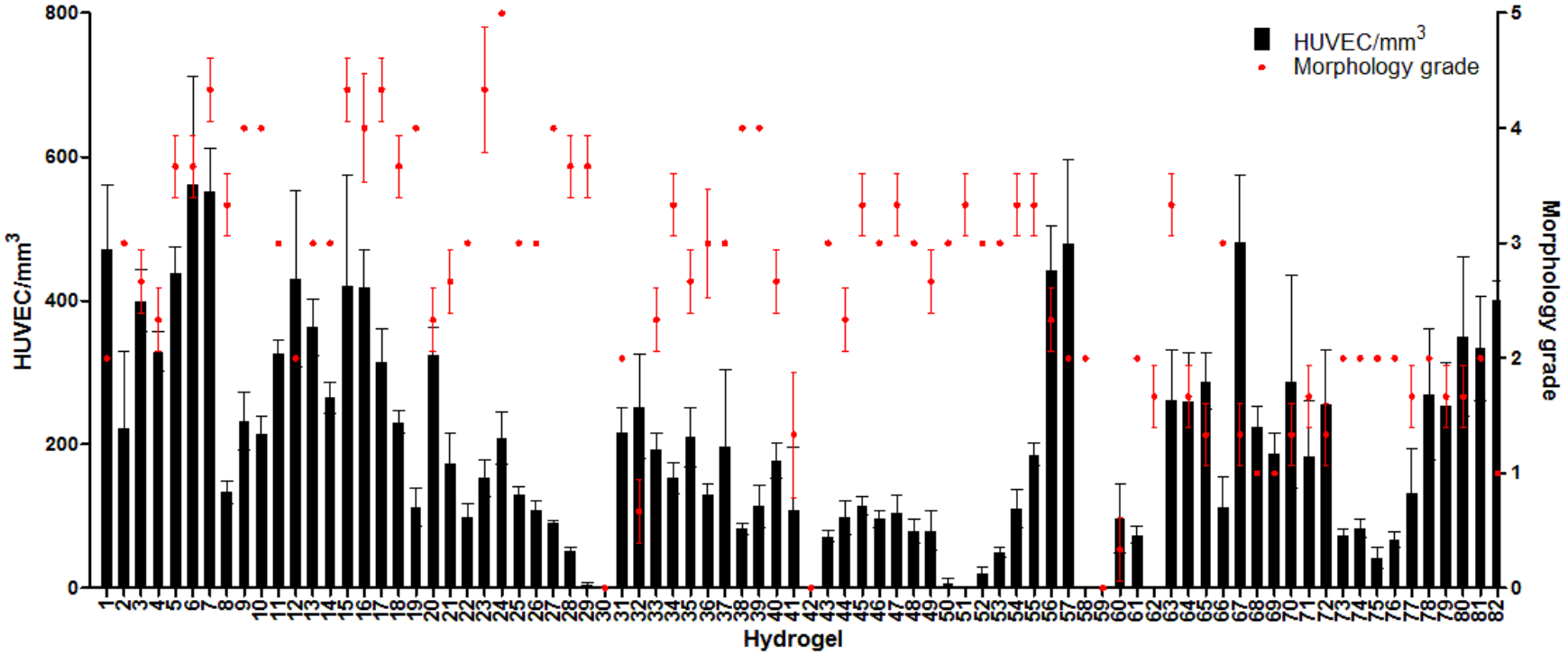

Table A1.1: Hydrogel compositions for the 250-member array. The number of drops printed per hydrogel feature is given for each component. All components were printed as solutions in water (2.5 %), ~ 300 pL/drop.

Hydrogel	RGD	LamIII	PEG_{2000}-CL	PEG_{3000}-CL	$(PEG\text{-}NH_2)_4$
1	800	0	800	0	0
2	900	0	700	0	0
3	1000	0	600	0	0
4	1100	0	500	0	0
5	1200	0	400	0	0
6	1300	0	300	0	0
7	1400	0	200	0	0
8	1500	0	100	0	0
9	700	0	900	0	0
10	600	0	1000	0	0
11	500	0	1100	0	0
12	400	0	1200	0	0
13	300	0	1300	0	0
14	200	0	1400	0	0
15	100	0	1500	0	0
16	800	0	800	0	200
17	900	0	700	0	200
18	1000	0	600	0	200
19	1100	0	500	0	200
20	1200	0	400	0	200
21	1300	0	300	0	200
22	1400	0	200	0	200
23	1500	0	100	0	200
24	700	0	900	0	200
25	600	0	1000	0	200
26	500	0	1100	0	200
27	400	0	1200	0	200
28	300	0	1300	0	200
29	200	0	1400	0	200
30	100	0	1500	0	200
31	1600	0	0	0	0
32	0	0	1600	0	0
33	800	0	0	800	0
34	900	0	0	700	0
35	1000	0	0	600	0
36	1100	0	0	500	0
37	1200	0	0	400	0

38	1300	0	0	300	0
39	1400	0	0	200	0
40	1500	0	0	100	0
41	700	0	0	900	0
42	600	0	0	1000	0
43	500	0	0	1100	0
44	400	0	0	1200	0
45	300	0	0	1300	0
46	200	0	0	1400	0
47	100	0	0	1500	0
48	800	0	0	800	200
49	900	0	0	700	200
50	1000	0	0	600	200
51	1100	0	0	500	200
52	1200	0	0	400	200
53	1300	0	0	300	200
54	1400	0	0	200	200
55	1500	0	0	100	200
56	700	0	0	900	200
57	600	0	0	1000	200
58	500	0	0	1100	200
59	400	0	0	1200	200
60	300	0	0	1300	200
61	200	0	0	1400	200
62	100	0	0	1500	200
63	0	800	800	0	0
64	0	900	700	0	0
65	0	1000	600	0	0
66	0	1100	500	0	0
67	0	1200	400	0	0
68	0	1300	300	0	0
69	0	1400	200	0	0
70	0	1500	100	0	0
71	0	700	900	0	0
72	0	600	1000	0	0
73	0	500	1100	0	0
74	0	400	1200	0	0
75	0	300	1300	0	0
76	0	200	1400	0	0
77	0	100	1500	0	0
78	0	800	800	0	200
79	0	900	700	0	200

80	0	1000	600	0	200
81	0	1100	500	0	200
82	0	1200	400	0	200
83	0	1300	300	0	200
84	0	1400	200	0	200
85	0	1500	100	0	200
86	0	700	900	0	200
87	0	600	1000	0	200
88	0	500	1100	0	200
89	0	400	1200	0	200
90	0	300	1300	0	200
91	0	200	1400	0	200
92	0	100	1500	0	200
93	0	800	0	800	0
94	0	900	0	700	0
95	0	1000	0	600	0
96	0	1100	0	500	0
97	0	1200	0	400	0
98	0	1300	0	300	0
99	0	1400	0	200	0
100	0	1500	0	100	0
101	0	700	0	900	0
102	0	600	0	1000	0
103	0	500	0	1100	0
104	0	400	0	1200	0
105	0	300	0	1300	0
106	0	200	0	1400	0
107	0	100	0	1500	0
108	0	800	0	800	200
109	0	900	0	700	200
110	0	1000	0	600	200
111	0	1100	0	500	200
112	0	1200	0	400	200
113	0	1300	0	300	200
114	0	1400	0	200	200
115	0	1500	0	100	200
116	0	700	0	900	200
117	0	600	0	1000	200
118	0	500	0	1100	200
119	0	400	0	1200	200
120	0	300	0	1300	200
121	0	200	0	1400	200

122	0	100	0	1500	200
123	200	200	1200	0	0
124	300	100	1200	0	0
125	100	300	1200	0	0
126	400	400	800	0	0
127	500	300	800	0	0
128	600	200	800	0	0
129	700	100	800	0	0
130	300	500	800	0	0
131	200	600	800	0	0
132	100	700	800	0	0
133	600	600	400	0	0
134	700	500	400	0	0
135	800	400	400	0	0
136	900	300	400	0	0
137	1000	200	400	0	0
138	1100	100	400	0	0
139	500	700	400	0	0
140	400	800	400	0	0
141	300	900	400	0	0
142	200	1000	400	0	0
143	100	1100	400	0	0
144	48	52	1500	0	0
145	100	100	1400	0	0
146	148	152	1300	0	0
147	248	252	1100	0	0
148	300	300	1000	0	0
149	344	348	900	0	0
150	448	452	700	0	0
151	500	500	600	0	0
152	548	552	500	0	0
153	648	652	300	0	0
154	700	700	200	0	0
155	200	200	0	1200	0
156	300	100	0	1200	0
157	100	300	0	1200	0
158	400	400	0	800	0
159	500	300	0	800	0
160	600	200	0	800	0
161	700	100	0	800	0
162	300	500	0	800	0
163	200	600	0	800	0

164	100	700	0	800	0
165	600	600	0	400	0
166	700	500	0	400	0
167	800	400	0	400	0
168	900	300	0	400	0
169	1000	200	0	400	0
170	1100	100	0	400	0
171	500	700	0	400	0
172	400	800	0	400	0
173	300	900	0	400	0
174	200	1000	0	400	0
175	100	1100	0	400	0
176	48	52	0	1500	0
177	100	100	0	1400	0
178	148	152	0	1300	0
179	248	252	0	1100	0
180	300	300	0	1000	0
181	344	348	0	900	0
182	448	452	0	700	0
183	500	500	0	600	0
184	548	552	0	500	0
185	648	652	0	300	0
186	700	700	0	200	0
187	200	200	1200	0	200
188	300	100	1200	0	200
189	100	300	1200	0	200
190	400	400	800	0	200
191	500	300	800	0	200
192	600	200	800	0	200
193	700	100	800	0	200
194	300	500	800	0	200
195	200	600	800	0	200
196	100	700	800	0	200
197	600	600	400	0	200
198	700	500	400	0	200
199	800	400	400	0	200
200	900	300	400	0	200
201	1000	200	400	0	200
202	1100	100	400	0	200
203	500	700	400	0	200
204	400	800	400	0	200
205	300	900	400	0	200

206	200	1000	400	0	200
207	100	1100	400	0	200
208	48	52	1500	0	200
209	100	100	1400	0	200
210	148	152	1300	0	200
211	248	252	1100	0	200
212	300	300	1000	0	200
213	344	348	900	0	200
214	448	452	700	0	200
215	500	500	600	0	200
216	548	552	500	0	200
217	648	652	300	0	200
218	700	700	200	0	200
219	200	200	0	1200	200
220	300	100	0	1200	200
221	100	300	0	1200	200
222	400	400	0	800	200
223	500	300	0	800	200
224	600	200	0	800	200
225	700	100	0	800	200
226	300	500	0	800	200
227	200	600	0	800	200
228	100	700	0	800	200
229	600	600	0	400	200
230	700	500	0	400	200
231	800	400	0	400	200
232	900	300	0	400	200
233	1000	200	0	400	200
234	1100	100	0	400	200
235	500	700	0	400	200
236	400	800	0	400	200
237	300	900	0	400	200
238	200	1000	0	400	200
239	100	1100	0	400	200
240	48	52	0	1500	200
241	100	100	0	1400	200
242	148	152	0	1300	200
243	248	252	0	1100	200
244	300	300	0	1000	200
245	344	348	0	900	200
246	448	452	0	700	200
247	500	500	0	600	200

248	548	552	0	500	200
249	648	652	0	300	200
250	700	700	0	200	200

Table A1.2: Hydrogel compositions for the 'hit array' screen of HUVEC. The number of drops printed per hydrogel feature is given for each component. All components were printed as solutions in water (2.5 %), ~ 300 pL/drop.

Hydrogel	RGD	LamIII	PEG_{2000}-CL	PEG_{3000}-CL	$(PEG\text{-}NH_2)_4$
1	700	0	900	0	200
2	600	0	1000	0	200
3	500	0	1100	0	200
4	400	0	1200	0	200
5	300	0	1300	0	200
6	500	0	0	1100	0
7	400	0	0	1200	0
8	300	0	0	1300	0
9	200	0	0	1400	0
10	100	0	0	1500	0
11	800	0	0	800	200
12	900	0	0	700	200
13	700	0	0	900	200
14	600	0	0	1000	200
15	500	0	0	1100	200
16	400	0	0	1200	200
17	300	0	0	1300	200
18	200	0	0	1400	200
19	100	0	0	1500	200
20	0	500	1100	0	0
21	0	400	1200	0	0
22	0	300	1300	0	0
23	0	200	1400	0	0
24	0	100	1500	0	0
25	0	400	1200	0	200
26	0	300	1300	0	200
27	0	200	1400	0	200
28	0	200	0	1400	200
29	0	100	0	1500	200

30	1100	0	500	0	0
31	200	0	0	1400	0
32	0	600	0	1000	200
33	400	400	800	0	0
34	500	300	800	0	0
35	600	200	800	0	0
36	700	100	800	0	0
37	248	252	1100	0	0
38	300	300	1000	0	0
39	344	348	900	0	0
40	448	452	700	0	0
41	500	500	600	0	0
42	100	300	1200	0	200
43	400	400	800	0	200
44	500	300	800	0	200
45	600	200	800	0	200
46	700	100	800	0	200
47	300	500	800	0	200
48	200	600	800	0	200
49	100	700	800	0	200
50	148	152	1300	0	200
51	248	252	1100	0	200
52	300	300	1000	0	200
53	344	348	900	0	200
54	448	452	700	0	200
55	500	500	600	0	200
56	500	300	0	800	0
57	600	200	0	800	0
58	700	100	0	800	0
59	300	500	0	800	0
60	200	600	0	800	0
61	100	700	0	800	0
62	148	152	0	1300	0
63	248	252	0	1100	0
64	300	300	0	1000	0

65	344	348	0	900	0
66	448	452	0	700	0
67	500	500	0	600	0
68	200	200	1200	0	200
69	300	100	1200	0	200
70	100	300	1200	0	200
71	400	400	800	0	200
72	500	300	800	0	200
73	600	200	800	0	200
74	700	100	800	0	200
75	300	500	800	0	200
76	200	600	800	0	200
77	100	700	800	0	200
78	100	100	1400	0	200
79	148	152	1300	0	200
80	248	252	1100	0	200
81	300	300	1000	0	200
82	344	348	900	0	200

A.2 Appendix for Chapter 3

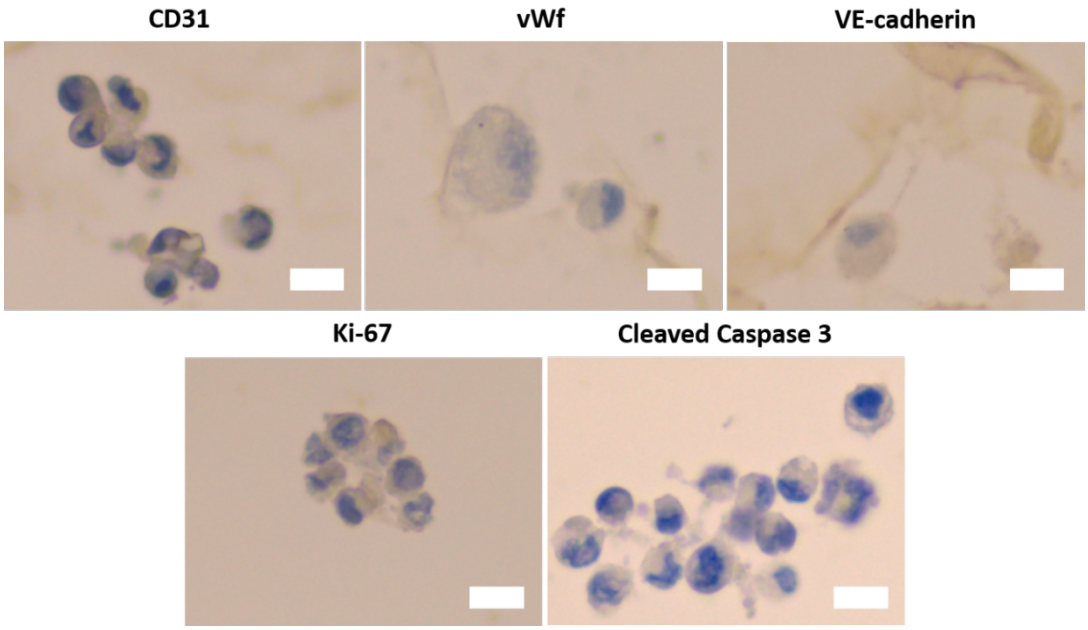

Figure A2.1: Negative controls for immunohistological analysis of endothelial (CD31, VE-cadherin, vWf), proliferation (Ki-67) and apoptosis (cleaved caspase 3) markers in HUVEC and after incubation in HG15 (4 or 30 days). Following cell incubation for the desired time point and cell fixation, the gels were embedded in agarose, paraffin-embedded, cut into slices, permeabilised and stained with secondary antibody only (no primary antibody) and haematoxylin. Visualisation was done with 3,3-diaminobenzidine (DAB). Scale bar 20 µm.

A.3 Appendix for Chapter 5

PU16	PU61	PU100	PU24	PU89	PU12	PU63	PU1
PU207	PU152	PU192	PU141	PU183	PU95	PU168	PU123
PA403	PU245	PA414	PU215	PU190	PU219	PU77	PU227
PA128	PA485	PA324	PA468	PA519	PA450	PA509	PA462
PA400	PA197	PA412	PA196	PA159	PA175	PA177	PA120
PA119	PA26	PA139	PA112	PA40	PA134	PA50	PA208
PU17	PU41	PU101	PU25	PU69	PU13	PU67	PU2
PU217	PU234	PU172	PU142	PU184	PU132	PU171	PU124
PA423	PU275	PA415	PU271	PA427	PU202	PU214	PU216
PA359	PA493	PA325	PA469	PA520	PA452	PA511	PA449
PA399	PA193	PA398	PA188	PA160	PA172	PA372	PA164
PA27	PA18	PA59	PA132	PA185	PA329	PA3	PA387
PU29	PU46	PU102	PU28	PU92	PU14	PU73	PU3
PA210	PU153	PU105	PU143	PU185	PU134	PU173	PU115
PA426	PU254	PA416	PU256	PU259	PU250	PU178	PU162
PA141	PA496	PA326	PA470	PA522	PA453	PA513	PA475
PA406	PA214	PA413	PA189	PA361	PA180	PA369	PA135
PA11	PA46	PA102	PA198	PA37	PA335	PA25	PA389
PU79	PU48	PU103	PU120	PU93	PU18	PU77	PU4
PU188	PU154	PU196	PU144	PU163	PU135	PU174	PU126
PA428	PU224	PA417	PU253	PU221	PU241	PU204	PU228
PA142	PA497	PA327	PA474	PA523	PA458	PA512	PA499
PA401	PA215	PA222	PA190	PA358	PA181	PA155	PA137
PA43	PA106	PA131	PA210	PA17	PA186	PA58	PA223
PU71	PU99	PU104	PU33	PU94	PU19	PU81	PU5
PU122	PU156	PU197	PU145	PU187	PU137	PU175	PU128
PA429	PU212	PA418	PU244	PU264	PU208	PU203	PU218
PA143	PA500	PA323	PA437	PA531	PA459	PA514	PA442
PA411	PA216	PA207	PA199	PA363	PA182	PA154	PA307
PA55	PA14	PA138	PA179	PA13	PA204	PA105	PA375
PU116	PU69	PU108	PU35	PU96	PU20	PU83	PU7
PU257	PU159	PU199	PU148	PU161	PU138	EMPTY	PU129
PA430	PU246	PA419	PU233	PA435	PU242	PU25	PU205
PA162	PA504	PA330	PA476	PA528	PA460	PA515	PA442
PA397	PA178	PA390	PA357	PA336	PA183	PA364	PA306
PA100	PA21	PA117	PA113	PA12	PA316	PA20	PA191
PU117	PU53	PU110	PU27	PU97	PU22	PU85	PU8
PU247	PU164	PU121	PU149	PU189	PU139	PU179	PU130
PA431	PU235	PA420	PU223	PU205	PU220	PU278	PU239
PA163	PA507	PA331	PA477	PA434	PA465	PA517	PA444
PA393	PA194	PA395	PA201	PA337	PA184	PA167	PA309
EMPTY	PA60	PA44	PA19	PA22	PA315	PA56	PA136
PU118	PU119	PU112	PU39	PU98	PU23	PU87	PU10
PU236	PU166	PU201	PU151	PU191	PU140	PU181	PU131
PA432	PU225	PA421	PU230	PU269	PU222	PU226	PU229
PA153	PA508	PA332	PA481	PA360	PA467	PA518	PA446
PA394	PA192	PA396	PA187	PA338	PA185	PA168	PA171
PA140	PA218	PA56	PA104	PA23	PA318	PA57	PA133

Figure A3.1: Lay-out of polymer microarray as printed.

Table A3.1: Compositions of polyacrylate/acrylamides used for microarray screening with CSC. For monomer abbreviations, see list at end of Appendix.

	M1	M2	M3	M1 ratio (mol %)	M2 ratio (mol %)	M3 ratio (mol %)
PA3	St	DEAA	-	90	10	-
PA11	MMA	DEAA	-	70	30	-
PA12	MMA	DEAA	-	50	50	-
PA13	MMA	DMAA	-	90	90	-
PA14	MMA	DMAA	-	70	30	-
PA17	MMA	PAA	-	70	30	-
PA18	MMA	PAA	-	50	50	-
PA19	MEMA	DEAA	-	90	10	-
PA20	MEMA	DEAA	-	70	30	-
PA21	MEMA	DEAA	-	50	50	-
PA22	MEMA	DMAA	-	90	10	-
PA23	MEMA	DMAA	-	70	30	-
PA25	MEMA	PAA	-	90	10	-
PA26	MEMA	PAA	-	70	30	-
PA27	MEMA	PAA	-	50	50	-
PA40	HEMA	DMAA	-	90	10	-
PA43	HEMA	PAA	-	90	10	-
PA44	HEMA	PAA	-	70	30	-
PA46	HPMA	DEAA	-	90	10	-
PA50	HPMA	DMAA	-	70	30	-
PA55	HBMA	DEAA	-	90	10	-
PA56	HBMA	DEAA	-	70	30	-
PA57	HBMA	DEAA	-	50	50	-
PA58	HBMA	DMAA	-	90	10	-
PA59	HBMA	DMAA	-	70	30	-
PA60	HBMA	DMAA	-	50	50	-
PA100	MEMA	DMAEMA	-	70	30	-
PA102	MEMA	DEAEA	-	90	10	-
PA104	MEMA	DEAEA	-	50	50	-
PA105	MEMA	DMAEA	-	90	10	-
PA106	MEMA	DMAEA	-	70	30	-
PA112	MEMA	BAEMA	-	70	30	-
PA113	MEMA	BAEMA	-	50	50	-
PA117	MEMA	BACOEA	-	90	10	-
PA119	MEMA	BACOEA	-	50	50	-
PA120	MEMA	DMVBA	-	90	10	-
PA128	MEMA	VI	-	50	50	-
PA131	MEMA	VPNO	-	50	50	-
PA132	MEMA	VP-4	-	90	10	-

PA133	MEMA	VP-4	-	70	30	-
PA134	MEMA	VP-4	-	50	50	-
PA135	MEMA	VP-2	-	90	10	-
PA136	MEMA	VP-2	-	70	30	-
PA137	MEMA	VP-2	-	50	50	-
PA138	MEMA	DAAA	-	90	10	-
PA139	MEMA	DAAA	-	70	30	-
PA140	MEMA	DAAA	-	50	50	-
PA141	MEMA	MNPMA	-	90	10	-
PA142	MEMA	MNPMA	-	70	30	-
PA143	MEMA	MNPMA	-	50	50	-
PA153	HEMA	DMAEMA	-	90	10	-
PA154	HEMA	DMAEMA	-	70	30	-
PA155	HEMA	DMAEMA	-	50	50	-
PA159	HEMA	DMAEA	-	90	10	-
PA160	HEMA	DMAEA	-	70	30	-
PA162	HEMA	MTEMA	-	90	10	-
PA163	HEMA	MTEMA	-	70	30	-
PA164	HEMA	MTEMA	-	50	50	-
PA167	HEMA	BAEMA	-	50	50	-
PA168	HEMA	DMAPMAA	-	90	10	-
PA171	HEMA	BACOEA	-	90	10	-
PA172	HEMA	BACOEA	-	70	30	-
PA175	HEMA	DMVBA	-	70	30	-
PA177	HEMA	VAA	-	90	10	-
PA178	HEMA	VAA	-	70	30	-
PA179	HEMA	VAA	-	50	50	-
PA180	HEMA	VI	-	90	10	-
PA181	HEMA	VI	-	70	30	-
PA182	HEMA	VI	-	50	50	-
PA183	HEMA	VPNO	-	90	10	-
PA184	HEMA	VPNO	-	70	30	-
PA185	HEMA	VPNO	-	50	50	-
PA186	HEMA	VP-4	-	90	10	-
PA187	HEMA	VP-4	-	70	30	-
PA188	HEMA	VP-4	-	50	50	-
PA189	HEMA	VP-2	-	90	10	-
PA190	HEMA	VP-2	-	70	30	-
PA191	HEMA	VP-2	-	50	50	-
PA192	HEMA	DAAA	-	90	10	-
PA193	HEMA	DAAA	-	70	30	-
PA194	HEMA	DAAA	-	50	50	-
PA196	HEMA	MNPMA	-	70	30	-

PA197	HEMA	MNPMA	-	50	50	-
PA198	MMA	A-H	-	90	10	-
PA199	MMA	A-H	-	70	30	-
PA201	MMA	AES-H	-	90	10	-
PA204	MMA	MA-H	-	90	10	-
PA207	MMA	AAG-H	-	90	10	-
PA208	MMA	AAG-H	-	70	30	-
PA210	MMA	EGMP-H	-	90	10	-
PA214	MEMA	A-H	-	70	30	-
PA215	MEMA	A-H	-	50	50	-
PA216	MEMA	AES-H	-	90	10	-
PA218	MEMA	AES-H	-	50	50	-
PA222	MEMA	AAG-H	-	90	10	-
PA223	MEMA	AAG-H	-	70	30	-
PA245	MEMA	A-H	DEAEA	70	10	20
PA306	MMA	GMA	DnBA	90	10	-
PA307	MMA	GMA	DnBA	70	30	-
PA309	MMA	GMA	DnHA	90	10	-
PA315	MMA	GMA	DBnA	90	10	-
PA316	MMA	GMA	DBnA	70	30	-
PA318	MMA	GMA	MnHA	90	10	-
PA323	MMA	GMA	cHMA	50	50	-
PA324	MMA	GMA	BnMA	90	10	-
PA325	MMA	GMA	BnMA	70	30	-
PA326	MMA	GMA	BnMA	50	50	-
PA327	MMA	GMA	MAEPy	90	10	-
PA329	MMA	GMA	MAEPy	50	50	-
PA330	MMA	GMA	Pyrle	90	10	-
PA331	MMA	GMA	Pyrle	70	30	-
PA332	MMA	GMA	Pyrle	50	50	-
PA335	MMA	GMA	MAPy	50	50	-
PA336	MMA	GMA	MAn	90	10	-
PA337	MMA	GMA	MAn	70	30	-
PA338	MMA	GMA	MAn	50	50	-
PA357	MMA	DMAEMA	-	90	10	-
PA358	MMA	DMAEMA	-	70	30	-
PA359	MMA	DMAEMA	-	50	50	-
PA360	MMA	DEAEA	-	90	10	-
PA361	MMA	DEAEA	-	70	30	-
PA363	MMA	DMAEA	-	90	10	-
PA364	MMA	DMAEA	-	70	30	-
PA369	HPMA	DMAEMA	-	90	10	-
PA372	HPMA	DEAEA	-	90	10	-

PA375	HPMA	DMAEA	-	90	10	-
PA387	HBMA	DMAEA	-	90	10	-
PA389	HBMA	DMAEA	-	50	50	-
PA390	EMA	DEAEMA	-	90	10	-
PA393	EMA	DMAEMA	-	90	10	-
PA394	EMA	DMAEMA	-	70	30	-
PA395	EMA	DMAEMA	-	50	50	-
PA396	EMA	DEAEA	-	90	10	-
PA397	EMA	DEAEA	-	70	30	-
PA398	EMA	DEAEA	-	50	50	-
PA399	EMA	DMAEA	-	90	10	-
PA400	EMA	DMAEA	-	70	30	-
PA401	EMA	DMAEA	-	50	50	-
PA403	BMA	DEAEMA	-	70	30	-
PA406	BMA	DMAEMA	-	70	30	-
PA411	BMA	DMAEA	-	90	10	-
PA412	BMA	DMAEA	-	70	30	-
PA413	BMA	DMAEA	-	50	50	-
PA414	MEMA	DEAEMA	MA	40	30	30
PA415	MEMA	DEAEMA	MA	60	10	30
PA416	MEMA	DEAEMA	MA	60	30	10
PA417	MEMA	DEAEMA	MA	80	10	10
PA418	MEMA	DEAEA	MA	40	30	30
PA419	MEMA	DEAEA	MA	60	10	30
PA420	MEMA	DEAEA	MA	60	30	10
PA421	MEMA	DEAEA	MA	80	10	10
PA423	MEMA	DEAEMA	BMA	60	10	30
PA426	MEMA	DEAEA	BMA	40	30	30
PA427	MEMA	DEAEA	BMA	60	10	30
PA428	MEMA	DEAEA	BMA	60	30	10
PA429	MEMA	DEAEA	BMA	80	10	10
PA430	MEMA	DEAEMA	MEA	40	30	30
PA431	MEMA	DEAEMA	MEA	60	10	30
PA432	MEMA	DEAEMA	MEA	60	30	10
PA434	MEMA	DEAEA	MEA	40	30	30
PA435	MEMA	DEAEA	MEA	60	10	30
PA437	MEMA	DEAEA	MEA	80	10	10
PA442	MEMA	DEAEA	DEGMEMA	40	30	30
PA443	MEMA	DEAEA	DEGMEMA	60	10	30
PA444	MEMA	DEAEA	DEGMEMA	60	30	10
PA446	MEMA	DEAEMA	THFFA	40	30	30
PA449	MEMA	DEAEMA	THFFA	80	10	10
PA450	MEMA	DEAEA	THFFA	40	30	30

PA452	MEMA	DEAEA	THFFA	60	30	10
PA453	MEMA	DEAEA	THFFA	80	10	10
PA458	MEMA	DEAEA	THFFMA	40	30	30
PA459	MEMA	DEAEA	THFFMA	60	10	30
PA460	MEMA	DEAEA	THFFMA	60	30	10
PA462	MEMA	DEAEMA	HEA	40	30	30
PA465	MEMA	DEAEMA	HEA	80	10	10
PA467	MEMA	DEAEA	HEA	60	10	30
PA468	MEMA	DEAEA	HEA	60	30	10
PA469	MEMA	DEAEA	HEA	80	10	10
PA470	MEMA	DEAEMA	HEMA	40	30	30
PA474	MEMA	DEAEA	HEMA	40	30	30
PA475	MEMA	DEAEA	HEMA	60	10	30
PA476	MEMA	DEAEA	HEMA	60	30	10
PA477	MEMA	DEAEA	HEMA	80	10	10
PA481	MEMA	DEAEMA	A-H	80	10	10
PA485	MEMA	DEAEA	A-H	80	10	10
PA493	MEMA	DEAEA	MA-H	80	10	10
PA496	MEMA	DEAEMA	DMAA	60	30	10
PA497	MEMA	DEAEMA	DMAA	80	10	10
PA499	MEMA	DEAEA	DMAA	60	10	30
PA500	MEMA	DEAEA	DMAA	60	30	10
PA504	MEMA	DEAEMA	DAAA	60	30	10
PA507	MEMA	DEAEA	DAAA	60	10	30
PA508	MEMA	DEAEA	DAAA	60	30	10
PA509	MEMA	DEAEA	DAAA	80	10	10
PA511	MEMA	DEAEMA	MMA	60	10	30
PA512	MEMA	DEAEMA	MMA	60	30	10
PA513	MEMA	DEAEMA	MMA	80	10	10
PA514	MEMA	DEAEA	MMA	40	30	30
PA515	MEMA	DEAEA	MMA	60	10	30
PA517	MEMA	DEAEA	MMA	80	10	10
PA518	MEMA	DEAEMA	St	40	30	30
PA519	MEMA	DEAEMA	St	60	10	30
PA520	MEMA	DEAEMA	St	60	30	10
PA522	MEMA	DEAEA	St	40	30	30
PA523	MEMA	DEAEA	St	60	10	30
PA528	MEMA	DEAEMA	-	70	30	-
PA531	MEMA	DEAEMA	-	55	45	-

Table A3.2: Compositions of polyurethanes used for microarray screening with CSCs. For monomer abbreviations, see list at end of Appendix.

	M1 (Diol)	Diol Mn (g/mol)	M2 (Diisocyanide)	M3 (Extender)	M1 ratio (mol %)	M2 ratio (mol %)	M3 ratio (mol %)
PU2	PEG	900	HDI	-	48.5	51.5	-
PU3	PEG	400	HDI	-	48.5	51.5	-
PU4	PPG	2000	HDI	-	48.5	51.5	-
PU5	PTMG	2000	HDI	-	48.5	51.5	-
PU7	PEG	900	BICH	-	48.5	51.5	-
PU8	PEG	400	BICH	-	48.5	51.5	-
PU10	PTMG	2000	BICH	-	48.5	51.5	-
PU12	PEG	900	TDI	-	48.5	51.5	-
PU13	PEG	400	TDI	-	48.5	51.5	-
PU14	PPG	2000	TDI	-	48.5	51.5	-
PU16	PEG	2000	MDI	-	48.5	51.5	-
PU17	PEG	900	MDI	-	48.5	51.5	-
PU18	PEG	400	MDI	-	48.5	51.5	-
PU19	PPG	2000	MDI	-	48.5	51.5	-
PU20	PTMG	2000	MDI	-	48.5	51.5	-
PU22	PEG	900	PDI	-	48.5	51.5	-
PU23	PEG	400	PDI	-	48.5	51.5	-
PU24	PPG	2000	PDI	-	48.5	51.5	-
PU25	PTMG	2000	PDI	-	48.5	51.5	-
PU27	PEG	900	HMDI	-	48.5	51.5	-
PU28	PEG	400	HMDI	-	48.5	51.5	-
PU29	PPG	2000	HMDI	-	48.5	51.5	-
PU33	PEG	900	HDI	BD	0.25	0.52	0.23
PU35	PEG	400	HDI	BD	0.25	0.52	0.23
PU39	PTMG	2000	HDI	BD	0.25	0.52	0.23
PU41	PEG	2000	BICH	BD	0.25	0.52	0.23
PU46	PEG	400	BICH	ED	0.25	0.52	0.23
PU48	PPG	2000	BICH	ED	0.25	0.52	0.23
PU53	PEG	900	TDI	BD	0.25	0.52	0.23
PU61	PEG	2000	MDI	BD	0.25	0.52	0.23
PU63	PEG	900	MDI	BD	0.25	0.52	0.23
PU67	PPG	2000	MDI	BD	0.25	0.52	0.23
PU69	PTMG	2000	MDI	BD	0.25	0.52	0.23
PU71	PEG	2000	PDI	BD	0.25	0.52	0.23
PU73	PEG	900	PDI	BD	0.25	0.52	0.23
PU77	PPG	2000	PDI	BD	0.25	0.52	0.23
PU79	PTMG	2000	PDI	BD	0.25	0.52	0.23
PU81	PEG	2000	HMDI	BD	0.25	0.52	0.23
PU83	PEG	900	HMDI	BD	0.25	0.52	0.23

PU85	PEG	400	HMDI	BD	0.25	0.52	0.23
PU87	PPG	2000	HMDI	BD	0.25	0.52	0.23
PU89	PTMG	2000	HMDI	BD	0.25	0.52	0.23
PU92	PTMG	1000	HDI	BD	0.485	0.515	-
PU93	PTMG	650	BICH	BD	0.485	0.515	-
PU94	PTMG	1000	BICH	BD	0.485	0.515	-
PU95	PTMG	650	MDI	BD	0.485	0.515	-
PU96	PTMG	1000	MDI	BD	0.485	0.515	-
PU97	PHNGAD	1800	BICH	DMAPD	0.25	0.52	0.23
PU98	PHNGAD	1800	BICH	DEAPD	0.25	0.52	0.23
PU99	PTMG	650	HDI	DMAPD	0.25	0.52	0.23
PU100	PTMG	1000	HDI	DMAPD	0.25	0.52	0.23
PU101	PTMG	650	BICH	DMAPD	0.25	0.52	0.23
PU102	PTMG	1000	BICH	DMAPD	0.25	0.52	0.23
PU103	PHNGAD	1800	MDI	DMAPD	0.25	0.52	0.23
PU104	PHNGAD	1800	MDI	DEAPD	0.25	0.52	0.23
PU105	PHNGAD	1800	HDI	DMAPD	0.25	0.52	0.23
PU108	PTMG	1000	HDI	DEAPD	0.25	0.52	0.23
PU110	PTMG	1000	BICH	DEAPD	0.25	0.52	0.23
PU112	PTMG	1000	MDI	DEAPD	0.25	0.52	0.23
PU115	PPG	1000	HDI	BD	0.485	0.515	-
PU116	PPG	425	BICH	BD	0.485	0.515	-
PU117	PPG	1000	BICH	BD	0.485	0.515	-
PU118	PPG	425	MDI	DMAPD	0.25	0.52	0.23
PU119	PPG	1000	MDI	DMAPD	0.25	0.52	0.23
PU120	PPG	425	BICH	DEAPD	0.25	0.52	0.23
PU121	PPG	1000	BICH	DEAPD	0.25	0.52	0.23
PU122	PPG	2000	BICH	DEAPD	0.25	0.52	0.23
PU123	PPG	2000	MDI	DMAPD	0.25	0.52	0.23
PU124	PPG	2000	TDI	DMAPD	0.25	0.52	0.23
PU126	PPG	425	TDI	DMAPD	0.25	0.52	0.23
PU128	PPG	2000	BICH	DMAPD	0.25	0.52	0.23
PU129	PPG	425	BICH	DMAPD	0.25	0.52	0.23
PU130	PTMG	650	TDI	DMAPD	0.25	0.52	0.23
PU131	PTMG	1000	TDI	DMAPD	0.25	0.52	0.23
PU132	PHNGAD	1800	BICH	BD	0.25	0.52	0.23
PU134	PHNGAD	1800	MDI	BD	0.25	0.52	0.23
PU135	PTMG	250	BICH	DMAPD	0.25	0.52	0.23
PU137	PTMG	250	BICH	BD	0.25	0.52	0.23
PU138	PTMG	250	BICH	EG	0.25	0.52	0.23
PU139	PTMG	650	BICH	EG	0.25	0.52	0.23
PU140	PTMG	1000	BICH	EG	0.25	0.52	0.23
PU141	PTMG	2000	BICH	EG	0.25	0.52	0.23

PU142	PTMG	250	BICH	PG	0.25	0.52	0.23
PU143	PTMG	650	BICH	PG	0.25	0.52	0.23
PU144	PTMG	1000	BICH	PG	0.25	0.52	0.23
PU145	PTMG	2000	BICH	PG	0.25	0.52	0.23
PU148	PTMG	250	HDI	BD	0.25	0.52	0.23
PU149	PTMG	250	HDI	EG	0.25	0.52	0.23
PU151	PTMG	1000	HDI	EG	0.25	0.52	0.23
PU152	PTMG	2000	HDI	EG	0.25	0.52	0.23
PU153	PTMG	250	HDI	PG	0.25	0.52	0.23
PU154	PTMG	650	HDI	PG	0.25	0.52	0.23
PU156	PTMG	2000	HDI	PG	0.25	0.52	0.23
PU159	PTMG	250	MDI	BD	0.25	0.52	0.23
PU161	PTMG	650	MDI	EG	0.25	0.52	0.23
PU162	PTMG	1000	MDI	EG	0.25	0.52	0.23
PU163	PTMG	2000	MDI	EG	0.25	0.52	0.23
PU164	PTMG	250	MDI	PG	0.25	0.52	0.23
PU166	PTMG	1000	MDI	PG	0.25	0.52	0.23
PU168	PTMG	250	BICH	-	48.5	51.5	-
PU171	PTMG	250	HDI	-	48.5	51.5	-
PU172	PTMG	650	HDI	-	48.5	51.5	-
PU173	PTMG	1000	HDI	-	48.5	51.5	-
PU174	PTMG	250	MDI	-	48.5	51.5	-
PU175	PTMG	650	MDI	-	48.5	51.5	-
PU178	PTMG	1000	HDI	NMPD	0.25	0.52	0.23
PU179	PTMG	2000	HDI	NMPD	0.25	0.52	0.23
PU181	PTMG	2000	BICH	NMPD	0.25	0.52	0.23
PU183	PTMG	1000	MDI	NMPD	0.25	0.52	0.23
PU184	PTMG	2000	MDI	NMPD	0.25	0.52	0.23
PU185	PHNAD	900	MDI	OFHD	0.17	0.52	0.33
PU187	PTMG	1000	BICH	OFHD	0.25	0.52	0.23
PU188	PTMG	2000	BICH	OFHD	0.25	0.52	0.23
PU189	PPG	1000	BICH	OFHD	0.17	0.52	0.33
PU190	PTMG	650	HDI	OFHD	0.25	0.52	0.23
PU191	PTMG	1000	HDI	OFHD	0.25	0.52	0.23
PU192	PTMG	2000	HDI	OFHD	0.25	0.52	0.23
PU196	PTMG	2000	MDI	OFHD	0.25	0.52	0.23
PU197	PTMG	650	BICH	DHM	0.25	0.52	0.23
PU199	PTMG	2000	BICH	DHM	0.25	0.52	0.23
PU201	PTMG	1000	HDI	DHM	0.25	0.52	0.23
PU202	PTMG	2000	HDI	DHM	0.25	0.52	0.23
PU203	PTMG	650	MDI	DHM	0.25	0.52	0.23
PU204	PTMG	1000	MDI	DHM	0.25	0.52	0.23
PU205	PTMG	2000	MDI	DHM	0.25	0.52	0.23

PU207	PPG	1000	BICH	OFHD	0.25	0.52	0.23
PU208	PPG	1000	MDI	OFHD	0.25	0.52	0.23
PU210	PPG	1000	BICH	PG	0.25	0.52	0.23
PU212	PHNAD	900	HDI	PG	0.25	0.52	0.23
PU214	PHNAD	900	MDI	PG	0.25	0.52	0.23
PU216	PHNAD	900	BICH	BD	0.25	0.52	0.23
PU217	PHNAD	900	MDI	BD	0.25	0.52	0.23
PU218	PHNAD	900	HDI	DMAPD	0.25	0.52	0.23
PU219	PHNAD	900	BICH	DMAPD	0.25	0.52	0.23
PU220	PHNAD	900	MDI	DMAPD	0.25	0.52	0.23
PU221	PHNAD	900	HDI	OFHD	0.25	0.52	0.23
PU222	PHNAD	900	BICH	OFHD	0.25	0.52	0.23
PU223	PHNAD	900	MDI	OFHD	0.25	0.52	0.23
PU224	PHNAD	900	HDI	-	48.5	51.5	-
PU225	PHNAD	900	BICH	-	48.5	51.5	-
PU226	PHNAD	900	MDI	-	48.5	51.5	-
PU227	PPG-PEG	1900	HDI	-	48.5	51.5	-
PU228	PPG-PEG	1900	BICH	-	48.5	51.5	-
PU229	PPG-PEG	1900	MDI	-	48.5	51.5	-
PU230	PPG-PEG	1900	HDI	BD	0.25	0.52	0.23
PU233	PPG-PEG	1900	HDI	OFHD	0.25	0.52	0.23
PU234	PPG-PEG	1900	BICH	OFHD	0.25	0.52	0.23
PU235	PPG-PEG	1900	MDI	OFHD	0.25	0.52	0.23
PU236	PPG-PEG	1900	HDI	PG	0.25	0.52	0.23
PU239	PPG-PEG	1900	HDI	DMAPD	0.25	0.52	0.23
PU241	PPG-PEG	1900	MDI	DMAPD	0.25	0.52	0.23
PU242	PPG-PEG	1900	HDI	EG	0.25	0.52	0.23
PU244	PPG-PEG	1900	MDI	EG	0.25	0.52	0.23
PU246	PHNGAD	1800	BICH	OFHD	0.25	0.52	0.23
PU247	PHNGAD	1800	MDI	OFHD	0.25	0.52	0.23
PU250	PHNGAD	1800	BICH	-	48.5	51.5	-
PU253	PPG-PEG	1900	MDI	DMAPD	0.17	0.52	0.33
PU254	PHNGAD	1800	BICH	BD	0.17	0.52	0.33
PU256	PPG	425	MDI	-	48.5	51.5	-
PU257	PTMG	1000	BICH	DMAPD	0.17	0.52	0.33
PU259	PTMG	2000	BICH	DMAPD	0.17	0.52	0.33
PU264	PTMG	1000	HDI	DMAPD	0.17	0.52	0.33
PU269	PPG	2000	MDI	DEAPD	0.25	0.52	0.23
PU271	PEG	400	MDI	DMAPD	0.25	0.52	0.23
PU275	PEG	400	MDI	-	48.5	51.5	-
PU278	PPG-PEG	1900	MDI	OFHD	0.17	0.52	0.33

A

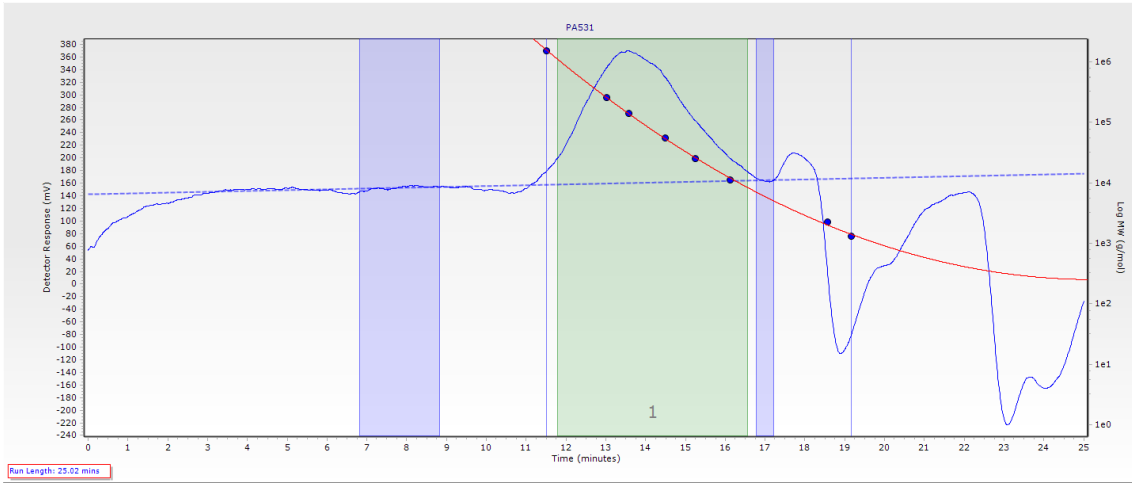
PA531
Detector Response (mV)
Log MW (g/mol)
Time (minutes)
Run Length: 25.02 mins

B

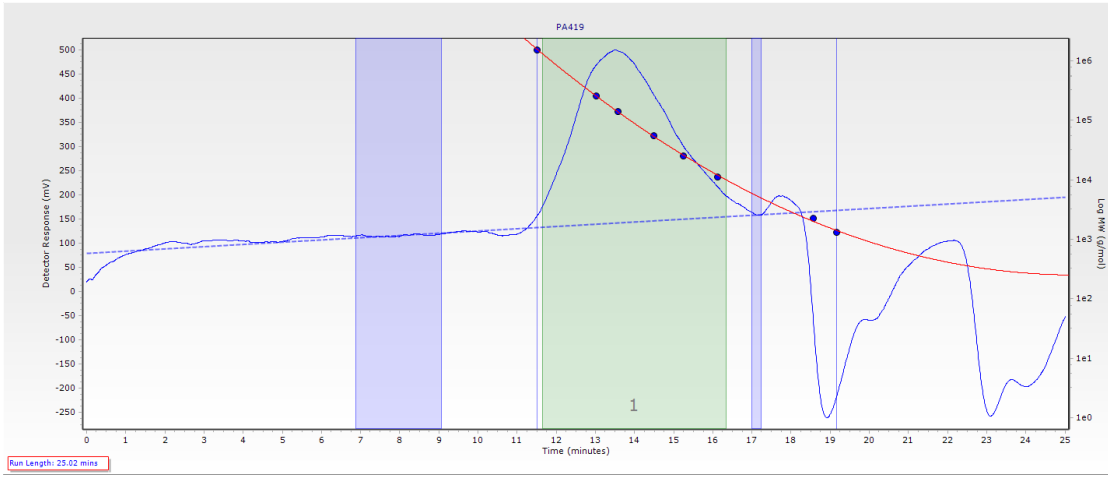
PA419
Detector Response (mV)
Log MW (g/mol)
Time (minutes)
Run Length: 25.02 mins

C

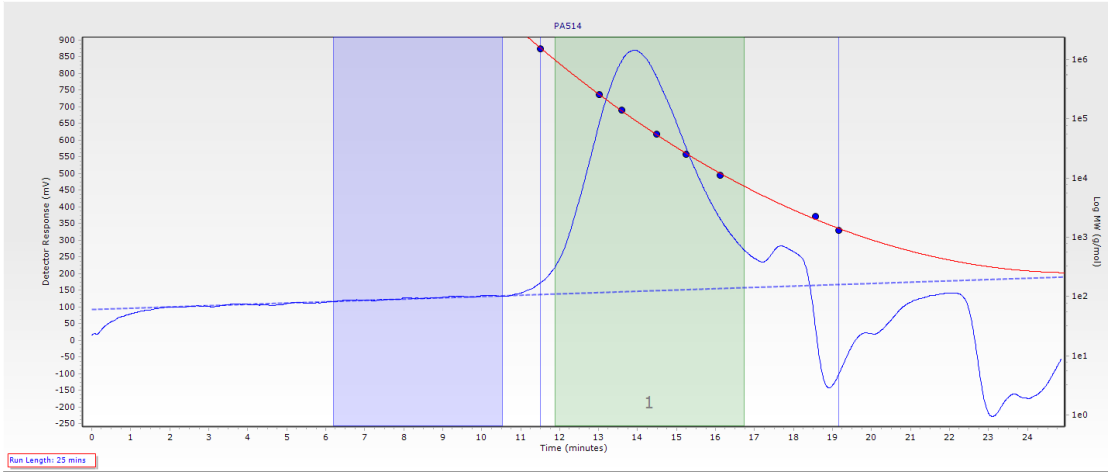
PA514
Detector Response (mV)
Log MW (g/mol)
Time (minutes)
Run Length: 25 mins

D

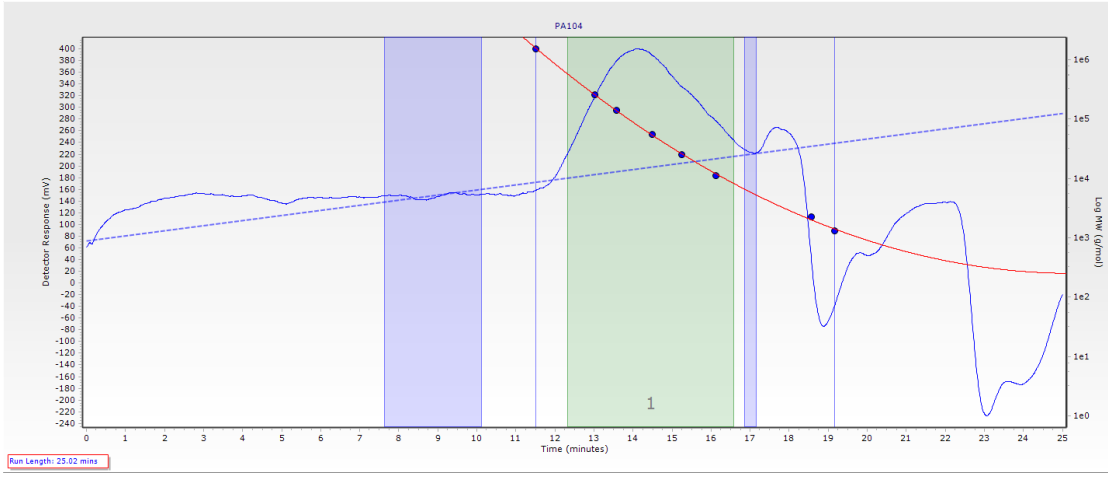
PA104
Detector Response (mV)
Log MW (g/mol)
Time (minutes)
1
Run Length: 25.02 mins

E

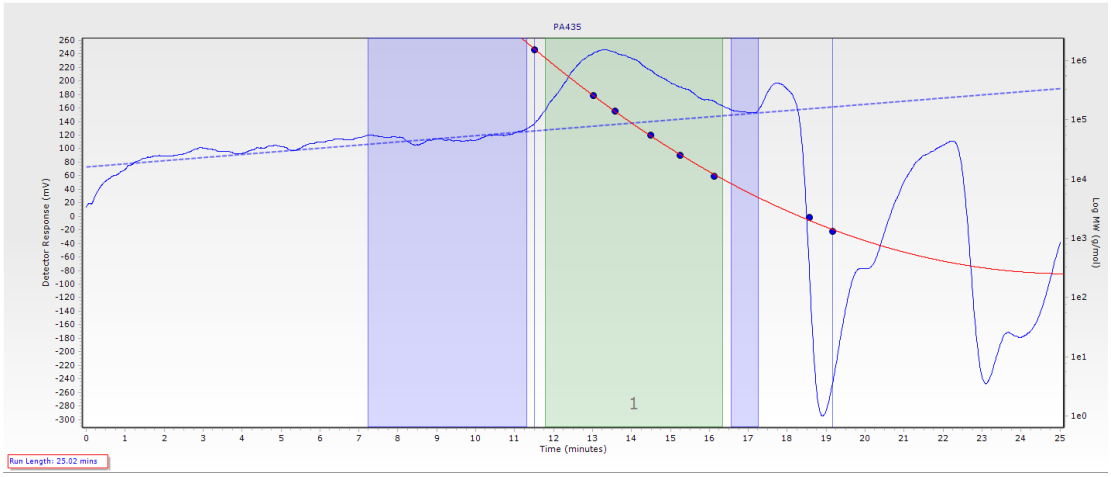
PA435
Detector Response (mV)
Log MW (g/mol)
Time (minutes)
1
Run Length: 25.02 mins

F

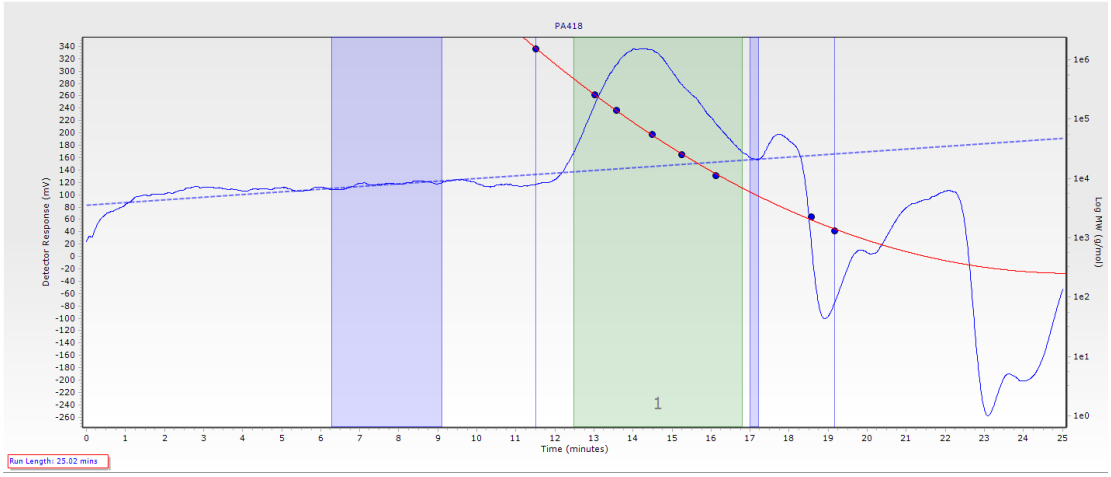
PA418
Detector Response (mV)
Log MW (g/mol)
Time (minutes)
1
Run Length: 25.02 mins

G

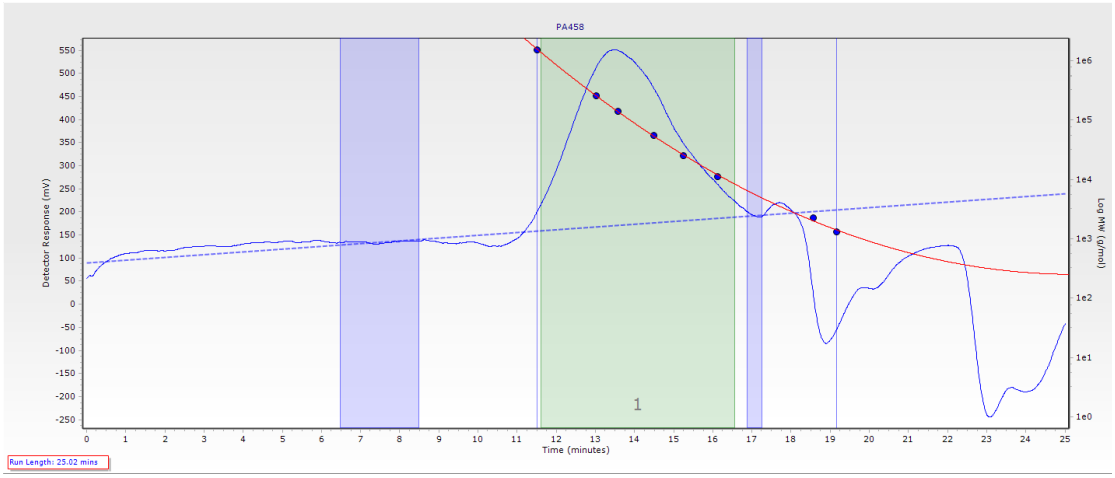
PA458
Detector Response (mV)
Log MW (g/mol)
Time (minutes)
1
Run Length: 25.02 mins

H

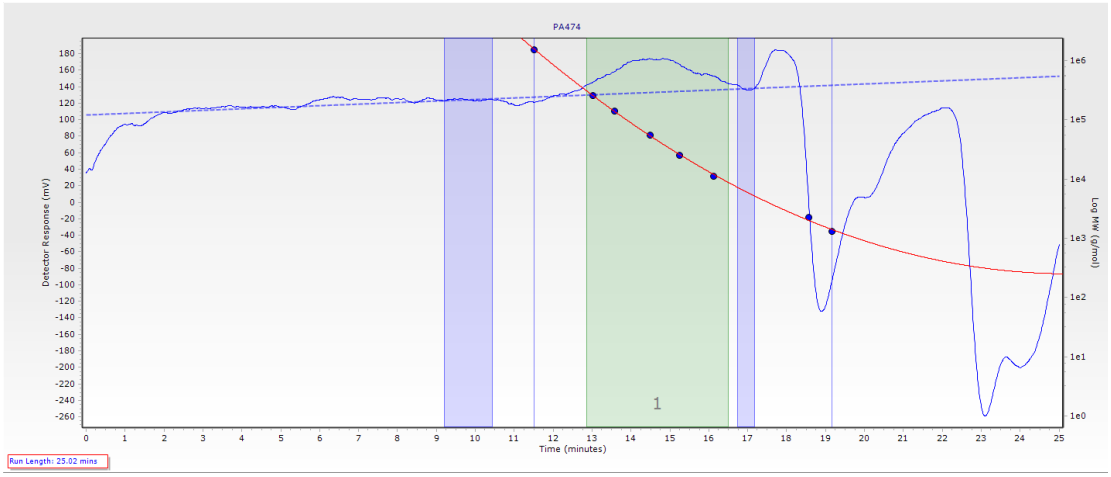
PA474
Detector Response (mV)
Log MW (g/mol)
Time (minutes)
1
Run Length: 25.02 mins

I

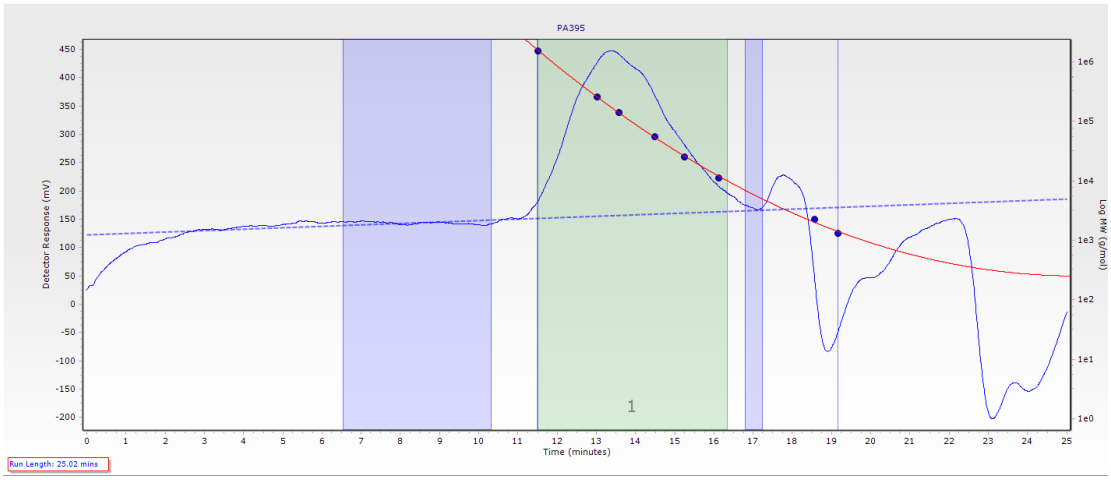
PA395
Detector Response (mV)
Log MW (g/mol)
Time (minutes)
1
Run Length: 25.02 mins

J

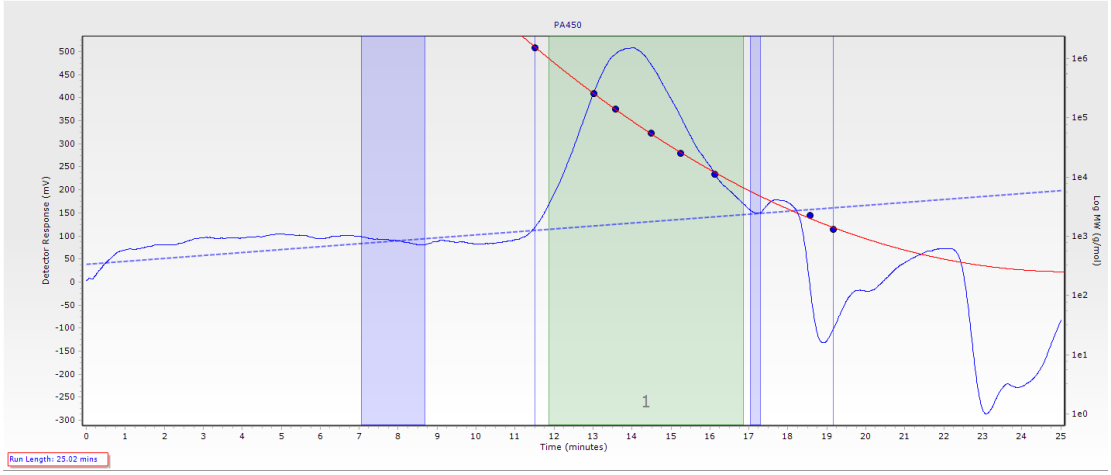

Figure A3.2: GPC traces of scaled-up polymers in Section§ 5.2 and 5.3. Y-axis = Detector Response (mV). X-axis = Time (minutes). **A.** PA531. **B.** PA419. **C.** PA514. **D.** PA104. **E.** PA435. **F.** PA418. **G.** PA458. **H.** PA474. **I.**PA395 **J.** PA450

PP1	PP1	PP1	PP1	PP2	PP2	PP2	PP2	PP3	PP3	PP3	PP3
PP4	PP4	PP4	PP4	PP5	PP5	PP5	PP5	PP6	PP6	PP6	PP6
PP7	PP7	PP7	PP7	PP8	PP8	PP8	PP8	PP9	PP9	PP9	PP9
PP10	PP10	PP10	PP10	PP11	PP11	PP11	PP11	PP12	PP12	PP12	PP12
PP13	PP13	PP13	PP13	PP14	PP14	PP14	PP14	PP15	PP15	PP15	PP15
PP16	PP16	PP16	PP16	PP17	PP17	PP17	PP17	PP18	PP18	PP18	PP18
PP19	PP19	PP19	PP19	PP20	PP20	PP20	PP20	PP21	PP21	PP21	PP21
PP22	PP22	PP22	PP22	PP23	PP23	PP23	PP23	PP24	PP24	PP24	PP24
PP25	PP25	PP25	PP25	PP26	PP26	PP26	PP26	PP27	PP27	PP27	PP27
PP28	PP28	PP28	PP28	PP29	PP29	PP29	PP29	PP30	PP30	PP30	PP30
PP31	PP31	PP31	PP31	PP32	PP32	PP32	PP32	PP33	PP33	PP33	PP33
PP34	PP34	PP34	PP34	PP35	PP35	PP35	PP35	PP36	PP36	PP36	PP36
PP37	PP37	PP37	PP37	PP38	PP38	PP38	PP38	PP39	PP39	PP39	PP39
PP40	PP40	PP40	PP40	PP41	PP41	PP41	PP41	PP42	PP42	PP42	PP42
PP43	PP43	PP43	PP43	PP44	PP44	PP44	PP44	PP45	PP45	PP45	PP45
PP46	PP46	PP46	PP46	PP47	PP47	PP47	PP47	PP48	PP48	PP48	PP48
PP49	PP49	PP49	PP49	PP50	PP50	PP50	PP50	PP51	PP51	PP51	PP51
PP52	PP52	PP52	PP52	PP53	PP53	PP53	PP53	PP54	PP54	PP54	PP54
PP55	PP55	PP55	PP55	PP56	PP56	PP56	PP56	PP57	PP57	PP57	PP57
PP58	PP58	PP58	PP58	PP59	PP59	PP59	PP59	PP60	PP60	PP60	PP60
PP61	PP61	PP61	PP61	PP62	PP62	PP62	PP62	PP63	PP63	PP63	PP63
PP64	PP64	PP64	PP64	PP65	PP65	PP65	PP65	PP66	PP66	PP66	PP66
PP67	PP67	PP67	PP67	PP68	PP68	PP68	PP68	PP69	PP69	PP69	PP69
PP70	PP70	PP70	PP70	PP71	PP71	PP71	PP71	PP72	PP72	PP72	PP72
PP73	PP73	PP73	PP73	PP74	PP74	PP74	PP74	PP75	PP75	PP75	PP75
PP76	PP76	PP76	PP76	PP77	PP77	PP77	PP77	PP78	PP78	PP78	PP78
PP79	PP79	PP79	PP79	PP80	PP80	PP80	PP80	PP81	PP81	PP81	PP81
PP82	PP82	PP82	PP82	PP83	PP83	PP83	PP83	PP84	PP84	PP84	PP84
PP85	PP85	PP85	PP85	PP86	PP86	PP86	PP86	PP87	PP87	PP87	PP87
PP88	PP88	PP88	PP88	PP89	PP89	PP89	PP89	PP90	PP90	PP90	PP90
PP91	PP91	PP91	PP91	PP92	PP92	PP92	PP92	PP93	PP93	PP93	PP93
PP94	PP94	PP94	PP94	PP95	PP95	PP95	PP95	PP96	PP96	PP96	PP96

Figure A3.3: Lay-out of peptide-containing polymer microarray as printed onto microscope glass slide. For polymer compositions see Table A3.3.

Table A3.3: Compositions of peptide-containing polymers used for microarray screening with pancreatic CSCs. For M1 and M2 abbreviation, see Table for polyacrylate/acrylamide library

Feature*	M1	M2	M3	M1 (%)‡	M2 (%)‡	M3 (%)‡
PP1	MEMA	DEAEA		7.2	7.2	0
PP2	MEMA	DEAEMA		7.2	7.2	0
PP3	MEMA	AH		7.2	7.2	0
PP4	MEMA	DMAAm		7.2	7.2	0
PP5	MMA	DEAEA		7.2	7.2	0
PP6	MMA	DEAEMA		7.2	7.2	0
PP7	MMA	AH		7.2	7.2	0
PP8	MMA	DMAAm		7.2	7.2	0
PP9	MEMA	DEAEA	Acrylamide-GRGDS	7.2	7.04	0.016
PP10	MEMA	DEAEMA	Acrylamide-GRGDS	7.2	7.04	0.016
PP11	MEMA	AH	Acrylamide-GRGDS	7.2	7.04	0.016
PP12	MEMA	DMAAm	Acrylamide-GRGDS	7.2	7.04	0.016
PP13	MMA	DEAEA	Acrylamide-GRGDS	7.2	7.04	0.016
PP14	MMA	DEAEMA	Acrylamide-GRGDS	7.2	7.04	0.016
PP15	MMA	AH	Acrylamide-GRGDS	7.2	7.04	0.016
PP16	MMA	DMAAm	Acrylamide-GRGDS	7.2	7.04	0.016
PP17	MEMA	DEAEA	Acrylamide-YIGSR	7.2	7.04	0.016
PP18	MEMA	DEAEMA	Acrylamide-YIGSR	7.2	7.04	0.016
PP19	MEMA	AH	Acrylamide-YIGSR	7.2	7.04	0.016
PP20	MEMA	DMAAm	Acrylamide-YIGSR	7.2	7.04	0.016
PP21	MMA	DEAEA	Acrylamide-YIGSR	7.2	7.04	0.016
PP22	MMA	DEAEMA	Acrylamide-YIGSR	7.2	7.04	0.016
PP23	MMA	AH	Acrylamide-YIGSR	7.2	7.04	0.016
PP24	MMA	DMAAm	Acrylamide-YIGSR	7.2	7.04	0.016
PP25	MEMA	DEAEA	Acrylamide-cRGDfK	7.2	7.04	0.016
PP26	MEMA	DEAEMA	Acrylamide-cRGDfK	7.2	7.04	0.016
PP27	MEMA	AH	Acrylamide-cRGDfK	7.2	7.04	0.016
PP28	MEMA	DMAAm	Acrylamide-cRGDfK	7.2	7.04	0.016
PP29	MMA	DEAEA	Acrylamide-cRGDfK	7.2	7.04	0.016
PP30	MMA	DEAEMA	Acrylamide-cRGDfK	7.2	7.04	0.016
PP31	MMA	AH	Acrylamide-cRGDfK	7.2	7.04	0.016
PP32	MMA	DMAAm	Acrylamide-cRGDfK	7.2	7.04	0.016
PP33	MEMA	DEAEA	Acrylamide-GRGDS	6.4	6.4	0.16
PP34	MEMA	DEAEMA	Acrylamide-GRGDS	6.4	6.4	0.16
PP35	MEMA	AH	Acrylamide-GRGDS	6.4	6.4	0.16
PP36	MEMA	DMAAm	Acrylamide-GRGDS	6.4	6.4	0.16
PP37	MMA	DEAEA	Acrylamide-GRGDS	6.4	6.4	0.16
PP38	MMA	DEAEMA	Acrylamide-GRGDS	6.4	6.4	0.16
PP39	MMA	AH	Acrylamide-GRGDS	6.4	6.4	0.16

PP40	MMA	DMAAm	Acrylamide-GRGDS	6.4	6.4	0.16
PP41	MEMA	DEAEA	Acrylamide-YIGSR	6.4	6.4	0.16
PP42	MEMA	DEAEMA	Acrylamide-YIGSR	6.4	6.4	0.16
PP43	MEMA	AH	Acrylamide-YIGSR	6.4	6.4	0.16
PP44	MEMA	DMAAm	Acrylamide-YIGSR	6.4	6.4	0.16
PP45	MMA	DEAEA	Acrylamide-YIGSR	6.4	6.4	0.16
PP46	MMA	DEAEMA	Acrylamide-YIGSR	6.4	6.4	0.16
PP47	MMA	AH	Acrylamide-YIGSR	6.4	6.4	0.16
PP48	MMA	DMAAm	Acrylamide-YIGSR	6.4	6.4	0.16
PP49	MEMA	DEAEA	Acrylamide-cRGDfK	6.4	6.4	0.16
PP50	MEMA	DEAEMA	Acrylamide-cRGDfK	6.4	6.4	0.16
PP51	MEMA	AH	Acrylamide-cRGDfK	6.4	6.4	0.16
PP52	MEMA	DMAAm	Acrylamide-cRGDfK	6.4	6.4	0.16
PP53	MMA	DEAEA	Acrylamide-cRGDfK	6.4	6.4	0.16
PP54	MMA	DEAEMA	Acrylamide-cRGDfK	6.4	6.4	0.16
PP55	MMA	AH	Acrylamide-cRGDfK	6.4	6.4	0.16
PP56	MMA	DMAAm	Acrylamide-cRGDfK	6.4	6.4	0.16
PP57	MEMA	DEAEA	Acrylamide-GRGDS	1.6	1.6	1.12
PP58	MEMA	DEAEMA	Acrylamide-GRGDS	1.6	1.6	1.12
PP59	MEMA	AH	Acrylamide-GRGDS	1.6	1.6	1.12
PP60	MEMA	DMAAm	Acrylamide-GRGDS	1.6	1.6	1.12
PP61	MMA	DEAEA	Acrylamide-GRGDS	1.6	1.6	1.12
PP62	MMA	DEAEMA	Acrylamide-GRGDS	1.6	1.6	1.12
PP63	MMA	AH	Acrylamide-GRGDS	1.6	1.6	1.12
PP64	MMA	DMAAm	Acrylamide-GRGDS	1.6	1.6	1.12
PP65	MEMA	DEAEA	Acrylamide-YIGSR	1.6	1.6	1.12
PP66	MEMA	DEAEMA	Acrylamide-YIGSR	1.6	1.6	1.12
PP67	MEMA	AH	Acrylamide-YIGSR	1.6	1.6	1.12
PP68	MEMA	DMAAm	Acrylamide-YIGSR	1.6	1.6	1.12
PP69	MMA	DEAEA	Acrylamide-YIGSR	1.6	1.6	1.12
PP70	MMA	DEAEMA	Acrylamide-YIGSR	1.6	1.6	1.12
PP71	MMA	AH	Acrylamide-YIGSR	1.6	1.6	1.12
PP72	MMA	DMAAm	Acrylamide-YIGSR	1.6	1.6	1.12
PP73	MEMA	DEAEA	Acrylamide-cRGDfK	1.6	1.6	1.12
PP74	MEMA	DEAEMA	Acrylamide-cRGDfK	1.6	1.6	1.12
PP75	MEMA	AH	Acrylamide-cRGDfK	1.6	1.6	1.12
PP76	MEMA	DMAAm	Acrylamide-cRGDfK	1.6	1.6	1.12
PP77	MMA	DEAEA	Acrylamide-cRGDfK	1.6	1.6	1.12
PP78	MMA	DEAEMA	Acrylamide-cRGDfK	1.6	1.6	1.12
PP79	MMA	AH	Acrylamide-cRGDfK	1.6	1.6	1.12
PP80	MMA	DMAAm	Acrylamide-cRGDfK	1.6	1.6	1.12
PP81	MEMA		Acrylamide-GRGDS	12.8	0	0.16

PP82	MEMA		Acrylamide-YIGSR	12.8	0	0.16
PP83	MEMA		Acrylamide-cRGDfK	12.8	0	0.16
PP84	MMA		Acrylamide-GRGDS	12.8	0	0.16
PP85	MMA		Acrylamide-YIGSR	12.8	0	0.16
PP86	MMA		Acrylamide-cRGDfK	12.8	0	0.16
PP87		DEAEA	Acrylamide-GRGDS	0	12.8	0.16
PP88		DEAEA	Acrylamide-YIGSR	0	12.8	0.16
PP89		DEAEA	Acrylamide-cRGDfK	0	12.8	0.16
PP90		DEAEMA	Acrylamide-GRGDS	0	12.8	0.16
PP91		DEAEMA	Acrylamide-YIGSR	0	12.8	0.16
PP92		DEAEMA	Acrylamide-cRGDfK	0	12.8	0.16
PP93		AH	Acrylamide-GRGDS	0	12.8	0.16
PP94		AH	Acrylamide-YIGSR	0	12.8	0.16
PP95		AH	Acrylamide-cRGDfK	0	12.8	0.16
PP96		DMAAm	Acrylamide-GRGDS	0	12.8	0.16

*For all polymers the concentration of 1-Hydroxycyclohexyl phenol ketone (initiator) and 1,6-diol diacrylate (cross-linker) were 2.4 % (w/v) and 6 % (w/v) respectively, the remaining % of each polymer being NMP solvent. ‡All % are given as % (w/v).

Monomer Abbreviations

Polyacylate/acrylamide library

A-H	Acrylic acid
AAG-(H)	2-acrylamidoglycolic acid
AES-H	Mono-2-(acryloyloxy)ethyl succinate
BACOEA	2-[[(butylamino)-carbonyl]oxy]ethylacrylate
BAEMA	2-(tert-butylamino)ethyl methacrylate
BMA	Butyl methacrylate
DAAA	Diacetone acrylamide
DEAA	Diethylacrylamide
DEAEA	2-(diethylamino)ethyl acrylate
DEAEMA	2-(diethylamino)ethyl methacrylate
DEGMEMA	Di(ethylene glycol) methyl ether methacrylate
DMAA(m)	Dimethylacrylamide
DMAEA	2-(dimethylamino)ethyl acrylate
DMAEMA	2-(dimethylamino)ethyl methacrylate
DMAPMAA	N,N-dimethylaminopropyl acrylamide

DMVBA	N,N-dimethylvinylbenzylamine
EGMP-H	Ethylene glycol methacrylate phosphate
EMA	Ethyl methacrylate
GMA	Glycidyl methacrylate
HBMA	Hydroxybutyl methacrylate
HEA	2-hydroxyethyl acrylate
HEMA	2-hydroxyethyl methacrylate
HPMA	Hydroxypropyl methacrylate
MA-(H)	Methacrylic acid
MEA	2-methoxyethylacrylate
MEMA	2-methoxymethylacrylate
MMA	Methyl methacrylate
MNPMA	2-methyl-2-nitropropyl methacrylate
MTEMA	2-(methylthio)ethyl methacrylate
PAA	N-isopropylacrylamide
St	Styrene
THFFA	Tetrahydrofurfuryl acrylate
THFFMA	Tetrahydrofurfuryl methacrylate
VAA	N-vinylacetamide
VI	1-vinylimidazole
VP-2	2-vinylpyridine
VP-4	4-vinylpyridine
VPNO	1-vinyl-2-pyrrolidinone

Amines for functionalisation with GMA-containing polymers

BnMa	N-benzylmethylamine
cHMA	Cyclohexanemethylamine
DnBa	Di-n-butylamine
MAEPy	2-(2-methylaminoethyl)pyridine
MAn	N-methylaniline
MnHA	N-methylhexylamine
Pyrle	Pyrrole

Polyurethane library

Diols

PEG	Poly(ethylene glycol)
PHNAD	Poly[1,6-hexanediol/neopentyl glycol-alt-adipic acid] diol
PHNGAD	Poly[1,6-hexanediol/neopentyl glycol/diethylene glycol-alt-adipic acid] diol
PPG	Poly)propylene glycol)
PPG-PEG	Poly)propylene glycol)- Poly(ethylene glycol)
PTMG	Poly(tetramethylene glycol)

Diisocyanides

BICH	1,3-bis(isocyanomethyl)cyclohexane
HDI	1,6-diisocyanohexane
HMDI	4,4′-methylenebis(cyclohexylisocyanate)
MDI	4,4′-methylenebis(phenylisocyanate)
PDI	1,4-diisocyanobenzene
TDI	4-methyl-1,3-phenylen diisocyanate

Extenders

BD	1,4-butanediol
DEAPD	3-diethylamino-1,2-propanediol
DHM	Diethyl bis(hydroxymethyl)malonate
DMAPD	3-dimethylamino-1,2-propanediol
EG	Ehtylene glycol
NMPD	2-nitro-2-methyl-1,3-propanediol
OFHD	2,2,3,3,4,4,5,5-octafluoro-1,6-hexanediol
PG	Propylene glycol